

Investigation of Psychophysiological and Electrophysiological Changes in Primary Open Angle Glaucoma

**Rizwan Malik
MBChB, MRCOphth**

**NIHR Biomedical Research Centre for Ophthalmology
Moorfields Eye Hospital Foundation Trust &
UCL Institute of Ophthalmology,
London**

**A thesis submitted for the degree of Doctor of Philosophy at
University College London (UCL)**

December 2010

Declaration

I, **Rizwan Malik**, confirm that the work presented in this thesis, *Investigation of psychophysiological and electrophysiological changes in primary open angle glaucoma* is my own. Where information has been derived from other sources, I confirm that this has been indicated in the thesis.

Signed _____

Rizwan Malik, MBChB, MRCOphth

Date _____

Dedication

This thesis is dedicated to my parents, my wife and my late aunt Nusrat.

'Glory be to You, we have no knowledge except what you have taught us' [Surah Baqarah, verse 32; The Holy Quran]

Contents

List of figures	15
List of Tables	19
List of Abbreviations	21
Abstract	24
CHAPTER 1: Introduction	27
SECTION A: Primary Open Angle Glaucoma -Definition, Aetiology and Prevalence	28
1.1 Primary open angle glaucoma definition.....	29
1.2 Prevalence	30
1.3 Glaucoma morbidity and economic burden	31
1.4 Risk factors for glaucoma.....	32
1.4.1 Race	32
1.4.2 Age.....	32
1.4.3 Intraocular Pressure	33
1.4.4 Family History.....	35
1.4.5 Baseline optic disc features.....	36
1.4.6 Myopia.....	37
1.4.7 Diastolic perfusion pressure.....	37
1.4.8 Systemic disease.....	38
1.5 Pathogenesis of POAG	38
1.5.1 Reduced aqueous outflow.....	38
1.5.2 Corticosteroid sensitivity.....	39
1.5.3 Immune-mediation.....	39

1.5.4	Blood-flow	39
1.5.5	Infectious aetiology	40
SECTION B: Psychophysical changes in primary open angle glaucoma		41
1.6	A brief evolution of perimetry.....	42
1.7	The normal visual field	43
1.8	The visual field in glaucoma	45
1.9	Modern clinical perimetry	47
1.91	The Humphrey field analyzer	48
1.92	The Octopus perimeter	48
1.9.3	Goldmann kinetic perimetry	48
1.9.4	The Henson perimeter	50
1.9.5	Other forms of perimetry.....	51
	High pass resolution perimetry (HPRP).....	51
	Frequency doubling technology (FDT).....	51
	Short-wavelength automated perimetry (SWAP).....	52
	Motion perimetry.....	53
	Oculokinetic perimetry	53
1.10	Perimetric strategies for static perimetry	54
1.10.1	Full Threshold strategy	54
1.10.2	Suprathreshold strategies	54
1.10.3	Bayesian Peirimetric strategies	54
1.11	Test locations for static perimetry	55
1.12	Problems associated with standard automated perimetry.....	56
1.12.1	Variability.....	56

1.12.2	Low diagnostic sensitivity.....	57
1.13	How can current perimetric techniques be improved on?.....	58
1.13.1	Improve sensitivity to detect glaucomatous loss.....	58
	Use of alternative stimuli.....	58
	Use of smaller ‘white’ stimuli than the Goldmann size III.....	60
1.13.2	Reduce variability.....	61
	Use of larger stimuli than the Goldmann III.....	61
	Alternative stimuli: sinusoidal stimuli.....	61
1.14	Differential light sensitivity.....	62
1.14.1	Definition.....	62
1.14.2	Units of measurement.....	62
1.15	Effect of background luminance.....	64
1.16	Psychophysical factors governing DLS.....	65
1.16.1	Spatial summation.....	65
	Clinical importance of spatial summation in glaucoma.....	65
	Does spatial summation change in glaucoma?.....	66
	Area of summation.....	67
	Effect of age.....	68
	Effect of eccentricity.....	68
	Spatial summation for specific ganglion cell classes.....	69
	Pre-neural factors affect spatial summation.....	69
1.16.2	Probability summation.....	70
1.16.3	Temporal summation.....	71
1.17	The structure-function relationship in glaucoma.....	71

1.17.1	Relating structure and function	71
1.17.2	The nature of the structure-function relationship.....	73
1.17.3	Factors influencing the structure-function relationship	76
SECTION C: Electrophysiological changes in primary open angle glaucoma		77
1.18	Role of Electrophysiology in Glaucoma.....	77
1.19	The Pattern ERG (PERG)	78
1.19.1	The Transient PERG	78
1.19.2	The Steady-State PERG.....	79
1.19.3	The PERG is affected by ganglion cell loss	80
1.19.4	The PERG in glaucoma.....	82
1.19.5	Separating normal from glaucoma on the basis of PERG measurements	83
1.19.6	Predicting OHT converters	85
1.19.7	The relationship between PERG and structural parameters of glaucomatous damage.....	85
1.19.8	The relationship between PERG and visual field measurements in glaucoma.....	87
1.19.9	Which PERG stimulus parameters are optimal for glaucoma detection?	89
	Reversal rate	89
	Check size	90
	Field size	91
1.19.10	Factors affecting precision of the PERG recording	92
1.20	The Photopic Negative Response (PhNR) of the Flash ERG	92

1.20.1	The flash ERG.....	92
1.20.2	The photopic negative response – characteristics & origins	93
1.20.3	Optimal conditions for PhNR recording	95
1.20.4	PhNR in Glaucoma.....	99
1.20.5	The S-Cone PhNR.....	101

CHAPTER 2: Development and evaluation of a linear perimetric staircase strategy for the assessment of glaucoma.....	102	
2.1	Aim.....	103
2.2	The rationale for a linear-increment perimetric strategy	104
2.3	Monte Carlo simulations	105
2.4	Methods	106
2.4.1	Linear units	106
2.4.2	Description of Monte Carlo computer simulation	106
2.4.3	Perimetric Strategies	110
	Full-threshold strategy	110
	Linear Strategies.....	110
2.4.4	Data Analysis	111
2.4.5	Collection of Clinical Data.....	112
	Subjects	112
	Perimetric conditions	113
	Apparatus	113
	Test reliability criteria	114
	Test locations	114
2.4.6	Analysis of pilot data and comparison with simulation data.....	115

2.5	Results	117
2.5.1	Results of the Monte Carlo simulations	117
	Results in dB units	117
	Bias	119
	Test-Retest variability	121
	Efficiency	124
2.5.2	Results from clinical data	127
	Measured sensitivities	127
	Test-retest variability	128
	Efficiency	132
2.6	Discussion	133
2.6.1	Summary of findings.....	133
2.6.2	Units of DLS measurement.....	134
2.6.3	Logarithmic versus linear steps for measuring linear DLS	135
2.6.4	Validating the variability predictions of the Monte Carlo model	137
2.6.5	Importance of findings	138
2.6.6	Comments on study methodology.....	139

CHAPTER 3: Development of novel perimetric stimuli for the assessment of

glaucoma.....	141	
3.1	Aims	142
3.2	Scaling stimulus size by estimates of ganglion cell density.....	143
3.3	Contrast sensitivity perimetry	146
3.4	An appropriate end-point for structure-function analyses.....	147
3.5	Methods.....	147

3.5.1	Participants.....	147
3.5.2	Perimetric conditions	149
3.5.3	Goldmann size III stimulus	149
3.5.4	New stimuli.....	149
	'Scaled' achromatic circular stimulus.....	149
	Gabor patch stimulus	155
3.5.5	Test apparatus.....	159
3.5.6	Imaging	159
3.5.7	Data analysis.....	160
	Variation of DLS and structure-function ratio across eccentricity.....	160
	Structure-function correlations	161
	Agreement of abnormality.....	162
	Application of the Hood-Kardon model.....	163
	Agreement analyses.....	164
3.6	Results I: Effects of scaling stimulus size by ganglion cell density	165
3.6.1	Participants.....	165
3.6.2	Variation of DLS and structure-function ratio across eccentricity in normal Eyes.....	166
3.6.3	Structure-function associations	169
3.6.4	Agreement of abnormality.....	172
3.7	Results II: Gabor patch perimetry	173
3.7.1	Participants.....	173
3.7.2	Variation of DLS and across eccentricity	174
3.7.3	Lower confidence limits for normality	175

3.7.4	Hood-Kardon fits	176
3.7.5	Bland-Altman analysis of agreement	177
3.8	Discussion: Scaled achromatic stimulus	180
3.8.1	Summary of main findings.....	180
3.8.2	Importance of findings	180
3.8.3	Scaling stimulus size and reducing eccentricity dependence	181
3.8.4	Units for structure-function comparisons.....	182
3.8.5	DLS within the central 10 degrees	184
3.8.6	Comments on study methodology.....	185
3.9	Discussion II: Gabor patch perimetry	186
3.9.1	Summary of main findings.....	186
3.9.2	Importance of findings	186
3.9.3	Lower variability around mean agreement for Gabor patch stimulus for locations at eccentricities greater than 20 degrees	187
3.9.4	Comments on study methodology.....	188
CHAPTER 4: The Photopic negative response of the Flash ERG and other functional measures of glaucomatous optic neuropathy.....		189
4.1	Aims	190
4.2	The photopic negative response and the pattern ERG	191
4.3	The photopic negative response and visual field indices.....	194
4.4	Methods.....	196
4.4.1	Study definition of glaucomatous optic neuropathy	196
4.4.2	Participants.....	197
4.4.3	Tests performed	198

4.4.4	Scanning laser ophthalmoscopy (HRT II Imaging)	198
4.4.5	Scanning Laser Polarimetry	199
4.4.6	Electrodiagnostic tests	200
	Pattern ERG	200
	Flash ERG	202
4.4.7	Data analysis	203
	Analysis of amplitudes and comparison of mean values	203
	Linear regression analysis of tPERG amplitude, SSPERG ratio and PhNR amplitude versus rim area	203
	Computation of a linear global visual field measure	204
	Mean value of MD, linear DLS and PhNR in normal and glaucomatous eyes	204
	The relationship between visual field measures and PhNR with RNFL thickness	204
	Agreement analyses	205
	Receiver Operator Curve Analysis	206
	Agreement of abnormal PERG and PhNR values	206
4.5	Results I: The photopic negative response and the pattern ERG	206
4.5.1	Mean and individual electrophysiological values	207
4.5.3	Relationship between the PERG, PhNR and rim area	208
4.5.4	ROC Analysis: PERG versus PhNR	212
4.5.5	Agreement of abnormal PERG and PhNR values	214
4.6	Results II: Global visual field indices and the photopic negative response	216

4.6.1	Participants.....	216
4.6.2	Relationship between visual field measures and the photopic negative response with nerve fibre layer thickness	218
4.6.3	ROC analysis: Visual field measures and PhNR	220
4.7	Discussion I: the PhNR and the PERG	225
4.7.1	Summary of findings.....	225
4.7.2	PhNR as a marker of ganglion cell loss in glaucoma	225
4.6.3	Conditions for recording the PhNR in the current study	227
4.7.4	Diagnostic accuracy of the PhNR and PERG and comparison with other studies	228
4.7.5	Comments on study methodology.....	229
4.7.6	Clinical relevance: electrophysiological evaluation of glaucomatous optic neuropathy.....	230
4.8	Discussion II: The PhNR and visual field measures of glaucomatous optic neuropathy.....	231
4.8.1	Summary of findings.....	231
4.8.2	Value of current sensitivity estimates.....	231
4.8.3	Relationship between the PhNR and RNFL thickness	233
4.8.4	Clinical usefulness of the PhNR.....	233
4.8.5	Comments on study methodology.....	233
CHAPTER 5: Conclusions & Further work		235
5.1	Conclusions.....	236
5.2	Further work.....	238
5.2.1	Perimetric strategies which utilise linear increments of sensitivity	238

5.2.2	Scaling stimulus sizes by estimates of ganglion cell density.....	238
5.2.3	Gabor patch perimetry.....	238
5.2.4	Agreement analyses for structure-function comparisons.....	239
5.2.5	The PhNR in glaucoma.....	239
Acknowledgments		242
References		245

List of figures

Figure 1.1: ‘Hill of vision’, Traquair (1938)	44
Figure 1.2 Spatial distribution of visual field defects in glaucoma,	47
Figure 1.3: Linear and dB increments on the (linear) same scale.....	63
Figure 1.4: Non-linear relationship between linear, L^{-1} and log (dB) units of DLS	63
Figure 1.5: A typical normal PERG trace	79
Figure 1.6: Transient PERG (P50-N95) amplitudes for Normal and Glaucoma groups from a published study (Garway-Heath, Holder et al. 2002).....	82
Figure 1.7: Simplified diagrammatic representation of the retina	93
Figure 1.8: Showing a normal human Photopic Negative Response,	94
Figure 2.1 Psychometric Functions (Frequency-of-Seeing Curves) obtained with the Weibull Function with a threshold (50% seen point) of 30 dB (= 1000 L^{-1})	108
Figure 2.2: Sample staircase runs	111
Figure 2.3: Test locations (left eye).....	115
Figure 2.4: Variability of DLS (dB) versus sensitivity (dB) as predicted by the Monte Carlo simulation	119
Figure 2.5: The effect of sensitivity on bias	121
Figure 2.6: Test-retest variability	123
Figure 2.7: Efficiency predictions from the Monte Carlo simulation.....	124
Figure 2.8: FT, Ln1 and Ln2 estimated test times for a full 24-2 visual field test.	126
Figure 2.9 Agreement of sensitivity values as measured by FT and Ln2	128
Figure 2.10: Variability (measured as the standard deviation of test-retest difference across locations with similar sensitivity) for FT and Ln2.....	129

Figure 2.11: Variability by sensitivity group.....	131
Figure 2.12: Mean number of trials taken for FT and Ln2 staircases to terminate. .	132
Figure 3.1: A re-analysis of empirical data (Garway-Heath et al. 2000) shows a dependence of DLS on eccentricity.....	150
Figure 3.2: Stimulus sizes on the VSG display monitor (to scale) for the scaled stimulus for the right eye.....	154
Figure 3.3: Diameter of scaled stimulus by retinal eccentricity	154
Figure 3.4: Gabor and achromatic scaled stimuli for the locations (3,-3), a; and (27,-3), b; are shown.....	158
Figure 3.5: Illustrating the locations in each analysis zone (A: <10 deg; B: 10-20 deg; C: > 20 deg).....	162
Figure 3.6: Variation of mean RNFL thickness across scan sector in normal Eyes ..	165
Figure 3.7: Mean DLS per eccentricity for normal subjects for DLS in (a) dB units and (b) Linear (L^{-1}) units	168
Figure 3.8: Variation of (log) structure-function ratio across eccentricity for the Goldmann size III and the scaled stimulus.....	169
Figure 3.9: DLS versus RNFL thickness for all locations	170
Figure 3.10: Comparison of the agreement between DLS and RNFL thickness	173
Figure 3.11: Variation of contrast sensitivity of the Gabor patch stimulus with eccentricity.....	175
Figure 3.12: Lower (95%) confidence limit for normal subjects at each eccentricity for the Gabor patch stimulus compared to the Goldmann size III and the scaled achromatic stimulus.....	176

Figure 3.13: Plots of RNFL thickness (μm) versus relative sensitivity for eccentricities of 4.2 and 27 degrees fitted with the Hood-Kardon model	177
Figure 3.14: Bland-Altman plots showing the difference versus the average of predicted RNFL thickness (from the Hood-Kardon Model) and measured RNFL thickness, μm for (a) 4.2 Degrees eccentricity; and (b) 27 degrees eccentricity	178
Figure 3.15: Bland-Altman mean (solid symbols) and standard deviation (error bars) of agreement for the Gabor patch stimulus across the range of eccentricities tested	179
Figure 4.1: The spatial correspondence of the retinal area stimulated by the PERG to the optic nerve head (ONH)	205
Figure 4.2: Scatterplot of individual values of the (a) tPERG, (b) SSPERG ratio and (c) PhNR.....	209
Figure 4.3: Recordings from one healthy volunteer (1) and 2 patients with primary open angle glaucoma (2,3).....	210
Figure 4.4: Plots of transient PERG N95—P50 amplitude, Steady State PERG ratio and PhNR amplitude versus rim area	211
Figure 4.5: ROC Analysis of transient (t) PERG amplitude, Steady-State (SS) PERG ratio and PhNR amplitude to identify glaucomatous optic neuropathy	213
Figure 4.6: Non-proportional Venn diagrams showing agreement of (a) abnormal transient PERG and (b) abnormal Steady-State PERG ratio with abnormal PhNR and abnormal MD in glaucoma patients.....	215
Figure 4.7: Pattern Standard Deviation (PSD) plots, RNFL thickness profile from GDxEcc and OCT RNFL 3.4 scans and flash ERG recordings showing the PhNR	

(marker '5') from (a) one healthy volunteer and (b,c) two patients with different severities of glaucoma	217
Figure 4.8: Relationship between Mean Deviation (MD, dB), linear DLS and PhNR with RNFL thickness. The column on the left shows plots for OCT RNFL thickness and those on the right for GDx.	219
Figure 4.9: Receiver Operator Characteristic (ROC) curves based on the presence of Glaucomatous Optic Neuropathy (GON) on HRT disc analysis.....	221
Figure 4.10: Venn diagrams (non-proportional) depicting agreement between visual field measures (a), (b) and the (c) photopic negative response with low Retinal nerve fibre layer thickness from OCT and GDx in eyes with glaucomatous optic neuropathy.....	223

List of Tables

Table 1.1: Reported prevalence of POAG	34
Table 1.2: Developments in perimetry	42
Table 1.3 Luminance values (in Asb) for the Goldmann perimeter,	50
Table 1.4: Types of perimetry and associated perimetric selective sensitivity	59
Table 1.5: Parameters used by various studies to record the PhNR	96
Table 2.1: Perimetric strategies simulated	110
Table 2.2: Mean sensitivity at each eccentricity for normal subjects	127
Table 3.1: Mean peak spatial frequency of the Gabor patch stimulus in relation to the achromatic ‘scaled’ circular stimulus at each eccentricity.....	157
Table 3.2: Coefficients of determination (R^2 values, in %) for linear regression of DLS against RNFL thickness	171
Table 4.1: Mean values for tPERG, SS PERG ratio and PhNR amplitude in normal (n=23) and glaucoma (n=30) groups.	207
Table 4.2: Sensitivities at fixed specificities of around 90% and areas under the ROC curves with corresponding criterion values for the transient PERG N95—P50 amplitude, SS PERG ratio and PhNR.....	214
Table 4.3: Comparison of parameters between the ‘normal’ and ‘glaucoma’ group	216
Table 4.4: Mean Deviation values, RNFL thickness and PhNR amplitudes for examples shown in <i>figure 4.7</i>	217
Table 4.5: Comparison of study sample size and diagnostic accuracy estimates of current study with previous studies of the PhNR in glaucoma	224

List of equations

$dB = 10[\log(L_{max}/x)]$ [1.1]	62
$P(x) = 1 - 2^{-(x/\alpha)^\beta}$ [2.1]	107
$R(x) = (1-FN)P(x) + FP(1-P(x)) = FP + (1-FP-FN)P(x)$ [2.2]	107
$\ln(SD) = 3.27 + 0.81 * \log(\alpha)$ [2.3]	108
$\beta = 10/(SD * \sqrt{2})$ [2.4]	108
$d = 2\sqrt{[37/\pi G]}$ [3.1]	152
$d_v = d / q_p$ [3.2]	152
$q_p = q_0 - 0.000014U^2$ [3.3]	152
$f = E/E_2$ [3.4]	153
$L(x,y) = L_m (1 + \sin [2\pi\omega(y-y_0)] (e^{-[(x-x_0)^2 + (y-y_0)^2]/(2\sigma^2)}))$ [3.5]	155
$\omega = (1/4) * (\text{Diameter of 'scaled' stimulus} / \text{Diameter of Goldmann III})$ [3.6]	156
$\omega = (\text{Diameter of scaled stimulus}) / 3.44$ [3.7]	156
$\omega = 1.72V(37/\pi G)$ [3.8]	156
$h = \sigma \omega = 0.75 \text{ octave}$ [3.9]	156
$\omega_m = \tan(E + 1/\omega) - \tan E$ [3.10]	157
$RNFL (dB) = 10 * \log_{10} RNFL (\mu m)$ [3.11]	161
$R = s_0 T + b$ for $T < 1.0$ [3.12]	163
$R = s_0 + b$ for $T \geq 1.0$ [3.13]	163
$R_{upper} = R_m + 2R_{sd}$ [3.14]	163
$R_{lower} = R_m - 2R_{sd}$ [3.15]	164
$95\% \text{ CI} = \text{mean } diff(RNFL_{pred}, RNFL_{meas}) \pm 1.96 \text{ sd } diff(RNFL_{pred}, RNFL_{meas})$ [3.16]	164
$R = s_0 T + b$ [4.1]	218

and $R = s_0 + b$ [4.2].....	218
Where $T = 10^{0.1 * MD}$ [4.3].....	218

List of Abbreviations

µm	micrometres
Asb	Apostilbs
Cpd	Cycles per degree
CRT	Cathode ray tube
dB	Decibel
Deg	Degrees
DLS	Differential light sensitivity
ERG	Electroretinogram
FDT	Frequency doubling technology
FN	False negative
FP	False positive
FT	Full-Threshold strategy
Goldmann III	Goldmann size III stimulus
HFA	Humphrey Field Analyzer
HRT	Heidelberg Retinal Tomograph
HVF	Humphrey visual field
Hz	Hertz
L	Lambert
Ln1	Linear 1 perimetric strategy
Ln2	Linear 2 perimetric strategy
Log	Logarithmic
m	Metres

MD	Mean Deviation
mm	Millimetres
MRA	Moorfields Regression Analysis
OCT	Ocular coherence tomography
ONH	Optic nerve head
p	Statistical probability value
PERG	Pattern electroretinogram
PhNR	Photopic negative response
POAG	Primary open angle glaucoma
PPA	Peri-papillary atrophy
PSD	Pattern Standard Deviation
RNFL	Retinal nerve fibre layer
ROC	Receiver operator curve
S-, L-, M- cone	'Short', 'Medium' and 'Long' wavelength cones
SAP	Standard automated perimetry
SD	Standard deviation
SE	Standard error
SITA	Swedish Interactive Thresholding Algorithm
SLO	Scanning laser ophthalmoscopy
SLP	Scanning laser polarimetry
SS PERG, tPERG	Steady-state and transient Pattern ERG
SWAP	Short-wavelength automated perimetry
TD	Total Deviation
VA	Visual acuity

VEP	Visual evoked potential
VSG	Visual Stimulus Generator

Abstract

The functional assessment of patients with primary open angle glaucoma (POAG) is important both for quantifying glaucomatous damage and for providing the clinician with an indication of the level of visual impairment from glaucoma. In its commonest form, perimetry is carried out using automated computerised techniques to bracket visual sensitivity (differential light sensitivity, DLS) at multiple test locations. Test parameters for contemporary standard automated perimetry (SAP) have largely been translated from the Goldmann kinetic parameter with minimal modification, with the use of an achromatic circular stimulus of a fixed size and perimetric strategies which utilise logarithmic (decibel, dB) increments of sensitivity. Perimetry is not without its problems: tests can often be unreliable and learning and fatigue effects contribute to test variability. Electrodiagnostic tests offer an alternative and objective means of functional assessment. In this regard, the photopic negative response (PhNR) is a technically easy test to perform and is not dependent on precise fixation stability or refractive correction. Following the introductory chapter (**Chapter 1**), the thesis consists of two broad areas of study: psychophysical (visual field) changes in POAG (**Chapters 2 and 3**) and electrophysiological changes in POAG (**Chapter 4**). **Chapter 2** explores the use of linear units for the measurement of DLS, with the development of new algorithms which yielded lower perimetric bias and variability compared to conventional dB-increment algorithms. Two new stimuli for perimetry were subsequently developed with the aim of improving correlation and agreement of DLS with structural parameters in POAG (**Chapter 3**). The electrophysiological investigations

demonstrated the PhNR to be as sensitive as global visual field measures and existing electrophysiological tests for the identification of functional loss associated with glaucomatous optic neuropathy (**Chapter 4**) and further refinement of this response for the diagnosis of glaucoma has been recommended (**Chapter 5**).

CHAPTER 1

Introduction

SECTION A:

Primary Open Angle Glaucoma - Definition, Aetiology and Prevalence

1.1 Primary open angle glaucoma definition

Definitions of primary open angle glaucoma (POAG) as given in some of the glaucoma textbooks have been given below:

(Duke-Elder 1954)- ‘..It is insidious in origin and slowly progressive, showing a triad of symptoms – field defects, cupping of the disc from a relatively early stage, and a rise of tension which, although phasic, eventually tends to be permanent... it occurs in eyes of any type, of any refractive error, the width of whose angles varies from wide to narrow as those of the general population.’

(Heilmann and Richardson 1978)– Glaucoma, Conceptions of a Disease: ‘Primary open-angle glaucoma is a genetically determined, chronic and progressive disease of insidious onset. The signs associated with this disease consist of elevated IOP, decreased outflow facility, optic nerve head damage and visual field defects.’

(Kanski 1989)– Glaucoma: ‘Primary open angle glaucoma is characterised by the following: (a) An IOP over 21 mmHg; (b) An open angle of normal appearance; (c) Glaucomatous cupping of the optic nerve head; (d) Visual field loss.’

(Chandler, Grant et al. 1997) -Chandler & Grant’s glaucoma: ‘POAG is a diagnosis of exclusion... the diagnosis is made by routine tonometry and by inspection of the optic nerve heads. The IOP at a given examination may be in a normal phase, but if the disc is abnormal, suspicion is aroused’

(Allingham and Shields 2005) - Shields’ Textbook of Glaucoma: ‘POAG is a multifactorial optic neuropathy in which there is a characteristic atrophy of the optic nerve. .. typically characterised by: (a) an IOP consistently above 21 mmHg in at least one eye; (b) an open, normal-appearing angle anterior chamber angle with

no ocular or systemic abnormality that may account for the elevated IOP and (c) typical ONH damage and / or glaucomatous visual field damage’.

Other definitions:

American Academy of Ophthalmology (2005): ‘Primary open-angle glaucoma is a progressive, chronic optic neuropathy in adults where intraocular pressure (IOP) and other currently unknown factors contribute to damage and in which, in the absence of other identifiable causes, there is a characteristic acquired atrophy of the optic nerve and loss of retinal ganglion cells and their axons. This is associated with an anterior chamber angle that is open by gonioscopic appearance.’

European Glaucoma Society Terminology and Guidelines for Glaucoma (European Glaucoma 2008) : ‘The open angle glaucomas are, chronic progressive optic neuropathies, that have in common characteristic morphological changes at the optic nerve head and retinal nerve fibre layer in the absence of ocular or congenital anomalies’

On the basis of these definitions, glaucoma, therefore, is consensually accepted as a group of conditions in which a characteristic optic neuropathy is the common denominator. The term ‘primary’ refers to the lack of any identifiable cause of the disease and ‘open angle’ is used to distinguish the condition from anatomic obstruction of the filtration angle.

1.2 Prevalence

Reports of glaucoma prevalence vary in the literature from under 0.5% (Hollows and Graham 1966) to nearly 9% (Mason, Kosoko et al. 1989). Racial and age

differences account for a considerable amount of this variation. The prevalence increases with age and is higher in 'black' populations (Tielsch, Sommer et al. 1991). Friedman et al. (2004) reported a prevalence of around 0.6% in the 40-49 age group compared with 7.3% in the over 80 years age group for a 'white' American population.

In the UK, a study in Bedford (age > 30 years) in 1968 documented a prevalence of 0.7% (Bankes, Perkins et al. 1968) and another study in Rhonda Valley (40-74 age range) 2 years earlier found a prevalence of less than half that number (Hollows and Graham 1966). More recently, the prevalence of POAG in a North London Eye Study for a random population aged 65 years and over was 3% (Reidy, Minassian et al. 1998).

1.3 Glaucoma morbidity and economic burden

POAG affects over 40 million people worldwide and is projected to affect nearly 60 million by 2020 (Quigley and Broman 2006). Glaucoma is the second cause of blindness worldwide and the leading cause of irreversible blindness (Quigley 1996). It is estimated that more than 5 million people will be (bilaterally) blind from the condition by 2020 (Quigley and Broman 2006) and nearly 15% of world blindness can be attributed to glaucoma (Thylefors and Negrel 1994). In the UK, glaucoma accounts for over 10% of blind registrations and a similar number of 'partial sight' registrations (Bunce and Wormald 2006).

Glaucoma, being chronic in nature and requiring life-time follow-up poses a significant economic burden to any health system. In 2002, management of glaucoma and ocular hypertensive patients in the UK totalled more than 300 million

pounds (Rouland, Berdeaux et al. 2005). The cost of treating a patient per year seems to be fairly similar in Europe compared to the United States and is over 1000 USD (\approx 700 pounds), (Kobelt-Nguyen, Gerdtham et al. 1998).

1.4 Risk factors for glaucoma

Knowledge of the factors associated with the development of POAG is essential for evaluating the risk profile of each individual with suspected glaucoma and appropriate monitoring of established patients.

1.4.1 Race

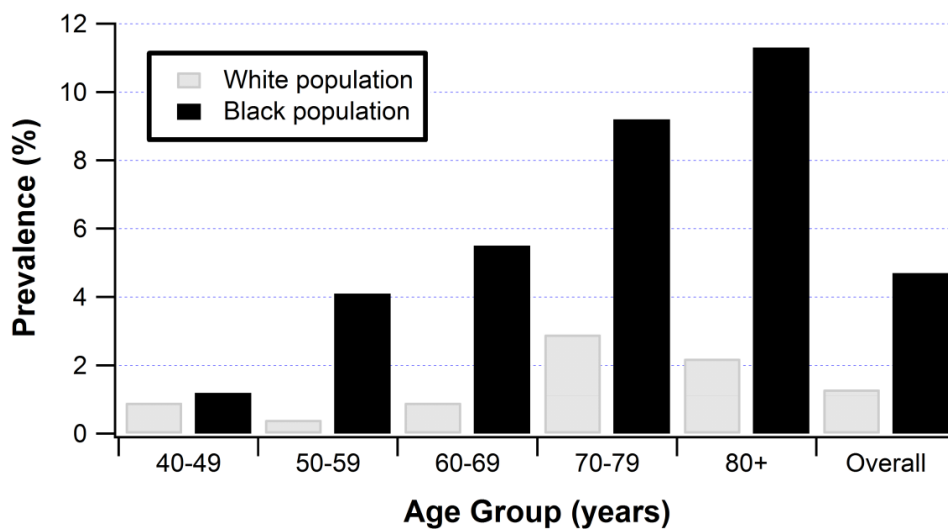
The lowest prevalence of POAG appears to be in 'White' populations and highest prevalence in 'Black' populations, with intermediary prevalence occupied by (Chinese and Indian) Asian populations. In the Baltimore Eye Study, the prevalence of POAG in the 50-59 age group in the Black population was 4.1% compared with just 0.4% for the white population in the same study (Tielsch, Sommer et al. 1991). For the 80+ age group, the respective prevalence was 11.3% and 2.2%. In the Ocular hypertension treatment study, (Gordon, Beiser et al. 2002), a lower corneal thickness and higher baseline cup-to-disc ratio (CDR) may have been confounding factors in the higher reported incidence of POAG in the black population.

1.4.2 Age

As outlined above and in **table 1.1**, the prevalence of POAG increases with age. The Baltimore Eye Survey (Friedman, Wolfs et al. 2004), the Barbados Eye Study (Leske, Connell et al. 1994) and a large study of the South Indian population (Ramakrishnan,

Nirmalan et al. 2003) have all documented such within-race increases. This may be an IOP-related effect in part, as there is a tendency of IOP to increase with age.

Figure 1.1: Prevalence of POAG in the 'white' and 'black' populations in the Baltimore Eye Study, Plotted from data in Tielsch et al. 1991



1.4.3 Intraocular Pressure

IOP is a quantitative objective measure and a modifiable risk factor for the development (and progression) of glaucoma and is therefore given considerable importance. The relative risk is related to the level of IOP (Heijl, Leske et al. 2002; Leske, Heijl et al. 2004) and the prevalence of POAG increases with IOP (Leske, Connell et al. 2001). In the Baltimore Eye Survey, the relative risk of glaucoma was 12.8 for an IOP in the range 22-24 mmHg compared to an IOP of less than 15 mmHg (Sommer, Tielsch et al. 1991).

Table 1.1: Reported prevalence of POAG

Study	Location	Race	Age (years)	Number	Prevalence (%)
Rhonda Valley	Rhonda Valley, UK	White	40-74	4231	0.3%
Bedford	Bedford, UK	White	>30	5941	0.7%
Frammingham	Frammingham, USA	White	52-85	2477	1.2%
St Lucia	St. Lucia, USA	Black	30-86	1679	8.8%
Baltimore Eye Study	Baltimore, USA	Black	>40	2913	1.3%
Beaver Dam	USA	White	43-84	4926	2.1%
Roscommon	Ireland	White	>50	2186	1.9%
Barbados Eye Study	Barbados	Black	40-84	4709	6.6%
Rotterdam Eye Study	Rotterdam, Netherlands	White	>55	3062	3.1%
Blue Mountains	Australia	White	>49	3654	3.0%
Mongolia	Mongolia	Oriental Asian	>40	1000	0.5%
Egna-Neumarket	Italy	White	>40	5816	1.4%
North London Eye Survey	London, UK	White	≥ 65	1547	3.0%
Andhra Pradesh Eye Study	Andhra Pradesh, India	Indian Asian	>40	1399	2.6%
Singapore	Singapore	Oriental Asian	40-79	1717	2.4%
Tamil Nadu 2003	Tamil Nadu, India	Indian Asian	>40	5150	1.7%

Key:

'White' race

'Black' race

'Asian' (Indian / oriental)

Similarly, the relative risk of POAG in the Barbados Eye Study was 10.5 for an IOP in the range 23-25 relative to an IOP of less than 17 mmHg (Leske, Connell et al. 2001). In both studies, the relative risk further increased with the level of IOP. One population based study in Australia estimated that the risk of POAG increased by 10% for every 1 mmHg increase in IOP (Le, Mukesh et al. 2003). Furthermore,

reduction of IOP in Ocular Hypertensive patients has been convincingly shown to reduce the incidence of POAG (Kass, Heuer et al. 2002) and reduce the rate of progression compared to no treatment (Heijl, Leske et al. 2002).

1.4.4 Family History

There is considerable evidence from large prevalence surveys for a positive family history of glaucoma (in a first degree relative) being associated with a higher risk of POAG compared to the absence of any family history. The risk is higher when a sibling is affected relative to a parent (Tielsch, Katz et al. 1994). In the Baltimore Eye Study, the (age-adjusted) odd ratios for glaucoma risk were 3.7, 2.2 and 1.1 for an affected sibling, parent and offspring respectively (Tielsch, Katz et al. 1994). In a population-based survey involving examination of nearly 500 siblings and offspring, the lifetime relative risk of glaucoma was 9.2 (Wolfs, Klaver et al. 1998). Risk profiling using a scoring system based on family history has been previously proposed (Hulsman, Houwing-Duistermaat et al. 2002). Interestingly, from both the Baltimore and Blue Mountain Eye Studies, the odds ratio for glaucoma in a first-degree relative appears to be higher when the affected individual has established (rather than newly-diagnosed) glaucoma (Tielsch, Katz et al. 1994; Mitchell, Rochtchina et al. 2002). This may reflect a greater awareness of glaucoma within families leading to more frequent or earlier glaucoma diagnosis.

The significance of a positive family history and the observation of concordance of POAG in monozygotic twins (Teikari 1987) have prompted a thorough investigation of possible genetic factors in POAG. At least 6 such genetic loci have been isolated. However, the lack of penetrance of POAG and the presence of genetic loci in

individuals without POAG points to a genetic susceptibility, with environmental factors playing a significant role.

1.4.5 Baseline optic disc features

Although a high CDR at baseline has been associated with a higher subsequent risk of developing glaucomatous field loss (Armaly, Krueger et al. 1980; Miglior, Pfeiffer et al. 2007), this is a difficult risk factor to interpret for 3 reasons. Firstly, some studies have used optic disc features as an inclusion criterion as well as a study endpoint (Gordon, Beiser et al. 2002), creating a bias in the analysis. Secondly, it is possible that such patients, who are often labelled as 'glaucoma suspects' in the clinical setting already have a subclinical preperimetric form of disease. Thirdly, the crude CDR value can be misleading without normalising for disc size and a high CDR may be an entirely normal finding in large discs (Garway-Heath, Ruben et al. 1998). The OHTS investigators estimated that for every 0.1 unit increase in baseline CDR, the incidence of POAG increased by 1.4 fold. Another study found the risk of glaucoma increased almost 9-fold with a CDR of 0.7 or more compared with a CDR of less than 0.7 (Mukesh, McCarty et al. 2002). A study of OHT patients at Moorfields Eye Hospital demonstrated that an abnormal rim area (using the Moorfields Regression Analysis of the Heidelberg Retinal Tomograph, HRT) at baseline of patients was associated with a higher risk of functional or structural conversion to glaucoma (Strouthidis, Gardiner et al. 2010).

The presence of peripapillary atrophy (PPA), which represents thinning of the retinal pigment epithelium surrounding the ONH, is also associated with glaucoma. PPA is divided into a peripheral alpha (α) and a peripheral beta (β) zone, with the

former being a frequent finding in normal eyes (Jonas, Nguyen et al. 1989). The latter form of PPA has been linked both to the development (Wilensky and Kolker 1976; Jonas, Nguyen et al. 1989) and progression of glaucoma (Uchida, Ugurlu et al. 1998), but is not a feature specific to the disease and is often found in myopic eyes. Optic disc haemorrhages are found with a higher frequency in glaucomatous eyes (Healey, Mitchell et al. 1998) and associated with progressive disease (Drance, Fairclough et al. 1977). Again, disc haemorrhages are not specific to glaucoma and the clinician should bear other causes of disc haemorrhage in mind when examining patients with this finding such as posterior vitreous detachment, proliferative retinal vascular disease (including diabetes), vein occlusions and systemic hypertension.

1.4.6 Myopia

In the Blue Mountains Study, the prevalence of POAG was much higher in myopic eyes (Mitchell, Hourihan et al. 1999). This finding is supported by other large population studies in the last decade (Weih, Nanjan et al. 2001; Wong, Klein et al. 2003).

1.4.7 Diastolic perfusion pressure

Although IOP tends to increase with diastolic blood pressure (Tielsch, Katz et al. 1995), systemic hypertension may be protective against POAG (Leske, Wu et al. 2002). In addition, there is considerable evidence for a link between low diastolic perfusion pressure (defined as diastolic BP – IOP) and the risk of POAG (Tielsch, Katz

et al. 1995; Bonomi, Marchini et al. 2000; Leske, Wu et al. 2002). Typically, a diastolic perfusion pressure of below 55 mmHg is considered to be abnormal.

1.4.8 Systemic disease

The association of diabetes with POAG appears to be controversial. Although the prevalence of POAG was higher in diabetics in the Beaver Dam, the Barbados Eye Study, the Rotterdam Study and the Blue Mountains Study (Klein, Klein et al. 1994; Leske, Connell et al. 1995; Dielemans, de Jong et al. 1996; Mitchell, Smith et al. 1997) other large studies have been unable to demonstrate such a link (Armstrong, Daily et al. 1960; Tielsch, Katz et al. 1995).

Grave's disease, which causes raised episcleral pressure and orbital congestion, has been connected with OHT and glaucoma (Cockerham, Pal et al. 1997). Recently, hypothyroidism has been suggested as a possible risk factor for POAG (Lin, Kang et al. 2010).

1.5 Pathogenesis of POAG

The pathogenesis of POAG remains largely unknown although a number of theories have been proposed:

1.5.1 Reduced aqueous outflow

Histologically, a number of abnormalities in the trabecular meshwork of glaucomatous eyes have been noted. These include changes in collagen morphology (Li and Yi 1985), increased amounts of stress markers such as myocillin (Lutjen-

Drecoll, May et al. 1998) proliferation of endothelial cells (Li and Yi 1985) and narrowed intratrabecular spaces (Finkelstein, Trope et al. 1990). Ageing causes similar changes in the trabecular meshwork (Miyazaki, Segawa et al. 1987). Oxidative (Li, Luna et al. 2007) and mechanical stress to the meshwork may be responsible for these changes (Luna, Li et al. 2009).

1.5.2 Corticosteroid sensitivity

Approximately 5% of the general population have an exaggerated response to topical steroids, causing an IOP elevation of 15 mmHg or more (Armaly 1967). This clinical finding has prompted the 'steroid-sensitivity' theory of POAG. On average, patients with POAG have a greater steroid sensitivity than control populations and there may be a degree of inheritance for this susceptibility (Becker and Hahn 1964).

1.5.3 Immune-mediation

Increased levels of immune markers and lymphocytes have been demonstrated in the trabecular meshwork of glaucomatous eyes, suggesting a possible immune trigger to the disease (Becker, Unger et al. 1963). Autoantibodies to a pro-apoptotic retinal protein called γ -enolase, have been isolated more frequently in glaucomatous patients than controls (Maruyama, Ohguro et al. 2000) as well as antibodies that cross-react with glucosaminoglycans (Tezel, Edward et al. 1999).

1.5.4 Blood-flow

Reduced ocular blood flow in glaucoma patients is a well-established finding and has been demonstrated using a variety of techniques, including fluorescein

angiography (Schwartz, Rieser et al. 1977), ultrasound Doppler (Nicolela, Drance et al. 1996; Butt, O'Brien et al. 1997) and Heidelberg retinal flowmetry (Embleton, Hosking et al. 2002). Ocular blood flow abnormalities are evident at a number of anatomical sites, including retrobulbar blood vessels (Nicolela, Drance et al. 1996), the optic disc (Schwartz, Rieser et al. 1977) and the choroid (Yin, Vaegan et al. 1997). Such patients may also have an abnormal peripheral circulation (O'Brien and Butt 1999). Vascular dysregulation has been labelled a major contributor to the development of glaucoma by some investigators (Flammer, Orgul et al. 2002). At present, although it is unanimously accepted that altered vascular regulation is a contributory factor in some patients with glaucoma, there appears to be little consensus on the optimal anatomical site for blood flow measurement, the precise measurements which should be made and values which should be regarded as abnormal.

1.5.5 Infectious aetiology

The incidence of *Helicobacter pylori* is higher in the gastrointestinal tracts of glaucoma patients compared to healthy controls, raising a possible role for *H.pylori* in the pathogenesis of glaucoma (Kountouras, Mylopoulos et al. 2001), with increased *H.pylori* antibodies being found in the aqueous samples of glaucoma patients compared to controls (Kountouras, Mylopoulos et al. 2003). However, the importance of *H.pylori* in the pathogenesis of glaucoma still appears to be controversial. Galloway, Warner et al. (2003) did not find a higher seropositivity for *H.pylori* in glaucoma patients.

SECTION B

Psychophysical changes in primary open angle glaucoma

1.6 A brief evolution of perimetry

Table 1.2 summarises the main developments leading to modern visual field testing.

Table 1.2: Developments in perimetry

Year	Development
Approx 400 BC	Hippocrates recorded existence of a hemianopia in a patient
150 BC	Ptolemy attempted to measure extent of visual field
1668	Mariotte discovered the 'blind spot'
1708	Boerhaave discovered scotoma in disease
1801	Thomas Young gave the first description of normal visual field and the blind spot
1825	Purkinje's description of visual field
1856	First use of clinical visual field testing with 'Campimeter' by Von Graefe. Demonstrated loss in peripheral field in glaucoma and related lesion to location of visual pathway lesion.
1867	De Wecker designed perimetric screen for clinical perimetry
1869	Richard Forster developed arc perimeter
1889	Introduction of 'Bjerrum screen' by Jannik Peterson Bjerrum with some information regarding depth of scotoma possible
1893	Groenouw developed concept of 'isoptres' of sensitivity
1933	Louise Sloan introduced concept of static stimuli for perimetry

1909-1949	Roenne, Sinclair, Traquair, Walker, Peter further developed perimetry with descriptions of normal and abnormal visual field
1949	Traquair's description of the 3-dimensional visual field as 'island in a sea of darkness'
1945	Introduction of Goldmann perimeter for kinetic perimetry
1962	Harms and Aulhorn produce first static perimeter
1972	Armaly developed suprathreshold testing
1973	Lynn and Tate develop computerized static perimetry US Patent #3,178,386 issued February 27, 1973 Lynn and Tate, "Automatic visual field examination including fixation monitoring and compensation"
1977-78	Development of computerised perimetry by Frankhauser, Heijl and Krakau

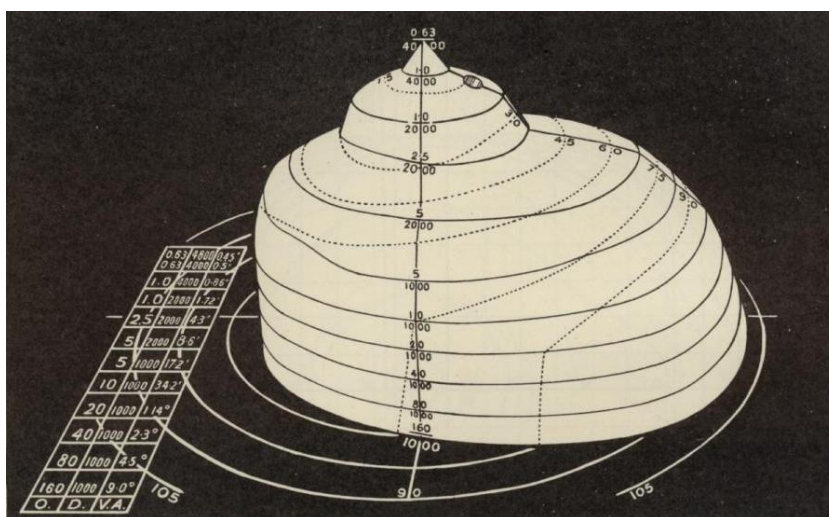
Table compiled from information from: (Whalen and Spaeth 1985) and (Silverstone and Hirsch 1986).

1.7 The normal visual field

Thomas Young, a British physician was the first to give a precise description of the visual field at the turn of the nineteenth century (Whalen and Spaeth 1985). Traquair's (1938) description of the normal visual field as an 'island of vision in a sea

of darkness' is familiar to most perimetrists, **figure 1.1**. The extent, in terms of length and width of the island, describes the size of the field of vision and the height represents the visual sensitivity. Traquair was the first to appreciate the 3-dimensional nature of the visual field. Isoptres are 'contours' on this island (similar to contours on a map) and describe lines of equal sensitivity (or equal height). The normal visual field subtends approximately 60 degrees superiorly and nasally, 70 degrees inferiorly and 100 degrees temporally.

Figure 1.1: 'Hill of vision', Traquair (1938)



The variation of sensitivity with eccentricity can be described by a sensitivity curve. For a fixed size stimulus at a given background luminance, DLS is typically highest at the fovea and falls with eccentricity. This constitutes the 'hill of vision'. Temporally at about 15 degrees eccentricity, the blind spot (which corresponds to the location of the optic nerve head in retina) produces a break in the normal sensitivity curve. In his book, Traquair (1938) gives detailed dimensions of the blind spot or *area coeca*, oval in shape with the long axis vertical, measuring approximately 5.5 by 7.5 degrees in size (Traquair 1938). The blind spot consists of an absolute scotoma surrounded by a relative scotoma (Armaly 1969).

Heijl, Lindgren et al (1987) recorded mean sensitivity for the size III stimulus presented at the conventional 30-2 locations in 95 healthy individuals. Age-corrected sensitivities (for a 50-year old subject) varied from 38 dB at the fovea to 25-28 dB at 30 degrees eccentricity, except in the superior periphery, where sensitivities tended to be lower (22-23 dB).

1.8 The visual field in glaucoma

The following types of visual field defects have been described in the glaucomatous eye:

1. *Diffuse sensitivity loss*

Although media opacity typically causes diffuse loss of sensitivity, a global reduction in sensitivity can be an indicator of glaucomatous functional loss (Drance 1991; Lachenmayr, Drance et al. 1992; Chauhan, LeBlanc et al. 1997). (1960) found that concentric contraction was common in glaucoma.

2. *Nasal step* (LeBlanc and Becker 1971; Werner and Beraskow 1979).

In some patients, this may be the only abnormality. This is a frequent defect in POAG (Lau, Liu et al. 2003).

3. *Arcuate defects*

a. 'Bjerrum' visual field defect (Harrington 1965)

This extends from the blind spot to the horizontal midline, arching above or below fixation.

b. Paracentral scotoma

These are defects usually between 10-20 degrees from fixation and can enlarge to involve the central field (Gramer, Gerlach et al. 1982)

c. Seidel scotoma

This is the term given to an early central arcuate defect which joins the blind spot, resembling an 'inverted comma'. This can progress to a Bjerrum scotoma.

4. *Vertical step*

Although characteristically hemianopic type defects occur in neurological lesions, they may also occur in glaucoma (Gilpin, Stewart et al. 1990)

5. *Visual field constriction*

Concentric constriction of the visual field may occur, especially in the nasal field (de Oliveira Rassi and Shields 1982; Flammer, Eppler et al. 1982).

6. *Blind spot enlargement*

Although this may occur in glaucoma, it is not specific for the disease (Drance 1969). Blaxter argued that such enlargement does not actually occur and represents arcuate scotoma which becomes connected with the blind spot in advanced disease (Blaxter 1950).

7. *Temporal defects*

Temporal sector defects can occur in the advanced stage of glaucomatous disease (Brais and Drance 1972). Conventional perimetry samples the temporal visual field poorly, with only 2 locations tested temporal to the blind spot.

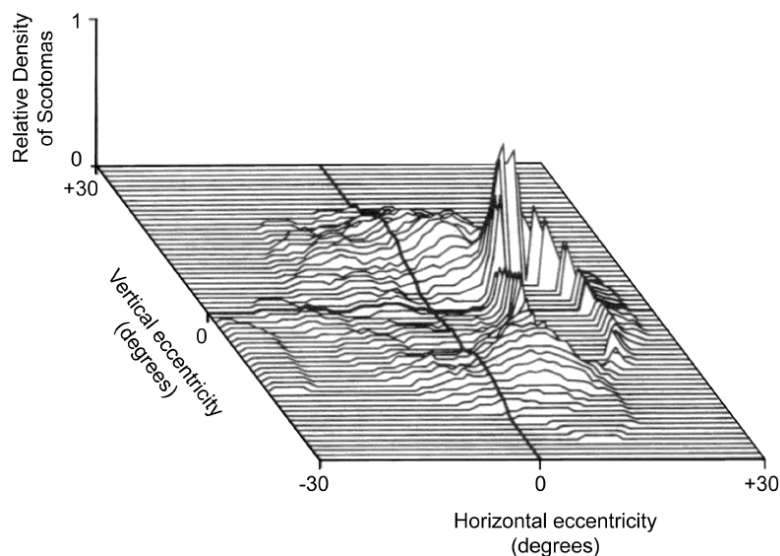
8. Advanced defects

Superior and inferior arcuate defects may merge, leaving just a temporal island of vision in advanced stages and eventually loss of the central visual field in progressive cases.

Hart and Becker (1982) described the spatial distribution of 'early' visual field defects in glaucoma **figure 1.2**, with defects around the physiological blind spot being most frequent.

Figure 1.2 Spatial distribution of visual field defects in glaucoma,

Adapted from: (Hart and Becker 1982)



1.9 Modern clinical perimetry

In the UK, more than 70% of hospital eye departments use SAP as the visual field test of choice (Gordon-Bennett, Ioannidis et al. 2008). Typically 54-72 locations are tested with the Goldmann size III stimulus and DLS recorded at each location.

Modern perimeters use automated methods to present a stimulus throughout the visual space. Most commonly, a constant size stimulus is presented and visual thresholds measured by varying the luminance. The word 'static' describes the motionless stimulus, in contrast to kinetic perimetry, which utilises a moving stimulus. After recording the data, statistical analyses may be applied to measures to compare sensitivities with aged-matched values and emphasize areas of 'focal' loss. The modern static 'white-on-white' perimeters in clinical use today are:

1.91 The Humphrey field analyzer

This consists of a 33 cm radius bowl on which the Goldmann stimuli I-V can be projected, with stimuli ranging from 0.08 to 10,000 asb (Silverstone and Hirsch 1986) with a temporal presentation of 0.2 s. The background luminance is 31.5 asb. The modern Humphrey Field Analyzers allow the use of a variety of test strategies and well as coloured stimuli.

1.92 The Octopus perimeter

The Octopus Perimeter utilises a 55 cm bowl. The earlier version (Octopus 201) permitted presentation of the largest five Goldmann stimuli. The later versions (500 E) allow presentation of the Goldmann size III only. The maximum stimulus luminance is a tenth of the Humphrey (1000 asb), with a much lower background luminance (4 asb).

1.9.3 Goldmann kinetic perimetry

Apart from stimulus size and luminance, kinetic perimetry introduces motion as another variable in the measurement of DLS. For a given stimulus luminance and size, the location at which the visibility of the stimulus changes is variable and dependent on the meridian and eccentricity.

The results of kinetic perimetry are dependent on the expertise of perimetrist and, in particular the speed at which the stimulus is presented. Goldmann suggested using a speed of 5 deg /s, whilst speeds of around 2 deg /s may also be acceptable (Henson 1993).

The Goldmann perimeter consists of a bowl of radius 30 cm. Stimuli are chosen from one of six sizes (Goldmann 0-Goldmann V) and one of 4 intensities (1,2,3,4) presented on a background of luminance 31.5 asb (10 cd/m²). The smallest stimulus is 1/16 mm², with each successive stimulus representing a four-fold increase in stimulus area (Anderson 1992). The stimuli are, in fact, oval in shape (ratio of axes length 1:√2) since the stimuli are projected at an angle of a 45 degrees (Greve 1973). The four intensities represent 31.5, 100, 315 and 1000 asb respectively. An isoptre is labelled by both stimulus size and intensity. Fixation can be directly monitored through a small telescope within the bowl.

For the Goldman perimeter, the maximum luminance is 1000 asb which equates to 316 cd/m² (**table 1.3**). The background luminance is 31.5 cd/m². The stimulus luminances available for the Goldmann perimeter are denoted by the numbers 1-4 and by the letters a-e. An increase from 1 to 2 represents an increase in stimulus intensity by 0.5 log units and an increase from 'a' to 'b' represents an increase of 0.1 log units. Each successive stimulus size represents a four-fold increase in area. The Goldmann size III stimulus, which has been adopted most widely for static clinical

perimetry, is 4 mm² in diameter on the Goldmann perimeter and subtends an angle of 0.43 degrees.

Table 1.3 Luminance values (in Asb) for the Goldmann perimeter,
adapted from (Portney and Hanible 1975)

Notation	a	B	C	d	E
1	12.5	16	20	25	31.5
2	40	50	63	80	100
3	125	160	200	250	315
4	400	500	630	800	1000

1.9.4 The Henson perimeter

Designed as the first computerised multi-location suprathreshold perimeter (Henson 1989; Henson 1989), test locations were optimised to correspond to regions of most frequent glaucomatous defects (Henson, Chauhan et al. 1988). The CFS2000 perimeter had a flat surface positioned 33 cm from the eye. The Henson perimeter allows a facility to test additional locations using a 'suprathreshold' strategy has undergone numerous generations of change. The 'CFS2000' model was essentially designed as a screening test with 3 levels of test ranging from 26 to 132 locations (Henson 1989). The later 'pro' models allows further quantification of defects using a full-threshold or 3 dB staircase with a single reversal. The latest model, the Henson Pro 7000 has a compact portable design ideal for domiciliary use.

Others perimeters such as the Dicon Autoperimeter, Krakau perimeter, Keta, Kowa, Tubinger and Fieldmaster perimeters are rarely used in hospital clinical practice and have not been discussed here.

1.9.5 Other forms of perimetry

High pass resolution perimetry (HRP)

The ability to resolve ring-shaped stimuli of varying size on a monitor with background luminance of 20 cd/m² is tested (Frisen 1987). The measured outcome is the smallest ring size that is discernable at 50 retinal locations within the central 30 degree field. The test is acceptable to patients (Dannheim et al. 1989) and fairly quick to perform (5 minutes per eye). The variability of measurements is not, like SAP, highly dependent on depth of perimetric defect (Chauhan and House 1991) possibly making it more suitable for the identification of progressive visual field loss than SAP (Chauhan, House et al. 1999). Measures from high-pass detection correlate with ganglion cell density (Popovic and Sjostrand 2005).

Frequency doubling technology (FDT)

The 'Frequency Doubling Illusion' refers to a grating of low spatial frequency which appears to 'double' when it undergoes a high temporal frequency (25 Hz) counter-flicker (Kelly 1981). The first generation of FDT tested a maximum of 19 points in the central 20 degrees of visual field (Alward 2000), although later generations have incorporated a larger number of test points. The FDT perimeter is portable, relatively cheap (Delgado, Nguyen et al. 2002) and it takes approximately 90 seconds to perform the test on a normal eye (Alward 2000), making it ideal for

screening. Its apparently high sensitivity in some studies has been attributed to its potential ability to selectively tap the magnocellular pathway. The first version of the FDT used stimuli 10 by 10 degrees in spatial extent and tested locations in the central 20 degrees. The modern FDT Matrix has a number of different tests including the 24-2, 30-2, 10-2 and Macula programmes. The 24-2 programme uses 5 degree targets and with 55 test locations in a similar arrangement to the Humphrey SAP 24-2 pattern.

Short-wavelength automated perimetry (SWAP)

SWAP is undertaken by presenting a blue Goldmann size V target on a yellow background (Sample and Weinreb 1990) and is available on the Humphrey Field Analyzer. Whilst some patients may have evidence of glaucomatous defects on SWAP which are not apparent on SAP, the converse is also true (Hart et al. 1991). A scurry of reports in the 90's implied that this test may detect losses and progression earlier than SAP (Sample and Weinreb 1992; Johnson, Adams et al. 1993; Johnson, Adams et al. 1993), but subsequent studies have demonstrated that SWAP has higher between-subject (Wild, Cubbidge et al. 1998) and higher test-retest variability than SAP (Kwon, Park et al. 1998). Van der Schoot, Reus et al. (2010) found that a number of patients with ocular hypertension who demonstrated conversion to glaucoma on SAP did not have reproducible defects on SAP. Patients with progressive glaucomatous optic neuropathy may have defects on SAP whilst SWAP is normal and vice versa (Sample, Medeiros et al. 2006). Some of the discrepancy may be due to inclusion of different control subjects in the normative

database. Sample et al. (2006) found that the sensitivity of both these tests to identify progressive optic neuropathy was around 50% at 80% specificity.

Motion perimetry

Patients with glaucoma exhibit abnormal motion perception compared with healthy volunteers (Wall and Ketoff 1995). The last decade has witnessed the development of a promising motion test for the detection of glaucoma, the Moorfields Motion Displacement Test (MDT). The original test consisted of a single line undergoing motion on a location just above the blind spot, presented on a BBC microcomputer monitor. Elevated motion thresholds have been demonstrated in regions of visual field defect (Westcott, Fitzke et al. 1998) and have been suggested as a predictor of defects on SAP (Baez, McNaught et al. 1995). The modern test consists of 32-line stimuli which are scaled in length by estimates of ganglion cell density. Multicentre validation of the Moorfields MDT to aid future commercial development is currently underway.

Oculokinetic perimetry

Unlike other forms of perimetry, which requires a subject to fix the eye on a central target, in Oculokinetic perimetry, the subject is asked to look at numbers (usually 1 to 100), stating whether a central target (black spot) is visible whilst looking at each number. This was originally developed in the UK as a community screening test (Damato 1985) and is quick (Greve 1973) and easy to perform but test specificity is an issue (Christoffersen, Fors et al. 1995; Chia, Goldberg et al. 1999; Yamada, Chen et al. 1999). Chia, Goldberg et al. (1999) found that Oculokinetic perimetry had a

specificity of 56% (and sensitivity of 86%) for detecting eyes which had defects on Humphrey Full-Threshold testing, often missing early defects.

1.10 Perimetric strategies for static perimetry

1.10.1 Full Threshold strategy

This is a repetitive bracketing strategy which employs a 'two reversal staircase' to measure estimate threshold (Spahr 1975). A stimulus is presented and, if not seen, a higher (by 4 dB) intensity stimulus is then presented. Once the stimulus is seen (as evidenced by an appropriate response), a 'reversal' of response is said to have occurred and a lower intensity (by 2dB) stimulus presented. The staircase terminates after the second reversal. The HFA records the sensitivity which corresponds to the stimulus intensity that was seen last for a given test location (Allergan Humphrey 1986).

1.10.2 Suprathreshold strategies

In simple terms, suprathreshold strategies determine whether a stimulus has been seen or not seen. A 'suprathreshold strategy with repeats' retests any missed points and changes them to 'seen' if the patient responds on repeat testing. A 'suprathreshold test' with quantification may provide some information regarding the depth of perimetric defect by presenting higher stimulus intensities at missed locations (Henson 1993). Although suprathreshold strategies do not provide the same quantification of DLS as FT strategies, they tend to reduce test time.

1.10.3 Bayesian Perimetric strategies

Bayesian adaptive threshold algorithms were first developed by Watson and Pelli (1983). Examples of Bayesian strategies include the QUEST, ZEST and SITA strategies. Such strategies compare a prior probability density function (PDF) with the patient responses to arrive at an expected distribution of thresholds. Generally, the procedure can terminate in one of 2 ways: after a fixed number of stimulus presentations or when the spread of measured PDF reaches a predetermined value. The Swedish Interactive Threshold Algorithm (SITA) Strategies are more time-efficient than FT (Bengtsson, Olsson et al. 1997) and reduce test time by varying the interval between stimulus presentations depending on the patient's response speed, not using 'catch trials' for the estimation of the false positive response rate and reducing the number of stimulus presentations by prior estimation of threshold by maximum likelihood procedures. Despite reduction in test time compared to FT, the test-retest variability of SITA is comparable to FT (Artes, Iwase et al. 2002). Pointwise DLS estimates using SITA are generally about 1dB higher than FT.

1.11 Test locations for static perimetry

Similar to the Octopus Program 32, the Humphrey '30-2' test grid consists of 76 retinal test locations to test the central 30 degrees of visual field, with locations distributed 6 degrees apart, offset from fixation by 3° vertical and 3° horizontal. The '30-1' grid examines additional locations along the horizontal midline but these do not assist the examiner in deciding whether a defect respects the horizontal meridian. The 24-2 grid consists of a reduced number (n=54) of locations with a similar spatial distribution. There appears to have been little attempt to modify

standard locations for perimetric assessment of glaucoma (Zeyen, Zulauf et al. 1993; Chauhan and Johnson 1994; Sugimoto, Schotzau et al. 1998) and it is likely that a certain number of minimum test locations are needed to maintain the sensitivity of the test (Sugimoto, Schotzau et al. 1998) .

1.12 Problems associated with standard automated perimetry

1.12.1 Variability

SAP measurements are confounded by high-test retest variability, particularly in regions with low sensitivity (Heijl, Lindgren et al. 1989; Piltz and Starita 1990; Artes, Iwase et al. 2002). High variability impedes the ability of the clinician to detect true visual field progression. It is estimated that more than 7 separate visual field tests are needed to detect change (Johnson 2001). In other words, on a practical basis, for a patient attending a hospital eye department for 6-monthly visual field tests, a 3-4 year interval may elapse before visual field progression is identified.

It has been speculated that microsaccadic eye movements may account for some of this variability. A stimulus may fall on an undamaged ganglion cell receptive field on one stimulus presentation but fall on a retinal location served by an affected ganglion cell on a subsequent presentation. This hypothesis would explain the increase in variability with increasing damage. Although Henson et al. (1996) concluded that fixation instability was not a major cause of perimetric variability, 'accurate' fixation was regarded as responses in which a patient's fixation was within one degree, so smaller movements may still be a cause of variability. Interestingly in their study, fixation beyond 30 minutes of arc occurred in almost

40% of the time in the most reliable patient. Wyatt, Dul et al. (2007) demonstrated that the variability of visual field measurements was correlated with the gradient of visual field sensitivity and such small movements could account for variability.

1.12.2 Low diagnostic sensitivity

White-on-white perimetry is traditionally thought to be insensitive to early glaucomatous losses and most clinicians would be aware of the statement 'more than 50% of ganglion cell axons are lost before visual field defects can be detected' derived from (Quigley, Dunkelberger et al. 1989) conclusion, which is one of the most frequent citations in ophthalmology (Ohba, Nakao et al. 2007). In their study, Quigley et al established normal ranges for RGC density at each visual field test location from only 5 eyes. Visual field testing was undertaken some time before histological examination of the enucleated eyes with kinetic perimetry. In a subsequent study by the same group, (Kerrigan-Baumrind, Quigley et al. 2000), the authors' concluded that 'at least 25% to 35% RGC loss is associated with statistical abnormalities in automated visual field testing', their confidence limits for normal RGC was large and their data did not support this conclusion. The standard deviation of RGC around the mean (534,000) was around 113,000 giving a lower 95% confidence limit of 300,000 RGC's i.e. nearly 60% of the mean value (or 40% loss).

Inspection of data from Harwerth's experiments from monkey eyes implied a curvilinear relationship between DLS (in dB) and percentage ganglion cell loss (Harwerth, Carter-Dawson et al. 1999) . Although the authors claimed a minimal change in DLS for ganglion cell losses up to 60%, their data shows a 6 dB loss in

perimetric sensitivity even with minimal ganglion cell loss. The apparent insensitivity of conventional perimetry to identify glaucomatous losses has been attributed to a ganglion cell 'reserve' which can be lost without measurable perimetric loss. This, in conjunction with the claim that alternative forms of perimetry may detect ganglion cell loss earlier in the course of disease has led to the 'reduced redundancy hypothesis' (Johnson 1994).

It is difficult to predict the sensitivity of SAP for identifying functional loss associated with glaucomatous optic neuropathy as most studies have used the results of white-on-white perimetry to classify glaucomatous eyes. A recent study, (Tafreshi, Sample et al. 2009) used disc appearance on stereophotographs to classify eyes as 'healthy controls' or 'glaucoma'. At a fixed specificity of around 95%, Pattern Standard Deviation (PSD) from SAP had a sensitivity of only 30-40% for identifying glaucomatous eyes based on the results of a single test. The sensitivity of FDT was similar.

1.13 How can current perimetric techniques be improved on?

1.13.1 Improve sensitivity to detect glaucomatous loss

Use of alternative stimuli

The histological observation that retinal ganglion cells served by larger diameter fibres may be selectively damaged in glaucoma (Quigley, Dunkelberger et al. 1989; Kerrigan-Baumrind, Quigley et al. 2000) has prompted the development of perimetry to target specific ganglion cell classes. However, subsequent analyses have suggested this could be an artefact of shrinkage in the histological sections (Morgan 2002). The mean dendritic field and cell body of parasol ganglion cells is

greater than for other retinal ganglion cells (Dacey and Petersen 1992). It has been argued that isolating responses from single ganglion cell classes may aid in earlier identification of abnormality in glaucoma. The parasol ganglion cells and midget ganglion cells form part of the magnocellular and parvocellular pathways respectively. The Koniocellular pathway contains diverse ganglion cell types. **Table 1.4** shows the types of stimuli designed to selectively ‘tap’ a subset of ganglion cells.

Table 1.4: Types of perimetry and associated perimetric selective sensitivity

Pathway	Ganglion cell type	Type of perimetry
Magnocellular	Parasol	FDT, motion detection
Parvocellular	Midget	HRP
Koniocellular	Small bistratified	SWAP

Although some studies have found that FDT may aid in identification of glaucomatous loss before SAP (Sample, Bosworth et al. 2000; Medeiros, Sample et al. 2004), 20% of patients with OHT only have FDT defects (Sample, Bosworth et al. 2000). Sample, Medeiros et al. (2006) found that global indices from FDT were abnormal in about 20% of OHT eyes, questioning its suitability for screening. FDT and SWAP may perform no better than SAP for a population of eyes based on ONH appearance (Tafreshi, Sample et al. 2009).

The Gabor patch stimulus is a sinusoidal patch surrounded by a Gaussian envelope (Gabor 1946). Gabor stimuli resemble the spatial response profile of cortical cells and may provoke a response from a smaller subgroup of ‘spatially-tuned’

mechanisms than a white circular stimulus. Harwerth, Carter-Dawson et al. (1999) used a 1 cycle per degree (cpd) Gabor patch stimulus in sine phase and found the sensitivity for this stimulus to be reduced compared to the Goldmann size III stimulus, with a tendency of Gabor patches to show more generalised perimetric loss. Hot, Dul et al. (2008) used a 0.4 degree cpd Gabor patch to test 20 glaucoma patients and 20 age-similar controls and found that contrast sensitivity measurements were more equivalent to rim area than SAP when measures were converted into percentage of mean normal. Contrast sensitivity has noted to improve following brimonidine therapy (Evans, Hosking et al. 2003), suggesting that this may be a sensitive measure of reversible glaucomatous optic nerve dysfunction.

Use of smaller 'white' stimuli than the Goldmann size III

It would seem logical that testing smaller retinal areas would improve the sensitivity to detect damage. Larger stimuli may fall on both normal and damaged retinal ganglion cell receptive fields resulting in near-normal sensitivity. Zalta and Burchfield (1990) tested patients with early glaucoma with both the Goldmann size I and Goldmann size III stimuli. The number of locations with defects of 6 dB or more was greater for the Goldmann size I stimulus, suggesting that this stimulus may be better suited to early detection of functional loss. Similarly, Gramer, Kontic et al. (1981) found that sensitivities were 6-10 dB lower with the Goldmann size I than the Goldmann size III in damaged locations. The main disadvantage of using a small stimulus is that DLS is often not recordable at very damaged locations and high test-retest variability (discussed below) and smaller stimuli are more affected by blur than larger ones (Anderson, McDowell et al. 2001).

1.13.2 Reduce variability

Use of larger stimuli than the Goldmann III

The Goldmann size V stimulus, which is 4 times the diameter or 16 times the area of the Goldmann size III, is associated with more uniform variability characteristics than the Goldmann size III (Wall, Woodward et al. 2009). Gilpin, Stewart et al. (1990) found a similar overall variability for the Goldmann size III compared to the Goldmann size V. The 'total fluctuation' (calculated from between-test and within-test) was similar for the Goldmann size III compared to the Goldmann sizes IV and V stimulus but lower for the Goldmann I and Goldmann II. Larger stimuli are less affected by optical blur than smaller stimulus sizes (Anderson, McDowell et al. 2001). Anderson, McDowell et al. (2001) found that an optical defocus of +1D affected contrast sensitivity for the Goldmann size III stimulus by approximately twice the amount compared to the same defocus for a size V stimulus in the fovea. The effect of blur on thresholds is eccentricity dependent (Weinreb and Perlman 1986).

Alternative stimuli: sinusoidal stimuli

The variability of the Frequency doubling technology stimulus is less dependent on sensitivity than the Goldmann size III stimulus (Chauhan and Johnson 1994; Spry, Johnson et al. 2001; Wall, Woodward et al. 2009). This effect, at least in part, may be a consequence of a larger stimulus. The peripheral stimuli of the FDTII stimulus subtend 10 by 10 degrees (Alward 2000). It has been argued that the improved sensitivity of the FDT may be a result of selectively tapping the magnocellular

pathway, although this hypothesis has been disputed (Swanson, Lee et al. 2010). Similar to the FDT stimulus, Gabor patch variability may exhibit less dependency on depth of perimetric defect than SAP (Pan and Swanson 2006; Hot, Dul et al. 2008).

1.14 Differential light sensitivity

1.14.1 Definition

Differential Light Sensitivity (DLS) describes the ratio of stimulus luminance to background luminance at threshold i.e. when the stimulus is just perceivable.

1.14.2 Units of measurement

The apostilb is a measure of illuminance or the incident flux per unit area and is historically used in visual field testing. One apostilb is equivalent to 0.318 cd/m^2 . It is important to note that dB units relate to the dynamic range of the perimeter and so dB values are not interchangeable between different perimeters.

The dB value of DLS for a given perimeter is given by:

$$\text{dB} = 10[\log(L_{\text{max}}/x)] \quad [1.1]$$

where L_{max} is the maximum stimulus luminance of the perimeter and x is the stimulus luminance in asb.

The decibel is a logarithmic metric of measurement relative to a specified reference level and is equivalent to one tenth of a bell. Specifically, decibels are used to express a ratio rather than an absolute quantity and are therefore dimensionless.

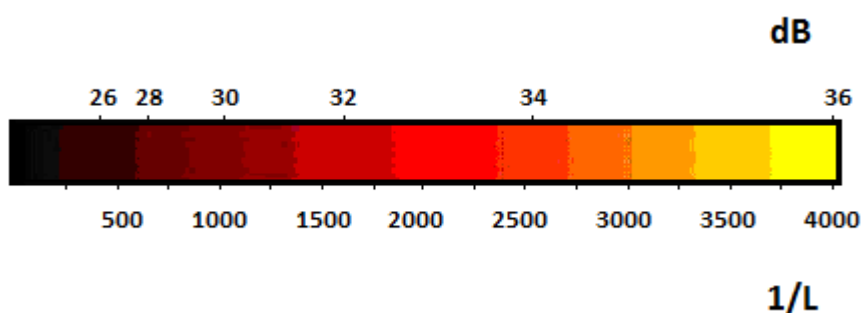
Decibels were first used to measure sound intensity, where they indicated losses of

sound intensity for a given length of telephone cable (Davis and Davis 1997) but now are commonly used to measure power or intensity levels. In perimetry, DLS is conventionally measured in decibel units, where:

$$L^{-1} = 10^{(\text{dB}/10)} \quad [1.2]$$

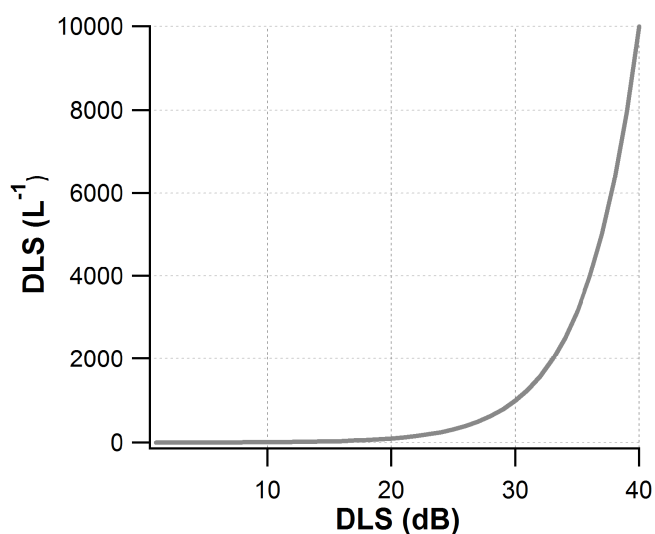
and L^{-1} represent a linear metric of sensitivity.

Figure 1.3: Linear and dB increments on the (linear) same scale



The relationship between dB and linear DLS is non-linear, **figure 1.4**

Figure 1.4: Non-linear relationship between linear, L^{-1} and log (dB) units of DLS



It is unclear why log units have become conventional for recording DLS: log units narrow the inter-individual range of DLS for a given location, thereby facilitating identification of abnormal values. The eye may respond to changes in stimulus intensity in a logarithmic manner. The Weber-Fechner law predicts that perceived change in sensation for a stimulus is related to the logarithmic increments in stimulus intensity and so it would seem appropriate to use logarithmic increments in stimulus luminance to achieve a change in perceived stimulus. Henson points out that the eye operates over a wide range of intensities in the order of 10^7 fold Henson (Henson 1993). Using a linear scale of sensitivity may make changes of sensitivity at the lower end of the scale less discernible.

Differential light sensitivity is conventionally measured in decibels (dB). This is a logarithmic scale, so that an increase of 3 dB represents a halving of light intensity (*figure 1.3*). When dB units are computed in a linearly-scaled metric of DLS, the relationship between these two units of DLS becomes apparent. The dB scale compresses the normal-sensitivity end of the scale and expands the low-sensitivity end. Zero (0) dB corresponds to the brightest stimulus intensity on a given perimeter. Values above this refer to an attenuation of maximum stimulus intensity.

1.15 Effect of background luminance

DLS is dependent on background luminance. For a given location in the central visual field and given individual, DLS is fairly constant between background luminances of between 100 and 1000 asb (31.5 – 315 cd/m²). For lower luminance levels, DLS increases proportionately with background luminance (Drance and

Anderson 1985). Differential light sensitivity also increases with pupil size (Wood, Wild et al. 1988) and after correction of refractive error (Anderson, McDowell et al. 2001).

1.16 Psychophysical factors governing DLS

1.16.1 Spatial summation

Spatial summation indicates the change in differential light threshold that occurs with an increase in stimulus size and has been thought to result from convergence of outputs from the photoreceptor to ganglion cells. Ricco's law states that, at threshold light sensitivity, $LA = C$, where L = luminance of the target; A = stimulus area and C = constant. The 'critical area' is defined as the largest area over which complete summation takes place. For areas larger than this, summation is described by the equation $LA^k = C$, where k = coefficient of summation ($0 \leq k \leq 1$). As the stimulus area increases beyond Ricco's area, the sensitivity increases at a lower rate. Probability summation predicts that, in this case, $k=0.25$ (Robson and Graham 1981; Feliuss et al. 1996). In this situation, threshold is thought to be governed by the detectors with the highest sensitivity. Pan and Swanson (2006) offered an alternative explanation for the shape of the spatial summation curve. A slope of one within Ricco's area and 0.25 for greater stimulus areas can be explained by mediation by cortical receptive fields of different peak spatial frequency.

Clinical importance of spatial summation in glaucoma

Wilensky, Mermelstein et al. (1986) noted that patients with glaucoma who failed to respond to maximum intensity stimuli (0 dB) with a Goldmann size III stimulus had a sensitivity of 5-25 dB higher when tested with a size V stimulus. This phenomenon of increased sensitivity with larger target sizes is most marked in glaucomatous eyes and has been observed by others (Dannheim and Drance 1974; Fellman, Lynn et al. 1989). 'Size Effects' have also been found in other conditions that reduce retinal sensitivity (Wilson 1967; Swanson, Felius et al. 2000). Smaller stimuli may be more likely to sample small areas of ganglion cell damage whereas larger stimuli may overlap both damaged and normal areas. It has been proposed that smaller stimuli may be more sensitive to small shifts in eye position (Felius, Swanson et al. 1996; Pan and Swanson 2006).

If spatial summation (k) in glaucoma is known then the light sensitivity may be representative of neuronal damage at a given location. Garway-Heath et al. (2000) hypothesised that $G^k = C/L$, where G was the number of ganglion cell receptive fields within the stimulus area. A linear relationship was found when L (in 1/Lamberts) was plotted against G^k . However, the assumption was made that spatial summation remains unchanged in the glaucomatous eye (Garway-Heath, Caprioli et al. 2000).

Does spatial summation change in glaucoma?

Dannheim and Drance (1974) examined spatial summation in small dense defects and found it to be variable (compared to areas of normal sensitivity) with small test targets. Fellman et al. (1998) used a 'bomb-cluster' analysis in which they tested the sensitivity of locations with both size V target and 19 size III targets within the same area. They also found that spatial summation becomes more complete in areas of

reduced sensitivity and postulated that glaucoma may affect ganglion cells with smaller receptive field centres preferentially.

Area of summation

Glezer (1965) proposed that Ricco's area corresponds to the size of the receptive field centre of a retinal ganglion cell. In agreement of this finding is the fact that the size of both parasol and midget ganglion cell dendritic area increases with eccentricity (Dacey and Petersen 1992). Clinically determined Ricco's area (Pan and Swanson 2006) exceeds anatomical dendritic field size (Dacey and Petersen 1992). This has led some investigators to speculate that Ricco's area may represent cortical, rather than ganglion cell receptive fields and (Pan and Swanson 2006) showed that observed spatial summation effects can be a result of detection by cortical mechanisms with different peak spatial frequency. Thomas found that the spatial summation occurs over a greater range when the longer dimension of the stimulus is varied than when the shorter dimension is varied, regardless of orientation (Thomas 1978). This axis-specific summation is a property of cortical cells. Also laser burns inducing retinal scotoma in monkey eyes have been noted to cause an increase in size of the projected cortical receptive fields (Gilbert and Wiesel 1992) and this may also explain the finding of larger critical area in glaucoma patients (compared with normal controls). Recently, Redmond and colleagues (Redmond, Garway-Heath et al. 2010) showed that the reduction of visual field sensitivity in glaucoma patients corresponds to an enlargement of the area of complete summation and the Ricco's area in a damaged eye is the same as the Ricco's area at the same visual field sensitivity in a healthy eye.

Effect of age

Danheim and Drance investigated spatial summation of normal individuals in the central 30° with target sizes ranging from 5 to 120 minutes of arc (Danheim and Drance 1971). They divided their study sample into three age groups (under 40 years; 40-49 years and 60 years and over). Although a reduction of retinal sensitivity with age was noted, the characteristics of spatial summation did not appear to change with age. They had 35 subjects in their sample, half of whom were under the age of 50 years (and therefore were not representative of the age of persons who develop open angle glaucoma). Similarly, Latham, Whitaker et al. (1993) found an effect of age. Scheffrin, Bieber (1998) investigated spatial summation for scotopic conditions after correcting for optical factors and changes in macular pigment density for age and found the area of complete summation to enlarge with age.

Effect of eccentricity

Sloan and Brown examined the effect of spatial summation with eccentricity with a Goldmann perimeter using Goldmann stimuli 0-V (Sloan and Brown 1962). Spatial summation was found to increase with distance from the fovea. Other reports are in agreement with this (Wilson 1967; Inui, Mimura et al. 1981). A linear relationship between eccentricity and critical area has been found with fundus-controlled perimetry (Inui, Mimura et al. 1981). Wilson proposed that the effect of a stimulus presented in a damaged area of visual field is similar to one presented at a peripheral location, and showed that spatial summation is more complete in

regions of the visual field where sensitivity is impaired (due to a pre- or post-geniculate lesion) compared with regions of normal sensitivity (Wilson 1967). Although light threshold increases with eccentricity, the shape of the summation curve does not change (Wilson 1970).

Spatial summation for specific ganglion cell classes

Felius, Swanson et al (1996) investigated critical areas for specific ganglion cell classes. They found that the critical area for red-on-white (r-w) was similar to that of white-on-white (w-w). The critical area for blue-on-yellow (b-y) detection was larger. However, they did not ensure chromatic isolation for the r-w condition for small stimuli (i.e. this may have been detected by the luminance pathway). Consequently, the actual critical area for r-w may be different than measured (Pan and Swanson 2006). For the b-y experiments, thresholds could not be determined for more than half the locations. The critical area is near, and often exceeds, the largest stimulus size on the Goldmann perimeter (Goldmann size V) for the b-y condition.

Pre-neural factors affect spatial summation

In routine clinical perimetry, only central refractive correction is usually achieved. Extra-foveal sensitivities are therefore affected by the amount of (uncorrected) peripheral defocus. Pupillary diffraction, refractive aberration and ocular media opacity blur a stimulus and affect spatial summation. Optical defocus, similar to stray light (Redmond, Zlatkova et al. 2010) may result in reduced contrast and a larger effective stimulus area due to a larger point spread function, resulting in

more ganglion cells being stimulated under the stimulus. It has been hypothesised that the change of Ricco's area that occurs with age in the fovea is solely a result of these pre-neural factors (Davila and Geisler 1991). Optical blur affects smaller size stimuli to a greater extent than larger stimuli (Anderson, McDowell et al. 2001). Anderson, McDowell et al. (2001) examined the effect of dioptic blur on detection thresholds of Goldmann size-equivalent I-V stimuli in both the fovea and at 30 degrees eccentricity and found that the effect to be greater for the larger stimuli at both locations. Optical blur affects gratings of lower spatial frequency less than those of higher spatial frequency (Campbell and Green 1965; Westheimer 1966). Levi and Klein (1990) assessed the effect of blur on line detection. The amount of blur was defined as a Gaussian function with standard deviation, σ . Intrinsic blur, B_i was defined as the blur value at which thresholds are degraded in the fovea. When the blur is less than B_i , they found that the line detection threshold obeyed Ricco's law. So far studies of spatial summation have not accounted for peripheral refractive error. Consequently, the amount of summation may have been incorrectly estimated.

1.16.2 Probability summation

Probability summation results from the interaction between homogenous neural mechanisms for the detection of a stimulus. In simplistic terms, a stimulus is detected when any of the underlying neural units is stimulated. For a stimulus larger than Ricco's area, the change of DLS with stimulus size has been traditionally attributed to probability summation, although detection by spatial filters with different peak spatial frequency provides a viable alternative explanation (Pan and Swanson 2006)

1.16.3 Temporal summation

This refers to the relationship between stimulus presentation time and threshold. By Bloch's law, for short stimulus durations (≈ 100 ms), the product of stimulus luminance and presentation time is constant (Henson 1993; Swanson, Pan et al. 2008). In other words, luminance is inversely related to the presentation time. For shorter stimulus presentation times (shorter than the 'critical time'), DLS is independent on presentation time. Temporal summation is further influenced by eccentricity, the level of adaptation and stimulus size.

1.17 The structure-function relationship in glaucoma

1.17.1 Relating structure and function

In order to relate psychophysical measurements in visual space to structural changes of the optic nerve head, the topographic relationship of visual field locations with respect to their circumferential location on the optic nerve head needs to be known. Many investigators have recognised the need for such a structure-function correspondence map. In their paper, Read and Spaeth (1974) produced a simplified retinotopic 'map' of the optic disc on the basis of observed visual field defects corresponding to disc damage in each of the 6 unequal sectors. Subsequently, Wirtscahfter, Becker et al. (1982) used illustrations from the primate nerve fibre layer to relate 12 unequal optic disc sectors to visual field regions. On the basis of planimetric data, Weber and Colleagues identified areas of focal neuroretinal rim thinning and related these to regions of visual field points with

depressed sensitivity (Weber, Dannheim et al. 1990) . The topographical relation of the inferior nerve fibre layer bundle was not studied, thereby producing only a partial correspondence map. The most widely utilised structure-function map was derived by Garway-Heath from 69 black-and-white photographs of the retinal nerve fibre layer in patients with discrete and traceable RNFL defects (Garway-Heath, Poinoosawmy et al. 2000) . The spatial arrangement of RNFL defects were related to visual field test locations by overlaying the 24-2 visual field test grid on individual photographs. The topographic destination of each of the 52 locations (excluding blind spot locations) was documented in terms of degree location (Temporal disc = 0 degrees). It is interesting to note that Garway-Heath's map, although extensively employed by a number of subsequent studies, (Garway-Heath, Holder et al. 2002; Schlottmann, De Cilla et al. 2004; Racette, Medeiros et al. 2007) represents an approximate and 'average' structure-function correspondence. The exact site of entry of nerve bundles into the optic nerve is often dependent on the position of the optic nerve head relative to the fovea and this is one source of structure-function correspondence variability (Garway-Heath, Poinoosawmy et al. 2000) constructed a correspondence map using HRT rim area data from 218 healthy eyes (109 subjects) and 166 glaucomatous eyes. They correlated pointwise visual field sensitivity with rim area (as a proportion of mean normal) in each sector. The structure-function correspondence of the optic disc sectors associated with the highest correlation coefficients were in general agreement with the map of (Garway-Heath, Poinoosawmy et al. 2000) apart from a few locations. The four locations temporal to the blind spot in Gardiner's map localised to quite different sectors of the optic disc. This may, in part be because of the disproportionately

lower number of visual field test locations in the temporal visual field. Ferreras, Pablo et al. (2008) used a similar approach to derive a correspondence map by evaluating the correlations between visual field and RNFL thickness data from OCT. For the purpose of comparing anatomical retinal ganglion cell counts with RNFL thickness in monkey eyes, (Harwerth, Vilupuru et al. 2007) derived a structure-function map for 10 OCT radial scan sectors, although the reasons for not using already established correspondence maps for this purpose are unclear. Recently, Jansonius, Nevalainen (2009) developed a novel mathematical model to describe the course of retinal nerve fibre layer trajectories from nerve fibre layer tracings of 27 fundus images. Points along trajectories were described in polar co-ordinates, using an equation with 2 free parameters. There appears to be considerable variability around the optic nerve head entry point for a given visual field location, typically spanning 20-30 degrees (Jansonius, Nevalainen et al. 2009). This is likely to be a major source of imprecision in the evaluation of structure-function relationships and a likely cause of poor structure-function correlation in some eyes. The next advancement for structure-function analyses may be to develop a maps which are 'individualised' for a given eye.

1.17.2 The nature of the structure-function relationship

Structural and functional measures are affected in glaucoma and both diminish with advancing disease (Read and Spaeth 1974). As neuroretinal rim area and retinal nerve fibre layer thickness are currently the best available substrate for neuronal loss, there has been long-standing interest in the relationship between these parameters and psychophysical measures in glaucoma. Read and Spaeth (1974) demonstrated a decline in visual field sensitivity was associated with progressive

disc cupping. There appeared to be minimal change in sensitivity for an increase in Cup-Disc-Ratio from 0.3 to 0.6, then sensitivity declined at a steeper rate than rim area. Subsequently, a number of researchers have demonstrated a curvilinear relationship between averaged visual field measures in dB with rim area (Airaksinen, Drance et al. 1985; Jonas and Grundler 1997; Bartz-Schmidt, Thumann et al. 1999; Garway-Heath, Viswanathan et al. 1999; Garway-Heath, Holder et al. 2002) and visual field measures in dB with RNFL thickness (Schlottmann, De Cilla et al. 2004; Mai, Reus et al. 2007; Horn, Mardin et al. 2009). This non-linear relationship had initially been attributed to a 'functional reserve' in ganglion cell number, but Garway-Heath demonstrated that that this non-linearity may be a consequence of measuring visual function in logarithmic units (Garway-Heath, Caprioli et al. 2000; Garway-Heath, Holder et al. 2002). Although the relationship between DLS (dB) and RA (mm^2) from HRT was found to curvilinear, a linear fit to the datapoints was inferred when the DLS values were 'unlogged'. Hood, Greenstein et al. (2002) showed that linear visual field measures are linearly related to the amplitude of the multifocal VEP and assumed that the latter represented a linear sum of ganglion cell responses. Harwerth, Carter-Dawson et al. (2004) also found a linear relationship between DLS and ganglion cell density when both were plotted in dB. They found the relationship to be eccentricity-dependent with slopes increasing with eccentricity. For normal eyes, empirical plots of DLS and ganglion cell number (both in log units) can be fitted with a bilinear (or 'hockey stick') function (Swanson, Felius et al. 2004). For DLS values less than 31.5 dB (peripheral locations), the plot has a slope of 1; for DLS greater or equal to 31.5 dB, the slope reduces by four-fold. Interestingly, this bears a striking resemblance to plots of spatial summation, which

predict a slope of around 0.25 (by probability summation) at stimulus areas exceeding Ricco's area. The Hockey-Stick model might also explain Harwerth's (2004) finding of increasing slopes at higher eccentricity.

Recently Hood and Kardon (2007) extrapolated the linear structure-function model to develop a model for relating structure and function, both in their conventional units of measurement (RNFL thickness in linear units, μm and DLS in dB). Their model relates the arithmetic mean of DLS values in superior and inferior arcuate bundles to RNFL thickness from OCT and recognises the need for a non-ganglion cell component ('base') of the RNFL in the structure-function relationship. The need for this comes from the observation that in eyes blind with glaucoma, RNFL thickness does not drop to zero, averaging about 30 μm (Sihota, Sony et al. 2006), although Hood and Kardon (2007) based their estimates of non-neuronal RNFL thickness on patients with unilateral anterior ischaemic optic neuropathy. For locations with extensive field loss (low sensitivity relative to mean normal), RNFL thickness is independent of DLS and equal to the 'base' RNFL thickness. At a relative DLS of 1 or greater (ie > 0 dB), RNFL is again independent of relative sensitivity and equal to mean RNFL thickness in healthy eyes.

Whilst 'measured structure' may not be representative of functioning axonal number (due to non-ganglion cell related tissue in the optic nerve) and may contribute to structure-function discordance, measured functional deficit can exceed functional impairment predicted from structural measurement alone (Harwerth, Vilupuru et al. 2007). Ganglion cell dysfunction (in addition to cell death) which may not result in structural change has been offered as a possible explanation for this finding.

1.17.3 Factors influencing the structure-function relationship

Linear regression analysis has been used most widely for an endpoint in structure-function analysis (Garway-Heath, Holder et al. 2002; Schlottmann, De Cilla et al. 2004; Bowd, Zangwill et al. 2006; Racette, Medeiros et al. 2007). Two discordant measures can correlate (Bland and Altman 1986) and regression analysis provides little information about the level of agreement between measures. The strength of the structure-function regression can be affected by sample size, range of glaucoma severity (Gonzalez-Hernandez, Pablo et al. 2009), units of perimetric measurement (Garway-Heath, Holder et al. 2002; Racette, Medeiros et al. 2007) and measurement variability. Analysing agreement between structural and functional parameters is complicated by different units of measurement. Some have computed each measure as a percentage of mean normal, allowing Bland-Altman plots of agreement to be graphed (Yang and Swanson 2007; Hot, Dul et al. 2008).

SECTION C

Electrophysiological changes in primary open angle glaucoma

1.18 Role of Electrophysiology in Glaucoma

In addition to the detection of functional abnormality in early stages of glaucomatous disease, electrophysiology may be useful for the individual risk assessment of patients at high risk of developing glaucoma (Pfeiffer, Tillmon et al. 1993) and provides an objective measure of optic nerve function in patients who are not able to perform perimetry reliably. Use of the PERG, in combination with

other functional tests, may increase the diagnostic precision for the detection of glaucoma (Martus, Korth et al. 1998).

Established visual field loss has been a prerequisite inclusion criterion for glaucomatous eyes in most studies of electrophysiology (Wanger and Persson 1983; Bach, Hiss et al. 1988; Korth, Horn et al. 1989; Parisi, Manni et al. 2001; Viswanathan, Frishman et al. 2001). As a result, patients with glaucomatous discs but normal visual fields have been excluded, resulting in reports of high glaucoma detection rates.

When comparing tests of visual function, disease presence must be defined by criteria other than the functional tests being investigated and preferably not by a functional criterion. Abnormal structural parameters, in the presence of statistically raised intra-ocular pressure provide a useful reference for the comparison of functional measurements. More recently, investigators are appreciating the need for a non-functional reference in studies of electrophysiology (Stroux, Korth et al. 2003; North, Jones et al. 2010; Tafreshi, Racette et al. 2010).

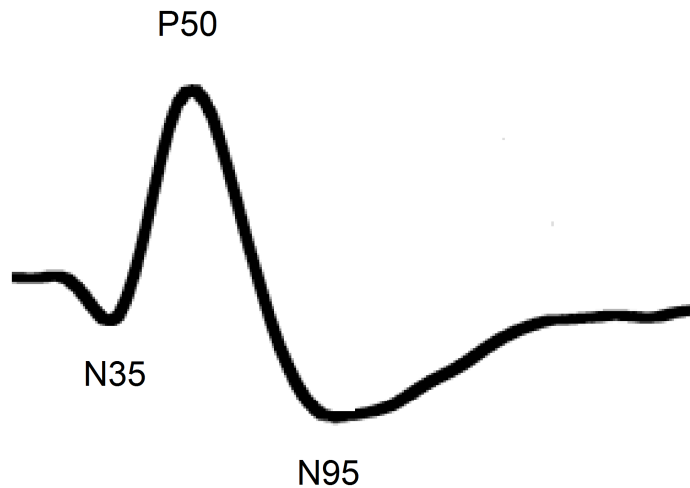
1.19 The Pattern ERG (PERG)

The PERG is a biphasic potential (*figure 1.5*) of much smaller amplitude than the flash ERG and is the response recorded to a (supra-threshold) pattern-reversal stimulus.

1.19.1 The Transient PERG

A transient PERG is a discrete response obtained at low temporal frequencies (<6 reversals/s, 3Hz) and consists of 3 distinct components (Holder 2001), **figure 1.5**:

Figure 1.5: A typical normal PERG trace



1. A small early negative component occurring around 35 ms, N35
2. A prominent positive component, P50
3. A larger late negative component, N95.

It is recommended that the P50 component of the PERG should be measured from the trough of the N35 to the peak of the P50 instead of from the baseline to the peak of the P50 (Bach, Hawlina et al. 2000), as the baseline may be difficult to discern in some cases. Measurement error in locating the baseline is a source of possible variability in recording P50 amplitude.

1.19.2 The Steady-State PERG

As the stimulus reversal rate is increased above 7 reversals per second, the P50 and N95 components fuse into a single waveform, which approximates to a sine wave.

This trace is known as the “steady-state PERG” recording.

1.19.3 The PERG is affected by ganglion cell loss

Although few observers have disputed ganglion cells as generators of the PERG (van den Berg, Riemslag et al. 1986), there is considerable evidence that the PERG is a useful measure of ganglion cell function.

Fiorentini demonstrated the steady-state PERG to be affected in a patient with unilateral optic neuritis and claimed similar findings in eyes with optic atrophy and chronic glaucoma (Fiorentini, Maffei et al. 1981). Maffei & Fiorentini proposed that ganglion cells may be essential to the normal PERG response when they found this response to be abolished in cat (Maffei and Fiorentini 1982) and monkey eyes with unilateral optic nerve transection (Maffei, Fiorentini et al. 1985), while the flash ERG response remained essentially normal. Retrograde histological loss of ganglion cells was verified histologically within the transected nerve. In pigeon eyes, findings have been to the contrary (Blondeau, Lamarche et al. 1987). Sectioning of the optic nerve did not have any lasting effects on PERG amplitude, suggesting that ganglion cells are not involved in the generation of the PERG in this species.

By simultaneous recording of the PERG and graded optic nerve potentials in artificially perfused enucleated cat eyes, Schuurmans and Berninger were able to show that both responses were affected similarly by changing stimulus check size (Schuurmans and Berninger 1984) .

In a human eye whose optic nerve was surgically resected for removal of a glioma, the PERG steady-state response (amplitude and implicit time) was diminished (Harrison, O'Connor et al. 1987).

Intra-retinal PERG recordings in the cat have shown that this response arises from the vicinity of the ganglion cell layer (Sieving and Steinberg 1987).

Bach (Bach 1992) demonstrated the need for intact optic nerve for a normal PERG response. They recorded PERG responses in 8 patients with unilateral optic neuropathy (2 of which had glaucoma). They showed that, in each case, the PERG amplitude in the affected eye was significantly less than the contralateral normal eye.

Holder (1987) reported the effect of optic neuropathy on the individual components of the transient PERG. In 36 patients with optic nerve disease, 29 (81%) exhibited a PERG abnormality which was confined to the N95 component. Two of these later developed a P50 abnormality in addition (Holder 1987). In a larger heterogeneous population of 520 eyes with clinical evidence of optic nerve dysfunction (optic nerve demyelination, optic nerve compression and hereditary optic atrophy), selective loss of the N95 was a common abnormality (Holder 1997).

Viswanathan, Frishman et al. (1999) demonstrated that blockage of ganglion cell spiking activity by administration of intravitreal tetrodotoxin (TTX) reduces the PERG trace in monkey eyes, thus providing further evidence for a ganglion cell origin for this response.

The response to a patterned high-frequency stimulus cannot be explained by changes in stimulus luminance alone (Berninger and Schuurmans 1985; Drasdo, Thompson et al. 1987; Viswanathan, Frishman et al. 2000) and it is highly likely that contrast or pattern, and possibly motion-sensitive pathways are involved in response generation (Dagnelie, de Vries et al. 1986). Cells with centre-surround receptive field properties probably, therefore, produce the response. The spatial-

tuning property is further supported by the fact that steady-state PERG amplitude is dependent on the size of the PERG check (Fiorentini, Maffei et al. 1981; van den Berg, Riemslag et al. 1986; Harrison, O'Connor et al. 1987; Pfeiffer, Birkner-Binder et al. 1991).

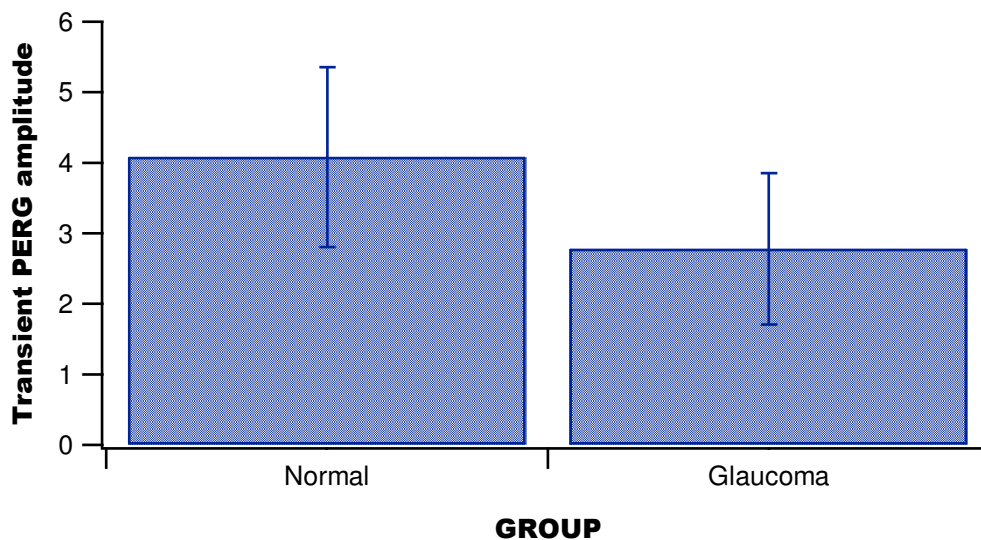
1.19.4 The PERG in glaucoma

Several studies have demonstrated differences in mean amplitudes between glaucomatous and normal eyes (Wanger and Persson 1983; O'Donoghue, Arden et al. 1992; Neoh, Kaye et al. 1994; Ruben, Arden et al. 1995; Martus, Korth et al. 1998; Garway-Heath, Holder et al. 2002), and the PERG can distinguish most eyes with glaucoma from normal eyes. Group differences for both steady-state (Bach, Hiss et al. 1988; Trick, Bickler-Bluth et al. 1988; Bach and Speidel-Fiaux 1989) and transient PERG amplitudes have been documented (Wanger and Persson 1983; Papst, Bopp et al. 1984; Neoh, Kaye et al. 1994; Ruben, Arden et al. 1995).

The amplitude reduction in glaucomatous eyes appears to be more marked in the N95 component. In one study of 16 normal eyes and 24 glaucomatous eyes, the mean P50 was similar in normal and glaucoma groups but the N95 amplitude was significantly different. Ninety-two percent of eyes with glaucoma had an abnormal P50/N95 ratio (Weinstein, Arden et al. 1988). Neoh, Kaye et al (1994) reported good separation between normal and glaucoma PERG amplitudes with the N95 component.

Figure 1.6: Transient PERG (P50-N95) amplitudes for Normal and Glaucoma groups from a published study (Garway-Heath, Holder et al. 2002). High inter-

individual variation of amplitudes across normal subjects and overlapping confidence intervals hinders individual separation of normal and glaucoma amplitudes. Error bars (mean \pm sd) shown.



1.19.5 *Separating normal from glaucoma on the basis of PERG measurements*

Although group PERG amplitudes in normal and glaucomatous subjects are different, the range of values in these two groups overlap (Ruben, Arden et al. 1995; Garway-Heath, Holder et al. 2002). This is, at least in part, due to the high variation of inter-individual PERG amplitudes across normal subjects (Holder 1987; Holopigian, Snow et al. 1988; Pfeiffer and Bach 1992; Trick 1992). For subjects aged between 18 and 48 years, the P50 component varied by a factor of 2 across normal individuals while the N95 varied by a factor of 2.2 (Holder 1987). Although the difference in mean PERG values is highly significant, classification on an individual basis is necessary for the test to be clinically useful.

Several studies have reported a high degree of separation between normal and glaucomatous eyes (O'Donaghue, Arden et al. 1992; Ruben, Arden et al. 1995). As

most of these have incorporated a visual-field-loss definition of glaucoma, the reported sensitivity and specificity rates are usually high.

Wanger and Persson (1983) found a reduction of the transient PERG (P50-N95) amplitude in 11 glaucomatous eyes. Their control group consisted of the fellow “normal” eyes, some of which had ocular hypertension; 2 patients were also on pilocarpine drops and miosis may have been a possible cause of abnormal PERG in these eyes. They employed a small check size (of 0.4 degrees). Poor visual acuity in at least 2 other patients may have contributed to abnormal PERG findings.

Bayer, Maag et al. (2002) reported a sensitivity and specificity of around 92% for the separation of normal eyes from those with glaucomatous field loss using the (transient PERG) P50-N95 amplitude. However, the separation of fellow eyes of these patients with glaucomatous optic neuropathy but normal fields from normal controls was less distinct (sensitivity 81%, specificity 61%). A recent study reported similar sensitivities for the PERG and SAP for a population selected on the basis of optic nerve head appearance (Tafreshi, Racette et al. 2010).

Maximal separation of individual normal and glaucomatous eyes can be achieved by optimising stimulus parameters (discussed below), and normalising amplitudes by age (Bach and Speidel-Fiaux 1989). The latter requires an understanding of PERG changes with age. Several investigators have reported a linear decline of PERG amplitude with age (Korth, Horn et al. 1989; Trick 1992; Garway-Heath, Holder et al. 2002), while in another study amplitudes declined only after about 65 years of age (Pfeiffer and Bach 1992). A PERG protocol optimised for glaucoma screening (PERGLA) has been shown to exhibit abnormality in suspect eyes (Forte, Ambrosio et al. 2010).

1.19.6 Predicting OHT converters

As only a small proportion of OHT patients eventually develop glaucoma: the conversion rate is around 1% per year, (Kitazawa, Horie et al. 1977; Lundberg, Wettrell et al. 1987) there has been some interest in the value of the PERG in predicting which patients are likely to “convert” to glaucoma.

Group mean PERG values have also been noted to be reduced in OHT eyes compared to normal eyes (Wanger and Persson 1983; Trick, Bickler-Bluth et al. 1988), and some have speculated that this may be a predictor of glaucoma. Patients who are deemed to have a high-risk of developing glaucoma (IOP greater than 26 mmHg and cup-to-disc ratio greater than 0.6) have been shown to have lower group PERG amplitudes than those at low risk (O'Donaghue, Arden et al. 1992).

In one observational study, 5 out of 12 patients with Ocular Hypertension (OHT) developed visual field defects (Pfeiffer, Tillmon et al. 1993). All of these had evidence of a pathological PERG before visual field defects became apparent. Furthermore, none of the eyes that had a normal PERG developed visual field changes. Although the period of observation was relatively short (mean 20 months) and the number of patients who developed glaucoma was small, the results of a median follow-up of more than 8 years was later published by the same group in 54 eyes (Bach, Unsoeld et al. 2006). Patients who developed visual field defects were found to have, on average, lower PERG amplitude to a 0.8 degree check size.

1.19.7 The relationship between PERG and structural parameters of glaucomatous damage

Presently, measurement of ganglion cell number in the living human eye is not possible. Histological studies in animals indicate that structural measurements of the optic nerve are related to ganglion cell number (Varma, Quigley et al. 1992; Yucel, Gupta et al. 1998). These surrogate parameters may, therefore, be useful substitutes for use in clinical studies to investigate the relationship between ganglion cell count and electrophysiological measures.

Several studies indicate that a direct relationship exists between structural measures of functioning retinal neural tissue and PERG amplitudes (Ringens, Vijfvinkel-Bruinenga et al. 1986; Salgarello, Colotto et al. 1999; Parisi, Manni et al. 2001; Garway-Heath, Holder et al. 2002).

Ringens, Vijfvinkel-Bruinenga et al. (1986) showed a correlation between PERG amplitude and cup to disc ratio (CDR). However, a high CDR can be a normal finding in eyes with a large optic disc (Garway-Heath, Ruben et al. 1998). PERG amplitudes are linearly related to optic nerve neuroretinal rim area (Korth, Horn et al. 1989; Garway-Heath, Holder et al. 2002). Salgarello, Colotto et al (1999) failed to find a similar relationship. They only included 12 glaucoma patients and their study may have lacked power to find a significant correlation between NRR area and PERG amplitude. However, they found that the PERG amplitude correlated with 'cup shape measure'. This is a vague parameter, which provides a "measure for the overall three-dimensional shape of the optic disc cupping", supposedly giving a numerical summary of the complex shape of the cup (Heidelberg-Engineering 2001) and it is not known how this parameter relates to ganglion cell number.

Parisi, Manni et al. (2001) investigated the relationship between average peripapillary RNFL thickness (measured by Ocular Coherence Tomography, OCT)

with PERG amplitudes in 30 glaucoma patients and 14 aged-matched controls. They found RNFL thickness correlated positively with PERG amplitude ($r=0.69$) and negatively with P50 implicit time ($r=-0.85$). The same group have reported a similar correlation in ocular hypertensive eyes (Parisi, Manni et al. 1999), and eyes with optic neuritis (Parisi 2003).

1.19.8 The relationship between PERG and visual field measurements in glaucoma

Several studies have reported an agreement of PERG amplitude with visual field indices in glaucoma. Neoh, Kaye et al. (1994) demonstrated significant correlations between PERG amplitudes and Pattern Standard Deviation (an index representing the degree of focal sensitivity loss) and proposed the use of PERG as an adjunct test when visual field findings are unreliable or equivocal.

As glaucomatous loss tends to be asymmetrical across the horizontal midline, Graham, Wong et al. (1994) suggested that an assessment of PERG hemifield ratio (upper hemifield PERG amplitude / lower hemifield PERG ratio), may be a sensitive indicator of glaucomatous damage. They selected 8 glaucoma patients (Mean Deviation range: -0.58 to -11.57 dB) with visual field loss in one hemisphere only. Although visual field defects were associated with PERG reductions in the corresponding hemisphere in 7 cases, one glaucoma patient had a PERG hemifield ratio within the normal range.

A study which compared psychophysical and electrodiagnostic tests for the detection of glaucoma reported the former to be more sensitive in early stages of disease (Stroux, Korth et al. 2003). Stroux, Korth et al et al. (2003) did not use visual

field loss as inclusion criteria for glaucoma patients, but based their definition on small neuro-retinal rim area in relation to the disc size. They found SAP to be more sensitive (at 80% specificity) than the PERG over the range of glaucoma severity (measured by loss of neuroretinal rim area) that they studied.

The relationship between DLS (in dB) and ganglion cell number is non-linear (Garway-Heath, Poinoosawmy et al. 2000; Harwerth, Crawford et al. 2002). If PERG amplitude is a direct measure of the number of functioning ganglion cells, then the relationship between DLS (in dB) and PERG amplitude is also expected to be non-linear. Garway-Heath, Holder et al. (2002) confirmed a curvilinear relationship between DLS (in dB) and PERG amplitude, but found a linear relationship when DLS was computed in 1/Lambert (L^{-1}) units. The L^{-1} unit represents a linearly-scaled measure of DLS. The curvilinear relationship between DLS (in dB) and PERG amplitudes may, therefore, simply reflect the logarithmic nature of the dB scale.

A higher correlation may exist between PERG amplitudes and visual field sensitivity than with PERG amplitudes and structural measures of the optic nerve (Garway-Heath, Holder et al. 2002). This may be expected, as both the PERG and perimetry measure aspects of visual function. Also, unlike structural measures, tests may indicate the level of ganglion cell dysfunction, in addition to cell death. Following artificial IOP elevation in normal eyes, there is a reduction in PERG amplitude (Colotto, Falsini et al. 1996), possibly secondary to ganglion cell dysfunction. A significant improvement of PERG amplitudes can occur after adequate control of IOP in ocular-hypertensive eyes (Ventura, Porciatti et al. 2005). Visual field changes may regress following adequate control of IOP (Katz, Spaeth et al. 1989), implying that reversible field loss may result from dysfunctional ganglion cells as well.

1.19.9 Which PERG stimulus parameters are optimal for glaucoma detection?

A specificity of 96% and sensitivity of 91% has been reported in one study (Bach and Speidel-Fiaux 1989) for distinguishing normal from glaucomatous eyes. It may be the choice of particular stimulus parameters that gave rise to this distinction. Parameters that potentially affect the ability of the PERG to detect functional loss in glaucoma follow.

Reversal rate

The ability to perceive flickering stimuli is reduced in glaucoma (Tyler 1981). This is consistent with the hypothesis that large diameter axons of the magnocellular pathway are preferentially lost in this condition (Quigley, Sanchez et al. 1987). Some investigators have argued that the PERG stimulates motion as well as contrast mechanisms (Dagnelie, de Vries et al. 1986) and this may provide a theoretical explanation for the greater involvement of the steady state (than the transient) PERG in early glaucoma (Bach 2001).

There are some advantages of recording a steady-state response instead of a transient PERG for the identification of glaucoma: more precise measurements may be obtained (Otto and Bach 1997) and the separation between glaucoma patients and normal controls is greater (Bach and Speidel-Fiaux 1989; Bach 2001).

However, recording of the steady-state PERG precludes assessment of the individual PERG components. Measurement of the N95 constituent may be invaluable as this has been shown to have a high degree of sensitivity in glaucoma (Weinstein, Arden et al. 1988). Data inspection from one study suggests that the

correlation of PERG amplitudes with optic disc neuro-retinal rim area may be higher for N95 amplitude compared to steady-state amplitude (Garway-Heath, Holder et al. 2002), although a statistical comparison of the two regression coefficients was not performed.

Check size

A check size of around 0.8° is conventionally used for PERG recording (Bach, Hawlina et al. 2000). PERG amplitudes (to small size check stimuli) are reduced more markedly in animal eyes with optic nerve transection (Harrison, O'Connor et al. 1987). In optic atrophy, PERG amplitudes to both small (0.8°) and large (15°) check sizes are reduced (Pfeiffer, Birkner-Binder et al. 1991).

However, in “early” stages of glaucoma steady-state amplitudes to small check sizes are affected to a greater extent (Bach and Speidel-Fiaux 1989; Bach 2001). It seems sensible, therefore, to compute the ratio of PERG amplitude to a small check size to PERG amplitude to a large check size (Bach 2001; Bach, Unsoeld et al. 2006). A study of check-size specific changes in monkey eyes with experimentally-induced unilateral glaucoma found that maximal discrimination of eyes with glaucoma from fellow normal eyes could be achieved using a small check size (Johnson, Drum et al. 1989). Similar findings have been demonstrated in human glaucoma. In one study, maximal separation of PERG amplitude from glaucomatous and normal eyes occurred with a check size of 0.8 degrees (Bach, Hiss et al. 1988). The findings of other observers have agreed with this. Korth et al. 1989 found that with a check size of 0.15 degree compared to 2.5 degrees, there was less overlap between PERG amplitudes of normal controls and glaucoma patients. Another study reported maximal sensitivity for detecting ocular hypertensive eyes with a check size of 1

degree (Trick, Bickler-Bluth et al. 1988). For acceptable recordings of a PERG with small check sizes, it is important that the visual acuity is normal and the eye is clear of media opacity. Either of these can result in artificially attenuated PERG amplitude (Leipert and Gottlob 1987).

The effect of defocus on the PERG recording is similar to early glaucoma, causing a selective reduction of amplitudes for small check sizes (Bach and Mathieu 2004). Uncorrected defocus can thus result in false-positive identification of glaucoma. The results of the PERG with a check size of 0.8 degrees are only considered valid when the visual acuity is at least 0.8 LogMar (equivalent to 6/38 Snellen), (Bach 2001).

Field size

The standard PERG stimulus suggested by the International Society for Clinical Electrophysiology in Vision (ISCEV) is 10 by 16 degrees (i.e. 5 by 8 degrees from the central fixation point), although "...for some applications, such as glaucoma assessment, a larger extent such as 30° may be more appropriate" (Bach, Hawlina et al. 2000). Typically, initial glaucomatous field defects often appear peripherally, outside 15° from fixation (Heijl and Lundqvist 1984). It may, therefore, seem suitable to use a PERG field of similar spatial extent. Although, the PERG stimulus typically only extends less than 20 degrees horizontally, the PERG often unveils evidence of ganglion cell impairment before field defects are apparent within the same retinal area. In 18 eyes with peripheral glaucomatous field defects and normal central (over 26 x 34 degrees) visual fields, 13 eyes had PERG abnormalities using a PERG field of the same size (Bach, Sulimma et al. 1997). The 'Freiburg paradigm'

employs a large field size (around 26 x 34 degrees) for evaluation of glaucoma (Bach 2001; Bach, Unsoeld et al. 2006).

1.19.10 Factors affecting precision of the PERG recording

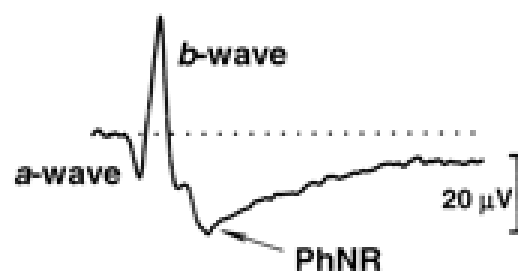
Low test-retest variability is necessary both for longitudinal monitoring of OHT patients for change and comparison of PERG amplitudes between normal subjects and glaucoma patients. It is necessary to distinguish between inter-sessional and intra-sessional variability, as replacement of electrodes represents a source of significant variability. Other potential sources of variability include physiological variability, pupil size, adaptive state of the eye, variability in stimulus parameters and variability of amplitude measurement. Systematic care should be exercised with placement of electrodes and recording should be performed in controlled ambient luminance conditions with frequent calibration of the stimulus display and recording system. After controlling for these factors, the mean inter-sessional coefficient of variability for PERG amplitude is around 10% (Otto and Bach 1997)

1.20 The Photopic Negative Response (PhNR) of the Flash ERG

1.20.1 The flash ERG

The full-field ERG represents the summed activity to the distal retina in response to a (suprathreshold) light flash. The ERG is classified according to its component waves: the main components are a negative 'a' wave and positive 'b' wave. The (negative) a wave originates from photoreceptors and may receive a contribution

Figure 1.8: Showing a normal human Photopic Negative Response, which follows the 'b' wave of the flash ERG, as illustrated by Viswanathan, Frishman et al. (2001) for a 16-year-old healthy subject



Viswanathan, Frishman et al. (1999) first described this component in eyes of macaques and noted that it was reduced in eyes with experimental glaucoma compared with contralateral normal control eyes. Furthermore, the PhNR was removed by the action of TTX, a drug which inhibits the spiking activity of retinal neurons (ganglion cells are the major elements that exhibit spiking activity), (Viswanathan, Frishman et al. 1999). It has also been demonstrated that the changes that occur to both the PhNR and the PERG are a consequence of reduced spiking activity of ganglion cells, (Viswanathan, Frishman et al. 1999). The PhNR, unlike the 'a' and 'b' waves of the flash ERG, can discriminate between normal and glaucomatous eyes in most cases (Viswanathan, Frishman et al. 2001), although this discrimination is somewhat hampered by high inter-individual variation of PhNR amplitudes across normal subjects. Amplitudes across normal human subjects may vary up to nearly 3-fold (Viswanathan, Frishman et al. 2001).

In patients with optic nerve atrophy (secondary to compression, trauma or inflammation), Gotoh, Machida et al. (2004) were able to demonstrate a reduction in PhNR in all of 10 eyes compared to the normal fellow eye. A progressive reduction in PhNR amplitude corresponded to thinning of the retinal nerve fibre layer and the reduction in PhNR seemed to precede the change in nerve fibre layer thickness.

1.20.3 Optimal conditions for PhNR recording

The specific test conditions needed to adequately isolate the PhNR may, at least in part, explain why changes in this response have only recently been described in glaucoma. A component of the flash ERG described by Spileers and co-workers which they termed the *photopic threshold response* (Spileers, Falcao-Reis et al. 1993), bears some resemblance to the PhNR described by Viswanathan, Frishman et al. (1999). The photopic threshold response (PTR) was evoked by a brief (0.1 to 1 ms) red flash in a light-adapted eye. It occurred 65-70 ms after the flash compared with the PhNR which has a mean latency of 72 ms in normal human eyes (Viswanathan, Frishman et al. 2001). Spileers, Falcao-Reis et al. (1993) speculated that this response, like the negative scotopic threshold response in dark-adapted eyes (which has similar latency) may originate from the inner retina.

In macaque eyes, Viswanathan, Frishman et al. (1999) recorded the PhNR by using red (630 nm wavelength) ganzfield flash (of duration ≤ 5 ms and > 200 ms) on a blue (450 nm) rod-saturating background.

Use of a brief, rather than prolonged ganzfield flash, may increase the sensitivity of the PhNR to detect glaucoma (area under ROC curve 0.98 and 0.94 for brief and prolonged flash respectively for macaque eyes, Viswanathan, Frishman et al. 1999).

The response to a brief flash ($\leq 5\text{ms}$) was maximal at low flash intensities (~ 0.7 log photopic trolands) but maximal difference between the glaucomatous eye and fellow control eye occurred at a higher (1.9 log photopic trolands) intensity.

It is difficult to compare the PhNR amplitude across studies because of varying stimulus conditions and reference points for measurement of this component (**table 1.5**).

Colotto, Falsini et al. (2000) used a white flash to elicit a photopic negative response. Their reported amplitudes were much smaller than those reported by Viswanathan, Frishman et al. (2001) in normal human eyes, with mean amplitude of only 1.92 μV . Cursiefen, Korth et al. (2001) used two separate conditions for recording the PhNR: for the first condition, they used a white flash on a white background and for the second condition, they used conditions similar to Viswanathan, Frishman et al. (1999). Mean amplitudes and latencies in both normal controls and glaucoma patients was higher for the white-on-white condition. However, the blue background used by them (2.5 log scot Td, compared to 3.7 log scot Td used by Viswanathan et al. 2001) may not have been sufficient to completely eliminate rod activity. The mean latencies of their photopic negative component for a red-on-blue flash are much different to that reported by Viswanathan, Frishman et al. (2001).

Table 1.5: Parameters used by various studies to record the PhNR

Study	flash	Background	Duration	Mean normal	Background	Latency	Numbers
-------	-------	------------	----------	-------------	------------	---------	---------

			of flash	PhNR amplitude (μV)	luminance		
Viswanathan et al. (1999)	Red (630 nm), varying intensity	Blue (450nm),	(i) $\leq 5\text{ms}$ and (ii) $< 200\text{ ms}$	$\sim 20\mu\text{V}$ + for brief and $\sim 38\mu\text{V}$ * for longer flash	3.7 log scot td	PhNR about 110 ms after flash	14 monkey eyes
Colotto et al. (2000)	White	White	200 ms	> 1.92	78 cd/m^2	“On” compone nt at 85- 90 ms.	11 patients with POAG and 8 patients with OHT
Viswanathan et al. (2001)	Red (630 nm) Optimal at flash intensity of 1.7 log photopic trolands.	Blue (450 nm)	(i) $< 6\text{ms}$ and (ii) 200 ms	~ 20	3.7 log scot td	$\sim 72\text{ ms}$	18 glaucoma patients & 62 normals
Cursiefen et al. (2001)	i. White ii Orange	i. white ii. blue		(i) ≥ 41.4 (ii) ≥ 31.3	i. 1.38 log scot td ii 2.5 log scot td	i. 140 ms ii. 114 ms	9 control eyes and 18 glaucomato us eyes
Fortune et al. (2003)	Red, varying intensity	Blue	1 ms	~ 100 *	3.16 cd/m^2 ($\sim 3.3\text{ log scot}$ td)	$\sim 75\text{ ms}$	23 normal monkey eyes 10 patients
Gotoh et al. (2004)	White	White (3.0 and 2.0 log cd/m^2)	3ms and 33.3 ms	~ 43 +	40 cd/m^2		with optic neuritis and 10

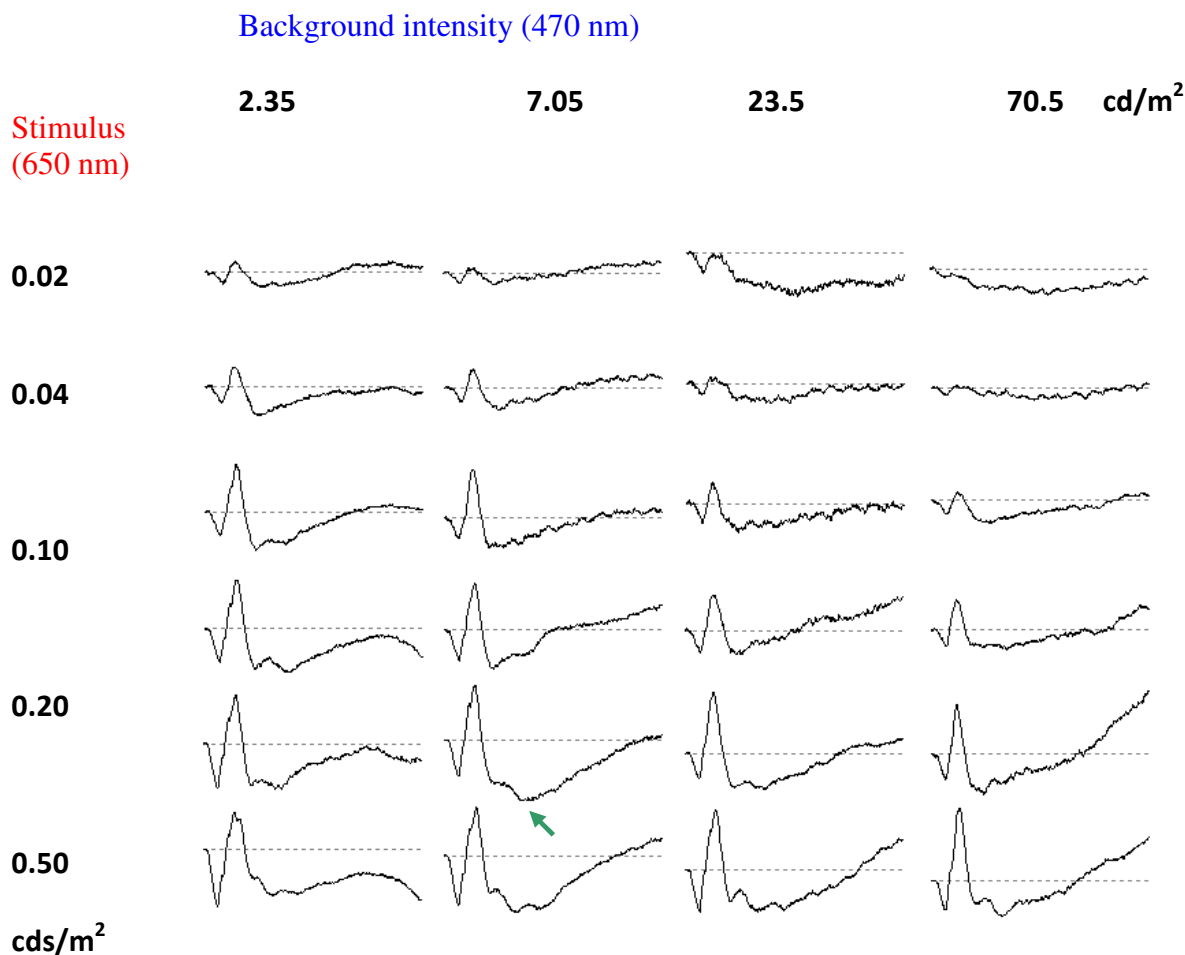
							aged- matched controls
Machida et al. 2008	Red (644), 1600 cd/m ²	Blue (470 nm)	3 ms	~30 μ V +	40 cd/m ²	~70 ms	53 patients (99 eyes), 28 controls (30 eyes)
Sustar et al. 2009	Red (635 nm) White	Blue (470nm)	4 ms	25 μ V 20 μ V	10 ph cd/m ² 130 sc cd/m ²		28 patients (28 eyes), 20 controls (40 eyes)
Drasdo et al. 2010	Red (650nm), 50 cd/m ²	Blue (450 nm),)	5ms	16 μ V	2.7 cd/m ² (>2000 sc trolands		30 POAG, 23 OHT, 28 controls

* Measured PhNR from trough of PhNR to peak of b wave; + Measured PhNR from baseline to trough of PhNR

Sustar, Cvenkel et al. (2009) used a variety of conditions to elicit the PhNR, including a monochromatic white stimulus and a red stimulus, both on a blue background. The amplitude reduction in glaucoma patients, relative to the amplitude in normals, was 68% for the red-flash ERG compared to 38% for the white flash ERG. Further ROC analysis suggested that the former condition had greater sensitivity for identifying glaucoma.

Figure 1.9 shows some PhNR recordings made in our research laboratory for a range of blue background and stimulus intensities.

Figure 1.9: Normal PhNR recordings from our department from a clinically normal right eye for a variety of stimulus and background conditions. The arrow indicates the PhNR for a 0.20 cds/m² flash and 7.05 cd/m² background



1.20.4 PhNR in Glaucoma

Measurement of the PhNR in glaucomatous optic neuropathy may aid in glaucoma diagnosis and has some potential technical advantages over the PERG: the patient does not need to be dark-adapted or fully refractively corrected and the recording takes less time to perform. Animal studies suggest that the reproducibility of the PhNR is high (Viswanathan, Frishman et al. 1999; Fortune, Bui et al. 2004). In glaucomatous eyes, the PhNR can be abnormal even when visual field losses are mild (Viswanathan, Frishman et al. 1999). Viswanathan, Frishman et al. (1999)

proposed several reasons for this: the PhNR may also reflect ganglion cell dysfunction due to raised IOP as well as ganglion cell death; the flash ERG tests a much wider retinal area than conventional perimetry which only examines the central visual field; the PhNR may be sensitive to functional abnormalities of other cells (astrocytes or Muller cells) which are not tapped in perimetry. However, the lack of agreement of PhNR amplitudes with visual field losses may be due to the relative insensitivity of white-on-white perimetry to detect early loss of ganglion cells and this hypothesis needs further investigation. If visual field measurements in linear units are an indicator of ganglion cell damage (Swanson, Felius et al. 2004), a high level of concordance between DLS in these units with PhNR (and PERG) amplitudes is expected.

Cursiefen, Korth et al. (2001) were unable to find a significant difference between PhNR amplitudes of normal and glaucoma patients for both sets of stimulus conditions which they studied (white flash on white background and orange flash on blue background) They included only 9 normal controls in their study.

PhNR amplitudes have been found to correlate with both visual field and structural indices of glaucomatous damage (Colotto, Falsini et al. 2000; Viswanathan, Frishman et al. 2001; Machida, Raz-Prag et al. 2008).

Recently, (North, Jones et al. 2010) concluded that the PERG P50-N95 is more sensitive to identification of GON (from stereo disc photography) than the PhNR. However, estimates of sensitivity at fixed high specificities or a statistical comparison of ROC areas for these two electrophysiological tests was not present in their paper.

1.20.5 The S-Cone PhNR

The finding that the short wave-length pathways are frequently impaired in the early stages of POAG (Greenstein, Hood et al. 1989) has prompted investigation of the S-Cone PhNR. This can be obtained using a 'silent substitution' method (Sawusch, Pokorny et al. 1987). However, its practical measurement is challenging: the wave is of small amplitude and has a low signal to noise ratio. The S-Cones constitute less than 10% of the cones (Marc and Sperling 1977).

Drasdo, Aldebasi et al. (2001) reported a high sensitivity and specificity of the S-Cone PhNR: the largest ROC area was obtained with the S-cone PhNR, followed by the PERG and then the L&M-cone PhNR. However, the number of subjects (18 glaucoma patients and 19 normal controls) was not sufficient to determine whether or not the differences between techniques were statistically significant. Although a follow-on study from the same group included 30 patients and 23 healthy controls, sensitivity values were not reported (North, Jones et al. 2010).

CHAPTER 2

Development and evaluation of a linear perimetric staircase strategy for the assessment of glaucoma

2.1 Aim

The purpose of the present study was to evaluate the sensitivity-dependence of accuracy, precision and efficiency of traditional logarithmic staircases when the results are expressed as linear perimetric sensitivity, and to develop strategies for which bias and precision are less dependent on sensitivity. Monte Carlo simulations of perimetric strategies were used to assess accuracy, precision and efficiency for both conventional logarithmic staircases and alternative linear staircases. The simulations were used to identify a linear strategy similar in overall efficiency to conventional logarithmic staircases. The predictions from the simulations were then evaluated by using both linear and logarithmic algorithms to measure perimetric sensitivity and variability in a group of patients with glaucoma and an age-similar control group.

2.2 The rationale for a linear-increment perimetric strategy

Standard automated perimetry (SAP) plays a central role in the assessment of visual function of patients with glaucoma, as do structural assessments of the optic nerve and the retinal nerve fibre layer (Weinreb and Khaw 2004). Converging empirical and theoretical analyses support the hypothesis that linear perimetric sensitivity correlates better with ganglion cell number than logarithmic sensitivity (Garway-Heath, Holder et al. 2002; Hood, Greenstein et al. 2002; Reus and Lemij 2004; Swanson, Feliuss et al. 2004). Evaluation of the hypothesis of linearity is confounded by the fact that conventional perimetric algorithms measure sensitivity in logarithmic steps, with the result that in linear units there are relatively few steps at high sensitivities and many steps near the lower limits of the testing apparatus (Harwerth, Carter-Dawson et al. 2005).

Logarithmic units (such as decibels) relate to the maximum stimulus luminance available for a given perimeter and represent certain attenuation from this maximum, so that 1 dB on a given instrument is not equivalent to 1 dB on another (under the same test conditions and background luminance) unless they have same dynamic range. For instance, the maximum stimulus on the Humphrey Field Analyzer is 10,000 apostilbs (asb), whilst that on the Goldmann perimeter is 1000 asb so that 1 dB represents a stimulus of 8000 asb on the Humphrey Field Analyzer but 800 asb on the Goldmann perimeter.

The use of logarithmic algorithms for measuring sensitivity with conventional perimetry is a potential source of bias and variability when sensitivity is converted to linear units for comparison with structural and electrophysiological

measurements. Conventional perimetric algorithms employ luminance increments at multiple locations in the visual field and report differential light sensitivity (DLS) in decibel (dB) units, where $10 \text{ dB} = 1 \text{ log unit of attenuation}$. Such algorithms typically use 4 – 7 trials per location in visual space and return about 20 possible sensitivities in 0.2 log unit steps. In linear units of sensitivity, the upper half of the range of possible sensitivities is therefore represented by only a few values, with most of the sensitivities compressed into the bottom 10% of the range. This makes it likely that, when sensitivity is scaled in linear units, the accuracy and precision of conventional perimetric algorithms will be lower in regions of high sensitivity than in regions of low sensitivity, and that test-time will show the opposite tendency. Sensitivity-dependence for accuracy, precision and efficiency are potentially serious complicating factors for comparisons of perimetric and structural measures of glaucomatous damage.

2.3 Monte Carlo simulations

Computer simulations have been extensively used to predict properties of perimetric strategies (Johnson, Chauhan et al. 1992; Chauhan and Johnson 1994; Spry, Bates et al. 2000; Turpin, McKendrick et al. 2003). Analysis of simulations has certain advantages over the use of data from human subjects for this purpose: computers are not subject to the effects of fatigue or emotion, a large number of permutations can be modelled in a short amount of time and bias of sensitivity measurement can be computed since the ‘true’ sensitivity is known. Monte Carlo simulations, which involve generation of random numbers, are widely used to analyze situations where a large number of outcomes are possible, such as nuclear

science, traffic flow systems and cancer therapy, as well as perimetry (Maloney 1990; Glass, Schaumberger et al. 1995; Anderson 2003).

2.4 Methods

2.4.1 Linear units

DLS values were expressed as linear perimetric sensitivity, using units of L^{-1} (1/Lambert), where 1.0 Lambert is the maximum stimulus luminance available on the Humphrey Field Analyzer. We used equation [1.2]

$$L^{-1} = 10^{(dB/10)}$$

where **dB** represents sensitivity in conventional perimetric units (number of 0.1 log unit steps from the maximum stimulus) and L^{-1} represents sensitivity in linear units. The high end of the normal range is about 34 dB (Heijl, Lindgren et al. 1987), which in linear sensitivity is 2512 L^{-1} , so we simulated responses for a sensitivity range of 0 to 2500 L^{-1} . A sensitivity of 1.0 L^{-1} corresponded to a threshold equal to the maximum stimulus luminance and sensitivities lower than this was scored as '0'.

2.4.2 Description of Monte Carlo computer simulation

For each perimetric strategy evaluated, Monte Carlo methods were used to simulate perimetric observers performing large numbers of staircases, for both normal-seeing and damaged regions of the visual field, using summary statistics to estimate accuracy, precision and efficiency. For a given stimulus presentation, the simulation yielded a response of either 'seen', or 'not seen'. When the response was 'seen', the staircase proceeded to a stimulus of lower luminance, and when the response was 'not seen' the staircase proceeded to a stimulus of higher luminance.

A *reversal* occurred when the change in stimulus luminance yielded a change in response from 'seen' to 'not seen' or vice versa. Until the first reversal, the *step size* in changing from one luminance to another was constant in either logarithmic units (conventional staircase) or in units of linear sensitivity (new staircases). After a reversal, the staircase either terminated (if the criterion number of reversals was met) or else the step size was reduced. When a staircase terminated, the simulated output sensitivity was set to the reciprocal of the last stimulus luminance with a response of 'seen'. If a response of 'seen' was not given even for the maximum stimulus, the simulated output sensitivity was set to zero.

For a given stimulus presentation, the response was generated by comparing a random number from the uniform distribution [0,1] with the *probability of responding function*, $R(x)$, where x is the luminance of the stimulus in Lamberts (since one Lambert is the maximum stimulus, values of x never exceeded 1.0). When the random number was greater than $R(x)$, the response was 'seen', otherwise the response was 'not seen'. The function $R(x)$ was defined by four parameters: threshold, α (the luminance, in Lamberts, that is seen 50% of the time); slope of Weibull function, β (determining intrinsic variability), **figure 2.1**; false negative rate, **FN** (the fraction of trials on which the stimulus was seen but not responded to); false positive rate, **FP** (the fraction of trials on which the stimulus was not seen yet a response was generated). The probability of seeing the stimulus, $P(x)$, was defined as

$$P(x) = 1 - 2^{-(x/\alpha)^\beta}, \quad [2.1]$$

and the probability of responding, $R(x)$ was defined as

$$R(x) = (1-FN)P(x) + FP(1-P(x)) = FP + (1-FP-FN)P(x) \quad [2.2]$$

It is well-established that variability in perimetric sensitivity tends to increase as sensitivity decreases. The simulations used two different models for this increase: intrinsic noise and heterogeneous damage. Intrinsic noise reflects the noise within the signal used for psychophysical sensitivity, and was modelled by varying the slope parameter, β , using the equation of Henson, Chaudry et al. (2000)

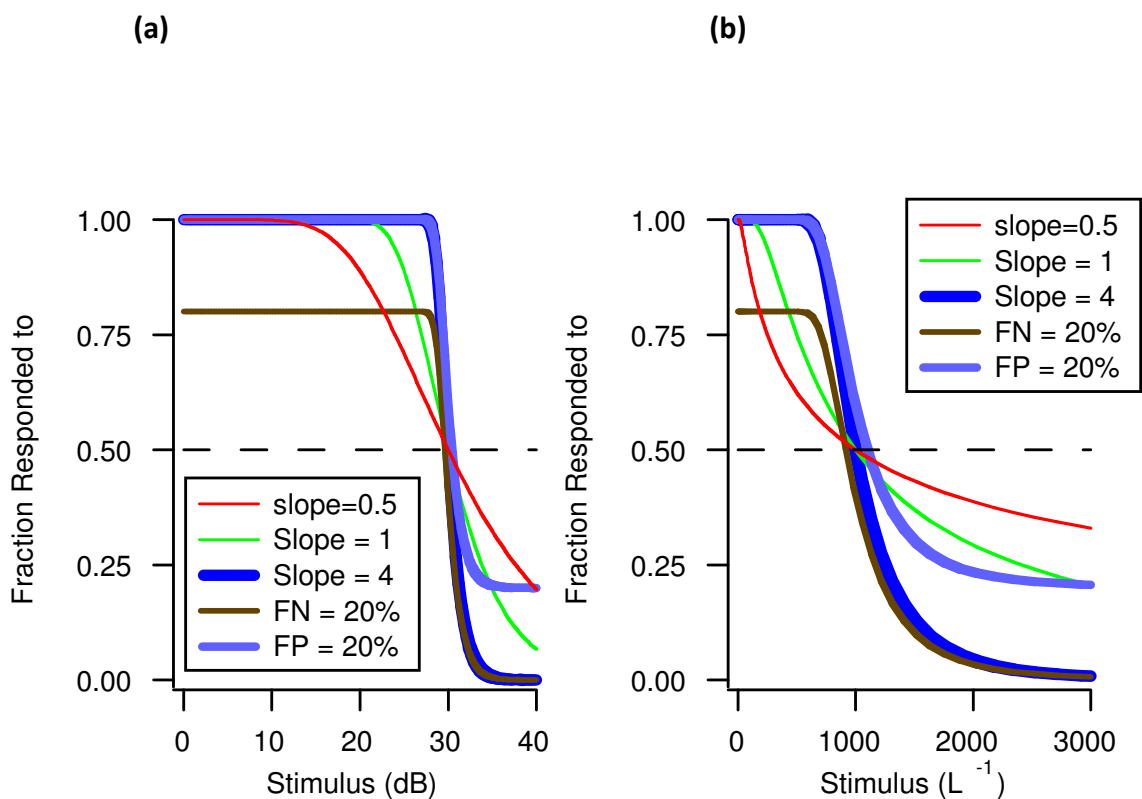
$$\ln(\text{SD}) = 3.27 + 0.81 \cdot \log(\alpha), \quad [2.3]$$

where SD is the standard deviation of noise in the perimetric signal (in dB units and $1/\alpha$ is the measured sensitivity. We then computed the slope parameter, β , from:

$$\beta = 10/(\text{SD} \cdot \sqrt{2}) \quad [2.4]$$

Figure 2.1 Psychometric Functions (Frequency-of-Seeing Curves) obtained with the Weibull Function corresponding to a threshold (50% seen point) of 30 dB (= 1000 L^{-1})

¹: **(a)** Psychometric functions in dB, **(b)** Psychometric functions in L^{-1} .



Typical slopes from equation (4) were 5.0 for a sensitivity of 36 dB (3981 L^{-1}) and 1.4 for a sensitivity of 20 dB (100 L^{-1}).

Heterogeneous damage was modelled by randomly removing ganglion cells from a mosaic and computing the effect on sensitivity of psychophysical spatial mechanisms which sample the responses of the degraded ganglion cell mosaics, using the model given by Swanson, Felius (2004). Shifts in eye position by 0.5 to 1.0 degrees are not uncommon in perimetry (Henson, Evans et al. 1996) and in damaged eyes such minor changes in stimulus location can cause dramatic changes in measured sensitivity (Fellman, Lynn et al. 1989). For each of seven levels of ganglion cell loss between 0% and 99%, values of threshold (α) were obtained for stimuli at thirteen different locations within $\pm 1^\circ$ of putative stimulus centre. This array of 13 values for threshold represents potential effects of normal fixational eye movements, and on each stimulus presentation the value for sensitivity was drawn randomly from this array of 13 values. Values for threshold were computed using spatial filters with a peak spatial frequency of 1.0 cycle per degree (cpd) sampling a sparse mosaic of ganglion cells with large receptive fields, as these yielded values for standard deviation versus sensitivity which were consistent with the equation of Henson et al. (2000) for the slope parameter, and for which perimetric loss remained a linear function of ganglion cell loss.

FP and FN were fixed at either 0.0 or 0.2, to mimic the responses of a reliable subject versus responses of an unreliable subject.

2.4.3 Perimetric Strategies

Four different perimetric strategies were simulated: the standard Full-Threshold (FT) strategy and 2 strategies, termed ‘Linear strategies’, which utilised linear sensitivity steps (**Table 2.1**). The total number of reversals and the step size at each reversal defined each strategy. For all strategies, the sensitivity value was taken as reciprocal of the ‘last seen’ stimulus luminance, or as zero when the maximum stimulus was not seen.

Full-threshold strategy

The Full-Threshold (FT) strategy of the Humphrey Field Analyzer was replicated. This strategy terminated after two reversals. The step size was 4 dB prior to the first reversal, then 2 dB until the second reversal (Allergan Humphrey, 1986).

Table 2.1: Perimetric strategies simulated

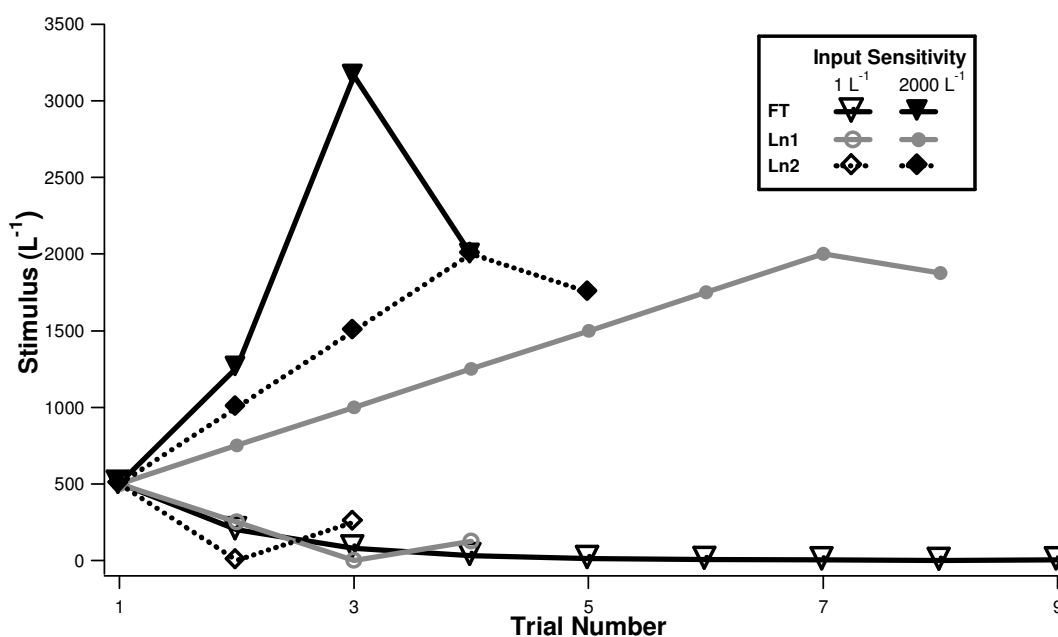
Strategy	Smallest Increment	Algorithm	No. of reversals
FT	2 dB	4–2 dB	2
Ln1	125 L ⁻¹	250-125 L ⁻¹	2
Ln2	250 L ⁻¹	500-250 L ⁻¹	2

Linear Strategies

The Linear strategies were designated Ln1 and Ln2; these were both 2-reversal strategies, **table 2.1**.

Figure 2.2 illustrates sample staircases from these four perimetric strategies with black symbols for the FT staircase and the Ln2 staircase (which had overall efficiency most like that of the FT staircase). Results are shown for an observer with minimal intrinsic and extrinsic noise, using a starting luminance corresponding to 500 L^{-1} and input sensitivities of 1 L^{-1} and 2000 L^{-1} . For an input sensitivity of 2000 L^{-1} , ($\alpha = 1/2000 \text{ L}$) the FT staircase had the smallest number of trials, while for a sensitivity of 1 L^{-1} ($\alpha = 1 \text{ L}$) the FT staircase had the largest number of trials.

Figure 2.2: Sample staircase runs for FT, Ln1 and Ln2 with a starting stimulus of 500 L^{-1} and an input sensitivity of 1 L^{-1} and 2000 L^{-1} .



2.4.4 Data Analysis

Bias was defined as the difference between the input sensitivity and the mean of the (thousand) output sensitivities obtained with simulated staircases. Bias was positive when mean staircase sensitivity was higher than input sensitivity and negative when mean (output) staircase sensitivity was lower than input sensitivity.

Test-retest variability (TRV) was computed as the standard deviation of 1000 output sensitivities for a given condition.

The *number of trials* for each staircase to run to completion was recorded. For each input sensitivity value, *perimetric efficiency* was defined as the inverse of the mean number of trials for the 1000 staircase runs. Therefore efficiency was low if, on average, a large number of trials were needed for a staircase to terminate. Simulations were implemented using Matlab 5.2.1 (The Mathworks, Inc., Natick, MA).

2.4.5 Collection of Clinical Data

In order to verify the clinical validity of predictions from the simulations, pilot data were gathered by testing 41 subjects with the FT and Ln2 perimetric strategies on 2 separate occasions. Prior to these 2 sessions, all subjects underwent a 'learning visit' to familiarise themselves with the nature of the test and the stimulus. The Ln2 strategy was chosen because the simulations suggested this to be more efficient than Ln1. The order of tests (FT / Ln2) was randomised and the number of tests for each strategy was counterbalanced across subjects.

Subjects

Twenty-one patients with glaucoma and 20 age-similar control subjects were recruited for this study. All participants were aged between 50 and 80 years, had best-corrected visual acuity 20/40 or better, spherical refraction < 7 D and cylinder ≤ 2D and did not have any other eye disease affecting the posterior segment. All the glaucoma patients were regular attendants at the Glaucoma Institute of SUNY State

College of Optometry. They all had evidence of reproducible visual field defects on at least 2 previous Humphrey Visual Field tests (average Mean Deviation, MD -6.7 dB, range -0.31 to -22.7). If both eyes were eligible, the eye with the least field damage was tested. The normal subjects all had passed a comprehensive eye examination at the University Optometric Center of SUNY and were excluded if there was a positive history of glaucoma within a first-degree relative. The study was conducted under an approval by the Institutional Review Board at SUNY and followed the tenets of the Declaration of Helsinki. After the purpose and procedures were discussed with each subject and informed consent was obtained prior to testing.

Perimetric conditions

The Goldmann size III stimulus is 0.43 degrees in diameter and is a standard stimulus used in clinical perimetry (Anderson 1992). This stimulus was presented on a mean background luminance of $10 \text{ cd} / \text{m}^2$. This background luminance allowed a large dynamic range of stimulus luminances. Stimuli were presented with a Gaussian temporal profile. The time constant of the Gaussian was 100 ms. Low temporal frequencies reduce the luminance required to reach the Weber region (Graham and Hood 1992). We used a fixed starting stimulus of 1000 L^{-1} (30 dB), at each location, to reduce test-time in normal-seeing regions of the visual field.

Apparatus

Stimuli were displayed on a 21" SONY Trinitron monitor driven by a VSG 2/5 system (Cambridge Research Systems, Rochester, Kent, UK). The resolution of this monitor

was set to 800 by 600 pixels. The visible portion subtended 54° by 42° at a viewing distance of 40 cm. The frame rate was 150 Hz. The VSG system provided 14-bit resolution for each phosphor. The VSG OptiCAL photometer was used to measure photometric values for each phosphor, to calibrate display gamma functions and produce a linear lookup table. A luminance meter (Minolta LS-100, Konica Minolta, Mahwah, NJ, USA) was used to ensure that the mean background luminance of the monitor was 10 cd/m².

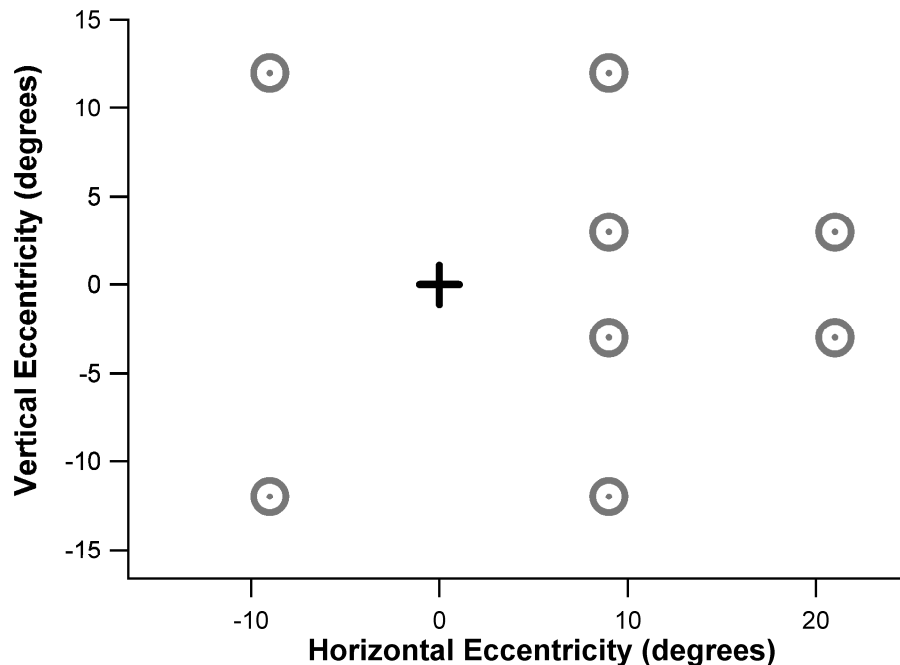
Test reliability criteria

Blank trials were presented at pseudo-random intervals, to provide an estimate of the false positive rate. Fixation was monitored with a CCTV video camera and using the Heijl-Krakau method. Tests were excluded and subsequently repeated when false-positive rate was greater than 20% or when fixation was deemed unstable (>30% fixation losses). Patients with deep defects and variable responses may not see the maximum available stimulus (15 dB on the VSG) all of the time (Bengtsson & Heijl 2000) and so false negative rate was not used as an indicator of test reliability.

Test locations

Stimuli were presented at 8 locations at eccentricities of 9.5, 15.0 and 21.2 degrees (**Figure 2.3**). These locations were chosen to reflect the distribution of the retinal nerve fibre pattern. Locations were symmetrical across the horizontal midline. Since glaucomatous loss tends to be asymmetrical, this arrangement allowed sampling of retinal locations with damage ranging from mild to severe within the same eye.

Figure 2.3: Test locations (left eye). Test locations (open grey symbols) are shown relative to the fixation point (solid black cross)



2.4.6 Analysis of pilot data and comparison with simulation data

For each point the *average sensitivity* of 2 tests for each of the 8 locations and each subject was computed as the means of the sensitivities measured by each of the two strategies, FT and Ln2.

Agreement of measured sensitivity values obtained by FT and Ln2 was evaluated using a Bland-Altman plot (Bland and Altman 1986) and was compared to corresponding (output) sensitivity values yielded by the Monte Carlo simulation. For the purposes of comparing the pilot and simulation data, output sensitivity values (rather than input sensitivity) were used, since in the practical situation *actual* sensitivity at a given test point is unknown and only a measured value is obtained by running a perimetric staircase.

Test-retest difference was defined as the difference in sensitivity at each location between the two tests (t_2-t_1) for each strategy. *Test-retest variability* was computed as the standard deviation of test-retest differences across all locations and all subjects for each of the two strategies. Tests where the maximum luminance stimulus was not seen on both occasions were excluded from variability analysis. Standard deviation from the simulations (1000 output sensitivities for each condition) was multiplied by the square root of two for direct comparison with the measured test-retest variability obtained from the pilot data.

2.5 Results

2.5.1 Results of the Monte Carlo simulations

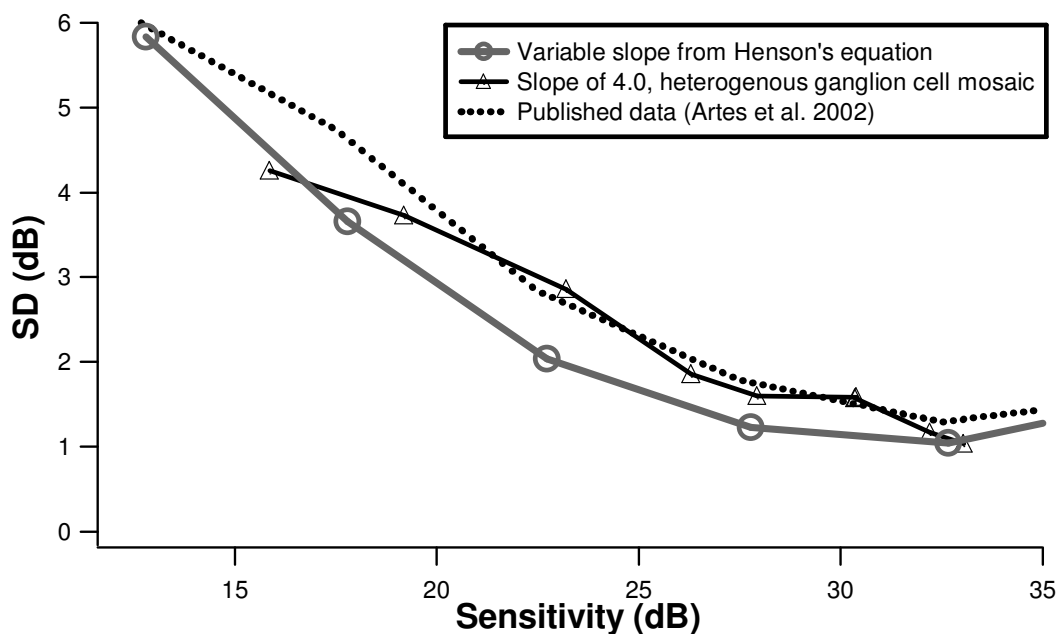
Results in dB units

Our goal was to evaluate the sensitivity-dependence of bias, variability and efficiency of FT and alternative staircases, when sensitivities are expressed in linear units. To demonstrate that our choice of parameters was consistent with data in the literature which expressed sensitivities in dB units, the relationship between simulated variability and sensitivity in dB units was qualitatively compared (**Figure 2.4**). A starting point of 500 L^{-1} (27 dB) was used for all these simulations. The solid grey line in **figure 2.4** shows results of the simulation for intrinsic variability modelled by varying the slope of the psychometric function according to Henson's equation. Henson's equation is not defined for sensitivities below 10 L^{-1} (10 dB). The variability of DLS measurement in dB is typically highest around 10 dB (Artes, Iwase et al. 2002), as measurement of variability for sensitivities below this value is limited by the maximum stimulus of the perimeter. Therefore, for these simulations in dB units and for input sensitivities below 10 L^{-1} , the psychometric function slope was fixed to 0.6 (this slope corresponded to an input sensitivity of 10 L^{-1}). Psychometric slopes below 0.6 gave rise to an artificial increase and higher estimates of variability for sensitivities in the range 10 – 15 dB. With this slope of 0.6, input sensitivities of $< 1 \text{ L}^{-1}$ (0 dB) sometimes yielded output sensitivities $\geq 10 \text{ dB}$. For a reliable estimate of dB variability for output sensitivities $\geq 10 \text{ L}^{-1}$ (10 dB), input sensitivities in the range of 0.016 to 10 L^{-1} (-18 dB to 10 dB) at 1 dB intervals were used. In accordance with the plot of Artes et al. (2002), average variability was plotted for 5 dB sensitivity bins. The solid black line shows the variability resulting from

heterogeneous ganglion cell damage interacting with minor changes in stimulus location. The two methods of simulating variability (slope of psychometric function and heterogeneous damage) exhibited similar qualitative trends: variability was less than 2 dB at high sensitivities (> 30 dB) and became much higher in regions of low sensitivity. This is consistent with previous reports of high variability in damaged regions of the visual field (Piltz & Starita, 1990; Chauhan, Tompkins, LeBlanc, McCormick, 1993; Artes et al. 2002). For comparison with published data, variability values from Artes et al. (2002) are also shown (dotted black line).

The variability predicted by the simulations using a variable psychometric function slope computed from Henson's equation was as much as 1 dB lower than the variability estimated by Artes et al. 2002. Further simulations (not shown) demonstrated that this difference could be explained by starting point effects. Our simulations used a fixed starting luminance corresponding to 500 L^{-1} (27 dB). Artes' data were obtained using the Full Threshold strategy of the Humphrey Field Analyzer, which uses a variable initial stimulus, suprathreshold to an initial estimate of sensitivity at each location.

Figure 2.4: Variability of DLS (dB) versus sensitivity (dB) as predicted by the Monte Carlo simulation for two conditions: a psychometric slope which varies with sensitivity according to Henson's equation ('variable slope') and for a fixed psychometric slope of 4 with sensitivity values obtained from a model of sparse ganglion cell loss sampled by a 1.0 c.p.d. spatial filter to represent effects of normal fixational eye movements.



Bias

Figure 2.5 shows the effect of sensitivity on bias for each of the 4 strategies, for starting luminances of 500 L^{-1} (left panels) and 2000 L^{-1} (right panels). In the absence of extraneous noise ($FP = FN = 0$) bias varied systematically with sensitivity, in the range -500 L^{-1} to $+650 \text{ L}^{-1}$ across strategies and sensitivities. The greatest underestimates were at higher sensitivities, dropping as low as -500 L^{-1} for the FT strategy, but not lower than -300 L^{-1} for the Linear strategies. The greatest overestimates were as high as $+650 \text{ L}^{-1}$ for the Ln1 strategy at a high starting stimulus, but for the FT and Ln2 staircases there were no overestimates exceeding

+400 L⁻¹. For a given strategy, bias varied by no more than 800 L⁻¹ across sensitivities.

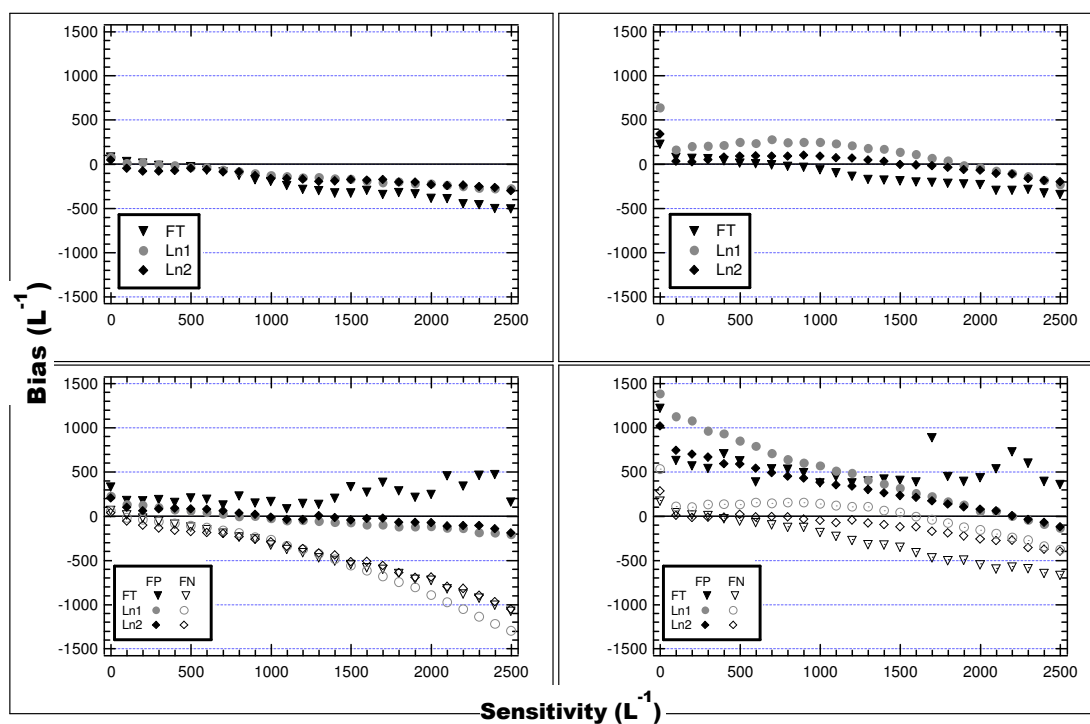
As shown in the lower panels of **figure 2.5**, much more extreme forms of bias were found in the presence of extraneous noise (FP = 0.2 or FN = 0.2). Generally, FP = 0.2 made bias more positive whilst FN = 0.2 made bias more negative. For a starting stimulus of 500 L⁻¹, with FP = 0.2 bias for FT increased from +100 L⁻¹ at low sensitivities to +500 L⁻¹ at high sensitivities, while bias for Ln1 and Ln2 showed much less variation with input sensitivity. For a starting luminance corresponding to 2000 L⁻¹, with FP = 0.2 all staircases yielded overestimates greater than 500 L⁻¹, and bias for linear staircases became highly dependent on input sensitivity, $r = 0.99$, slope = -0.54 for Ln1; $r = 0.96$; $r = 0.98$, slope = -0.37 for Ln2 (p values for slope < 0.0001 in both cases).

For FN = 0.20, bias for all 3 staircases became increasingly negative at high sensitivities, more rapidly for a starting stimulus of 2000 L⁻¹.

Figure 2.5: The effect of sensitivity on bias for FT and the 2 Linear Strategies Ln1 and Ln2. Simulations for two different starting stimuli are shown. The top graphs show results for minimal extraneous noise ($FP=FN=0$). The bottom graphs illustrate the effect of introducing FP or FN rate of 20% ($FP = \text{False Positive}$, $FN = \text{False Negative}$, $FT = \text{Full Threshold strategy}$, $Ln1$ and $Ln2 = \text{Linear Strategies}$, $L^{-1} = 1/\text{Lambert}$).

a. Starting $500 L^{-1}$

b. Starting $2000 L^{-1}$



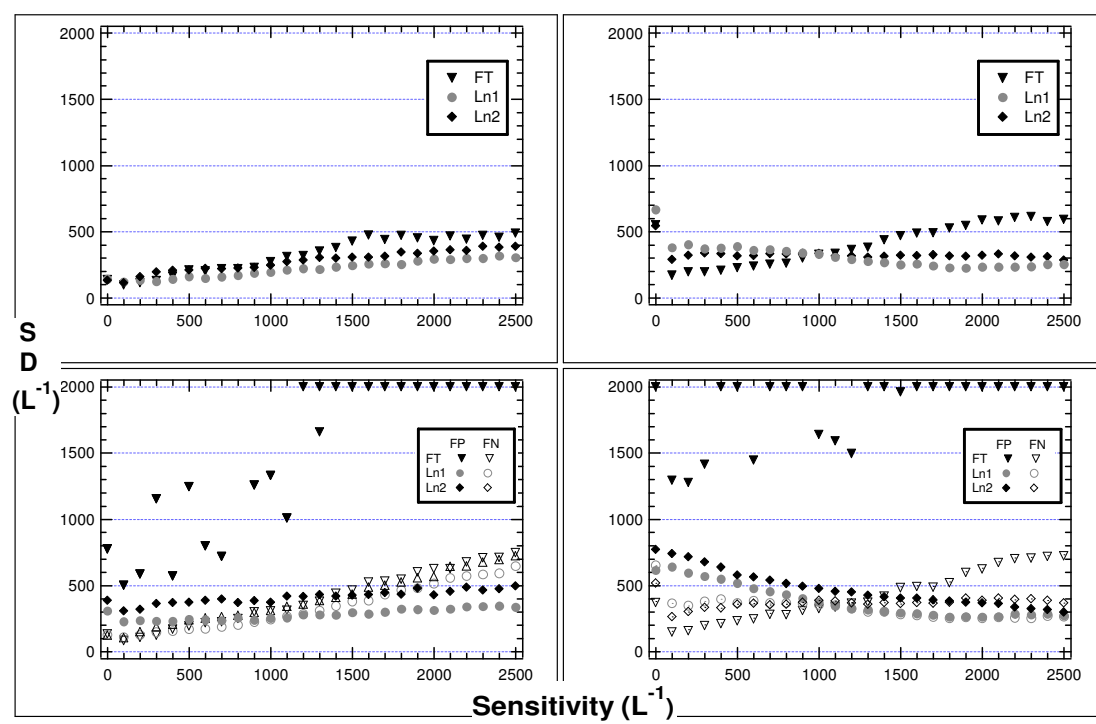
Test-Retest variability

Qualitatively, results were similar for intrinsic noise and heterogeneous damage (*figure 2.4*), and in *figure 2.6* are shown for intrinsic noise. In general, variability was less dependent on sensitivity for the linear staircases than for the logarithmic (FT) staircases. When extraneous noise was eliminated (upper panels), variability for

FT and linear staircases changed by 400 L^{-1} across sensitivities, with variability for linear staircases being highest at 1 L^{-1} . For sensitivities above 1500 L^{-1} (32 dB), variability was lower for linear strategies than for FT. The Linear strategy with the smallest final step size (Ln1) had the least variability over most of the sensitivity range.

Extraneous noise (lower 2 graphs, **figure 2.6**) increased variability for all staircases. This was most pronounced for $\text{FP} = 0.2$, where variability for FT often exceeded 2000 L^{-1} (shown in Figure 4 with symbols pinned at 2000 L^{-1}). For the Linear staircases variability rarely exceeded 500 L^{-1} and never exceeded 800 L^{-1} . For Ln1 and Ln2, sensitivity-dependence with $\text{FP} = 0.2$ was greater for a starting point of 2000 L^{-1} ($z = 7.8$, $p < 0.0001$ for Ln1 and $z = 16.5$, $p < 0.0001$ for Ln2) while for $\text{FN} = 0.2$ sensitivity-dependence was greater for a starting point of 500 L^{-1} ($z=8.4$, $p < 0.0001$ for Ln1 and $z = 19.7$, $p < 0.0001$ for Ln2)

Figure 2.6: Test-retest variability (measured as the standard deviation of 1000 staircase runs) for minimal extraneous noise, $FP=FN=0$ (top graphs) and FP / FN rates of 20% (bottom graphs). The graphs on the left show simulations for a starting stimulus of $500 L^{-1}$. Variability for runs with a starting stimulus of $2000 L^{-1}$ are shown on the right. With 20% FP , SD values for FT exceeded $2000 L^{-1}$ at sensitivities above $1500 L^{-1}$ and are shown pinned at $2000 L^{-1}$. (FP = False Positive, FN = False Negative, FT = Full Threshold strategy, $Ln1$ and $Ln2$ = Linear Strategies, $L^{-1} = 1/\text{Lambert}$).



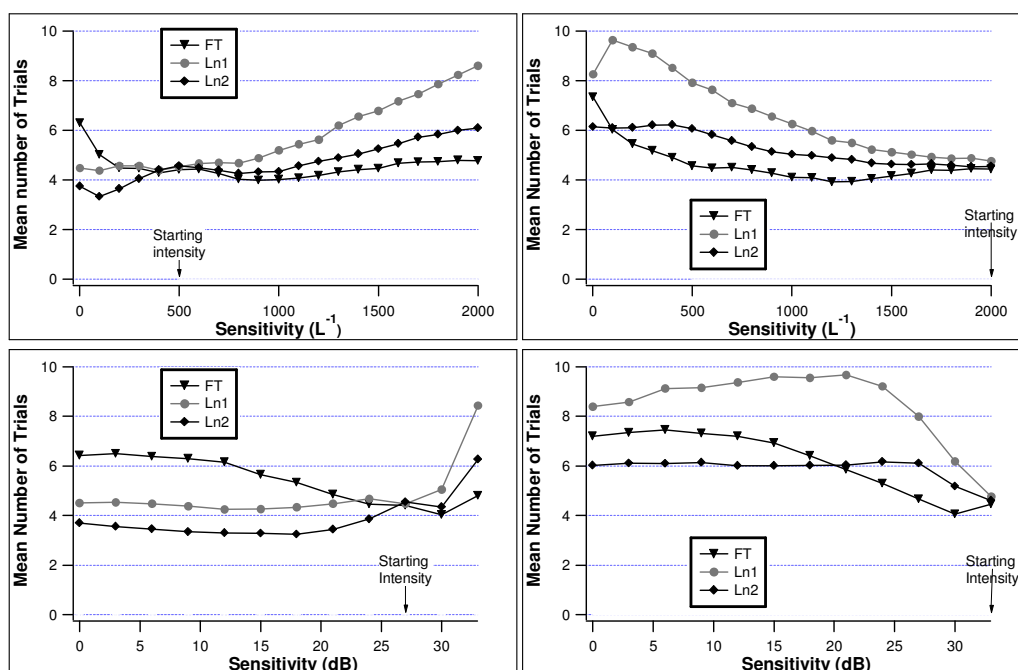
Efficiency

Efficiency for FT and Linear strategies had opposite forms of sensitivity-dependence: FT tended to be more efficient at high sensitivities whilst the Linear strategies tended to be more efficient at low sensitivities (**figure 2.7**). For a starting stimulus of 500 L⁻¹ (27 dB), linear staircases had the highest efficiency for locations with sensitivity 0 - 20 dB, while the FT staircase had the greatest efficiency for locations with sensitivity 27 – 33 dB. Change to a starting stimulus of 2000 L⁻¹ (33 dB) caused a decrease in efficiency of Linear strategies at sensitivities 0 – 30 dB.

Figure 2.7: Efficiency predictions from the Monte Carlo simulation. Efficiency for linear and dB algorithms are shown for two different starting points: 500 L⁻¹ (left graphs) and 2000 L⁻¹ (right graphs) and for sensitivity scaled in both in linear metrics (top graphs) and dB metrics (bottom graphs). (SD = standard deviation, FT = Full threshold, Ln1 and Ln2 = Linear strategies, L⁻¹ = 1/Lambert).

a. Starting 500 L⁻¹

b. Starting 2000 L⁻¹

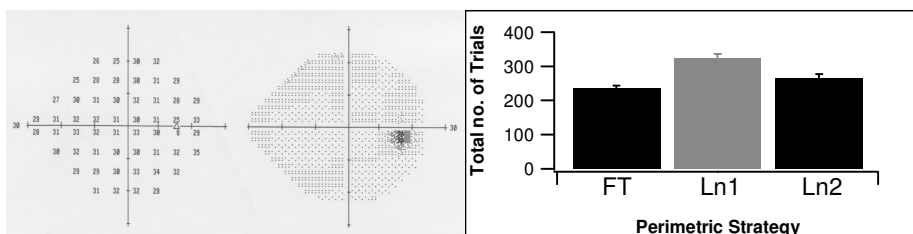


To compare potential efficiencies of the staircases in patients with varying amounts of visual field loss, we selected 24-2 SITA Standard field test results from one control subject and 3 patients with glaucoma (**figure 2.8**). For each field, dB sensitivities at all 54 locations were converted to L^{-1} and used as input sensitivities for the Monte Carlo simulation, with a starting stimulus of $500 L^{-1}$, false positive and false negative rates of zero. Psychometric slopes from Henson's equation were computed. Each simulation generated all 54 staircases and used the total number of trials as an estimate of test duration. This was repeated for a total of 100 simulations per visual field, and mean test durations were computed. For the fields with minimal or no loss (top two panels), FT had the shortest test duration. For the fields with moderate or advanced damage (lower two panels), test duration increased for FT and decreased for the Linear staircases, so Ln1 and Ln2 had lower test durations than FT. Of the Linear strategies, Ln2 had the shortest test duration.

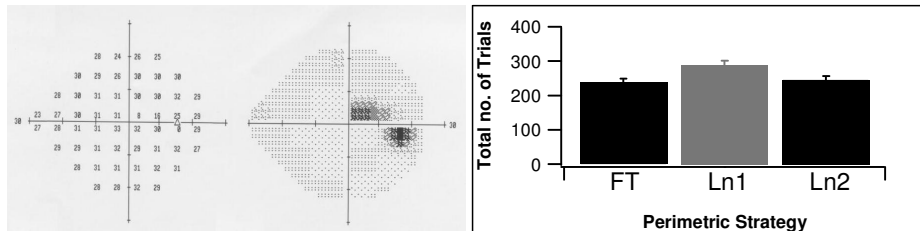
Figure 2.8: FT, Ln1 and Ln2 estimated test times for a full 24-2 visual field test.

Sensitivities were obtained from 24-2 SITA Standard Visual Field tests for one normal subject **(a)** and three glaucoma patients with varying amounts of field loss **(b), (c)** and **(d)**. The sensitivities obtained in dB units were converted to linear (L^{-1}) units and used as input sensitivities for our Monte Carlo simulation to estimate the total test time (total number of trials) for each of the perimetric strategies for a 54-location test. The Ln2 and FT strategies (both black solid bars) were comparable in efficiency.

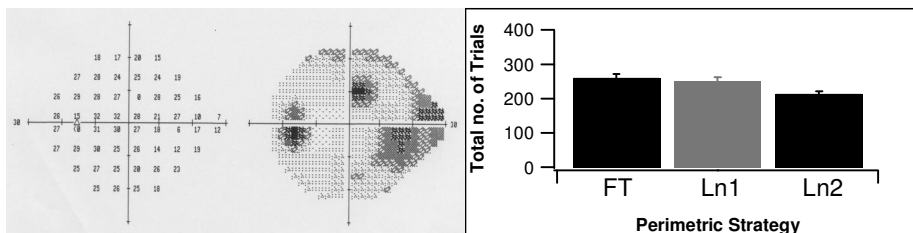
a. Right eye, MD +0.1 dB



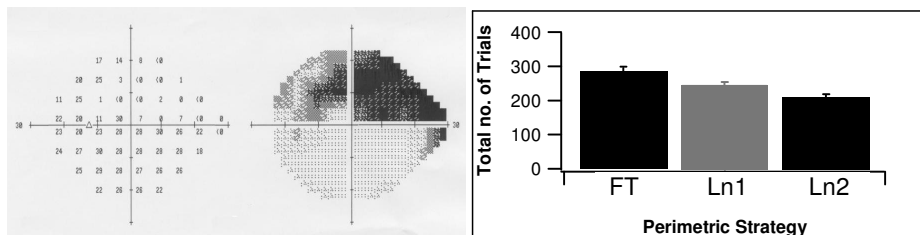
b. Right eye, MD -1.94 dB



c. Left eye, MD -6.72



d. Left eye, MD -12



2.5.2 Results from clinical data

Measured sensitivities

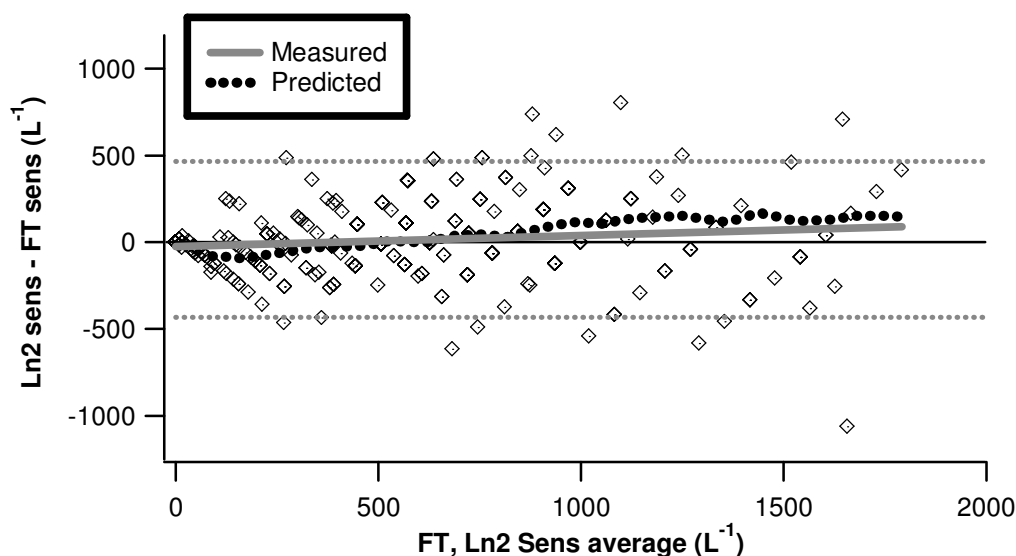
Measured mean sensitivities obtained with FT and Ln2 were similar for the 20 control subjects at each of the 3 eccentricities (**Table 2.2**).

Table 2.2: Mean sensitivity at each eccentricity for normal subjects

Eccentricity (degrees)	9.5	15.0	21.2
FT Sensitivity, L ⁻¹ (m ± sd)	1140 ± 403	797 ± 355	707 ± 228
Ln2 Sensitivity, L ⁻¹ (m ± sd)	1250 ± 387	814 ± 304	735 ± 265

When data from both patient and control groups were combined, analysis of agreement (**figure 2.9**) found no significant mean difference between sensitivities obtained with the FT and Ln2 staircases (mean = 16 L⁻¹, 95% limits for agreement - 435 to +467 L⁻¹). There was a tendency for the difference between FT and Ln2 sensitivities to increase with average sensitivity ($r^2 = 0.01$, slope = 0.06, $p = 0.03$), with Ln2 giving a higher value than FT at higher average sensitivities.

Figure 2.9 Agreement of sensitivity values as measured by FT and Ln2 for the clinical data (open symbols), 95% limits for agreement 467-435 L^{-1} , mean difference = 16 L^{-1} . The solid grey line shows the regression line for these points ($r^2 = 0.01$, slope=0.06, $p=0.03$). The dotted line shows the prediction obtained by the Monte Carlo simulation. (FT = full threshold, Ln2 = Linear 2 strategy, $L^{-1} = 1/\text{Lambert}$).

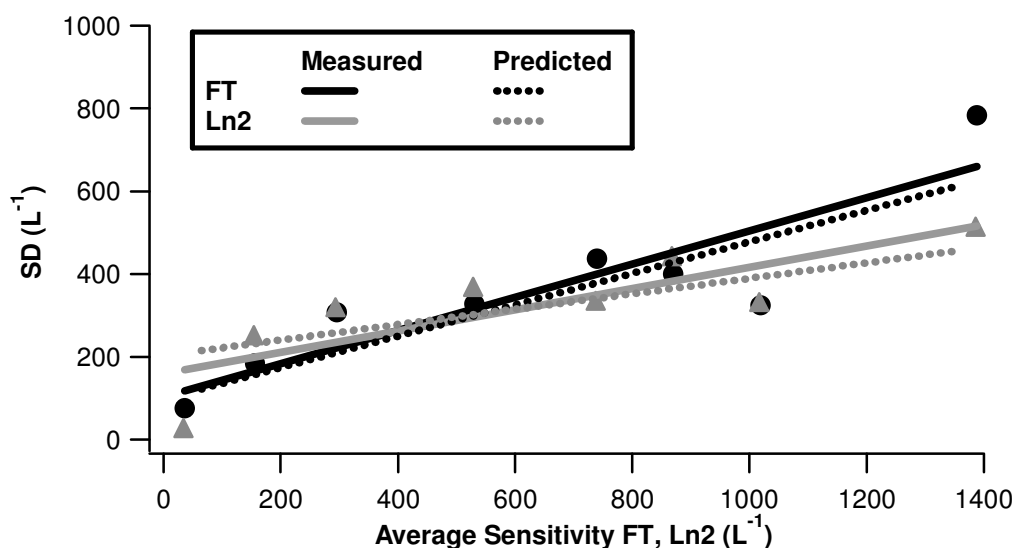


Test-retest variability

Test-retest variability was calculated as the standard deviation of test-retest difference at each location separately for each subject. For the clinical data (solid symbols), sensitivity was grouped into eight bins and the standard deviation (SD) of test-retest difference for each bin was computed (**figure 2.10**). The solid lines show the regression lines for these points. The dotted lines show the predicted standard deviations from the simulations. For both predicted and measured values of FT and Ln2, SD was well described by a linear fit in each case (p value for slopes < 0.05). As expected, the sensitivity-dependence of the variability was greater for FT than for Ln2. The slopes of the regression lines for measured data for FT (Slope 0.40, SE

0.085) and Ln2 (Slope 0.26, SE 0.072) were different ($z=1.70$, $p=0.04$). In each case, the slopes of the regression lines for the predicted values and measured values were similar ($z = 0.25$, $p = 0.4$ for FT; $z = 0.97$, $p = 0.17$ for Ln2).

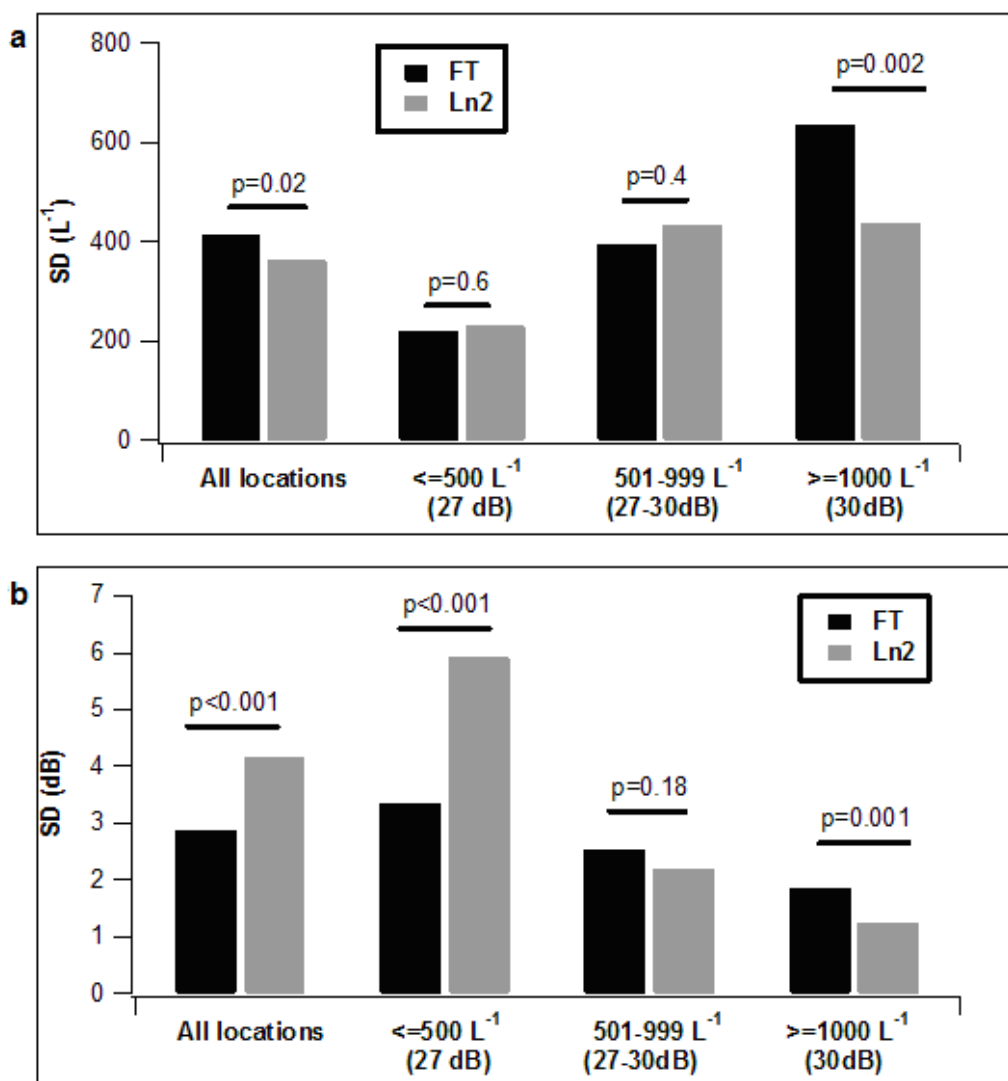
Figure 2.10: Variability (measured as the standard deviation of test-retest difference across locations with similar sensitivity) for FT and Ln2 (solid symbols). The regression lines for these points are shown (solid lines). The dotted lines show predictions from the Monte Carlo simulation. (SD = standard deviation, FT = Full Threshold, Ln2 = Linear 2 strategy, $L^{-1} = 1/\text{Lambert}$).



Pointwise test-retest differences were divided into 3 discrete sensitivity groups ($1 - 500 L^{-1}$, $501 - 999 L^{-1}$ and $\geq 1000 L^{-1}$), and comparisons of variability for FT and Ln2 was computed in L^{-1} (**figure 2.11a**) This revealed significantly higher variability for FT in the group with high sensitivities ($F = 2.1$, $p = 0.002$) but not for the groups with intermediate or low sensitivity ($F < 1.3$, $p > 0.35$).

Although the primary purpose of the study was to assess the effect of the type of staircase step (log versus linear) on variability, for comparison, we also analysed pointwise test-retest differences in dB units (**figure 2.11b**). As expected, this showed that for dB units, variability increased for FT and Ln2 as sensitivity decreased. Variability was still higher for FT compared to Ln2 at higher ($\geq 1000 \text{ L}^{-1}$) sensitivities ($F = 2.32$, $p = 0.001$) but no different at intermediate sensitivities (501 - 999 L^{-1}), $F = 1.34$, $p = 0.18$. At low sensitivities, variability (in dB) for FT was much lower than Ln2 ($F = 3.15$, $p < 0.001$).

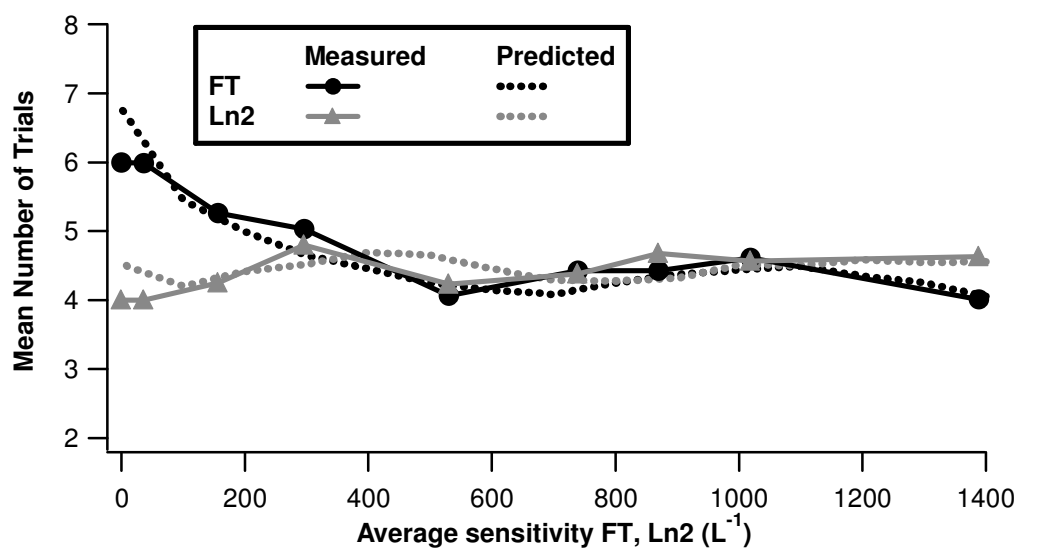
Figure 2.11: Variability by sensitivity group for FT and Ln2 for the pilot data. The first set of bars show the standard deviation across all locations. The next 3 sets of bars show the standard deviation for locations with sensitivity $\leq 500 L^{-1}$ (27 dB) 501-999 L^{-1} (27-30 dB) and $\geq 1000 L^{-1}$ (30 dB) respectively. P values (F-test) for comparison of variances between FT and Ln2 are shown for each group. The top graph, a, shows variability (vertical axes) computed in linear units. Variability computed in dB is shown in the bottom graph, 10b, for comparison. (SD = standard deviation, FT = full threshold, Ln2 = Linear 3 strategy, $L^{-1} = 1/\text{Lambert}$).



Efficiency

The mean sensitivities for the control group for the different test eccentricities are given in **table 2.2**. At all locations tested the mean sensitivities were in the range 700 –1300 L^{-1} , for which both FT and Ln2 staircases are predicted to have similar efficiency (upper left of **figure 2.7**). Across all subjects, the mean number of trials required for a staircase to terminate is shown in **figure 2.12** for each sensitivity value. The mean number of trials was indeed quite similar for sensitivities of 700 – 1300 L^{-1} ($t < 1.5$, $p > 0.15$ for all average measured sensitivities ≥ 700 and $< 1300 L^{-1}$), and as predicted (dotted lines) the Linear staircase was more efficient at low sensitivities. The total number of trials across all locations and all subjects was 4580 for FT and 4353 for Ln2 respectively.

Figure 2.12: Mean number of trials taken for FT and Ln2 staircases to terminate across the sensitivity range (mean of 2 tests). The dotted lines show predictions from the Monte Carlo simulation. (FT = Full Threshold, Ln2 = Linear 2 strategy, $L^{-1} = 1/\text{Lambert}$).



2.6 Discussion

2.6.1 Summary of findings

Conventional perimetric algorithms return sensitivities in equal logarithmic steps, while structural and electrophysiological measures are typically returned in linear steps. The conversion of perimetric data to linear sensitivity could produce substantial statistical artefacts due to sensitivity-dependence for bias, variability and/or efficiency. We used Monte Carlo simulations to evaluate sensitivity-dependence of these three factors for conventional strategies, as well as for three strategies returning sensitivity in equal linear steps. The simulations identified a Linear staircase, Ln2, which was expected to have similar efficiency to the conventional logarithmic full-threshold (FT) strategy when averaged across locations with a range of degrees of loss (**figure 2.8**), and to have weaker sensitivity-dependence than conventional staircases. These predictions were tested by making repeated measures of perimetric sensitivity of patients with glaucoma and control subjects, using both logarithmic and linear staircases.

As predicted, the Ln2 staircase reduced sensitivity-dependence for both efficiency and precision (**figures 2.10, 2.12**). Sensitivity-dependence of bias cannot be directly determined, as the true sensitivity for a given location is unknown, but the data gathered with FT and Ln2 staircases do conform to the prediction that the difference between sensitivities measured with Ln2 and FT increases with sensitivity (**figure 2.9**).

2.6.2 *Units of DLS measurement*

In conventional perimetry sensitivity is measured with dB steps, for which a 3 dB decrease in DLS is equivalent to a doubling of luminance. The use of logarithmic steps has some advantages: the variation of normal thresholds across eccentricity (Heijl, Lindgren et al. 1987) is smaller with logarithmic units, and use of dB units compresses the normal range of sensitivities while expanding the range of abnormal sensitivities, thereby facilitating the identification of abnormal levels of sensitivity. However, DLS in dB units may not be linearly related to the number of functioning ganglion cells, particularly in the early stages of glaucomatous disease (Harwerth, Carter-Dawson et al. 1999; Swanson, Feliuss et al. 2004).

The complex relationship between DLS (in dB) and structural measures makes it difficult to accurately grade the severity of glaucoma, particularly in the early stages of disease. The impression of a 'functional reserve' may result from the logarithmic nature of the dB scale (Garway-Heath, Poinoosawmy et al. 2000; Garway-Heath, Holder et al. 2002). Linear units of DLS may provide a more precise indication of underlying ganglion cell number. Both theoretical (Swanson, Feliuss et al. 2004) and clinical evidence (Garway-Heath, Holder et al. 2002; Reus and Lemij 2004; Schlottmann, De Cilla et al. 2004) suggests that a continuous (linear) structure-function relationship may be obtained if DLS is computed in a linear metric of sensitivity.

Studies of electrophysiology have also provided support for the linear relationship between ganglion cell damage and a linear sensitivity. A linear relationship exists between DLS in linear units and Pattern ERG (PERG) amplitude (Garway-Heath, Holder et al. 2002) PERG amplitude is thought to reflect the number of functioning

ganglion cells. Hood, Greenstein et al. (2002) reported a linear relationship between the log ratio (right versus left eye) of multifocal visual evoked potential amplitude and log ratio visual field losses and postulated that both these parameters may be directly related to the local loss of ganglion cells.

The relationship between structural and functional measures can be linearised by plotting both parameters in logarithmic units (Harwerth, Carter-Dawson et al. 2004; Harwerth, Carter-Dawson et al. 2005) but there is currently no agreed method of measuring optic disc and retinal nerve fibre layer parameters in logarithmic metrics. Several investigators have converted dB values to linear sensitivity to aid structure / function comparisons (Garway-Heath, Holder et al. 2002; Schlottmann, De Cilla et al. 2004; Harwerth, Carter-Dawson et al. 2005). Inspection of data from these studies suggests that dB perimetric sensitivity, when scaled in linear units, exhibits large variability particularly at higher sensitivities. The aim of the present study was to evaluate the effects of measuring linear sensitivity with dB steps and test the hypothesis that measurement of linear sensitivity with linear steps would reduce the effect of sensitivity on variability. The results of our study, comparing log and linear steps, are specific for linear measures of DLS and the variability findings are intended to be interpreted in the context of the linear model of structure / function relationship. The interpretation of variability in dB units, outside the linear structure function model, may be misleading (**figure 2.11**), as apparently large variability in dB units at low sensitivity may actually be low variability in terms of structural units.

2.6.3 Logarithmic versus linear steps for measuring linear DLS

By Fechner's law, equal steps in the change of the apparent brightness of a stimulus is related to the logarithm of the luminance increment and therefore the use of logarithmic steps may provide a representation of the corresponding changes in sensory magnitude.

Our results suggest that the precision, bias and efficiency of linear DLS measurement is, to some extent, determined by the size of the stimulus steps in relation to the underlying sensitivity. The precision of a sensitivity estimate is largely determined by the staircase step size in relation to the slope of the psychometric function. In general, the psychometric function slope is shallow at low sensitivities and steep at high sensitivities. In linear units, the number of possible sensitivity outcomes obtained with a dB-increment staircase is relatively low at low sensitivities and high at high sensitivities. In linear units, this results in lower precision at higher sensitivities and higher precision at lower sensitivities. The inverse occurs when sensitivity is measured with a linear-increment staircase (**figure 2.10**). One might argue, therefore, that whilst a linear strategy may be suited to detecting loss at higher sensitivities (for the detection of glaucoma), a dB staircase may be more suitable for detecting progression of established disease. Therefore, the identification of which algorithm is 'best' depends on the question or task in question. We have selected a strategy that we believe is more appropriate for structure/function analyses, where the step size is selected in the context of a linear model of the structure / function relationship, for which there is growing evidence. The Ln2 algorithm results in greater precision at higher sensitivities and lesser precision at lower sensitivities, when compared with the dB scale. Assuming a linear structure / function relationship, a 2 dB loss from 0 to -2dB represents a 37%

loss in ganglion cells, yet a 2 dB loss from -10dB to -12dB is equivalent to only 3.7% loss (from 90% to 93.7% loss). In this scenario, when trying to quantify structural damage from a functional test, it makes little sense to have high precision at low sensitivity and low precision at high sensitivity. In alternative scenarios, such as the evaluation a subject's ability to manage in his / her visual environment, measuring small amounts of remaining visual function with greater precision may be more important. There is a reciprocal relationship between precision and efficiency, so that an increase in precision occurs at the cost of reduced efficiency.

Various algorithms are possible, depending on the purpose for field testing. These include a 'hybrid' log-linear scale, with linear increments for higher sensitivities, switching to log increments for lower sensitivities, an algorithm where the step size is a percentage of the previous luminance value (this would fall somewhere between the linear and logarithmic staircase), or an algorithm which matches the step size to the estimated threshold.

2.6.4 Validating the variability predictions of the Monte Carlo model

The usefulness of conventional perimetry for monitoring glaucoma has been limited by high test-retest variability in damaged regions of the visual field: more than seven visual fields may be required to accurately determine progression of disease (Johnson 2001). The simulations replicated this finding (**figure 2.4**), in that the magnitude of test-retest variability in simulations of the standard FT strategy was similar to previous clinical studies.

Heijl, Lindgren et al. (1987) reported a standard deviation for intertest variability of around 2 dB at sensitivities between 30 and 35 dB (in normal eyes). Piltz and Starita

(1990) shows SDs of about 1 – 2 dB at a mean sensitivity of 30 dB, and SDs ranging from 4 to 10 dB at a mean sensitivity of 15 dB. Artes, Iwase et al. (2002) found a mean root-mean-square (RMS)-error of between 5 and 6 dB at a mean sensitivity of 15 dB, and a mean RMS error of less than 2dB at sensitivities in the range 30 – 35 dB. These findings are consistent with values obtained from the simulations (SD near 6 dB for an input sensitivity of 15 dB, and near 1 dB for an input sensitivity of 30 dB, *figure 2.4*).

2.6.5 Importance of findings

The simulations and clinical data both found that the use of a conventional dB-increment staircase results in lower number of trials and higher linear-unit variability in areas of the visual field with higher sensitivities. The simulations demonstrated that, in the absence of extraneous noise, the FT staircase should have a tendency to underestimate sensitivity in regions of high sensitivity, and that this bias will vary with starting luminance for subjects with substantial extraneous noise. These forms of sensitivity-dependence for the FT staircase could produce artefacts when FT sensitivities are converted to linear units for comparisons with structural indices, and could potentially produce a curvilinear relation even when the underlying relation is linear. The increase in variability with sensitivity for FT staircases is likely to decrease the strength of correlations between structural and visual field measurements, especially if many locations tested have near-normal sensitivities. The use of Linear staircases to measure perimetric sensitivity could potentially reduce these sources of artefact in structure-function comparisons.

Greater accuracy and improved precision at normal sensitivities has important implications for the early detection of glaucoma, particularly for inexperienced perimetric subjects with a high false positive rate. The normal sensitivity for an average 50-year-old at a peripheral nasal location is 29 dB (800 L^{-1}) (Heijl, Lindgren et al. 1987). The simulations suggest that the SD of variability for a subject with a FP rate of 20% at this sensitivity is more than halved with the use of Ln2 rather than FT (**figure 2.6**). Hence, it is expected that the ability to detect early defects at such locations would be greatly improved with the use of linear steps. This has important implications for glaucoma screening and diagnosis.

This study has shown that, when DLS is measured in linear units, the relation between variability and sensitivity is inverted from that found with dB units: variability of sensitivities derived from the FT staircase (dB staircase algorithm) is greater in areas with higher sensitivity (**Figures 2.6 & 2.11**). The use of linear staircases made variability less dependent on sensitivity, so that sensitivity estimates would have nearly equal variability at all levels of sensitivity. It was also found that FT tends to be less efficient in regions with reduced sensitivity, which means that patients with more profound defects will tend to require a larger number of trials, increasing the likelihood that prolonged test time will produce fatigue effects.

2.6.6 Comments on study methodology

For this study, fixed levels of extraneous noise were employed. For a given individual, the lapse (FN) or guess (FP) rate may vary with factors such as the length of the test, the location being tested and the time of day. Some investigators have

tried to overcome this problem by using computer simulations that are based on stimulus-response data from actual subjects (Chauhan and Johnson 1994). The present simulations provided a method of introducing extraneous noise that did not require human subjects. With this approach, a large number of noise conditions could be modelled in a short time.

For the simulations, the relationship between sensitivity and the slope of the psychometric function, as given by Henson, Chaudry et al. (2000) has been utilised. In general, slopes are steep in normal sensitivity regions and shallow in defective regions of the visual field. However, some patients with glaucoma can have shallow slopes in normal sensitivity regions (Chauhan, Tompkins et al. 1993). The simulations allowed the effects of slope and sensitivity to be considered separately. Although, for the purpose of the simulations reported here, a variable slope (dependent on the underlying sensitivity value) was employed, the simulation also allowed the use of fixed levels of slope at any sensitivity value. These simulations (not shown) found that intrinsic noise increased variability and that the sensitivity-dependence of variability increased as the slope (β) was reduced.

It should be noted that Henson's equation has not been validated for sensitivities below 10 dB (10 L^{-1}) (Henson, Chaudry et al. 2000), so simulated values of bias, variability and efficiency computed for an input sensitivity of 1 L^{-1} (**figures 2.5-2.7**) should be interpreted with caution.

CHAPTER 3

Development of novel perimetric stimuli for the assessment of glaucoma

3.1 Aims

The purpose of investigations in this chapter is to evaluate:

(i) The effect of scaling the diameter of an achromatic circular stimulus by estimates of ganglion cell receptive field density on the structure-function relationship in glaucoma. The hypothesis to be tested is that, by reducing the dependence of sensitivity on eccentricity, RNFL thickness will explain a greater amount of variance in DLS than for conventional perimetry with the Goldmann size III stimulus and will create a linear structure-function relationship across test eccentricities.

(ii) The agreement between DLS and RNFL thickness for a Gabor patch stimulus, with peak spatial frequency scaled by estimates of ganglion cell receptive density. The hypothesis to be tested was that the Gabor patch stimulus, by achieving complete spatial summation, would achieve better agreement than the Goldmann size III stimulus over the range of eccentricities tested.

3.2 Scaling stimulus size by estimates of ganglion cell density

Standard automated perimetry (SAP), involving the presentation of a white circular stimulus on a background of uniform intensity to determine differential light sensitivity (DLS), remains the mainstay of functional assessment in patients with suspected or established glaucoma and is one of the most frequently performed clinical psychophysical test in these individuals.

The era of Hans Goldmann led to a standardisation of clinical 'white-on-white' perimetry (Anderson 1992), in particular the use of six stimuli of fixed size for kinetic testing ('Goldmann size 0' to 'Goldmann size V') varying in area by a 3 log unit range. These have been imported into contemporary automated perimetry (Goldmann 1999). SAP utilises a constant size stimulus, typically the Goldmann size III stimulus (0.43 degree in diameter), at all test locations. Measurement of DLS with the Goldmann size III stimulus results in a characteristic 'hill of vision' sensitivity profile in normal eyes (Sloan and Brown 1962), with a measured sensitivity declining by 0.7 log units from 10 to 30 degrees eccentricity and corresponding ganglion cell coverage by the Goldmann size III stimulus declining from approximately 200 to 15 ganglion cells. The use of this fixed stimulus across the visual space is associated with DLS values (Wilson 1970; Kasai, Takahashi et al. 1993; Latham, Whitaker et al. 1993) and structure-function slopes which are dependent on eccentricity (Harwerth, Carter-Dawson et al. 2004).

Inspection of data derived from monkey eyes suggests that the slope of the relationship between DLS and ganglion cell number varies across standard perimetric test field (central 30 degrees) (Harwerth, Carter-Dawson et al. 2004),

implying that a greater loss of ganglion cells within the central 10 degrees eccentricity is necessary to yield the same loss in visual sensitivity than at 30 degrees eccentricity.

Measurements from Pattern Electroretinography (PERG), which are believed to represent ganglion cell activity, can indicate functional impairment in the central visual field of glaucoma patients without apparent perimetric loss in the same region (Bach, Sulimma et al. 1997). Although alternatives to conventional 'white-on-white' perimetry have been developed in an attempt to improve the sensitivity of perimetry to detect functional loss associated with glaucomatous optic neuropathy (Johnson, Adams et al. 1993), assessment of the effects of scaling the conventional 'white' stimulus by ganglion receptive density to improve perimetric sensitivity and structure/function correlations has not been investigated in depth. The Goldmann size I stimulus may identify visual field defects which may be less apparent with the Goldmann size III stimulus (Zalta and Burchfield 1990).

The use of appropriate scaling to equate peripheral and central sensitivity has been suggested as a possible method to reduce the eccentricity dependence of DLS (Wild, Wood et al. 1987; Latham, Whitaker et al. 1993; Garway-Heath, Poinoosawmy et al. 2000). Wilson (1970) showed that spatial summation curves from different eccentricities were essentially identical after a suitable horizontal translation. The derivation of magnification factors to represent cortical scaling of projected retinal stimuli attracted renewed attention in the 1980's and 90's (Wild, Wood et al. 1987; Latham, Whitaker et al. 1993), but no structural substrate was possible to suggest a constant relationship between DLS and ganglion cell number. More recently,

(Garway-Heath, Poinoosawmy et al. 2000) demonstrated, with empirical data, that scaling of DLS by a 'summation exponent' (which varied with eccentricity) created a linear relationship between DLS measured in linear units and estimated ganglion cell number across locations at all eccentricities. Pan and Swanson (2006) provided a neural interpretation for this spatial exponent in terms of spatial summation by cortical processes. Inspection of their analysis suggests that DLS shows minimal variation with eccentricity when the stimulus is scaled by critical area at each location.

For stimulus sizes equal or smaller to Ricco's area, DLS is linearly related to ganglion cell receptive field density with a slope of 1 dB/dB. In the central 13 degrees, the Goldmann size III exceeds Ricco's area for complete summation and the slope becomes shallower (Swanson, Feliuss et al. 2004). By varying stimulus size by estimates of ganglion cell receptive field density (and therefore Ricco's area) it is expected that the structure-function slope would be more constant across eccentricity, giving rise to approximately equivalent changes of DLS for changes in RNFL thickness at each location.

As direct quantification of ganglion cell numbers in the living eye is not yet possible, structural parameters, which correlate with ganglion cell number (Yucel, Gupta et al. 1998) are often used as surrogate measures for comparison with functional measures as optic disc rim area.

3.3 Contrast sensitivity perimetry

Stimuli, which tap low spatial frequency mechanisms, such as Gabor patches (sinusoidal grating with a gaussian envelope), may be suitable for identifying perimetric defects (Lundh and Gottvall 1995; Bodis-Wollner and Brannan 1997; Harwerth, Crawford et al. 2002).

At low spatial frequencies, sensitivity to grating stimuli is minimally affected by eccentricity (Pointer and Hess 1989) and optical defocus (Campbell and Green 1965; Westheimer 1966). The spatial properties of Gabor stimuli are considered to resemble the spatial profiles of the receptive fields of low level visual cortical neurons (Marcelja 1980). Harwerth noted that a 1 cycle per degree (cpd) Gabor patch possesses the characteristics of a very small stimulus in that it is sensitive to early losses, despite being more than twice the spatial extent of the Goldmann size III stimulus (Harwerth, Crawford et al. 2002). Mean test-retest variability is lower for Gabor stimuli compared to the Goldmann size III stimulus (Pan and Swanson 2006; Hot, Dul et al. 2008). Further, the test-retest variability is less dependent on depth of defect for such sinusoidal stimuli relative to the Goldmann size III stimulus (Artes, Iwase et al. 2002; Hot, Dul et al. 2008). Literature regarding structure-function relationships for spatially-localising stimuli is scarce. Hot, Dul et al (2008) found that depth of perimetric defect for a 0.4 cpd Gabor patch more closely matched the amount of percentage rim area loss (from HRT) than perimetric defect for the Goldmann size III using SAP.

Similar to an achromatic circular stimulus scaled in size by estimates of ganglion cell density, it is expected that scaling a Gabor patch stimulus in size would give rise to constant contrast sensitivity across eccentricity.

3.4 An appropriate end-point for structure-function analyses

Visual field measurements are assumed to reflect functioning ganglion cell activity and structural parameters of the optic nerve head provide a non-invasive measure of the ganglion cell count in a living eye. Regression analysis has been used extensively as an endpoint for evaluating the relationship between DLS and structural measures in glaucoma (Garway-Heath, Holder et al. 2002; Schlottmann, De Cilla et al. 2004; Bowd, Zangwill et al. 2006; Racette, Medeiros et al. 2007). However, this type of analysis provides little information about the concordance of two measures (Altman and Bland 1983). Bland-Altman plots (Bland and Altman 1986) have been widely employed in medical statistics to analyse the agreement for 2 measures which are in the same units. The Hood-Kardon model, (Hood and Kardon 2007), provides a method of relating DLS (in dB) to RNFL thickness (in μm) so for a given DLS value; the 'equivalent' RNFL thickness value can be estimated. Measured values of RNFL can therefore be compared with such predicted DLS-derived RNFL thickness.

3.5 Methods

3.5.1 Participants

Ninety-eight patients and 65 age-similar healthy volunteers were recruited for this study. All participants were White European and above 40 years of age, and had corrected visual acuity of 20/30 or better, spherical refraction ≤ 6 D and cylinder ≤ 2 D, open anterior chamber angles and no other eye conditions affecting the posterior segment. All patients and healthy subjects were experienced in perimetry, having performed at least one reliable test (defined as $\leq 15\%$ false positives, $\leq 25\%$ false negatives and $\leq 25\%$ fixation losses) prior to taking part in the study.

Patients were selected on the basis of statistically raised intraocular pressure (IOP) at presentation (≥ 21 mmHg). To reduce selection bias, patients were not selected on the basis of abnormal optic head (or nerve fibre layer) appearance or on the basis of visual field status. This inclusion criterion, based solely on IOP and not on structural or visual field measurements, was aimed at reducing potential bias with regard to pre-conceived notions of 'normal' and 'abnormal' functional parameters and allowed the inclusion of both ocular hypertensive (OHT) patients who had normal optic nerve head structure and visual fields and glaucomatous patients with a wide range of disease.

All patients were regular attendees to Moorfields Eye Hospital. If both eyes were eligible, one eye was selected at random. The control subjects all had normal intraocular pressure (≤ 21 mmHg) and were excluded if there was a positive history of glaucoma within a first-degree relative. The study was conducted under an approval by Moorfields and Whittington Regional Ethics' Committee and followed the tenets of the Declaration of Helsinki. The purpose and procedures were discussed with each subject and written informed consent was obtained prior to testing.

3.5.2 Perimetric conditions

All participants were tested with a Gabor patch stimulus and with the scaled achromatic circular and Goldmann size III stimulus. To avoid fatigue affects, testing with the Goldmann size III stimulus was performed on the first visit whilst the scaled achromatic stimulus and Gabor patch perimetry was performed at the second visit. Tests with these 2 stimuli were randomized and counterbalanced across all study participants, all of whom had previous experience with SAP.

3.5.3 Goldmann size III stimulus

The Goldmann size III stimulus is 0.43 degrees in diameter and is a standard stimulus used in clinical perimetry (Anderson 1992). Thresholds were measured in dB (where a 1 dB decrease in sensitivity is a 0.1 log unit increase in stimulus luminance, and the 0 dB stimulus is the maximum stimulus luminance the device can produce) using the SITA-Standard Strategy at the conventional 54 locations (spaced 6 degrees apart) of the Humphrey Field Analyzer II-i series (Carl Zeiss, Humphrey Division, Dublin, CA). Standard test conditions with a mean background luminance of 31.5 Asb ($10 \text{ cd} / \text{m}^2$) and a temporal presentation of 200 ms were employed. From the raw dB DLS values at each location, values were converted to linear DLS using equation [1.2].

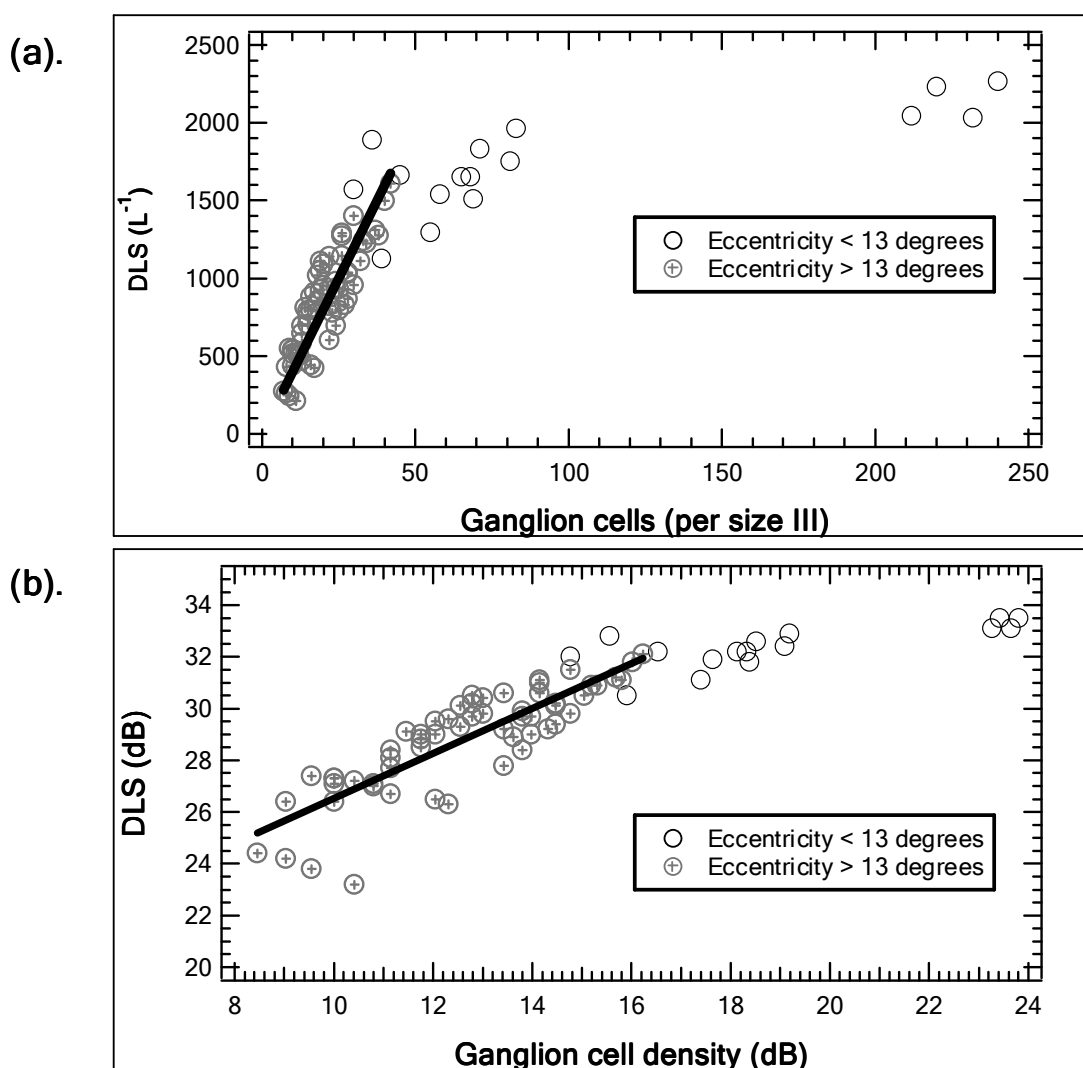
3.5.4 New stimuli

'Scaled' achromatic circular stimulus

The stimulus sizes were designed to cover an approximately equal number of ganglion cell receptive fields at each location and were derived from a published map of ganglion cell receptive field density (Garway-Heath, Poinoosawmy et al. 2000). This map was based on histological counts of ganglion cell number at differing eccentricities (Curcio and Allen 1990) and accounted for the lateral displacement of ganglion cells around the fovea.

A re-analysis (Swanson, Felius et al. 2004) of the Garway-Heath et al. (2000) data suggested that the relationship between DLS and ganglion cell number was linear for locations outside 13 degrees eccentricity when DLS and ganglion cell receptive field density were both scaled in linear units ($R^2 = 0.75$, $p < 0.001$) and dB units ($R^2 = 0.72$, $p < 0.001$), **figure 3.1**. The plot in **figure 3.1** has a linear region with a slope of approximately 37 L^{-1} per size III. The scaled stimulus was designed to cover 37 ganglion cell receptive fields at each location, according to the previously described model (Garway-Heath, Caprioli et al. 2000; Garway-Heath, Poinoosawmy et al. 2000; Swanson, Felius et al. 2004).

Figure 3.1: A re-analysis of empirical data (Garway-Heath et al. 2000) shows a dependence of DLS on eccentricity. *The variation of DLS was approximately linear for locations outside 13 degrees eccentricity for both DLS and ganglion cell density in (a) linear and (b) log units*



Assuming a regular arrangement of receptive fields, the diameter, d , of the stimulus at each location (in mm) was calculated from the area covered occupied by 37 ganglion cell receptive field centroids:

$$\begin{aligned} d &= \sqrt{[4 (37/G)] / \pi} \\ d &= 2\sqrt{[37/ \pi G]} \end{aligned} \quad [3.1]$$

Where G was the estimated ganglion cell receptive field density (number / mm²) from the map of Garway-Heath et al. (2000).

The diameter, in degrees of visual angle, was

$$d_v = d / q_p \quad [3.2]$$

The conversion factor q_p was computed from

$$q_p = q_0 - 0.000014U^2 \quad [3.3]$$

where U was the angle of retinal eccentricity in degrees and q_0 = conversion factor for the fovea (0.286mm/°), (Bennett, Rudnicka et al. 1994).

Stimulus sizes are shown (to scale) in **figure 3.2**. The smallest stimulus of 0.17 degrees was presented at location (3, -3 degrees) and the largest stimulus of 0.84 degrees at (-27, 3 degrees). This gave almost a 5-fold variation of stimulus diameter and 24-fold variation in stimulus area across locations.

Stimulus sizes were compared to critical areas derived from studies of spatial summation (**figure 3.3**) and data from studies of magnification perimetry. The data from Latham et al. (Latham, Whitaker et al. 1993; Latham, Whitaker et al. 1994) are particularly relevant to the present study as they calculated magnification factors which equated sensitivity across eccentricity (a flat ‘hill of vision’) with a background luminance similar to that used in this study for both kinetic and static perimetry. The diameter of the stimulus size necessary to equate sensitivity across eccentricity was computed from the scaling factor, f

$$f = E/E_2 \quad [3.4]$$

Where the E_2 value represented the eccentricity at which the foveal stimulus (0.108 deg) increased to remain perceivable at eccentricity E . Values of E_2 are given in their publications for 4 different meridians for 10 young normal healthy volunteers. These scaling factors were used to derive stimulus diameters for comparison at the 8 eccentricities tested in the present study (4.2, 9.5, 12.7, 15.3, 17.5, 21.2, 22.8 and 27.2 degrees). The size of the scaled stimulus (derived from the RGC receptive field data) is generally comparable across eccentricity to stimulus sizes derived from Latham’s data, particularly for scaling factors derived for static perimetry (‘Latham’), **figure 3.3b**.

Figure 3.2: Stimulus sizes on the VSG display monitor (to scale) for the scaled stimulus for the right eye

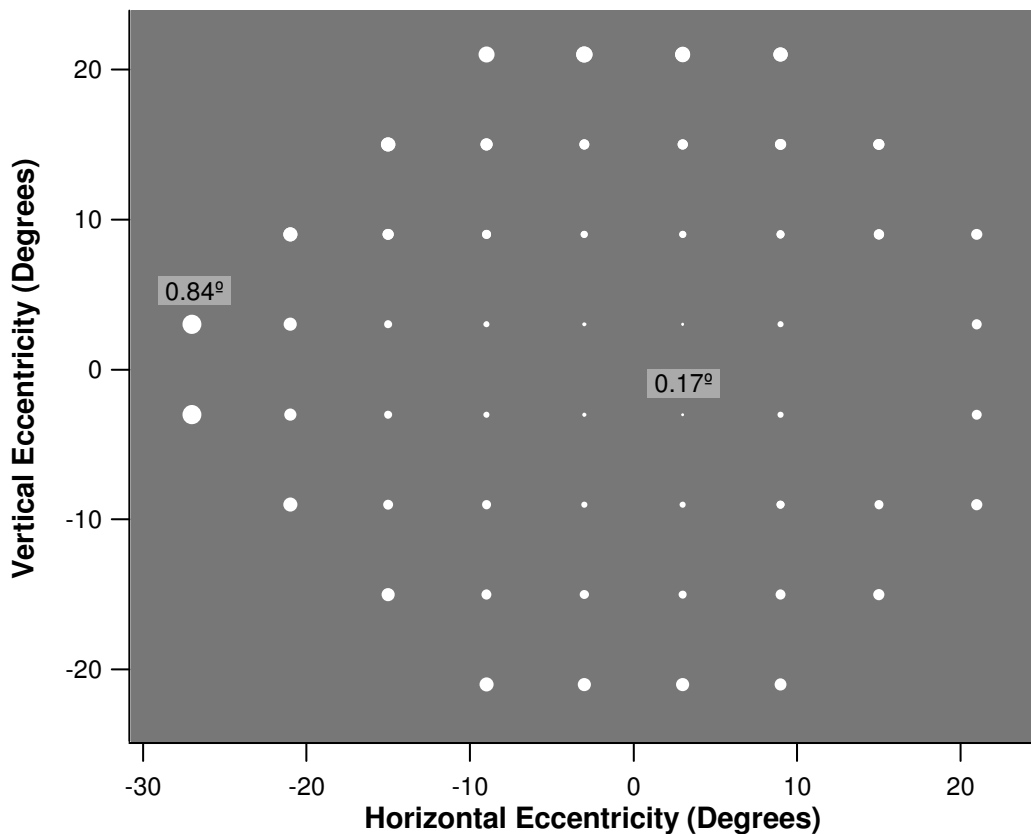
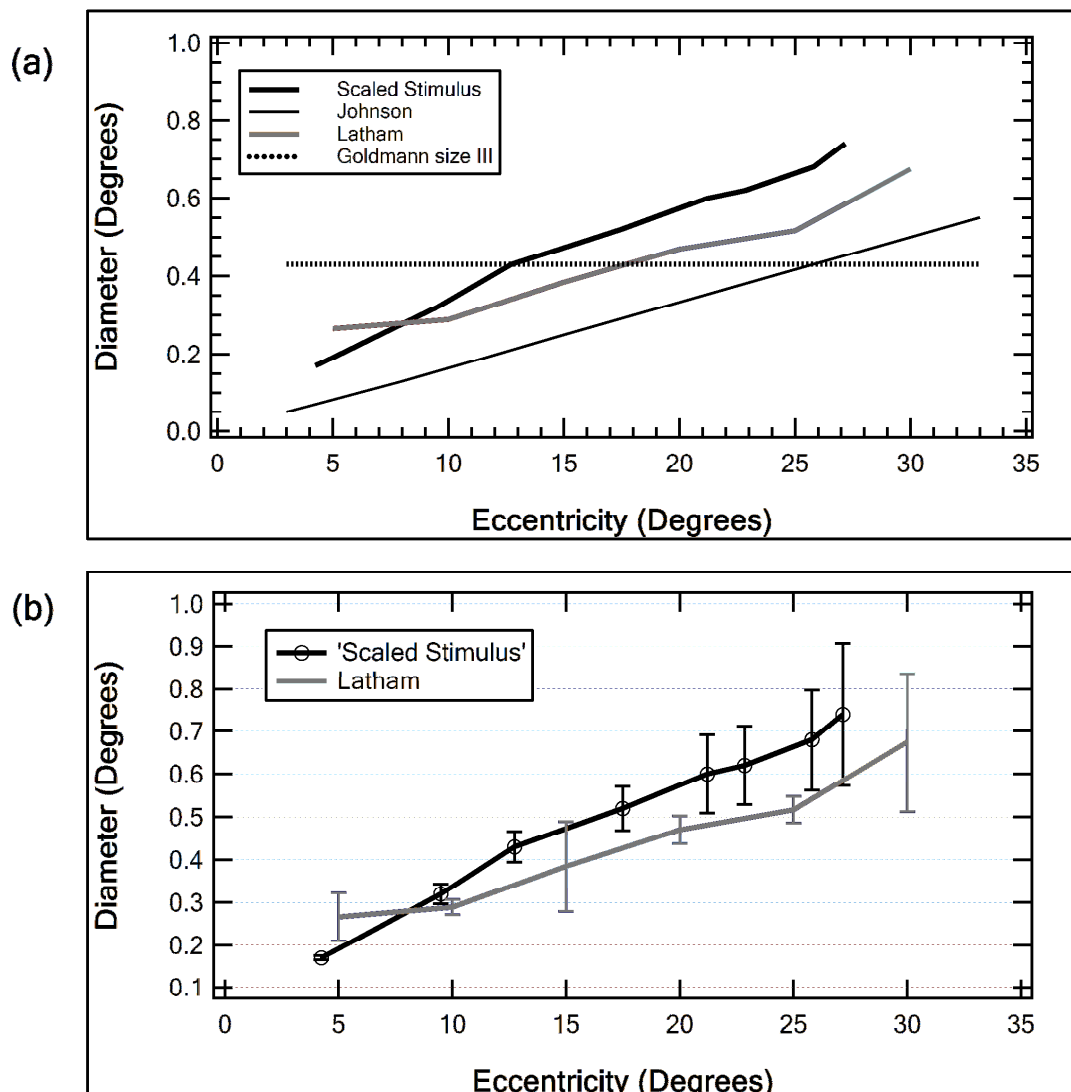


Figure 3.3: Diameter of scaled stimulus by retinal eccentricity (a) The diameter of the scaled stimulus used in this study in relation to critical area at differing eccentricities in other studies (Latham 1993; Johnson 1978) and the Goldmann size III stimulus. **(b)** The mean and standard deviation (error bars) of stimulus diameters across locations for a given eccentricity are compared to those derived from Latham's data for static perimetry



Gabor patch stimulus

A Gabor patch in sine phase was selected to avoid a DC component:

$$L(x,y) = L_m (1+ \text{Sin} [2\pi\omega(y-y_0)] (e^{-[(x-x_0)^2+(y-y_0)^2]/(2\sigma^2)})) \quad [3.5]$$

Where L_m is the mean luminance (10 cd/m^2); $L(x,y)$ is the luminance at the coordinate (x,y) relative to the centre of the stimulus (x_0,y_0) ; σ is the space constant of

the Gaussian window.. The peak spatial frequency of the Gabor, ω , was dependent on the estimated ganglion cell density at each location and was inversely related to the size of the achromatic stimulus relative to the Goldmann size III:

$$\omega = 0.215 / ((1/4) * (\text{Diameter of 'scaled' stimulus})) \quad [3.6]$$

$$\omega = (\text{Diameter of scaled stimulus}) / 4.65 \quad [3.7]$$

In terms of ganglion cell density, G at each location,

$$\omega = 0.215 / \{[2\sqrt{(37/\pi G)}] / q_p\}$$

$$\omega = [q_p \sqrt{(\pi G)}] / 56.6 \quad [3.8]$$

The peak spatial frequency of the stimulus varied from 0.23 cpd at 27 degrees eccentricity to 1.23 cpd at 4.2 degrees. The spatial frequency of the Gabor patch stimulus decreased with increasing eccentricity whilst its size increased: the space constant of the Gabor patch increased with eccentricity to maintain a constant bandwidth so that:

Bandwidth,

$$h = \sigma \omega = 0.75 \text{ octave} \quad [3.9]$$

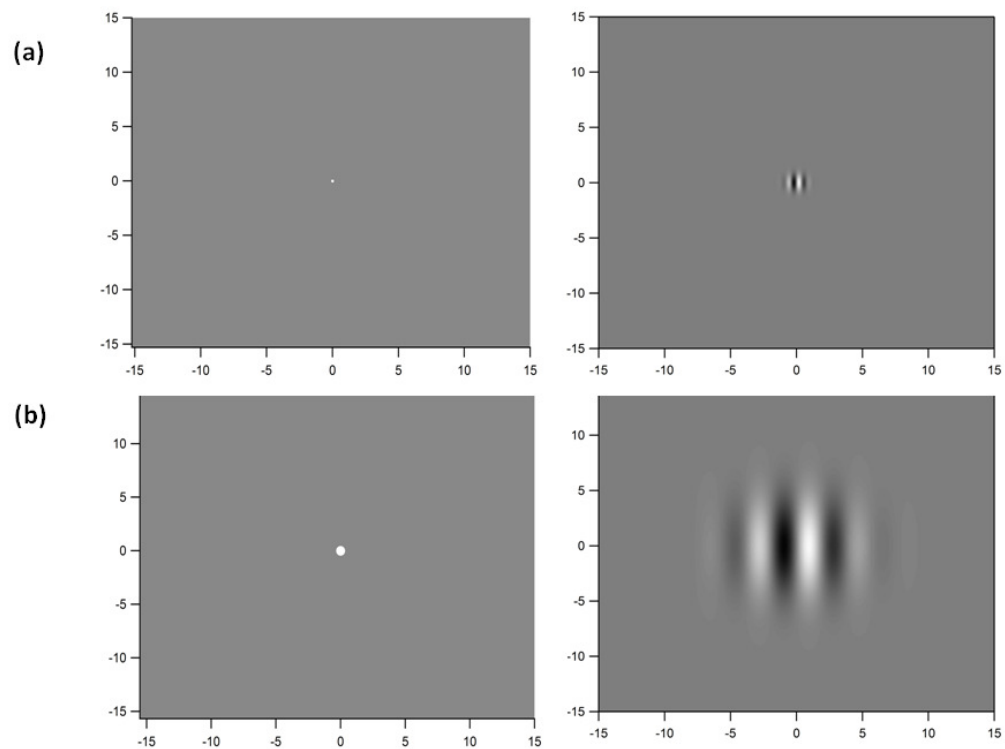
The peak spatial frequency of the Gabor patch, in cycles per mm ω_m , was further scaled for eccentricity to account for the flat monitor and varying distance of the eye to the stimulus:

$$\omega_m = \tan(E+1/\omega) - \tan E \quad [3.10]$$

Table 3.1: Mean peak spatial frequency of the Gabor patch stimulus in relation to the achromatic ‘scaled’ circular stimulus at each eccentricity. Mean \pm standard deviation across locations for each eccentricity are shown

Eccentricity (deg)	Scaled stimulus diameter (deg)	Peak spatial frequency Gabor patch (cpd)
4.2	0.17 \pm 0.004	1.23 \pm 0.03
9.5	0.32 \pm 0.02	0.68 \pm 0.05
12.7	0.43 \pm 0.04	0.50 \pm 0.04
15.3	0.46 \pm 0.06	0.50 \pm 0.06
17.5	0.52 \pm 0.05	0.42 \pm 0.04
21.2	0.60 \pm 0.09	0.37 \pm 0.06
22.8	0.62 \pm 0.06	0.35 \pm 0.05
27.2	0.83 \pm 0.01	0.26 \pm 0.003

Figure 3.4: Gabor and achromatic scaled stimuli for the locations (3,-3), a; and (27,-3), b; are shown. The Gabor stimuli (right hand side) are shown in relation to the achromatic circular stimuli (left hand side). Here the x- and y-axis co-ordinates are relative to the centre of the stimulus



Test strategy

A strategy similar to the Full Threshold strategy of the Humphrey Field Analyzer (Allergan-Humphrey 1986) was used to bracket sensitivity at 52 locations of the Humphrey Field. This strategy used increments of 4 dB prior to the first reversal, 2 dB thereafter and terminated after 2 reversals. The sensitivity corresponding to the last seen stimulus luminance was recorded in dB. DLS in linear units was obtained using equation [2.1].

Similarly for the Gabor patch stimulus, this strategy used increments of 0.4 log units prior to the first reversal, 0.2 log units thereafter and terminated after 2 reversals.

3.5.5 Test apparatus

Stimuli were displayed on a F520 21" SONY Trinitron monitor driven by a VSG 2/5 system (Cambridge Research Systems, Rochester, Kent, UK) with appropriate full-aperture lenses for foveal (near) correction. This near correction was obtained by adjusting the participant's usual near prescription with 0.25 DS lenses to obtain maximal subjective clarity for a reading chart at the test distance. The resolution of this monitor was set to 800 by 600 pixels. The visible portion subtended 78° by 62° at a viewing distance of 25 cm. The frame rate was 100 Hz. The VSG system provided 14-bit resolution for each phosphor. Photometric values for each phosphor were measured with the VSG OptiCAL photometer. The mean background luminance of the monitor was set to 10 cd/m² so that thresholds could be directly compared to those measured with the Goldmann size III stimulus from the Humphrey field perimeter. A luminance meter (Minolta LS-100, Konica Minolta, Mahwah, NJ, USA) was used to verify this background luminance value. Luminance measurements were made at four random locations on the monitor and were found to be within 10% of the mean value.

3.5.6 Imaging

All subjects underwent imaging with Optical Coherence Tomography using the software (version 2.0/0406) of the third generation OCT (Stratus OCT 3, Model 3000, Carl Zeiss Meditec, Humphrey Division, Dublin, CA, USA) to obtain measurements of

the peripapillary Retinal Nerve Fibre Layer (RNFL). The RNFL 3.4 Scan protocol gives RNFL values for 12 equal clock-hour sectors with a circular annulus of default radius 3.4 mm centered on the optic nerve head. Prior to scanning, eyes were dilated with 1% tropicamide and the alignment of the eye was checked. The focus, Z-offset and image polarization were optimized. Internal fixation was used.

Three sequential circular scans were obtained. The 3 separate images were evaluated and the highest quality image, in terms of scan signal strength and centration on the optic nerve head, was selected. The *RNFL thickness analysis* was performed using the instrument software to give RNFL thickness measurements for 12 equal (30 degree) radial sectors, **figure 3.6**.

3.5.7 Data analysis

Variation of DLS and structure-function ratio across eccentricity

Mean DLS was computed as the average of DLS (in linear units) at each eccentricity separately for all healthy normal eyes. Pointwise DLS values were related to clock-hour RNFL thickness values obtained with OCT imaging using a published structure-function correspondence map (Garway-Heath, Poinoosawmy et al. 2000). The *structure-function ratio* was defined as the ratio of DLS to RNFL thickness at each point and was computed for each individual and location separately. This gave an estimate for each test point of the ratio of DLS to ganglion cell number. The *mean structure-function ratio* was computed for all normal eyes. The mean DLS at each eccentricity was compared for the Goldmann size III stimulus and the scaled stimulus.

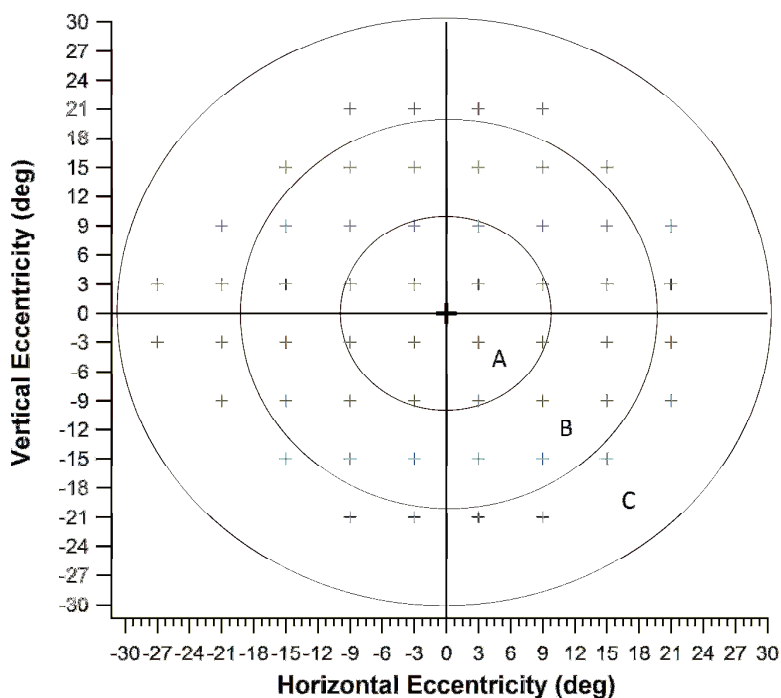
Structure-function correlations

The structure-function relationship was analysed for different eccentricities. Relationships were summarized for locations in 3 zones - Zone A: locations within 10 degrees eccentricity; Zone B: Locations between 10 and 20 degrees eccentricity and Zone C: locations outside 20 degrees eccentricity, **figure 3.5**. Mean DLS was plotted against RNFL thickness (from the OCT sectors corresponding to the visual field points) for each zone separately and with both DLS and RNFL thickness in linear-linear units (i.e. L^{-1} and μm) and dB-dB units. Decibel values for RNFL thickness were obtained by:

$$\text{RNFL (dB)} = 10 * \log_{10} \text{RNFL } (\mu m) \quad [3.11]$$

Arithmetic rather than geometric means were used for average dB values of DLS and RNFL thickness since averaging DLS in linear units is thought to provide a closer representation of functioning ganglion cell activity (Hood, Greenstein et al. 2002; Swanson, Felius et al. 2004).

Figure 3.5: Illustrating the locations in each analysis zone (A: <10 deg; B: 10-20 deg; C: > 20 deg)



Agreement of abnormality

In a clinical environment, the diagnosis of glaucoma hinges on the presence of abnormal psychophysical and/or structural parameters. Agreement between abnormal structural and functional parameters strengthens this diagnosis increases the likelihood that disease is present (Garway-Heath 2008).

Abnormal points were identified as those lying outside the one-sided 95% confidence prediction limits derived from normal eyes. The percentage of patient points which were abnormal for DLS and RNFL separately was computed as a fraction of the total number of patient locations. The agreement in terms of normal

/ abnormal DLS and normal / abnormal RNFL thickness was depicted using bar charts and Venn diagrams.

Application of the Hood-Kardon model

The Hood-Kardon model (Hood and Kardon 2007) was used to derive ‘predicted’ RNFL thickness values from DLS which was then compared to measured RNFL thickness as described below.

Plots of RNFL thickness versus sensitivity were fitted with the Hood-Kardon model (Hood and Kardon 2007). RNFL values (R) are related to *relative sensitivity*, T by the equations:

$$R = s_0T + b \quad \text{for } T < 1.0 \quad [3.12] \quad \text{and}$$

$$R = s_0 + b \quad \text{for } T \geq 1.0 \quad [3.13]$$

T was computed as the ratio of the measured sensitivity and the mean normal sensitivity for each eccentricity. The base (non axonal contribution) level of RNFL thickness, b was computed from a third of the mean normal RNFL thickness at each eccentricity separately; s_0 is the other (non-neural) RNFL component due to RGC axons.

Approximate 95% confidence limits for predicted RNFL thickness were computed from normal between-subject variability, so that for a relative sensitivity of 1, the approximate upper and lower confidence limits were

$$R_{\text{upper}} = R_m + 2R_{sd} \quad [3.14]$$

$$R_{\text{lower}} = R_m - 2R_{sd} \quad [3.15]$$

Where R_m and R_{sd} were the mean and standard deviation respectively of measured RNFL thickness in normal subjects for a given eccentricity.

Agreement analyses

The agreement between two measures, which are in the same units, can be computed using a Bland-Altman plot (Bland and Altman 1986). To obtain both RNFL and DLS measures in common units, values of *predicted* RNFL thickness were obtained for each value of CS using the Hood-Kardon equations [3.7] and [3.8]. These were compared to each measured value of CS at the same location. A Bland-Altman plot was obtained by plotting the difference ($RNFL_{\text{pred}} - RNFL_{\text{meas}}$) of the $\text{diff}(RNFL_{\text{pred}}, RNFL_{\text{meas}})$ against the average, $\text{av}(RNFL_{\text{pred}} - RNFL_{\text{meas}})$. The mean difference indicated the average bias of $RNFL_{\text{pred}}$ relative to $RNFL_{\text{meas}}$. The 95% confidence limits around this mean were calculated from

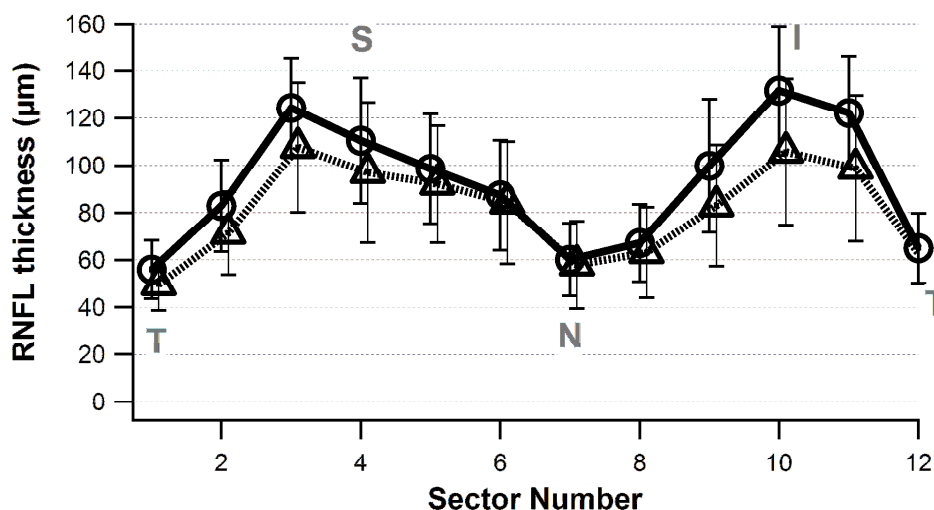
$$95\% \text{ CI} = \text{mean } \text{diff}(RNFL_{\text{pred}}, RNFL_{\text{meas}}) \pm 1.96 \text{ sd } \text{diff}(RNFL_{\text{pred}}, RNFL_{\text{meas}}) \quad [3.16]$$

3.6 Results I: Effects of scaling stimulus size by ganglion cell density

3.6.1 Participants

The mean (\pm sd) ages of the normal (67 ± 9 years) volunteers and patients (66 ± 10 years) were similar ($t=0.65$, $p=0.52$; $F=1.23$, $p=0.37$). The mean ($m \pm$ sd) RNFL thickness across sectors was $92 \pm 10 \mu\text{m}$ in normal subjects compared with $81 \pm 16 \mu\text{m}$ in patients ($t=4.9$, $p<0.01$). The Mean Deviation for patients was -1.2 ± 1.2 dB compared to -0.3 ± 1.2 dB for normal subjects ($t=3.3$, $p=0.001$).

Figure 3.6: Variation of mean RNFL thickness across scan sector in healthy (solid lines) and patient (dotted) eyes (n=65). Error bars represent SD across eyes. T = Temporal; S = Superior; N = Nasal; I = Inferior disc sector



3.6.2 Variation of DLS and structure-function ratio across eccentricity in normal Eyes

The variation of DLS with eccentricity for the Goldmann size III stimulus and the scaled stimulus is shown in **figure 3.7**.

For the scaled stimulus, in both dB and linear units, DLS remained approximately constant for eccentricities greater than 4.2 degrees. Mean DLS in dB varied from 27.0 dB to 28.5 dB (a difference of 1.5 dB), and 540 L^{-1} to 710 L^{-1} (1.3-fold difference) at 10 and 27 deg eccentricity, respectively, **figure 3.7**. However, for locations at 4.2 degrees, DLS for the scaled stimulus was 40% (240 L^{-1}) of the mean DLS at greater eccentricities

For the Goldmann size III stimulus, DLS declined monotonically with eccentricity. Mean DLS in dB varied from 31.3 dB to 27.0 dB (a difference of 4.3 dB), and 1700 L^{-1} to 500 L^{-1} (3.4-fold difference) at 10 and 27 deg eccentricity, respectively.

The standard error of these mean DLS values was small and no greater than 9% of the mean value.

The standard deviations of mean DLS across eccentricity were 380 L^{-1} and 160 L^{-1} for size III and scaled stimuli, respectively ($F=6.06$, $p=0.03$). The variation of mean DLS in linear units with eccentricity was roughly linear for the Goldmann size III ($R^2=0.98$, $p<0.001$) and the scaled stimulus ($R^2=0.61$, $p=0.02$). The dependence of DLS on eccentricity was smaller ($z= 7.2$, $p<0.001$) for the scaled stimulus compared to the Goldmann size III stimulus (all eccentricities).

The logarithm of the structure-function ratio is versus eccentricity is shown as in **figure 3.8**. The log of the ratio was used plotted against eccentricity rather than the

ratio as the latter is dependent on whether DLS/RNFL or RNFL/DLS is plotted. Between 4 deg and 27 deg, the structure-function log ratio varied by 0.8 log unit from 1.4 at 4 degrees to 0.64 at 27 degrees for the Goldmann size III and by 0.3 log unit from 0.53 to 0.80 for the scaled stimulus. The standard deviation of mean log ratio was 0.21 across eccentricities for Goldmann size III and 0.1 for the scaled stimulus. The structure function ratio was less dependent on eccentricity for the scaled stimulus compared to than for the Goldmann size III stimulus ($z=5.9$, $p<0.001$). With locations at 4.2 degrees eccentricity excluded, the change of the log ratio was 1.01-fold for the scaled stimulus and the slope of the linear regression line was close to zero (slope <0.01 , $R^2=0.49$, $p=0.08$).

Figure 3.7: Mean DLS per eccentricity for normal subjects for DLS in (a) dB units and (b) Linear (L^{-1}) units

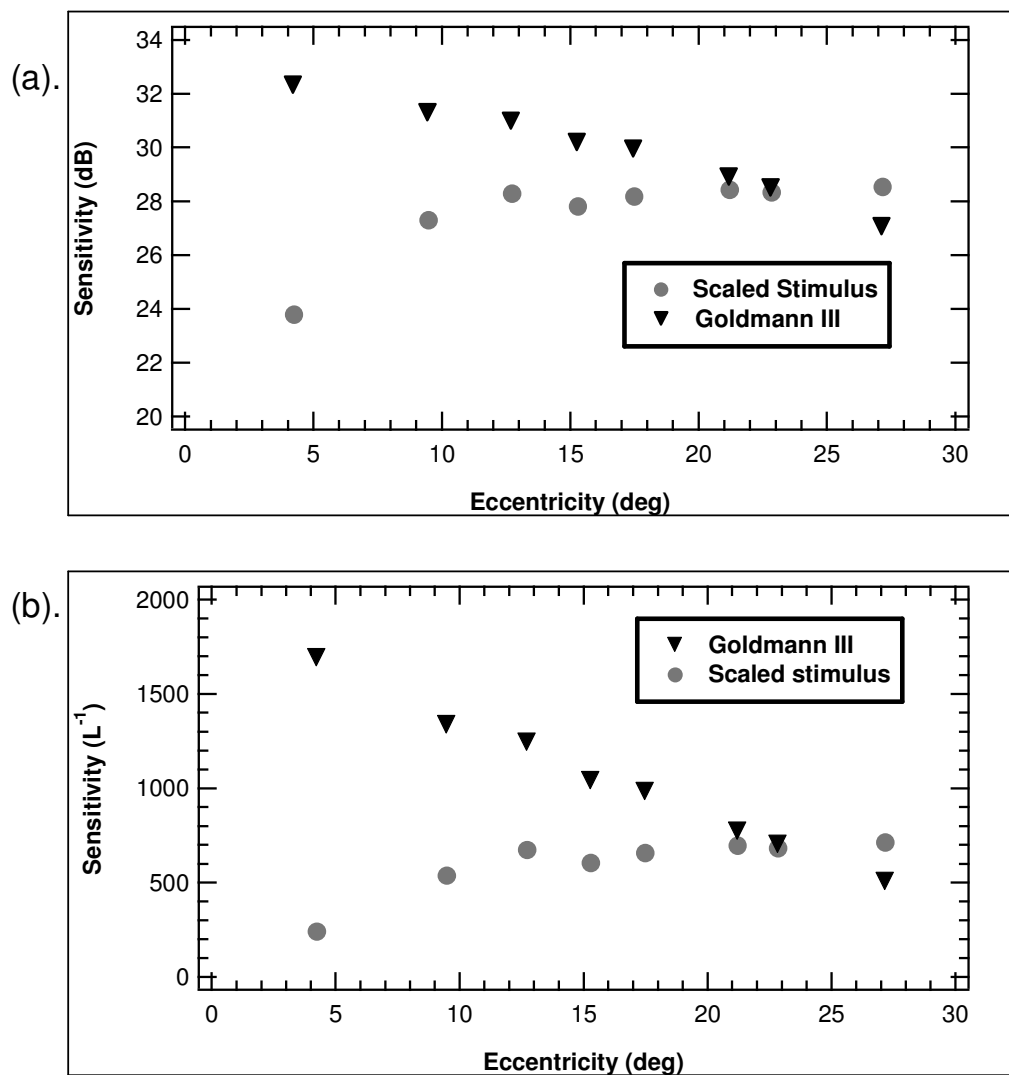
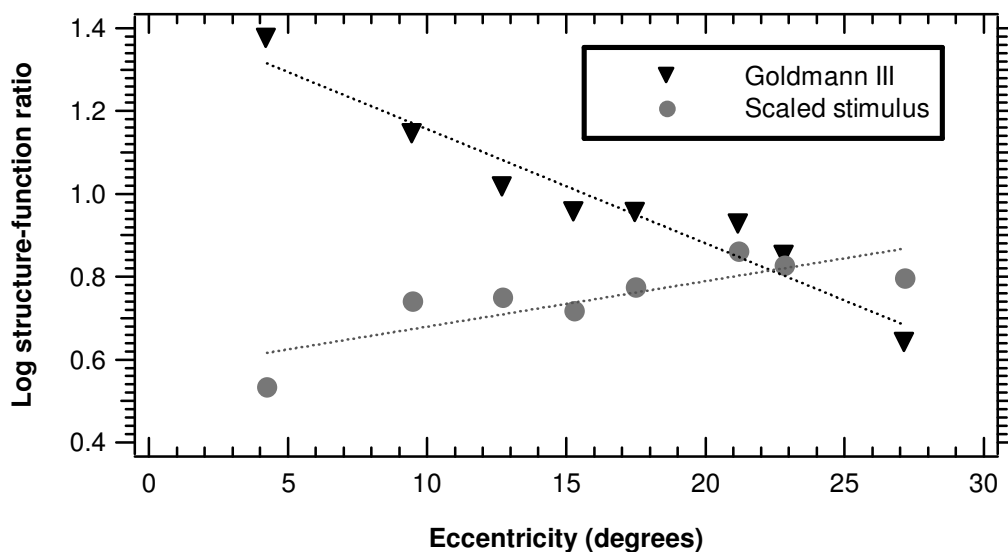


Figure 3.8: Variation of (log) structure-function ratio across eccentricity for the Goldmann size III and the scaled stimulus

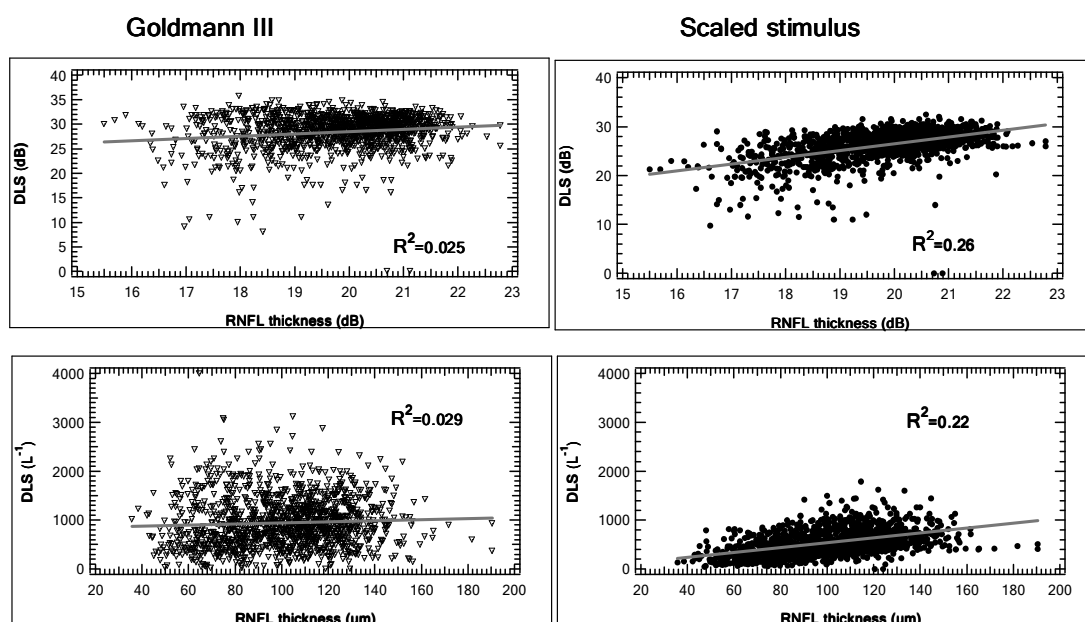


3.6.3 Structure-function associations

This analysis was performed with data from both patients and normal volunteers combined to obtain a wide range of DLS and RNFL values. Associations of DLS with RNFL thickness were assessed by averaging all locations for a given eccentricity in a given individual. **Figure 3.9** shows scatterplots of DLS versus RNFL thickness fitted with linear regression lines for the Goldmann size III stimulus (left) and the scaled stimuli (right). The top plots show structural and functional values in dB-dB units and the bottom plots show them in linear-linear units. With locations averaged across eccentricity, the strength of the association between DLS and RNFL thickness for all points was higher for the scaled stimulus ($R^2=0.22$ for linear-linear and

$R^2=0.26$ for dB-dB) compared to the Goldmann size III ($R^2=0.03$ for linear-linear and dB-dB), both for DLS and RNFL thickness in linear-linear and dB-dB units ($t>4.9$, $p<0.001$).

Figure 3.9: DLS versus RNFL thickness for all locations (after averaging across eccentricity) both with DLS-RNFL in dB-dB units (top graphs) and linear-linear units (bottom 2 graphs).



To examine the variation in the strength of the structure-function relation with eccentricity, locations were grouped into 3 zones. The coefficients of determination for linear regression of DLS versus RNFL thickness in different eccentricity zones are shown in **table 3.2**.

Table 3.2: Coefficients of determination (R^2 values, in %) for linear regression of DLS against RNFL thickness for locations within 10 degrees (Zone A); locations between 10-20 degrees (Zone B) and Locations outside 20 degrees (Zone C) for **(a)** dB-dB units and **(b)** linear-linear units. p values for the comparison of R^2 values for the Goldmann and scaled stimuli are shown in the last column.

(a)

Zone	Goldmann III	Scaled stimulus	N	P
A	4%	35%	326	<0.001
B	29%	24%	489	0.23
C	8%	12%	489	0.48

(b)

Zone	Goldmann III	Scaled stimulus	N	P
A	1%	34%	326	<0.001
B	17%	15%	489	0.76
C	4%	13%	489	0.10

Across zones, R-square values varied from 1% to 29% for the Goldmann size III stimulus and from 12% to 35% for the scaled stimulus. For Zone A locations, the structure-function association was much higher for the scaled stimulus regardless of the units ($t > 4.6$, $p < 0.001$). For locations outside 10 degrees (Zones B and C), the

strength of linear regression was similar for both stimuli for linear-linear and dB-dB units ($t < 1.7$, $p > 0.9$).

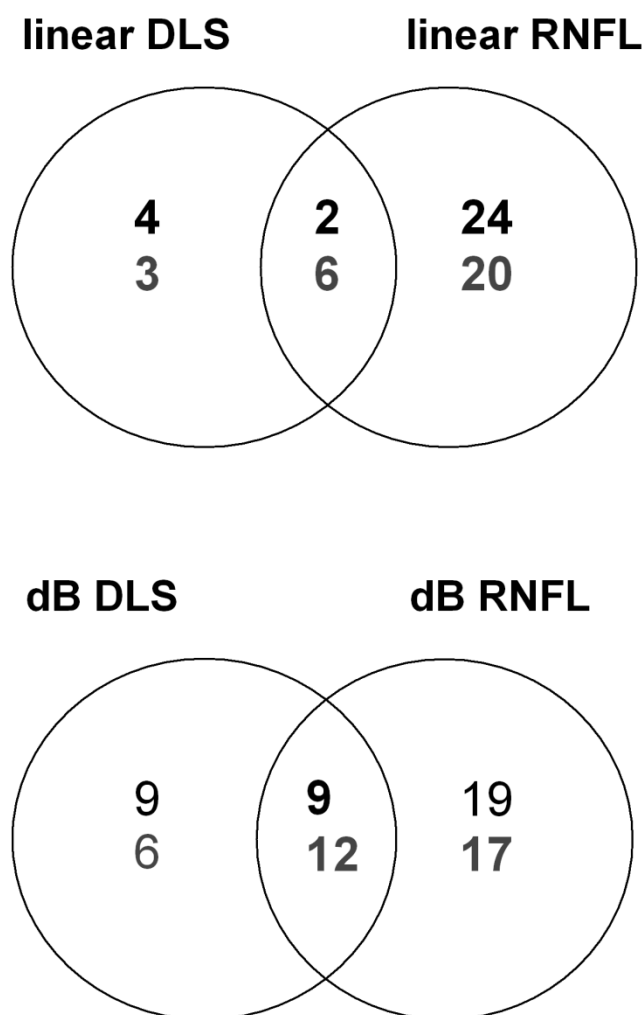
3.6.4 Agreement of abnormality

The 95% confidence prediction limits for normality were computed for DLS and RNFL thickness separately from the data of 65 normal eyes. The percentage of abnormal values (below 95% confidence limits for normality) for DLS and RNFL thickness is depicted in **figure 3.10**. The Venn diagrams in this figure show agreement between DLS and RNFL thickness with both computed in linear-linear units (top diagram) and dB-dB units (bottom diagram) for the 98 patients. Values for the Goldmann size III (black font) and scaled stimulus (grey font) have been compared. In linear units, a greater number of values were abnormal for RNFL thickness than DLS (Chi-square=13.4, $p < 0.001$). In linear-linear units, 2% of values were abnormal for both DLS and RNFL thickness for the Goldmann size III compared to 6% for the scaled stimulus (Chi-square=1.2, $p = 0.08$). Corresponding figures for DLS and RNFL thickness in dB-dB were 9% and 12% respectively (Chi-square=0.21, $p = 0.03$).

The agreement of abnormality between DLS and RNFL thickness, by eccentricity zone, is shown in **figure 3.10**. For locations within 20 degrees, the fraction of abnormal points was similar for the scaled stimulus and the Goldmann size III stimulus ($\chi^2 > 0.3$, $P > 0.3$ in each case). Outside 20 degrees, the proportions of points abnormal for both DLS and RNFL thickness were higher for the scaled stimulus

compared to the Goldmann size III ($\chi^2 = 1.3$, $p=0.08$ for linear-linear and $\chi^2 = 2.7$, $p=0.10$ for dB-dB) but this did not reach statistical significance in this sample.

Figure 3.10: Comparison of the agreement between DLS and RNFL thickness (in terms of percentage of abnormal points) for the Goldmann size III (black font) and the Scaled stimulus (grey, lower figures), $n=784$



3.7 Results II: Gabor patch perimetry

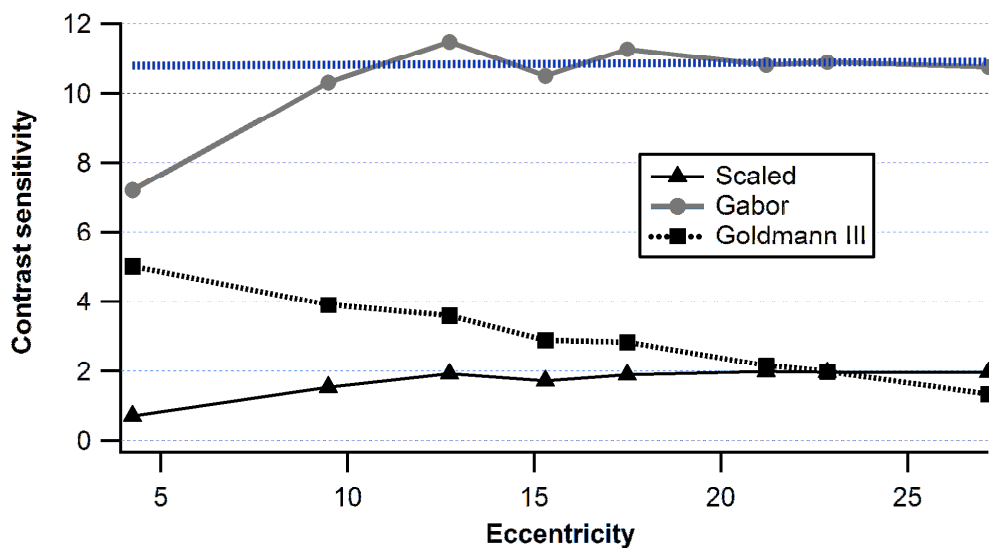
3.7.1 Participants

The mean age ($m \pm sd$) of the glaucoma patients (66 ± 12 ; range 41-85 years) was similar ($t = 0.53$, $p = 0.60$) to the healthy volunteers (65 ± 8 ; range 78-85 years). The average MD was significantly lower ($t = 4.3$, $p < 0.001$) for the glaucoma) patients ($MD = -1.53 \pm 2.10$ dB) than for the healthy volunteers ($MD = -0.18 \pm 1.10$ dB)

3.7.2 Variation of DLS and across eccentricity

Contrast sensitivity for the Gabor patch stimulus was fairly constant across the range of eccentricities tested, **figure 3.11**. With locations at the eccentricity 4.2 degrees excluded, the slope ($-0.006 \text{ L}^{-1}\text{deg}^{-1}$) of the regression (dotted blue) line was close to zero with an intercept at a CS of 10. The mean CS at 4.2 degrees (8.0 ± 3.2) was lower than this intercept value, indicating that scaling of the peak spatial frequency at this eccentricity did not yield the constant sensitivity achieved at other locations.

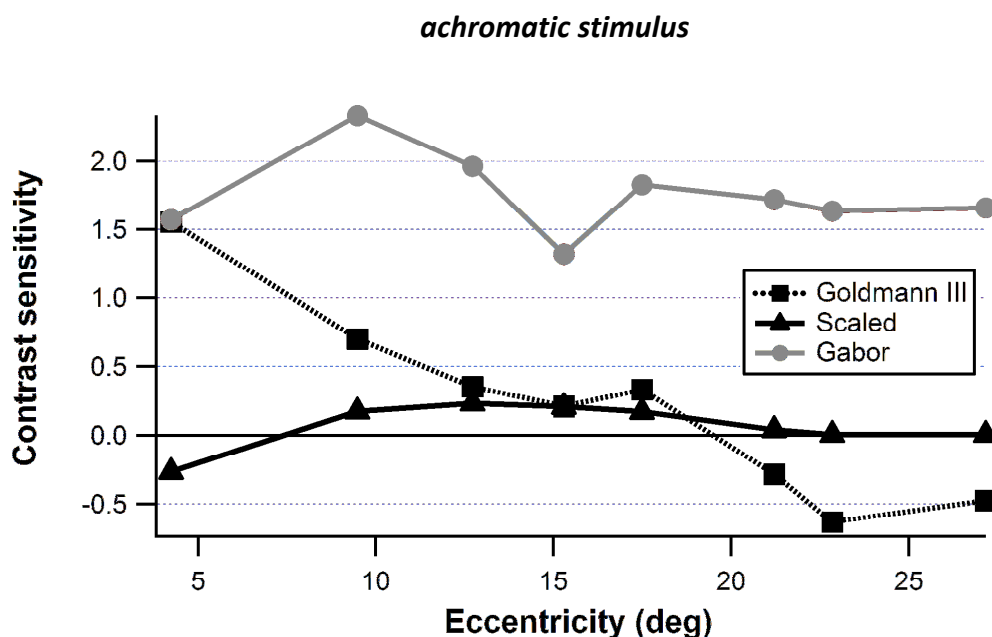
Figure 3.11: Variation of contrast sensitivity of the Gabor patch stimulus with eccentricity. DLS has been plotted in CS for both the achromatic scaled stimulus and the Goldmann size III for comparison



3.7.3 Lower confidence limits for normality

Figure 3.12 shows the lower 95% confidence limit at each eccentricity for the 3 stimuli in contrast sensitivity. For the Gabor patch stimulus, this limit remained above 1 at all eccentricities tested whereas the lower 95% limit was close to zero for the scaled achromatic stimulus at eccentricities greater than 20 degrees.

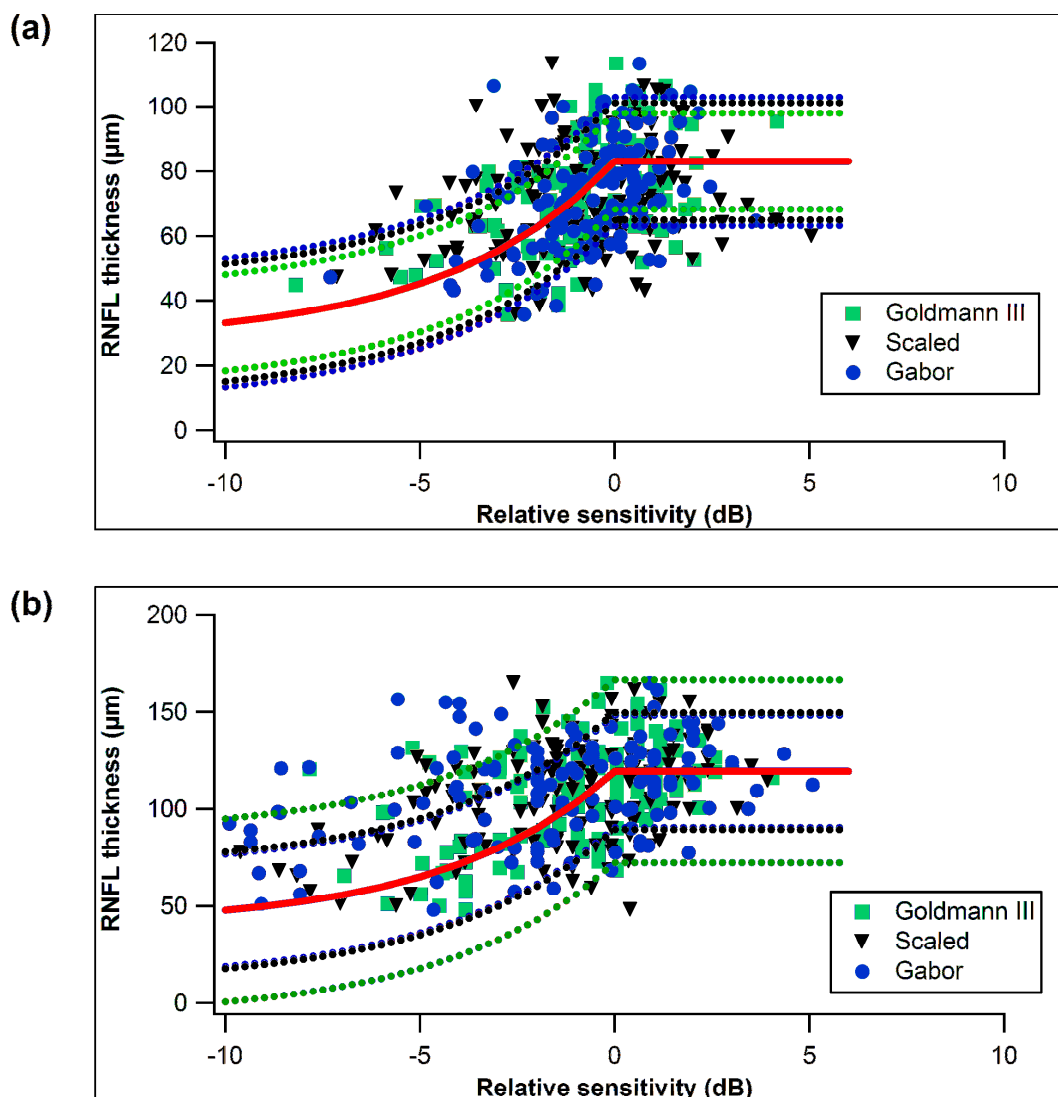
Figure 3.12: Lower (95%) confidence limit for normal subjects at each eccentricity for the Gabor patch stimulus compared to the Goldmann size III and the scaled



3.7.4 Hood-Kardon fits

Figure 3.13 shows the scatterplots (solid symbols) of measured RNFL thickness against relative sensitivity (as defined in equations above). The red line indicates the fitted predicted RNFL values computed from the Hood-Kardon equations [3.12, 3.13] with the confidence limits indicated by the dotted lines. Overall, for all 3 stimuli, a lower proportion of measured points fell above the line of ‘Hood-Kardon’ fit than below ($\chi^2 > 11.3$, $p < 0.0008$).

Figure 3.13: Plots of RNFL thickness (μm) versus relative sensitivity for eccentricities of 4.2 and 27 degrees fitted with the Hood-Kardon model

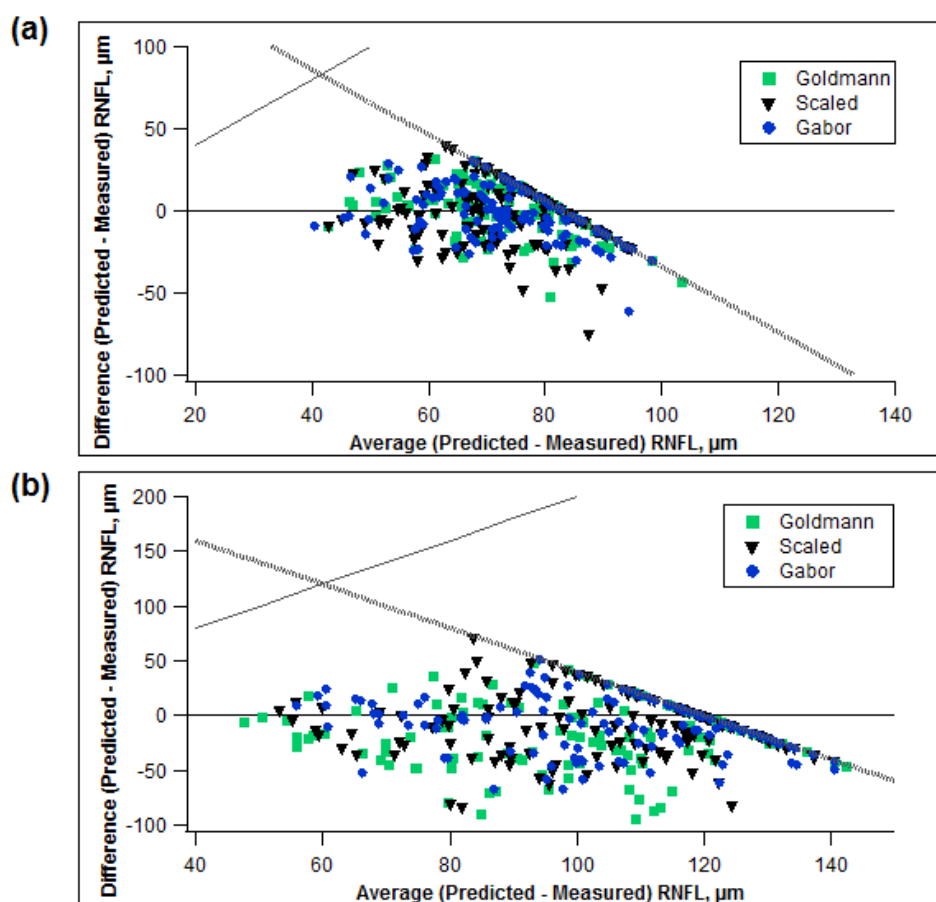


3.7.5 Bland-Altman analysis of agreement

Bland Altman plots of the difference between predicted RNFL values (from the Hood-Kardon model) and measured RNFL thickness versus the average of these two parameters, $av(\text{RNFL}_{\text{predicted}} - \text{RNFL}_{\text{measured}})$, are shown in **figure 3.14** for the

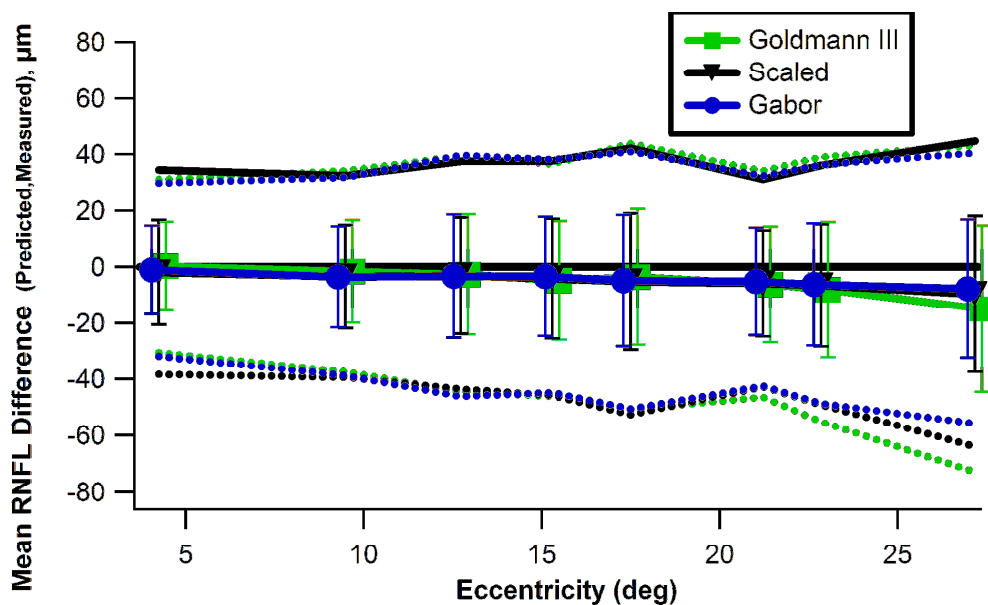
eccentricities of 4.2 and 27 degrees eccentricity. At higher values of $av(\text{predicted, measured RNFL, } \mu\text{m})$, a 'ceiling effect' for the $\text{diff}(\text{predicted, measured RNFL, } \mu\text{m})$ was observed due the 'cap' on predicted RNFL values from the Hood-Kardon equation (solid grey line, **figure 3.14**) whilst the lower limit on RNFL thickness also imposes a limit (dotted grey line).

Figure 3.14: Bland-Altman plots showing the difference versus the average of predicted RNFL thickness (from the Hood-Kardon Model) and measured RNFL thickness, μm for (a) 4.2 Degrees eccentricity; and (b) 27 degrees eccentricity. The dotted grey line and the solid grey lines on the graph shows limits on the agreement difference which is imposed by the Hood-Kardon Model.



The average difference was close to zero across eccentricity (**figure 3.15**) indicating that, on average, predicted values were in agreement with measured values of RNFL. However, the typical standard deviation around these mean values was 20 μm , so that the 95% CI for the difference was approximately $\pm 40 \mu\text{m}$. The sd of the difference was similar for the Gabor patch and Goldmann size III for all eccentricities ($F < 1.4$, $p > 0.03$) except the greatest eccentricity tested: for 27.2 degrees, the sd was lower for the Gabor patch than the Goldmann size III ($F = 2.07$, $p < 0.001$).

Figure 3.15: Bland-Altman mean (solid symbols) and standard deviation (error bars) of agreement for the Gabor patch stimulus across the range of eccentricities tested



3.8 Discussion: Scaled achromatic stimulus

3.8.1 Summary of main findings

For the scaled stimulus sensitivity was independent of eccentricity from 10 deg to 30 deg (**figure 3.7**), and for these eccentricities the scaled stimuli resulted in a relatively constant structure-function ratio while the ratio for size III decreased by 0.6 unit as eccentricity increased. Scaling strengthened the structure/function (DLS versus RNFL thickness) relationship, with RNFL accounting for 26% of the variance in DLS for the scaled stimulus, compared to 3% for the Goldmann size III stimulus.

3.8.2 Importance of findings

Scaling stimulus size by an estimate of regional ganglion cell density created a more constant structure/function relationship across eccentricity compared to the use of a single-sized stimulus at all locations.

It is expected that this would facilitate identification of glaucomatous damage, particularly at central field locations. The finding of a very poor structure/function relation with the Goldmann size III stimulus may explain why glaucomatous damage is thought to be uncommon at central locations until later stages of the disease. Studies of Pattern ERG amplitudes demonstrate functional losses within the macula in glaucoma patients with SAP sensitivity at central locations within the normal range (Bach, Sulimma et al. 1997), suggesting that losses near fixation may remain undetected on conventional perimetry (with the Goldmann size III stimulus). Within the central 10 degrees, more than 30% of the variance in DLS for the scaled stimulus could be accounted for by RNFL thickness, compared with less than 5% for the Goldmann size III stimulus (**table 3.2**).

3.8.3 *Scaling stimulus size and reducing eccentricity dependence*

Early efforts to vary test target size with eccentricity to improve the efficiency to detect early perimetric losses have largely been ignored in modern-day perimetry, where a constant size stimulus is presented throughout the visual field. Goldmann appreciated the need to use small stimuli in the central field and larger stimuli at peripheral locations, as DLS measurement in the periphery is limited by stimulus intensity with small target sizes, particularly in pathological cases (Goldmann 1999). He suggested that size of the kinetic visual field could be equated for different size stimuli by an appropriate scaling of the stimulus luminance by a 'filter value'.

A number of reports have suggested that eccentricity-dependence can be reduced by scaling DLS. Wilson (1970) demonstrated that spatial summation curves at different eccentricities could be superimposed with a horizontal shift (along the sensitivity axis), suggesting the dependence of eccentricity could be reduced by suitable correction. Garway-Heath et al. (2000) compared perimetric data (gathered with the size III stimulus) from Heijl's study (Heijl, Lindgren et al. 1987) of normal subjects and histological ganglion cell counts from Curcio and Allen (1990). The relationship between DLS and the theoretical number of ganglion cells (G) under the Goldmann size III stimulus was linear when DLS was plotted against G^k , where k was termed the coefficient of spatial summation. The value of k varies with both eccentricity and stimulus size (Garway-Heath, Caprioli et al. 2000; Pan and Swanson 2006).

Our scaled stimulus was designed to cover a constant number of ganglion cells across eccentricity. The relative uniformity of DLS across eccentricity suggests that

that this was largely achieved, except at 4.2 degrees eccentricity, where the stimulus size was smaller than that needed to achieve a constant threshold across all eccentricities.

The stimulation of retinal neural units, and the resultant change in DLS, is governed by the area of the stimulus in relation to the critical area for a given location. The scaled stimulus used in the present study was comparable to size to the critical areas derived from studies of spatial summation, (**figure 3.3**) and to scaled stimuli derived from magnification scaling: around 0.20 degrees diameter for static perimetry at 4 degrees eccentricity, (Latham, Whitaker et al. 1994).

Within the central 10 degrees, where the Goldmann size III stimulus is larger than the critical area (**figure 3.3**), the change of DLS with RGC loss in glaucoma is likely to be affected by 'cortical redundancy', where each of the cortical neural units mediating detection samples only a portion of ganglion cells under the stimulus (Pan and Swanson 2006). In this case, ganglion cell damage may not result in abnormal DLS as long as at least one of the neural units samples an undamaged patch of ganglion cells, resulting in poorer structure-function correlations for the Goldmann size III.

3.8.4 Units for structure-function comparisons

Although the primary aim of the present study was to evaluate the effect of scaling stimulus size on structure-function relations, certain inferences can be made regarding the use of linear-linear and log-log units for structure-function comparisons.

Conventionally structural parameters are recorded in linear units whereas visual field sensitivity is recorded in log units. The present study provides support for the linearity of the structure-function relationship for both linear-linear (Garway-Heath, Holder et al. 2002) and log-log units (Harwerth, Carter-Dawson et al. 2004). Further, this linearity has been demonstrated in a population of normal eyes and those with relatively early glaucomatous damage (mean MD -1.18, range -7.7 to 1.9 dB), rather than patients with extreme glaucomatous damage. Previous studies have included a large percentage of glaucomatous eyes with a Mean Deviation loss of greater than 5dB. In one study, one quarter of patients had a MD worse than -5dB (Garway-Heath, Holder et al. 2002; the study by Schlottmann, De Cilla et al. (2004) included patients with a MD of between 0.26 dB and -20.33 dB (with a mean of -6.92 dB); in the study by Reuss and Lemij (2004), the mean MD was -9.39 ± 7.45 dB (SD). As Anderson pointed out, the demonstration of a structure-function relationship in a population ranging from normal to end-stage glaucoma is of little value for the detection of early glaucoma (Anderson 2006).

The interest in linear units for DLS stems from the observation that visual sensitivity in dB relates non-linearly to structural measures. A 1 dB loss of ganglion cells represents a loss of 21% in linear units, whereas a loss of 3 dB corresponds to loss of 50%. Further, for a given amount of dB DLS loss, the predicted ganglion cell loss depends on the test location and varies with the eccentricity and spatial summation coefficient (Garway-Heath, Caprioli et al. 2000). A 3 dB loss may correspond to a loss of nearly 70% of ganglion cells at central locations compared to 30% in the superior periphery. Scaling stimulus size by test location, as in the present study, may reduce this dependence on eccentricity.

Use of linear perimetric DLS expands the normal end of the range of values and compresses the lower-sensitivity end of the range relative to the dB DLS scale. For instance in the present study, the DLS values for the Goldmann size III in normal subjects spanned from 500 L^{-1} (26 dB) to 1700 L^{-1} (32 dB), which represents approximately 70% of the range of values in linear units but only 20% of the range in dB units. Use of linear units increases the variation of DLS across eccentricity for the Goldmann size III stimulus. This effect of increased variation across eccentricity is reduced with scaling stimulus size by estimates of ganglion cell density.

3.8.5 DLS within the central 10 degrees

With locations at 4.2 degrees excluded, DLS remained fairly constant across eccentricity, indicating that the stimulus may be tapping a constant number of ganglion cells across the central 27 degrees. Optical blur for the small stimulus or inappropriate scaling of the stimulus within the macula may account for the decline of sensitivity at the 4.2-degree eccentricity. The mean diameter of the scaled stimulus (0.17 degrees) at 4.2 degrees is in reasonable agreement with critical area from studies of spatial summation. Johnson reported a critical area of 0.17 at 3 degrees (background luminance 3.18 cd/m^2); Dannheim and Drance (1971) found a critical area of 0.12 degrees at 5 degrees eccentricity (same background luminance). Changes in DLS across the central retina may not be entirely accounted for by changes in ganglion cell density (Latham, Whitaker et al. 1993). Within the macula, sensitivity is likely to be governed by cortical and optical factors rather than ganglion cell density (Thibos 1998).

This is, in part, likely to be a sensitivity-related effect. In dB units, variability increases as DLS falls (as stimulus size gets smaller). In linear units, however, variability tends to decrease at lower sensitivities (see Chapter 2). Further work is needed to investigate the test-retest variability of the scaled stimulus at different eccentricities.

3.8.6 Comments on study methodology

Comparison between the Goldmann size III stimulus and the scaled stimulus may be confounded by two factors. Firstly, the order of tests was not randomised for the two stimuli. All subjects underwent testing with the Goldmann size III stimulus under standard clinical test conditions prior to undergoing testing on the customised CRT display because patients were already familiar with this form of perimetry. Secondly, the perimetric strategies used to measure DLS were different for the two stimuli. The SITA standard strategy was used to measure DLS for the Goldmann size III stimulus whereas the Full Threshold strategy was replicated for measuring DLS for the scaled stimulus. The SITA standard strategy was chosen as this is currently the method employed in the clinical setting and takes up to 50% less time to perform than full threshold testing (Bengtsson and Heijl 1998). Measured DLS is, on average, measured 1 dB higher by the SITA standard strategy (which uses a likelihood procedure to estimate threshold) than the full threshold strategy which uses a staircase and measures sensitivity as the last seen stimulus luminance. The effect of higher measured DLS (in dB) with SITA-standard is not sensitivity-dependent (Bengtsson and Heijl 1998; Artes, Iwase et al. 2002). For the Goldmann size III mean DLS varied from 500 L^{-1} (27 dB) to 1700 L^{-1} (32 dB) with the SITA

standard strategy. For the same individuals, mean DLS is expected to be about 1 dB lower across the range of 400 (26 dB) to 1260 (31 dB) with a Full-Threshold algorithm. Measurement of DLS with the SITA standard strategy, may therefore, have an effect of increasing the eccentricity dependence of DLS in linear units, although this effect is expected to be small.

3.9 Discussion II: Gabor patch perimetry

3.9.1 Summary of main findings

For both the Gabor patch stimulus and the Goldmann size III, there was, on average agreement between predicted and measured DLS measurements indicating that, overall structure and functional parameters agree over the range of eccentricities tested. For the furthest locations from eccentricity tested (27.2 deg), the precision around this structure-function agreement was higher for the Gabor patch stimulus compared to the Goldmann size III; at all other eccentricities, the precision of agreement was similar for the 2 stimuli.

For measurement of DLS in linear units, Gabor patch perimetry may aid identification of abnormality as the lower 95% confidence limit for normality remains above zero at all eccentricities, when sensitivity is measured in linear units (*figure 3.12*).

3.9.2 Importance of findings

The findings of this study are in agreement with those of Harwerth (2006), who noted that SAP and RNFL measures were quantitatively similar when both were converted to ganglion cell (GC) density from a model derived from monkey eyes

(Harwerth, Carter-Dawson et al. 2004). For GC density estimates, the standard deviation of predicted GC density for a measured GC density of 40 dB was about 3 dB (Harwerth and Quigley 2006); on a linear scale this yields 95% confidence limits around the prediction from around 30% (lower limit) to nearly 400% (upper limit) of mean normal. For the agreement method presented here, 95% confidence limits ranged from 70% to 170% of mean normal. The current study provides a method of analysing agreement between structural and functional measures in glaucoma by converting DLS to 'equivalent' RNFL. An alternative approach is to express both measures in common metrics and to compute each quantity as a fraction of mean normal (Hot, Dul et al. 2008). Using this method, Hot, Dul et al. (2008) found that, on average contrast sensitivity showed similar degree of loss to rim area for a range of glaucomatous loss, although they did not show a Bland-Altman plot of the same data. In a number of previous studies, structure-function regression analysis has been utilised as an endpoint for structure-function comparisons (Garway-Heath, Holder et al. 2002; Reus and Lemij 2004; Bowd, Zangwill et al. 2006) but this type of analysis provides limited information regarding the concordancy of these 2 measures.

3.9.3 Lower variability around mean agreement for Gabor patch stimulus for locations at eccentricities greater than 20 degrees

The effect of peripheral refractive blur on DLS may explain the low variability around mean agreement for the Gabor. Blur has minimal effect on thresholds for low spatial frequency gratings at 30 degrees eccentricity (Pointer and Hess 1989). In contrast, sensitivity for the Goldmann size III stimulus diminishes approximately

75% from a 2D defocus at the same eccentricity (Anderson 2001). Astigmatism increases from 0 in the fovea to over 5D at 40 degrees eccentricity in normal eyes.

3.9.4 Comments on study methodology

Similar to the scaled achromatic stimulus presented in the previous section, the Gabor patch stimulus achieved constant sensitivity at all eccentricities except 4.2 degrees. As the peak spatial frequency of the Gabor patch stimulus at the closest location to the fovea was 1.2 cpd, it is unlikely to have been affected by optical defocus, given that firstly low spatial frequency gratings are minimally affected by optical blur near the fovea and secondly participants were all corrected for foveal refractive error. All participants had vision acuity of 6/9 or better and had acuity checked at the test distance. Therefore, it is likely that the spatial frequency of the stimulus at this location was too high to achieve constant sensitivity. Keltgen and Swanson (2009) investigated spatial scale across the central visual field and found that it did not decline as rapidly as ganglion cell density with eccentricity.

The method of agreement analysis presented here utilises the Hood-Kardon model for predicting RNFL thickness from contrast sensitivity. Bias in the RNFL estimation by the model, therefore contributes to any error in the difference of predicted and measured RNFL thickness. A number of assumptions are made in the Hood-Kardon model, for instance: RNFL thickness is independent of sensitivity in eyes with a relative sensitivity greater than zero and the 'base' non-ganglion cell related RNFL thickness is a constant percentage of overall thickness for healthy eyes.

CHAPTER 4

The Photopic negative response of the Flash ERG and other functional measures of glaucomatous optic neuropathy

4.1 Aims

The purpose of investigations in this chapter was to compare:

- (i) The ability of the PERG and the PhNR response of the flash ERG for identifying functional loss associated with glaucomatous optic neuropathy (GON). The diagnostic accuracy of both the transient PERG (N95—P50) amplitude and the PERG ratio from steady-state recordings were compared to the PhNR using a structural reference for glaucoma diagnosis.
- (ii) The structure-function relationships for DLS and the PhNR using RNFL thickness measurements from both ocular coherence tomography (OCT) and scanning laser polarimetry (SLP). The hypothesis that the PhNR has similar diagnostic capability for identifying GON to global measures of visual field loss in a population defined by optic nerve head appearance was also tested.

4.2 The photopic negative response and the pattern ERG

Primary open angle glaucoma is characterised by death and loss of retinal ganglion cells (Quigley, Dunkelberger et al. 1989; Harwerth, Carter-Dawson et al. 1999) and progressive nerve fibre atrophy (Varma, Quigley et al. 1992). Non-invasive tests which provide an objective measure of ganglion cell activity are an invaluable tool for glaucoma diagnosis and evaluating disease progression.

The Pattern ERG (PERG) is one such objective marker of ganglion cell function. Maffei and Fiorentini's early experiments demonstrated an abolished PERG response in an animal eye whose optic nerve was surgically transected (Maffei and Fiorentini 1982; Maffei, Fiorentini et al. 1985). Subsequent studies have reported the PERG to be affected in glaucoma and other optic neuropathies (Holder 1987; Bach, Hiss et al. 1988). Whilst mean group amplitudes in glaucomatous eyes are often reduced compared to normal eyes (Wanger and Persson 1983; O'Donoghue, Arden et al. 1992; Neoh, Kaye et al. 1994; Ruben, Arden et al. 1995; Martus, Korth et al. 1998; Garway-Heath, Holder et al. 2002), the diagnostic ability of the PERG at an individual level is limited by high normal inter-individual variability (Bach, Hiss et al. 1988), high test-retest variability (Holopigian, Snow et al. 1988) and substantial overlap of individual amplitudes from normal and glaucomatous eyes (Korth, Horn et al. 1989; Ruben, Arden et al. 1995; Garway-Heath, Holder et al. 2002; Hood, Xu et al. 2005). Typically, PERG amplitudes vary by a factor of more than 3 across normal subjects.

Accounting for age-effects may aid in reducing the normal variation of PERG amplitudes in normal eyes, but the precise variation of PERG amplitude with age is

controversial: some investigators have reported a linear reduction of PERG amplitude with age (Korth, Horn et al. 1989; Trick 1992), whilst another study showed amplitudes to decline only after 65 years of age (Bach and Speidel-Faux 1989). Further, the rate of decline may depend on the spatial characteristics of the stimulus (Trick 1992). Since PERG amplitudes to small check stimuli are preferentially affected in glaucoma (Bach and Speidel-Fiaux 1989; Korth, Horn et al. 1989; Pfeiffer, Birkner-Binder et al. 1991). Bach has advocated the use of the 'PERG ratio' from steady-state (SS) recordings, where PERG amplitudes to a small check stimulus are normalised by PERG amplitude to a large check stimulus within the same eye (Bach 2001). The PERG ratio measure has been shown to improve the sensitivity of the PERG to identify glaucoma (Bach, Hiss et al. 1988) and to be a predictor of ocular hypertensive individuals at risk of developing glaucoma (Bach, Unsoeld et al. 2006). Rapid stimulation with the PERG stimulus through SS recording may reveal a more pronounced amplitude reduction in glaucomatous eyes compared with transient PERG recording (Bach and Speidel-Fiaux 1989) and accordingly, the 'Freiburg paradigm' utilises the PERG ratio from SS PERG recordings (Bach 2001).

Historically, the flash Electroretinogram was regarded as having little role in the diagnosis of glaucoma (Leydhecker 1950). The components of the flash ERG reflect the activity of photoreceptor rods and cones as well as bipolar cells. Although there is an indirect suggestion that bipolar cells may be affected by glaucoma (Wassle, Chun et al. 1987), the 'a' and 'b' waves of the flash ERG can be normal in eyes even blind with the condition (Bach, Gerling et al. 1992). However, refinement of electrodiagnostic testing and recording techniques has allowed the identification of

finer components of the flash ERG which may be altered by ganglion cell loss. Relatively recently, a slow negative component following the 'b' wave termed the *photopic negative response* by Viswanathan, Frishman (1999) has been shown to be dependent on ganglion cell activity.

Unlike the PERG, precise fixation stability and a meticulous correction of optical refraction are largely not necessary for recording the flash ERG. Measurement of the PhNR, therefore, offers a potential means of gauging ganglion cell activity in patients who are unable to fixate precisely for the PERG and psychophysical tests or who have poor visual acuity. PhNR amplitudes correlate with visual field and structural measures of glaucoma (Machida, Gotoh et al. 2008).

Drasdo, Aldebasi et al. (2001) compared the PhNR elicited by stimulation of the L&M cones and the S cones, separately, with the transient PERG and found a mean reduction in the magnitude of both types of PhNR response and the PERG in glaucomatous eyes. The area under the ROC curve was 0.86, 0.73 and 0.81 for the S cone PhNR, L&M cone PhNR and the PERG, respectively, and the authors proposed this S-cone response to be a selective indicator of early glaucomatous damage. However, the practical measurement of the S-cone PhNR is challenging: the wave is of small amplitude and has a high noise / signal ratio. The S cones constitute less than 10% of all cones (Marc and Sperling 1977).

A source of bias affecting studies of the PERG and flash ERG for the identification of glaucoma is the selective inclusion of glaucoma cases with established field loss on conventional perimetry. This precludes meaningful comparison of the diagnostic ability of electrophysiological tests with visual field testing (because all subjects have visual field loss, by definition) and the stringent definition of glaucoma, with

possible omission of milder cases of disease, is a potential source of inaccuracy in the reporting of the ability of diagnostic tests (Medeiros 2007).

4.3 The photopic negative response and visual field indices

Visual field testing, in the form of Standard Automated Perimetry (SAP) which involves thresholding of Differential Light Sensitivity (DLS) at a number of pre-defined retinal locations, remains the gold standard functional test for the assessment of glaucomatous optic neuropathy (GON). Although electrodiagnostic tests such as the Pattern ERG and multifocal VEP have exhibited some potential for glaucoma diagnosis, their usefulness has been limited by high interindividual variability (Pfeiffer and Bach 1992; Trick 1992; Dandekar, Ales et al. 2007) and low diagnostic sensitivity (Stroux, Korth et al. 2003) relative to SAP.

The Flash Electroretinogram (ERG), which is technically easier to record than the Pattern ERG and has a relatively higher signal-noise amplitude, has been traditionally rendered redundant for the diagnosis of glaucoma but the Photopic Negative Response (PhNR) has shown promising potential in this regard during the last decade (Colotto, Falsini et al. 2000; Drasdo, Aldebasi et al. 2001; Viswanathan, Frishman et al. 2001; Machida, Gotoh et al. 2008). PhNR amplitudes are reduced in glaucomatous eyes compared with normal eyes (Viswanathan, Frishman et al. 1999; Viswanathan, Frishman et al. 2001; Machida, Gotoh et al. 2008) and this response is related to both structural and psychophysical measures of glaucoma in human eyes (Colotto, Falsini et al. 2000; Viswanathan, Frishman et al. 2001; Machida, Gotoh et al. 2008). The PhNR is a ganglion cell-dependent response which can reliably

distinguish eyes with glaucomatous visual field loss from 'normal' eyes (Viswanathan, Frishman et al. 1999).

Presently, there are no reliable estimates of diagnostic accuracy for the PhNR compared to SAP. The sensitivity of any new diagnostic test should be reported relative to the sensitivity of the 'gold standard' test and its role in the diagnostic pathway should be apparent (Bossuyt, Reitsma et al. 2003). To date, studies of the PhNR in glaucoma have used the results of SAP as an inclusion criterion (Colotto, Falsini et al. 2000; Viswanathan, Frishman et al. 2001; Machida, Gotoh et al. 2008), thereby not allowing a fair comparison of the sensitivity and specificity of the PhNR with SAP for the assessment of GON.

To quantify disease stage, the relationship between clinical markers of disease severity and ganglion cell number should be apparent. Structural and functional parameters are assumed to be related to ganglion cell number in glaucoma and both diminish as disease advances (Heijl, Bengtsson et al. 2009). The relationship between DLS and surrogate measures of ganglion cell number is recognised but the association between the PhNR and retinal nerve fibre layer has only recently gained interest (Machida, Gotoh et al. 2008). Global indices, such as Mean Deviation (MD) from SAP provide a summary measure of the visual field and are useful for disease staging (Katz 1999). Both MD (Ajtony, Balla et al. 2007) and average DLS measures, measured in decibels dB, are related to structural parameters in glaucoma in a non-linear manner (Garway-Heath, Holder et al. 2002; Schlottmann, De Cilla et al. 2004). Once DLS is 'unlogged', the structure-function relationship becomes more linear (Garway-Heath, Holder et al. 2002). For the PhNR to serve as a clinical indicator of

disease stage, its relationship to Retinal Nerve Fibre Layer thickness requires detailed evaluation.

Ocular Coherence Tomography (OCT) and Scanning Laser Polarimetry (SLP) both provide an objective and reproducible (Budenz, Fredette et al. 2008; Mai and Lemij 2008) means of measuring ocular RNFL thickness through different technologies. SLP utilises the birefringence property of the RNFL whilst OCT employs interference characteristics of a reflected and reference light beam to construct a tomographic retinal image.

4.4 Methods

4.4.1 Study definition of glaucomatous optic neuropathy

Perimetric and electrodiagnostic tests both provide assessments of visual function and test results are correlated (Garway-Heath, Holder et al. 2002). Therefore, visual fields were not used to define the glaucoma cohort in order to minimise selection bias in the test population, and to allow a comparison of the diagnostic precision of the electrophysiological tests with visual field testing.

Instead, a structural definition of normality and glaucoma was used in order to compare the psychophysical / electrophysiological tests against a (non function-related) common reference. The structural definition allowed the potential inclusion of patients with ocular hypertertension (OHT) and GON, but normal visual fields, and normal or abnormal electrophysiology.

The structural definition for glaucoma was an 'outside normal limits' Heidelberg retina tomograph (HRT) Moorfields Regression Analysis (MRA) classification

(Wollstein, Garway-Heath et al. 1998) in the context of raised intraocular pressure at diagnosis. The prior probability for glaucoma, based on raised IOP, is about 40% (population prevalence of raised IOP = 3.5%, population prevalence of glaucoma with raised IOP = 1.4%, $1.4/3.5 = 0.4$), (Bonomi, Marchini et al. 1998). The likelihood ratio for the HRT MRA 'outside normal limits' classification, for a population with a visual field average (standard deviation) mean deviation of $-4.87 (\pm 3.9)$ dB and a normal-field normal group, is 19.4 (Zangwill, Jain et al. 2007). A pre-test probability of 40% combined with a likelihood ratio of 19.4 gives a post-test probability of 93% (Garway-Heath and Friedman 2006; Garway-Heath 2008). Thus the definition of glaucoma in this cohort can be given in probabilistic terms, and independently of the outcome measure of the study.

The structural definition for normal subjects was a 'within normal limits' HRT MRA classification in the context of normal IOP (always <22 mmHg). The prior probability for glaucoma, based on a normal IOP is about 0.6% (population prevalence of normal IOP = 96.5%, population prevalence of normal tension glaucoma 0.6%, $0.6/96.5 = 0.0062$). The likelihood ratio for the HRT MRA 'within normal limits' classification is 0.35 (Medeiros, Zangwill et al. 2004). A pre-test probability of 0.6% combined with a likelihood ratio of 0.35 gives rise to a post-test probability of 0.2%.

4.4.2 *Participants*

Thirty patients and 23 age-similar healthy volunteers were recruited between September 2004 and August 2006. The patients were recruited from the OHT and glaucoma clinics and from a pool of referrals from the primary care service ('phenotyping clinic'). Common inclusion criteria for patients and healthy

volunteers were: age above 40 years, white European ethnicity, spherical refractive error less than 6D and cylindrical refractive error less than 2D and visual acuity 20/30 or better. Recruitment was limited to subjects of white ethnic origin as optic disc morphology is known to vary amongst different racial groups and the accuracy of the HRT to identify GON may be race-dependent (Zelevsky et al. 2006). Additionally, normal subjects were excluded if there was any previous history of ocular disease affecting the posterior segment or a positive family history of glaucoma in a first degree relative.

4.4.3 Tests performed

Electrodiagnostic tests were performed within 4 months of imaging. Participants attended for 2 study visits: Imaging with the Scanning laser ophthalmoscope (HRTII) was performed at the first visit and electrodiagnostic tests were undertaken on a subsequent visit.

All glaucoma patients were regular attendees at clinics at Moorfields Eye Hospital and all the healthy volunteers took part in a parallel psychophysics study. The results of recent (within 6 months) and reliable (fixation losses $\leq 33\%$, false positive rate $\leq 15\%$) visual field testing using Standard Automated Perimetry (SAP; Humphrey Field Analyzer II-i series, Carl Zeiss, Humphrey Division, Dublin, CA) using the SITA-Standard test strategy. Global indices from visual field measures (Mean Deviation, MD; Pattern Standard Deviation, PSD) were used to provide a marker of glaucoma severity.

4.4.4 Scanning laser ophthalmoscopy (HRT II Imaging)

All participants were imaged using the HRT. The mean topography of 3 images was acquired using the available software and were later recomputed using the HRTIII software (version 3.0) which had become available during the course of the study. Only high quality images with a mean standard deviation of mean pixel height (MPHD) of less than 50 μm were accepted. The optic nerve head contour line was drawn by one of two experienced technicians and subsequently checked by a clinician (RM). Rim area was computed using the standard reference plane.

4.4.5 Scanning Laser Polarimetry

All participants underwent imaging with the GDx Nerve Fiber Analyzer, software version 5.5.1; Carl-Zeiss Meditec, Dublin, CA) to permit an estimation of the RNFL thickness using the 'enhanced corneal compensation' setting . Only well-centered, well-focused, evenly illuminated images of high quality were accepted. Images with a quality ('Q' score) of less than 8 were discarded. A detailed description of this software is given elsewhere (Reus, Zhou et al. 2006). The GDxVCC utilises a variable corneal compensator that allows compensation for birefringence arising from the anterior segment.

Images of the macula were first obtained to assess the magnitude and axis of corneal birefringence. Three compensated' images of the peripapillary RNFL were then acquired automatically and combined to generate a mean image. The reflection image of the fundus was used to mark an ellipse around the margin of the optic disc. The GDxVCC software positioned a circle of annulus of inner diameter 54 pixels and width 8 pixels on the centre of the ellipse to give 256 evenly-distributed retardation values around the circle. The average retardation for each sector

(temporal; superior; nasal; inferior) could be determined as well as the overall circumferential 'TNSIT' average.

4.4.6 Electrodiagnostic tests

All PERG and flash ERG test results were reported by a consultant electrophysiologist and measurements were performed by an electrodiagnostic technician. Both were masked to the subject diagnosis.

Pattern ERG

1. Transient PERG

The conditions for recording and measurement of the transient PERG was consistent with the recommendations proposed by the International Society for Clinical Electrophysiology of Vision (Bach, Hawlina et al. 2000; Holder, Brigell et al. 2007). The stimulating field was provided by a CRT monitor (Mitsubishi Diamon Plus 230 50cm visible screen) with a refresh rate of 87.5Hz. Recordings were obtained using corneal and lateral canthal gold foil electrodes with a viewing distance of 152 cm using the usual distance refractive correction.

The checkerboard stimulus subtended 14.8° by 10.4° on the retina and comprised checks of high contrast (between 95% and 98%), with each check subtending 0.75°. Transient responses were recorded at a pattern-reversal rate of 4.4 rev/s. Approximately 150 responses were averaged for each recording and at least 3 responses were recorded for each eye. The magnitude of the transient response was measured from the peak of the P50 component to the trough of the N95

component (Holder, Brigell et al. 2007). For simplicity, this N95—P50 amplitude measurement is referred to hereafter as the ‘transient PERG (tPERG) amplitude’.

2. Steady-state PERG

The steady state PERG was recorded with a larger field size than the transient PERG (36 by 27 deg) by reducing the eye-monitor distance to 60 cm. An appropriate refractive correction for near was used. This larger field size has been advocated to be better suited to the early detection of glaucoma by stimulating a larger retinal area (Bach, Hiss et al. 1988; Bach, Hawlina et al. 2000). To replicate the ‘Freiburg PERG paradigm, (Bach, Hiss et al. 1988; Bach and Speidel-Fiaux 1989; Bach 2001), both small and large check stimuli were employed. The small check stimulus subtended 0.8 degrees at the test distance, whilst the large check size subtended 13 degrees. For this large check condition, the screen contained only four square-shaped checks. Recordings were made at a fixed stimulus frequency of 8Hz (16 rev/s). At this frequency, the measured stimulus rate was 7.9 Hz (15.8 rev/s).

Trend artefacts were corrected. Steady-state PERG amplitudes were analysed using a customised macro in Igor Pro (4.09, Wavemetrics Inc., Inc., Lake Oswego, OR) to isolate the response amplitude at 7.9 Hz. A ‘window’ function was not used to filter the recordings as this can introduce measurement artefacts and is not considered necessary for SS PERG potentials when the exact stimulus frequency is known (Bach and Meigen 1999). A discrete Fourier transform was computed with an integer number of waveform cycles.

Flash ERG

1. Standard ERG

Standard photopic ERG's were obtained with a stimulus frequency of both 2Hz and 30Hz after pupillary dilatation with 1% tropicamide and 2.5% phenylephrine and light adaptation for 8 minutes. A standard (white) flash ERG was performed to exclude a general cone abnormality and to provide baseline measurements of the 'a' and 'b' wave under photopic conditions.

2. PhNR recording

The PhNR was recorded with conditions similar to that used by Viswanathan and colleagues (Viswanathan, Frishman et al. 1999; Viswanathan, Frishman et al. 2001). A red flash (wavelength 655 nm) of 5 ms duration and intensity 660 cd/m^2 on a blue rod-saturating background (425 nm) of luminance 4.9, 1.6 and 0.49 cd/m^2 was employed. The results in terms of sensitivity / specificity analysis were very almost identical for each of these 3 background luminances and the results for one of these conditions (background luminance of 0.49 cd/m^2) is presented here for simplicity. Consistent with the methodology of Viswanathan et al. (1999, 2001), the amplitude of the PhNR was measured from the baseline to trough following the 'b'-wave at approximately 70 ms. In most individuals, 2 distinct negative components followed the 'b' wave at latencies of approximately 55 ms and 70 ms. The observation of 2 distinct negative components following the 'b' wave has been noted by other investigators (Gotoh, Machida et al. 2004; Machida, Gotoh et al. 2008). We used only the latter of these as prior pilot studies done in our laboratory revealed that

the first negative response at around 55 ms is often unrecordable in healthy eyes (unpublished data).

4.4.7 Data analysis

Analysis of amplitudes and comparison of mean values

For the transient PERG amplitude, steady-state PERG ratio and PhNR, mean values from normal and glaucomatous eyes were compared using a two-tailed t-test. Data distribution was approximately Gaussian for each of the 3 measures.

Variances of PERG and PhNR measures for the healthy volunteers were compared with an F-test by computing each as a fraction of the corresponding mean value.

Linear regression analysis of tPERG amplitude, SSPERG ratio and PhNR amplitude versus rim area

PERG and PhNR measures were plotted against corresponding HRT neuroretinal rim area. To evaluate spatial correspondence of the PERG field size to the optic nerve head (ONH), the size of the PERG checker-board was overlaid on a standard 24-2 visual field grid. The correspondence of retinal location to the ONH has previously been reported (Garway-Heath, Poinoosawmy et al. 2000). The transient PERG field (14.8 by 10 degrees) maps to the temporal HRT disc sector whilst the steady state field (36 by 27 deg) localises to most sectors except the nasal sector (*figure 4.1*). As the PhNR is a panretinal response, global HRT rim area measures were used for the regression analysis of PhNR amplitude versus rim area. *Figure 4.1* illustrates the rim area sectors which were used for regression analysis for the transient and steady-state PERG.

Computation of a linear global visual field measure

Some preliminary work has previously been initiated for developing global visual field indices in linear units (Dul, Malik et al. 2004). For each value of the 52 values of DLS (dB) obtained for each participant, pointwise Linear values of DLS (L^{-1}) were obtained by equation [1.2].

The average of these 52 values was taken as a global measure of visual field damage, in linear units, for each individual and was denoted by the term average '*linear DLS*' hereafter.

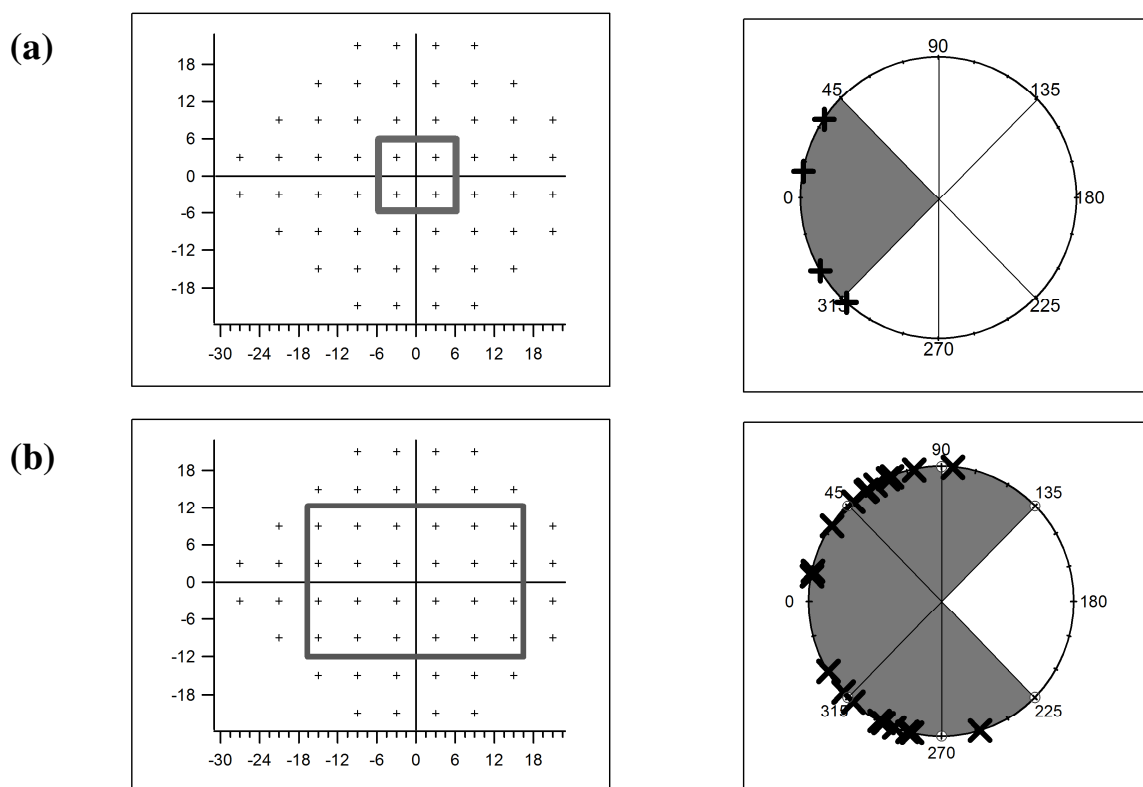
Mean value of MD, linear DLS and PhNR in normal and glaucomatous eyes

The average values of MD, linear DLS and PhNR amplitude were compared in normal and glaucomatous eyes using a two-tailed t-test.

The relationship between visual field measures and PhNR with RNFL thickness

The relationship between MD and PhNR was analysed. Linear regression coefficients for plots of Linear DLS versus RNFL thickness and PhNR versus RNFL thickness were compared.

Figure 4.1: The spatial correspondence of the retinal area stimulated by the PERG to the optic nerve head (ONH) was estimated by overlaying the PERG field size (a) Transient PERG; (b) Steady-State PERG field) on a standard 24-2 Humphrey visual field test grid. Points for the right eye are shown. The black crosses indicate points mapped to the ONH from within the PERG field. The shaded grey areas indicate rim area sectors for the HRT which were used for linear regression analysis of PERG measures versus rim area.



Agreement analyses

The agreement between (abnormally) low RNFL thickness and functional (PhNR, MD and average linear DLS) was depicted using Venn diagrams. The criterion values

corresponding to a specificity of around 90% identified from the ROC analysis were used as 'cut-off' values to demarcate low values of each parameter.

Receiver Operator Curve Analysis

ROC curves for discrimination of normal and glaucomatous eyes were plotted for the tPERG, SSPERG ratio and PhNR. The area under the ROC curve for the PhNR was compared that for the tPERG and the SSPERG ratio. The sensitivity of each parameter to identify glaucomatous optic neuropathy for a fixed specificity of around 90% was assessed. Similar ROC curves were plotted for the visual field measures (linear DLS, MD) and the PhNR. Statistical tests and ROC analysis was carried out with MedCalc (version 7.4).

Agreement of abnormal PERG and PhNR values

The criterion values corresponding to 90% specificity identified by ROC analysis were used as cut-off values to classify individual values as 'normal' or 'abnormal'. The agreement of abnormal PERG and PhNR measures in eyes with GON was depicted by means of a Venn diagram.

4.5 Results I: The photopic negative response and the pattern ERG

The mean \pm SD age of the 30 glaucoma patients (69.8 ± 7.1 years) was similar ($t=1.8$, $p=0.08$) to the mean age of the 23 healthy volunteers tested (66.3 ± 7.4 years).

The average (\pm SD) MD from SAP (-5.5 ± 6.40 dB) and global rim area (0.78 ± 0.30 mm²) of the patients was less ($t>3.9$, $p<0.001$) than the normal subjects (average

MD -0.12 ± 1.24 dB; global rim area 1.42 ± 0.26 mm²). Seven of the glaucoma patients did not have any evidence of field loss on SAP.

4.5.1 Mean and individual electrophysiological values

The mean 'a' wave (-49.9 ± 13.1 μ V for normals and -44.8 ± 11.2 μ V for glaucoma patients) and 'b' wave amplitudes (53.4 ± 21.4 μ V for normals and 56.2 ± 19.6 μ V for patients), for the red flash on the blue background condition, were similar ($t < 0.5$, $p > 0.10$ in each case) for normal subjects and glaucoma patients. Mean values for the tPERG, SSERG ratio and PhNR shown in **table 4.1**. The mean tPERG, SSERG ratio and PhNR were all significantly different in glaucomatous eyes compared to normal eyes ($t > 3.0$, $p < 0.01$).

Table 4.1: Mean values for tPERG, SSERG ratio and PhNR amplitude in normal (n=23) and glaucoma (n=30) groups. *'Transient PERG amplitude' indicates measurement of N95 from peak of P50, PhNR = Photopic Negative Response, SS = Steady-State, tPERG= transient Pattern Electroretinogram, MD = Mean Deviation*

	MD (dB)	Transient PERG N95 Amplitude (μ V)	Steady State PERG ratio	PhNR (μ V)
Normal	-0.12 ± 1.24	3.27 ± 0.91	1.10 ± 0.28	-28.4 ± 10.3
Glaucoma	-5.5 ± 6.40	2.42 ± 0.78	0.88 ± 0.22	-17.3 ± 12.8
	t=4.0	t = 3.66	t = 3.19	t = 3.40
	P<0.001	P <0.001	P = 0.0024	P = 0.0013

With measures computed as a percentage of mean normal, the standard deviation of the tPERG (28%) and SSPERG ratio (26%) across normal individuals was similar ($F=1.7$, $p=0.22$; $F=1.15$, $p=0.74$, respectively) to that of the PhNR (36%).

The arrows in **figure 4.2** indicate measurements from a normal subject ('1') and 2 glaucoma patients ('2' and '3'). The black dotted lines show the criterion values identified by ROC analysis (see section below) corresponding to 90% specificity. The raw PERG and flash ERG recordings for these participants are shown in **figure 4.3**. For the tPERG, SSPERG ratio and PhNR, there was substantial overlap of the distribution of individual measures between normal and glaucomatous eyes. The normal subject ('1') was 56 years of age and had a tPERG amplitude (4.0 μV), SSPERG ratio (1.47) and PhNR (-52.6 μV) within the normal range. Patient 2 (age 74 years, MD -7.7 dB) had a tPERG amplitude of 1.29 μV and a PhNR amplitude of -1.29 μV . The SSPERG amplitude to the 0.8 check was 0.69 μV and to the 13 degree check was 1.42 μV , giving a PERG ratio of 0.49. The second patient shown ('3') was 70 years of age and had extensive field loss on conventional automated 24-2 perimetry (MD -12 dB). The tPERG amplitude was subnormal (2.6 μV). SSPERG amplitudes to the 0.8 and 13 degree check sizes were 3.31 μV and 3.85 μV respectively (PERG ratio = 0.86) and the PhNR amplitude was also low (-3.5 μV).

4.5.3 Relationship between the PERG, PhNR and rim area

Figure 4.4 shows plots of tPERG amplitude, SSPERG ratio and PhNR versus rim area. In each case, the relationship was approximately linear. R^2 values for linear regression were similar ($t=0.24$, $p=0.81$) for the plot of tPERG versus rim area

($R^2=0.21$) and PhNR versus rim area ($R^2=0.17$); R^2 values for SSPERG ratio ($R^2=0.17$) and PhNR versus rim area were also similar ($t=0.01$, $p=0.99$).

Figure 4.2: Scatterplot of individual values of the (a) tPERG, (b) SSPERG ratio and (c) PhNR in normal (average Mean Deviation, MD -0.12 ± 1.24 dB) and glaucomatous eyes (average MD -5.5 ± 6.40 dB). Arrow indicate values for one normal healthy volunteer (1) and 2 glaucoma patients (2,3) whose recordings are shown in **Figure 5 and discussed in the text. The horizontal dashed lines indicate the criterion values corresponding to 90% specificity.**

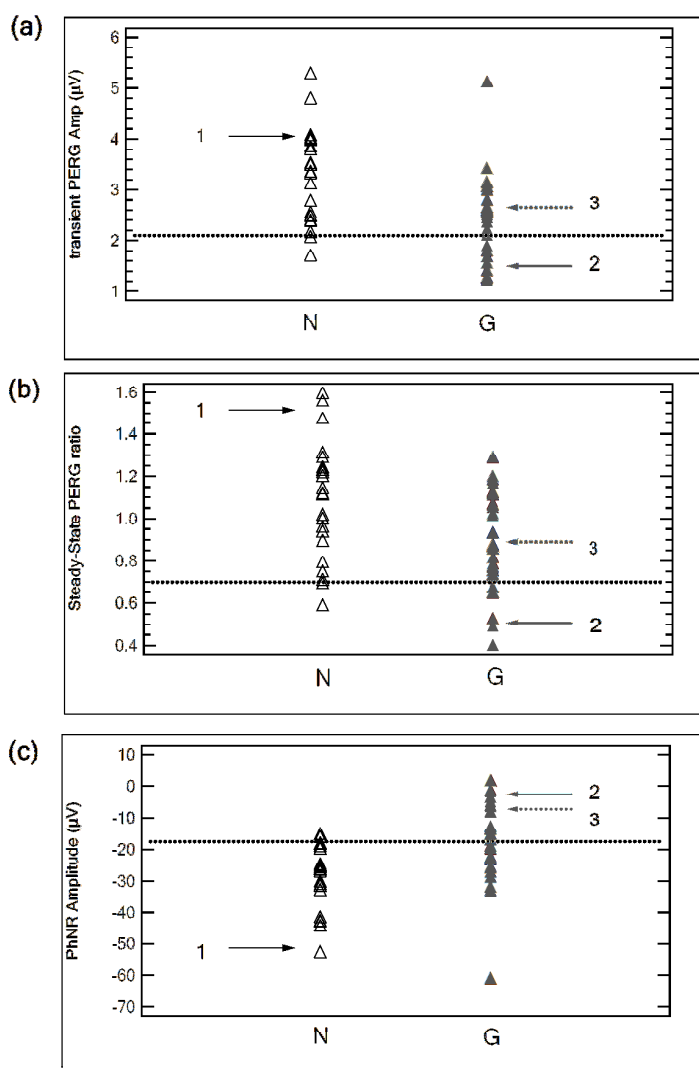
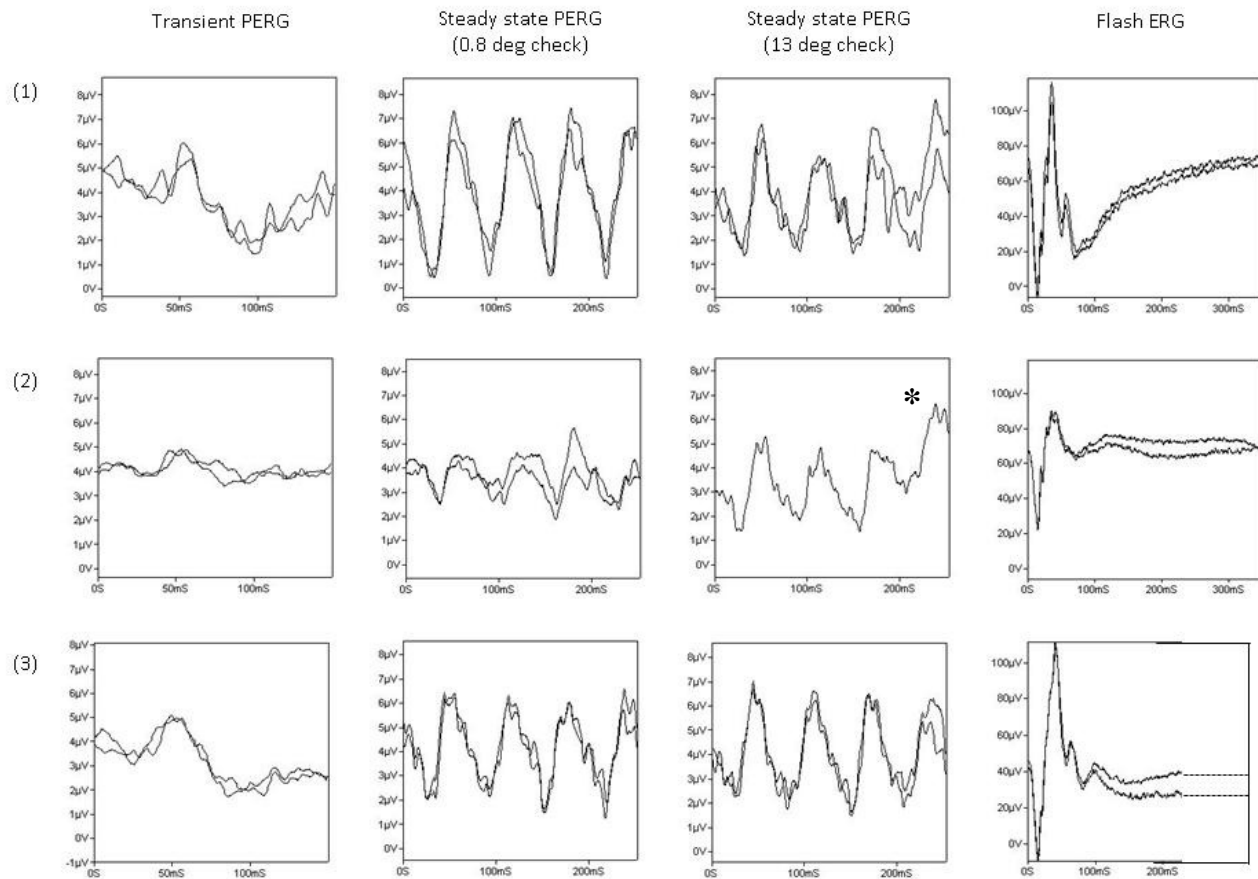
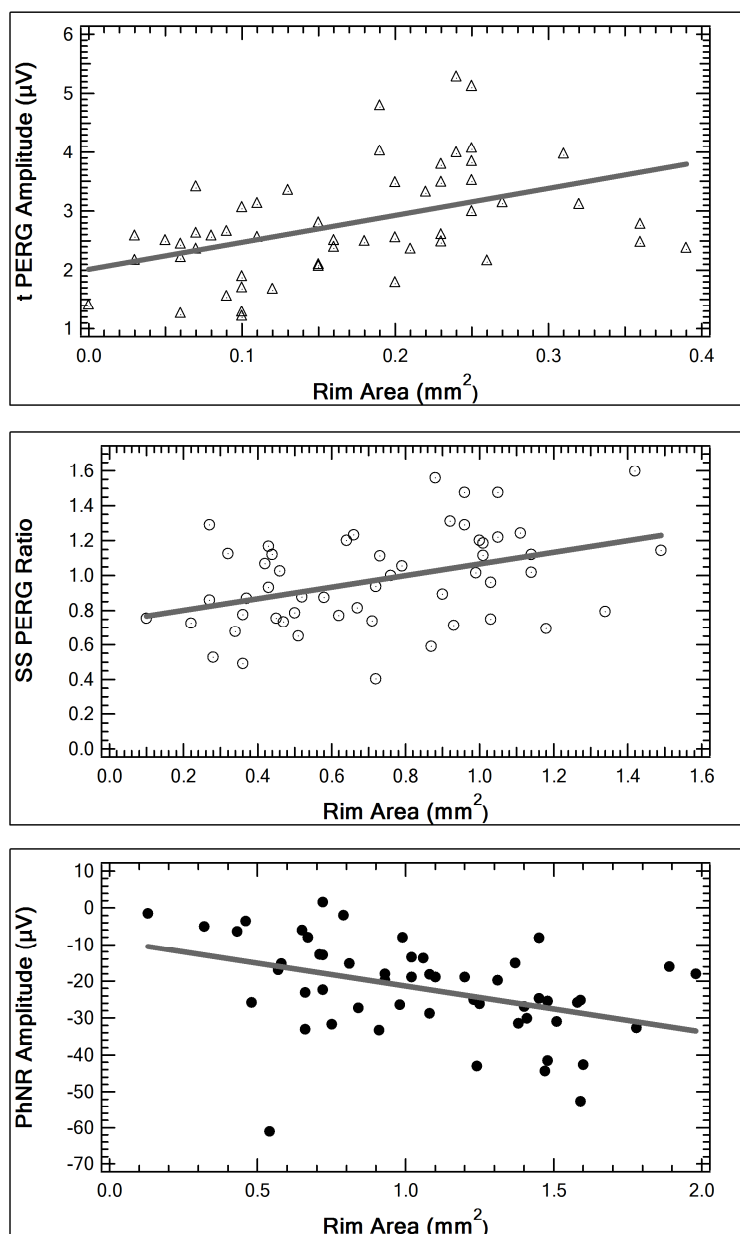


Figure 4.3: Recordings from one healthy volunteer (1) and 2 patients with primary open angle glaucoma (2,3)



Repeat recordings are shown in each case, except one large check (13 degree) steady state PERG recording, where a repeat was not available *

Figure 4.4: Plots of transient PERG N95—P50 amplitude, Steady State PERG ratio and PhNR amplitude versus rim area for normal eyes (average Mean Deviation, MD -0.12 ± 1.24 dB) and glaucomatous eyes (average MD -5.5 ± 6.40 dB). The grey lines indicate the linear regression in each case. R^2 values were 0.21, 0.17 and 0.17 for the tPERG, SS PERG ratio and PhNR respectively.



4.5.4 ROC Analysis: PERG versus PhNR

Plots of sensitivity versus 1-specificity are shown in **figure 4.5**. The total area under the ROC curve was similar ($p>0.60$) for the PERG measures (Area 0.75 for tPERG and 0.72 for SSPERG ratio) and PhNR (0.77). Sensitivities at fixed specificity of 90% were approximately 30%, 17% and 57% for the tPERG amplitude, SSPERG ratio and PhNR respectively (**table 4.2**). The criterion values identified by ROC analysis corresponding to 90% specificity are also shown in **table 4.2** and indicated on the graphs in **figure 4.5**.

As the results of conventional automated perimetry did not serve as an inclusion criterion for this study, the sensitivity / specificity of perimetry to identify GON in the study population was estimated to provide a reference accuracy of a gold-standard functional test to detect GON. In the same population, the MD had a sensitivity of around 67% at 90% specificity with a total area under the ROC curve of 0.87. Two markers of focal field loss were used. Firstly, a pattern standard deviation (PSD) value below 1% on SAP has been shown to be an efficient discriminatory index for separating glaucomatous from normal eyes (Johnson, Sample et al. 2002). This definition gave a sensitivity of 60% and specificity of 100% to identify GON. Secondly, the criterion based on the European Glaucoma Society guidelines (European Glaucoma Society 2008) for glaucomatous field loss was employed (3 or more abnormal points confirmed on 2 tests with $p<5\%$ of being normal, one of which should be $p<1\%$ and not be contiguous with the blind spot). This second visual field definition of glaucoma gave a sensitivity of 80% and specificity of 100% (dashed arrow, **figure 4.5**). Hence it is estimated that, in the given population, for

specificity around 90%, perimetry has sensitivity in the range 64-79% for the detection of GON.

Figure 4.5: ROC Analysis of transient (t) PERG amplitude, Steady-State (SS) PERG ratio and PhNR amplitude to identify glaucomatous optic neuropathy. The ROC curve for Mean Deviation (MD) from visual field data is shown for comparison. Point sensitivity estimates for 90% specificity are shown for 2 visual field criteria (PSD<1%, solid arrow) and the European Glaucoma Society field loss criteria (dashed arrow).

See text for further details.

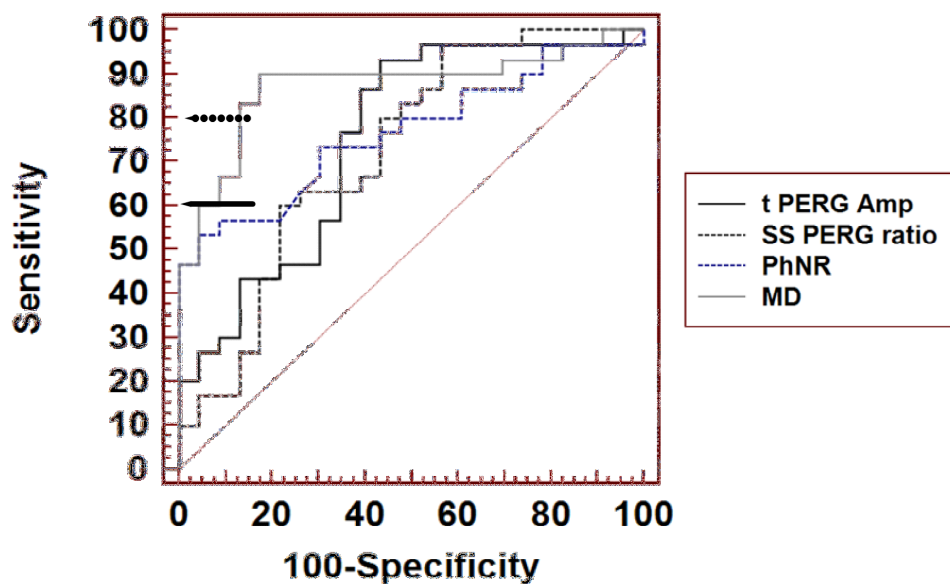


Table 4.2: Sensitivities at fixed specificities of around 90% and areas under the ROC curves with corresponding criterion values for the transient PERG N95—P50 amplitude, SS PERG ratio and PhNR (PERG=Pattern ERG, SS=Steady-State, MD=Mean Deviation, PhNR=Photopic Negative Response).

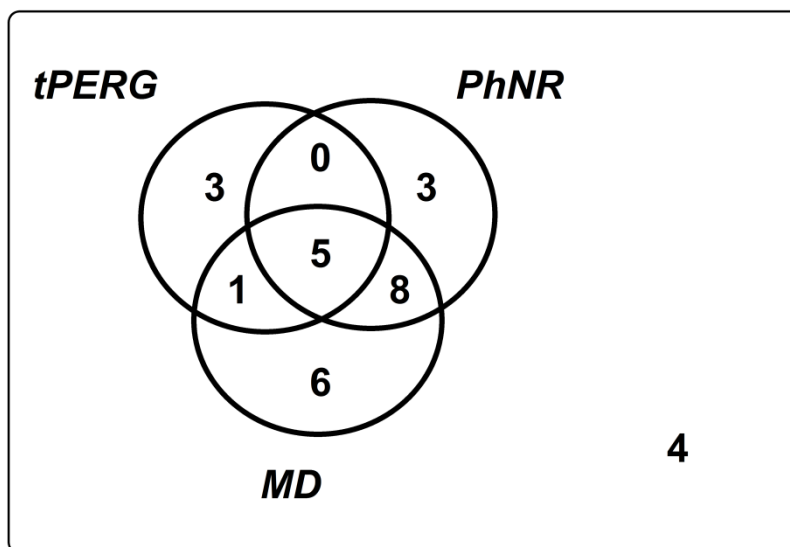
	Criterion value	Area under ROC Curve	Specificity (95% C.I.)	Sensitivity (95% C.I.)
Transient PERG	≤ 2.1 μV	0.75	90 (72—99)	30 (15—49)
SS PERG ratio	≤ 0.7 μV	0.72	91 (72—99)	17 (6—35)
PhNR	> -17.5 μV	0.77	91 (72—99)	57 (37—75)
MD	<-1.7 dB	0.87	91 (72-99)	67 (47-83)

4.5.5 Agreement of abnormal PERG and PhNR values

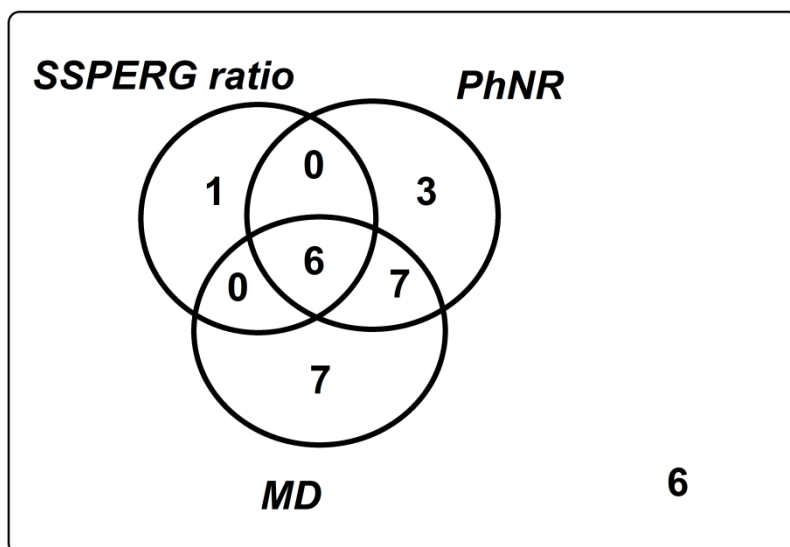
Agreement between abnormal PERG, PhNR and Mean Deviation, MD values in eyes with GON is depicted in **figure 4.6** Criterion values corresponding to 90% specificity were used to identify each variable as subnormal. Accordingly, values of MD equal or below to -1.7 dB were classified as abnormal. The tPERG amplitude and PhNR were both abnormal in 5 patients. Similarly, the SSPERG ratio and PhNR were both abnormal in 6 patients. Four patients had abnormal tPERG amplitude but PhNR in the normal range whilst only 1 had abnormal SSPERG and normal PhNR.

Figure 4.6: Non-proportional Venn diagrams showing agreement of (a) abnormal transient PERG and (b) abnormal Steady-State PERG ratio with abnormal PhNR and abnormal MD in glaucoma patients using the criterion values identified by ROC analysis corresponding to 90% specificity

(a)



(b)



4.6 Results II: Global visual field indices and the photopic negative response

4.6.1 Participants

The characteristics of the glaucoma patients and healthy volunteers is summarised in **table 4.3**.

Table 4.3: Comparison of parameters between the 'normal' and 'glaucoma' group

	Age (years)	Mean Deviation (dB)	Average DLS (L^{-1})	OCT RNFL average (μm)	GDxECC TNSIT average (μm)	PhNR (μV)
Normal	66 \pm 7.2	-5.9 \pm 6.5	1008 \pm 280	97 \pm 6.9	55 \pm 5.2	-28.4 \pm 10.3
Glaucoma	70 \pm 7.4	-0.12 \pm 1.2	650 \pm 299	64 \pm 15	37 \pm 6.3	-17.0 \pm 12.5
P	0.03	<0.001	<0.001	<0.001	<0.001	<0.001

On average, patients were 4 years older than the healthy volunteers. The Mean Deviation, average DLS (linear units, L^{-1}), PhNR amplitude and RNFL thickness were all lower in the glaucoma group compared with the 'normal' group.

Sample data from our study is displayed in **figure 4.7** which shows Visual field pattern standard deviation (PSD) plots, RNFL thickness measurements and flash ERG recordings from one healthy volunteer (a) and two glaucoma patients. For the flash ERG recordings, marker '5' indicates the position of the trough of the PhNR. The measurements obtained from this data are summarised in **table 4.4**.

Figure 4.7: Pattern Standard Deviation (PSD) plots, RNFL thickness profile from GDxEcc and OCT RNFL 3.4 scans and flash ERG recordings showing the PhNR (marker '5') from (a) one healthy volunteer and (b,c) two patients with different severities of glaucoma

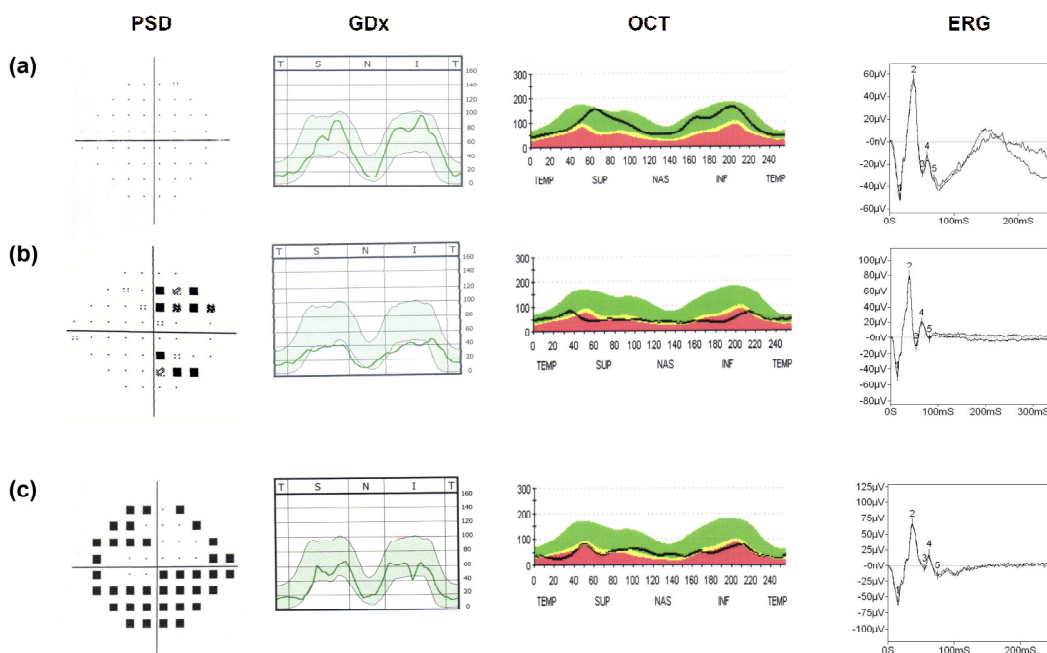


Table 4.4: Mean Deviation values, RNFL thickness and PhNR amplitudes for examples shown in figure 4.7

	Status	MD (dB)	RNFL thickness μm		PhNR amplitude, μV
			OCT	GDx	
a	Normal	-0.13	90	51	-32.7
b	Patient	-1.71	48	30	-1.4
c	Patient	-19.3	49	30	-15.1

4.6.2 Relationship between visual field measures and the photopic negative response with nerve fibre layer thickness

Figure 4.8 shows the relationship between MD and the PhNR with RNFL thickness measurements from both OCT (left-hand column) and GDx (right-hand column).

Figure 4.8 (a-c) show the relationship of visual field measures with RNFL thickness and **(d)** shows the relationship of the PhNR to RNFL thickness. The relationship between MD and OCT RNFL thickness was non-linear and has been fitted with a polynomial regression with 3 terms ($R^2=0.56$; regression equation: $y = -47 + 1.01x - 0.0054 x^2$). Similarly, the relationship between MD and GDx RNFL thickness appeared curvilinear, although the regression coefficients for a polynomial fit ($R^2=0.28$) and linear fit ($R^2=0.27$) were similar.

The same data has been plotted with the RNFL (R) transposed on the 'y-axis' and fitted with the Hood-Hardon (2007) model (b), dashed line. For this fit, the equation

$$R = s_0T + b \quad [4.1]$$

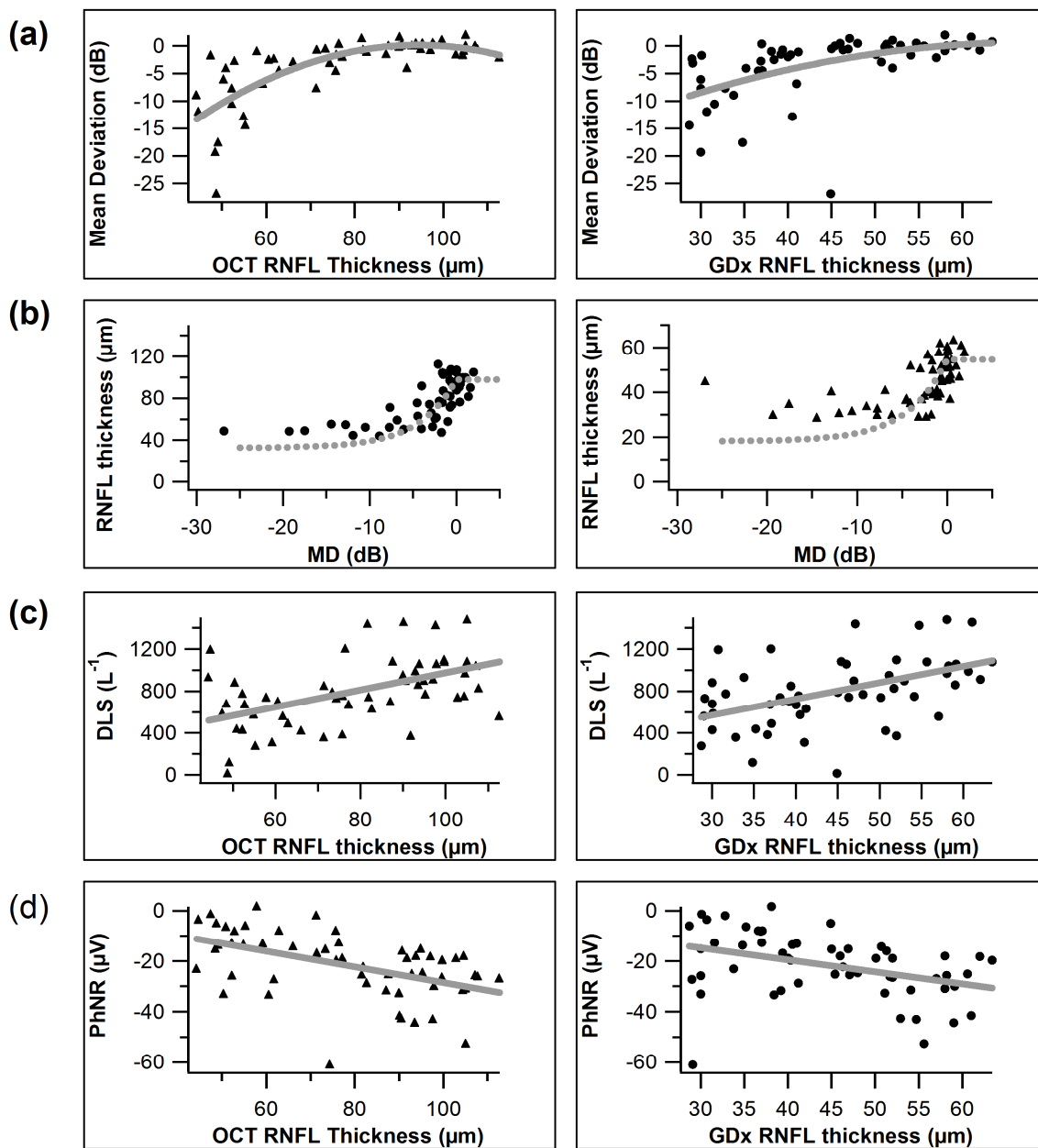
was used for values of $T < 1.0$

$$\text{and } R = s_0 + b \quad [4.2]$$

for values of $T \geq 1.0$

$$\text{Where } T = 10^{0.1 * MD}; \quad [4.3]$$

Figure 4.8: Relationship between Mean Deviation (MD, dB), linear DLS and PhNR with RNFL thickness. The column on the left shows plots for OCT RNFL thickness and those on the right for GDx.



s_0 was the non-ganglion cell related component of the RNFL and approximated to third of the mean normal RNFL thickness and b was the residual 'functional' component of the RNFL. S_0 was computed from the mean RNFL thickness for the 23 healthy volunteers tested.

The relationship between linear DLS and RNFL thickness ($R^2 = 0.25$ for OCT; $R^2 = 0.23$ for GDx) and between the PhNR amplitude and RNFL thickness ($R^2 = 0.25$ for OCT and $R^2 = 0.17$) were approximately linear with similar regression coefficients ($t < 0.35$, $p > 0.73$ in each case).

4.6.3 ROC analysis: Visual field measures and PhNR

ROC curves were plotted for MD, Linear DLS and the PhNR amplitude using the presence of GON from HRT as the classifying variable, **figure 4.9**. The whole area under the curve was comparable ($Z > 0.70$, $p > 0.10$ in each case) for both visual field measures (0.89 for MD; 0.84 for Linear DLS) and the PhNR (0.78). Sensitivities for a fixed specificity of around 90% were also similar ($Z > 1.10$, $p > 0.10$) for MD (sensitivity $\approx 69\%$) compared with the PhNR (sensitivity $\approx 56\%$) and Linear DLS (sensitivity $\approx 72\%$) compared with the PhNR.

Figure 4.9: Receiver Operator Characteristic (ROC) curves based on the presence of Glaucomatous Optic Neuropathy (GON) on HRT disc analysis. Linear DLS = Differential Light Sensitivity (linear units, L^{-1}); MD = Mean Deviation (dB); PhNR = amplitude of photopic negative response (μV)

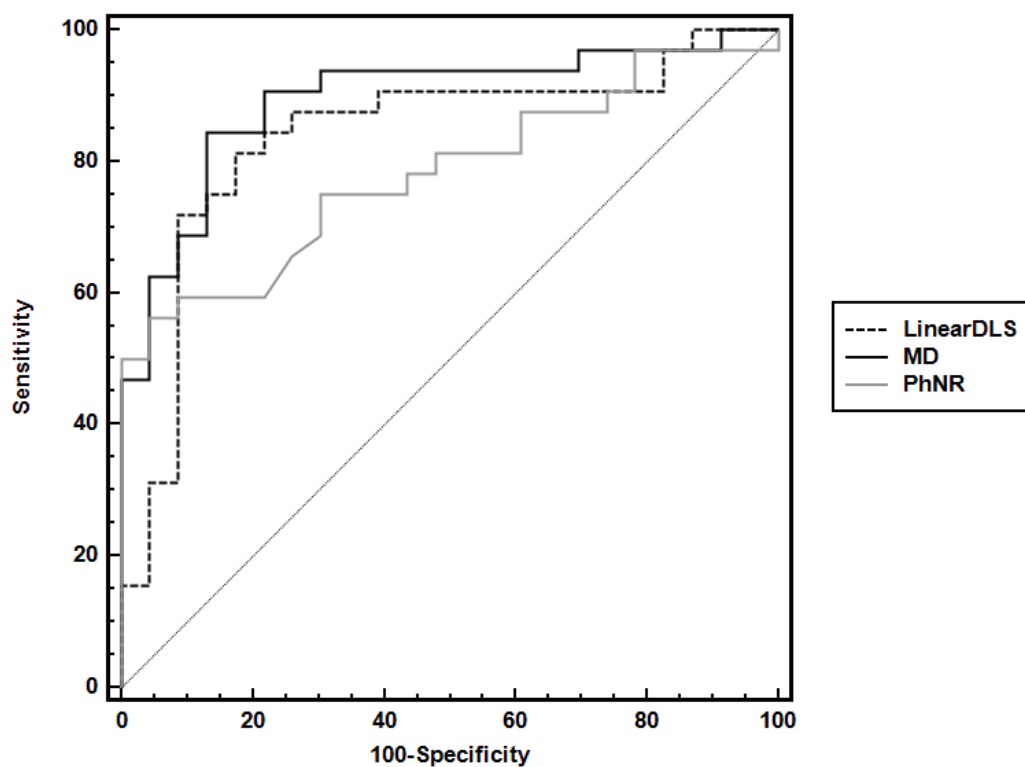


Figure 4.10 illustrates the agreement between Visual field measures and the PhNR with RNFL measurements from OCT and GDx in eyes with GON in the form of Venn Diagrams. Criterion values (MD, Linear DLS, OCT RNFL thickness and GDx RNFL thickness) corresponding to 90% specificity for each parameter were used as cut-off values for normality. The left-hand column shows agreement between RNFL thickness from OCT with visual field measures (**a,b**) and the PhNR (**c**), whilst the right hand column shows these plots for GDx RNFL thickness. For both OCT and GDx, 22-23 eyes had low MD and 17-18 eyes had a low PhNR (**c**). The proportion of patients with GON identified by global visual field measures and the PhNR were therefore comparable.

Figure 4.10: Venn diagrams (non-proportional) depicting agreement between visual field measures (a), (b) and the (c) photopic negative response with low Retinal nerve fibre layer thickness from OCT and GDx in eyes with glaucomatous optic neuropathy. Criterion values corresponding to 90% specificity have been used as cut-off values to define abnormally low values. MD= Mean Deviation; GDx = GDx

RNFL thickness; OCT = OCT RNFL thickness

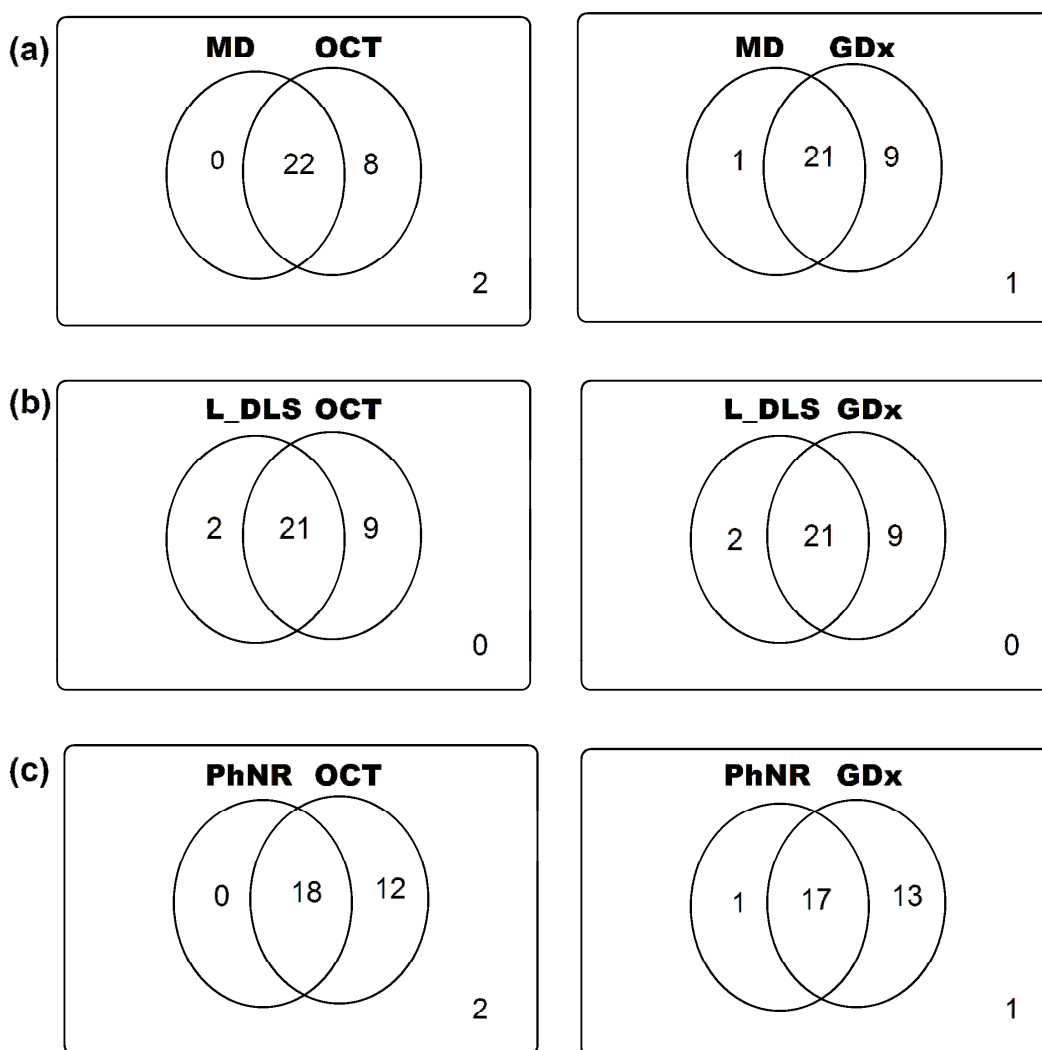


Table 4.5: Comparison of study sample size and diagnostic accuracy estimates of current study with previous studies of the PhNR in glaucoma

Study	Number of normal eyes	Number of glaucoma eyes	VF based inclusion?	Area under ROC curve	patients with MD >-6 dB (%)	Sensitivity at ≈90% specificity
Viswanathan et al. (2001)	18	62	Yes	0.96	16	83
Wakili et al. (2008)	37	37	Yes	≈0.8*	?	~60
Machida et al. (2008)	30 (28 subjects)	99 eyes (53 patients)	Yes	0.79	20	77
Present study	23	32	No	0.78	63	56

*Exact ROC area reported varied with flash energy used

4.7 Discussion I: the PhNR and the PERG

4.7.1 Summary of findings

Whilst both PERG and PhNR measures correlated with neuroretinal rim area (figure 2), these measures, were at best, approximately 60% sensitive at 90% specificity for the identification of functional loss associated with GON (**figure 4.5**).

Inspection of the analyses from the current study suggests that over the range of specificities, the PhNR was at least as sensitive as the PERG for the detection of GON (**table 4.2**). For higher (>80%) specificities, the PhNR was a more sensitive marker than the SSPERG ratio and at least as sensitive as the tPERG. There is incomplete agreement between abnormal PERG and PhNR in glaucomatous eyes, with the PhNR being abnormal in some eyes and the PERG being abnormal in others (**figure 4.6**).

4.7.2 PhNR as a marker of ganglion cell loss in glaucoma

Traditionally the flash ERG has been considered to have little role in the diagnosis of glaucoma. The 'a' and 'b' waves are often normal in eyes with extensive field loss (Leydhecker 1950, Bach, Gerling et al. 1992). However, affection of finer components of the flash ERG has been described. The scotopic threshold response, STR (Graham and Vaegan 1991; Korth, Nguyen et al. 1994; Frishman, Shen et al. 1996) and oscillatory potentials (Gur, Zeevi et al. 1987; Vaegan, Graham et al. 1991) may be affected to some extent in glaucoma. Recording of the scotopic threshold response requires adequate (≥ 40 minutes) dark adaptation, extensive signal averaging and the response is relatively small. The degree of the affection of the

STR in glaucoma is controversial (Sieving 1991). In contrast, there is mounting evidence for the consistent involvement PhNR in glaucoma (Viswanathan, Frishman et al. 1999; Colotto, Falsini et al. 2000; Drasdo, Aldebasi et al. 2001; Viswanathan, Frishman et al. 2001; Machida, Gotoh et al. 2008; Wakili, Horn et al. 2008; North, Jones et al. 2010).

Viswanathan, Frishman et al. (1999) first described the PhNR component in eyes of macaques and noted that it was reduced in eyes with experimental glaucoma compared with contralateral normal control eyes. Furthermore, the PhNR was removed by the action of tetrodotoxin (TTX), a drug which inhibits the spiking activity of retinal neurons (predominantly ganglion cells), (Viswanathan, Frishman et al. 1999, Viswanathan, Frishman et al. 2000). The changes that occur to both the PhNR and the PERG in glaucoma are a consequence of reduced spiking activity of ganglion cells, (Viswanathan, Frishman et al. 1999). The PhNR, unlike the 'a' and 'b' waves of the flash ERG, can discriminate between normal and glaucomatous human eyes in most cases (Viswanathan, Frishman et al. 2001). PhNR amplitudes correlate with both structural and psychophysical measures of glaucoma (Viswanathan, Frishman et al. 2001; Colotto, Falsini et al, 2001; Machida, Gotoh et al. 2008). Loss of the PhNR has been observed in other optic neuropathies apart from glaucoma (Gotoh, Falsini et al. 2004).

The findings of (Cursiefen, Korth et al. 2001) are contrary to those of this study. They failed to demonstrate a difference in mean amplitude between normal subjects and glaucoma patients when they recorded the PhNR using either a white flash on a low white background or an orange flash on a blue background. Although their study included only a small number of control subjects (6 subjects for the

orange flash condition), thereby raising the possibility of a statistical artefact, their stimulus conditions were quite different from those used in the current study and those described by Viswanathan, Frishman et al. (2001), (see discussion below). The orange flash was of a different colour (Cursiefen does not state exact wavelength used), the flash duration was much shorter (in μs range rather than ms) and produced by a Xenon discharge tube, rather than by light emitting diodes (LED's) as in the present study. The intensity of the blue background was lower (2.5 Log scot Td) than used by Viswanathan, Frishman et al. 2001 (3.7 Log scot Td), raising the possibility of a mixed cone-rod response rather than a pure cone response. This speculation is supported by the higher PhNR amplitudes and a PhNR response with a different latency (around 115 ms compared with 60-70 ms in the present study and Viswanathan, Frishman et al. (2001)).

4.6.3 Conditions for recording the PhNR in the current study

The stimulus conditions employed in the current study are not different to those described by Viswanathan, Frishman et al. (2001) for recording the PhNR in human subjects. Our stimulus duration (5 ms), stimulus wavelength (655 nm), background intensity (365.4 scot cd/m^2 (0.49 phot cd/m^2) \approx 4.15 log scotopic Td for 7mm pupil) and wavelength (425 nm) are comparable to that from Viswanathan et al. (red flash duration 6ms, wavelength 630 nm, background blue intensity 3.7 log scot Td). Their mean amplitude in normal subjects ($\sim 25\mu\text{V}$) is also similar to the present study ($28\mu\text{V}$). For simplicity, we have reported the results with a blue background of 0.49 cd/m^2 , although ROC curves for the PhNR for a variety of blue luminance backgrounds in the range 0.16 – 4.9 cd/m^2 were almost identical. Although a white

stimulus may be used to elicit the PhNR (Colotto, Falsini et al 2000), PhNR amplitudes using a red stimulus have recently been shown to have higher sensitivity for identifying glaucoma and show a better correlation with visual field measures than amplitudes obtained with a white stimulus (Sustar, Cvenkel et al. 2009), possibly because of a more 'selective' ganglion cell response elicited with the red-on-blue conditions.

4.7.4 Diagnostic accuracy of the PhNR and PERG and comparison with other studies

Sensitivity estimates for the PERG around specificities of 90% generally vary from 80 to over 90% (Bach and Speidel-Fiaux 1989; Ruben, Arden et al. 1995; Graham, Drance et al. 1996). These studies have largely included glaucoma with established field loss as cases and this may explain the lower sensitivity of 17-30% in our population for the PERG, in which field loss was not a prerequisite for study inclusion. Bach's studies (Bach, Hiss et al. 1988; Bach and Speidel-Fiaux 1989; Pfeiffer and Bach 1992) have included glaucomatous eyes classified by the Aulhorn field grading system of 1 and 2 (Aulhorn 1977). By definition, eyes with grade 2 field defects have early to moderate field loss ('spot or arcuate defects not connected with the blind spot'). Stroux (2003) estimated the sensitivity of the PERG at various degrees of neuroretinal rim loss. For rim losses of 0 to 1 mm², sensitivity estimates were between 35% and 60% at 80% specificity, which is comparable for the sensitivity of the tPERG and SSPERG ratio in this study (~43% at 80% specificity, **figure 4.5**).

Sensitivity estimates for the PhNR are more limited. Viswanathan et al.'s ROC analysis (Viswanathan, Frishman et al. 2001) revealed a sensitivity of around 83% at 90% specificity. Their glaucoma patients included a range of visual field loss (MD range -1.3 to -16.8 dB) all with proven field loss on conventional perimetry. Machida et al. (2008) reported a sensitivity of around 90% for separating normal eyes from perimetric glaucoma. The sensitivity fell to 57% (at the 'optimal cut-off' criterion) for the identification of early field defects (defined as Mean Deviation higher than -6 dB). Their total ROC area for the PhNR (0.79) was similar to the present study (ROC area for PhNR = 0.77).

4.7.5 Comments on study methodology

The sensitivity estimates in this study are specific to the study population and to the diagnostic reference used. Although a non-vision function reference may be more appropriate for the comparison of 2 different functional tests of glaucomatous loss, the HRT is estimated to be around 60-70% sensitive at 90% specificity (Ford, Artes et al. 2003). The likelihood of false identification of glaucoma was minimised by choosing further characteristics which minimised the chance of glaucoma in normal subjects (IOP \leq 21 mmHg, absence of family history of glaucoma).

The sensitivity estimates of the SSPERG ratio from the present study are considerably lower than previously reported (Bach, Hiss et al. 1988). Whilst population differences may account for some of the discrepancy, the possibility of recording or measurement artefact in our study should be considered. Any degradation of retinal image quality through optical defocus or reduced acuity can result in artificially low PERG amplitude, especially for small size check sizes

However, as our study included only patients with distance visual acuity of 20/30 or better and meticulous subjective refraction was obtained for the test distance, artefacts arising from reduced acuity are likely to be negligible. A second source of artefact can result from improper analysis of the steady-state waveform. This can arise if the refresh rate of the viewing monitor is not considered, trend artefacts are not corrected prior to waveform analysis, or a sub-integer number of waveforms are used for discrete Fourier transform (Bach and Meigen 1999). Such sources of analysis artefact have been specifically avoided in this study.

The current study included a sample size of 53, so that each single observation represents 2% of the data. Some investigators recommend at least 50 diseased and 50 normal control subjects for accurate ROC analysis (Metz 1978). However, with the exception of one study (Machida, Gotoh et al. 2008), ROC studies of the human PhNR have included fewer than 20 glaucoma patients (Colotto, Falsini et al. 2000; Cursiefen, Korth et al. 2001; Viswanathan, Frishman et al. 2001).

4.7.6 Clinical relevance: electrophysiological evaluation of glaucomatous optic neuropathy

In the study population, the PhNR was found to be at least as sensitive as the PERG for the identification of GON. Given the relative ease of recording the flash ERG, the potentially higher signal-to-noise ratio and the lack of need for precise fixation stability, it is recommended that the flash ERG with measurement of the PhNR (in addition to the PERG) be performed in all patients referred for electrodiagnostic evaluation of glaucoma.

For meaningful clinical application of the data, the diagnostic sensitivity of summary visual field indices was evaluated in the same group of patients and normals as the electrophysiological tests. The PhNR, which is assumed to be a global retinal response, had sensitivity no better than the MD. Using a definition for glaucoma based on PSD gave a higher diagnostic sensitivity, suggesting that measures which include spatial information are superior to MD or to the PhNR.

4.8 Discussion II: The PhNR and visual field measures of glaucomatous optic neuropathy

4.8.1 Summary of findings

Data from this study confirms that the PhNR is reduced in patients with glaucoma compared to healthy eyes. Further, for this study population, the PhNR was found to be linearly related to RNFL thickness and had comparable sensitivity to global measures of visual field loss from SAP for the detection of GON. Similar to MD, the PhNR was abnormally low in a high proportion of eyes with GON.

4.8.2 Value of current sensitivity estimates

To date existing studies of the PhNR have used visual field loss on SAP as an inclusion for glaucoma patients (Viswanathan, Frishman et al. 2001; Machida, Raz-Prag et al. 2008; Wakili, Horn et al. 2008), with sensitivity estimates of between 60 to over 80% at 90% specificity (**table 4.4**) compared to a sensitivity of nearly 60% in the current study. The difference in sensitivity is likely to reflect populations of differing glaucoma severity. For the validation of any new diagnostic test, sensitivity

and specificity should be benchmarked against an existing 'gold standard' test modality (Bossuyt, Irwig et al. 2006). As SAP is currently the reference test for the identification of functional loss associated with GON, MD from SAP was used for comparison with PhNR amplitude from normal and glaucomatous eyes. In addition, results of SAP were not used as an inclusion criterion to define 'normal' or 'glaucoma'. Inclusion of patients with field defects and GON would have resulted in the elimination of patients with pre-perimetric glaucoma from the study and is likely to have resulted in biased estimates of diagnostic accuracy for the PhNR. The effects of spectrum bias on sensitivity and specificity estimates have been described (Medeiros, Ng et al. 2007). Estimates of diagnostic accuracy from the current study are invaluable for powering future studies for the use of the PhNR for glaucoma diagnosis.

Table 4.5 provides a summary of the sensitivity estimates for the PhNR available in the literature for human eyes. The study by Machida, Gotoh et al. (2008) provides the largest study to date. It is unclear why whilst most glaucoma patients in this study had both eyes tested; only 30 eyes from 28 normal subjects were tested. Further, the paired nature of the data was not taken into account for their data analysis. It is considerable likely that patients with severe glaucoma in one eye, had a similarly affected fellow eye, with reduced PhNR amplitudes in both eyes. A higher proportion of eyes in our study (20 eyes, 63%) had mild visual field defects (MD > -6 dB) compared to Machida et al. (20 eyes, 20%) and the study by Viswanathan, Frishman et al. (2001) and this is likely to explain the difference in sensitivity values between the studies.

4.8.3 Relationship between the PhNR and RNFL thickness

Similar to linear measures of DLS (Garway-Heath, Holder et al. 2002; Schlottmann, De Cilla et al. 2004) and the Pattern ERG response (Garway-Heath, Holder et al. 2002), the PhNR is linearly related to structural parameters (Machida, Gotoh et al; 2008, Machida, Toba et al. 2008), suggesting that the amplitude of the PhNR response is related linearly to ganglion cell number. A reduction in the PhNR may, therefore, linearly relate to a loss in ganglion cell number, although this hypothesis would require longitudinal evaluation of a group of patients with progressive disease.

4.8.4 Clinical usefulness of the PhNR

Whilst inspection estimates of sensitivity and specificity from this study would indicate that the PhNR would not be a useful screening test for patients with glaucoma, the diagnostic capability of the PhNR was comparable to Mean Deviation in the study population. It is possible that with further refinements in recording techniques, reducing the inter-individual range of the PhNR and testing focal retinal areas (Machida, Toba et al. 2008) would further assist in improving the sensitivity of this response. Such an objective marker of ganglion cell function would be invaluable in glaucoma suspects who are unable to fixate for SAP.

4.8.5 Comments on study methodology

In the present study, the healthy volunteers were, on average, 4 years younger than the glaucoma patients. As there was no evidence for an age-related decline of PhNR or RNFL in the normal group ($R^2 < 0.1$, $p > 0.20$ for PhNR, RNFL and MD plots versus

age), it is unlikely that this difference between ages in the 2 groups would have altered the findings of this study.

The PhNR has been compared with MD rather than focal measures of visual field damage. This has allowed a 'like-for-like' comparison of field measures with the PhNR of the flash ERG, which is presumed to be a summed panretinal response. In clinical practice, clusters of reproducible abnormal visual field points are more reliable for detecting deviation from normality. Machida, Toba et al. (2008) measured the PhNR response from glaucomatous eyes using the focal ERG response. PhNR abnormalities were shown to correspond spatially to regions of, in some cases minimal, DLS deficit on SAP. A specificity of 84% using 'combined criteria' (ie abnormal PhNR in any one of the 3 retinal areas tested) yielded a sensitivity of 95% using this technique.

Although the number of participants in the current study compares favourably with previous studies of the PhNR in glaucoma (**table 4.5**), the confidence limits around sensitivity around sensitivity estimates from ROC analysis are large (typical range \approx 30% for each criterion value). Therefore, the results of ROC analysis should be interpreted with some caution. Nevertheless, the current study provides an adequate justification for undertaking a larger study for comparing the PhNR and visual field measures for the identification of functional loss associated with GON and for refining factors which may further improve the diagnostic precision of the PhNR.

CHAPTER 5

Conclusions & Further work

5.1 Conclusions

1. Monte Carlo simulations and clinical pilot data support the hypothesis that the dependence of bias, variability and efficiency on linear sensitivity can be reduced with the use of linear DLS steps.
2. The use of perimetric strategies which utilise linear steps for perimetric sensitivity can reduce extremes of variability in normal regions of the visual field, giving rise to relatively uniform variability characteristics across the sensitivity range. It is likely that this would improve the precision of measurements in normal regions of the field, when DLS is recorded in linear units, potentially narrowing the normal range of linear sensitivity.
3. Scaling the diameter of an achromatic circular stimulus by estimates of location-specific ganglion cell density results in:
 - a. more uniform DLS across eccentricity than the Goldmann size III stimulus
 - b. a linear relationship of DLS versus RNFL thickness across different eccentricities
4. Use of a Gabor patch stimulus (with peak spatial frequency scaled by ganglion cell density) yields higher agreement between structural and functional measures at extremes of eccentricity (30 degrees).

5. The sensitivity of the PhNR, for the detection of GON in the study population, is similar:
 - a. to the Pattern ERG
 - b. to indices of global visual field loss

5.2 Further work

5.2.1 *Perimetric strategies which utilise linear increments of sensitivity*

It remains to be ascertained clinically whether use of algorithms which measure sensitivity in linear steps leads to better agreement between perimetric and structural measures of ganglion cell damage in the initial stages of disease and earlier identification of glaucoma.

5.2.2 *Scaling stimulus sizes by estimates of ganglion cell density*

Further work on scaling factors may produce greater uniformity of DLS with eccentricity for the scaled stimulus, particularly for locations close to fixation. Exploration of the effect of optical blur and test-retest variability, at different eccentricities, on DLS for the scaled stimulus may elucidate reasons for poorer structure-function agreement with this stimulus within the central 10 degrees.

For linear DLS, the dependence of bias and variability on sensitivity can be reduced with the use of algorithms which employ linear, rather than logarithmic, staircase steps (as demonstrated in **Chapter 1**). Use of such a perimetric staircase to measure linear DLS may further reduce the eccentricity dependence of DLS for the scaled stimulus.

5.2.3 *Gabor patch perimetry*

Test-retest variability may be lower for the Gabor stimulus than the Goldmann size III (Pan, Swanson and Dul, 2006). Lower test-retest variability and between-subject

variability may aid in identification of abnormality, though this hypothesis requires further evaluation.

5.2.4 *Agreement analyses for structure-function comparisons*

Due to the limitations of regression analysis, agreement between structural and functional measures has been used as an endpoint for structure-function analysis (**Chapter 3**), after converting DLS to 'equivalent RNFL thickness'. Use of the same units for both parameters allowed a Bland-Altman plot to be graphed for qualitative structure-function agreement. The Hood-Kardon model caps RNFL thickness at mean normal, causing a ceiling effect in the Bland-Altman plot. A recent model proposed by Harwerth (Harwerth, Wheat et al. 2010), which extrapolates a model from monkey eyes, does not limit RNFL thickness in normal eyes. Further work is needed firstly to establish whether the Hood-Kardon model can accurately be applied to normal eyes and secondly whether the Harwerth model predicts RNFL thickness (based on DLS) better than the Hood-Kardon model.

5.2.5 *The PhNR in glaucoma*

The interindividual variation of normal PERG measures in this study was similar to the PhNR. A further evaluation of interindividual variability of the PhNR in a larger group of subjects may further assist in narrowing the range of normal PhNR values and improving the diagnostic ability of this test. PhNR amplitude may decline linearly with age (Viswanathan, Frishman et al. 2001) and a more detailed evaluation of this relationship is necessary. Another main source of variability, namely test-retest variability has not been quantified in this study. Data on test-

retest variability of the PhNR in human eyes is limited. In one study, the PhNR was within $\pm 13\%$ of the mean amplitude on repeated testing of 6 normal subjects (Viswanathan, Frishman et al. 2001). In adult rhesus monkeys, the test-test variability of the PhNR is similar to the 'a' and 'b' waves of the flash ERG (Fortune, Bui et al. 2004). The coefficient of variation in these eyes was around 10-20% which is comparable to that of the PERG (Otto and Bach 1997). In one recent study (Machida, Gotoh et al. 2008), the variability of the PhNR was evaluated in 22 glaucomatous and 22 healthy eyes. The coefficient of variation was $8.7 \pm 5.4\%$ in normal eyes and $14.6 \pm 10.9\%$ in glaucomatous eyes, suggesting that variability may be affected by the stage of disease.

Recently, the focal PhNR response has been described as having high sensitivity for the detection of glaucoma, with amplitudes correlating with SAP measures (Machida, Toba et al 2008). The focal flash ERG is elicited by stimulating focal areas of the retina, with the potential ability to identify more discrete areas of damage than the full-field flash ERG. A comparison of the sensitivity and variability of the focal and full-field PhNR for glaucoma of varying severity would delineate the role of these responses for the detection of GON.

The results of the present study warrant further exploration of the role of the PhNR for glaucoma diagnosis. In particular, the sensitivity and specificity for this response needs to be evaluated in a larger group of patients with early neuroretinal rim loss and concordance with visual field indices assessed. A logical extension of the current work would be to compare the PhNR with the focal PhNR and focal measures of visual field damage for the detection of GON.

Acknowledgments

I would like to thank the following for their assistance during my PhD:

David, 'Ted', Garway-Heath, International Glaucoma Association Professor of Ophthalmology & Glaucoma Theme Lead, NIHR Biomedical Research Centre for Ophthalmology for acting as my PhD supervisor, for his inspirational ideas and ongoing mentorship.

Bill Swanson, Professor of Optometry, Indiana University School of Optometry, USA for his continuous guidance, attention to detail, availability during my PhD and for accepting me as a visiting Research Fellow to his laboratory at SUNY College of Optometry, New York, USA between September 2003 and March 2004. The work presented in Chapter 2 was done directly under his guidance.

Fred Fitzke, Professor of Physiological Optics & Psychophysics, UCL Institute of Ophthalmology, for acting as my second PhD supervisor.

David Crabb, Professor of Statistics and Measurement Vision, City University for his advice on data analysis presented in Chapters 3 and 4.

Graham Holder, Professor of Electrophysiology, Moorfields Eye Hospital, for his advice on electrophysiology methodology and for validating the recordings used in this thesis (Chapter 4).

Patricio Schlottmann, formerly Research Fellow, Glaucoma Research Unit, Moorfields Eye Hospital for undertaking electrophysiological testing (Chapter 4).

Edward White, Senior Phenotyping Technician, Glaucoma Research Unit, Moorfields Eye Hospital, for his assistance in undertaking imaging and psychophysical tests (Chapters 3 & 4).

Chris Hogg, Clinical Scientist, Electrophysiology Department, Moorfields Eye Hospital, for assisting with technical aspects of recording the photopic negative response (Chapter 4).

Janine Shewry, formerly Phenotyping Technician Glaucoma Research Unit, Moorfields Eye Hospital, for helping with imaging and psychophysical tests (Chapters 3 & 4).

Andrew Carter, Senior Technician, Electrophysiology Department, Moorfields Eye Hospital for assisting with electrodiagnostic testing (Chapter 4).

Aachal Kotecha, Gay Verdon-Roe, Nicholas Strouthidis and Tony Redmond, Post-doctoral Research Fellows, Glaucoma Research Unit for discussing research ideas.

Francesca Amalfitano, UKGTS Co-coordinator, Moorfields Eye Hospital for assistance with patient recruitment (Chapter 3).

May Ellis, Study Co-ordinator, SUNY State College of Optometry, New York for her assistance with patient recruitment (Chapter 2).

Elisa Surkis, Computer programmer, SUNY State College of Optometry, New York, for writing the perimetry software programme used in Chapters 2 and 3.

Mitchell Dul and Richard Maddona, Consultant Optometrists at SUNY State College of Optometry, New York for help with patient recruitment (Chapter 2).

Richard Seeberan, Database Developer, Research & Development, Moorfields Eye Hospital for developing the 'structure-function' database (Chapters 2-4)

Tuan Ho, Publications Manager, Glaucoma Research Unit, Moorfields Eye Hospital, for suggestions on the layout of the thesis and proof-reading parts of Chapter 1.

The patients and healthy volunteers who have attended repeatedly to undertake hours of testing.

I would like to thank the *Guide Dogs for the Blind* for funding my 3-year Research Fellowship.

Finally, I would like to thank my wife, Afshan, for her patience during my PhD, my parents and brother and sisters for their support.

References

- American Academy of Ophthalmology (2005). Glaucoma. San Francisco, Calif., American Academy of Ophthalmology.
- Airaksinen, P. J., S. M. Drance, et al. (1985). "Neuroretinal rim areas and visual field indices in glaucoma." Am J Ophthalmol **99**(2): 107-110.
- Allergan-Humphrey (1986). The field analyzer primer, Allergan Humphrey, San Leandro, California.
- Allingham, R. R. and M. B. T. o. g. Shields (2005). Shields' textbook of glaucoma. Philadelphia, Pa. ; London, Lippincott Williams & Wilkins.
- Alward, W. L. (2000). "Frequency doubling technology perimetry for the detection of glaucomatous visual field loss." Am J Ophthalmol **129**(3): 376-378.
- Anderson, A. J. (2003). "Spatial resolution of the tendency-oriented perimetry algorithm." Invest Ophthalmol Vis Sci **44**(5): 1962-1968.
- Anderson, D. R. (1992). Automated static perimetry, Mosby Year Book.
- Anderson, R. S. (2006). "The psychophysics of glaucoma: improving the structure/function relationship." Prog Retin Eye Res **25**(1): 79-97.
- Anderson, R. S., D. R. McDowell, et al. (2001). "Effect of localized defocus on detection thresholds for different sized targets in the fovea and periphery." Acta Ophthalmol Scand **79**(1): 60-63.
- Armaly, M. F. (1967). "Inheritance of dexamethasone hypertension and glaucoma." Arch Ophthalmol **77**(6): 747-751.
- Armaly, M. F. (1969). "The size and location of the normal blind spot." Arch Ophthalmol **81**(2): 192-201.

- Armaly, M. F., D. E. Krueger, et al. (1980). "Biostatistical analysis of the collaborative glaucoma study. I. Summary report of the risk factors for glaucomatous visual-field defects." Arch Ophthalmol **98**(12): 2163-2171.
- Armstrong, J. R., R. K. Daily, et al. (1960). "The incidence of glaucoma in diabetes mellitus. A comparison with the incidence of glaucoma in the general population." Am J Ophthalmol **50**: 55-63.
- Artes, P. H., A. Iwase, et al. (2002). "Properties of perimetric threshold estimates from Full Threshold, SITA Standard, and SITA Fast strategies." Invest Ophthalmol Vis Sci **43**(8): 2654-2659.
- Aulhorn, E. (1977). "Frequency distribution in early glaucomatous visual field defects." Docum Ophthal Proc Series **14**: 17-83.
- Aulhorn, E. and H. Harms (1960). "[Papillary change and visual field disorder in glaucoma.]." Ophthalmologica **139**: 279-285.
- Bach, M. (2001). "Electrophysiological approaches for early detection of glaucoma." Eur J Ophthalmol **11 Suppl 2**: S41-49.
- Bach, M., Gerling, J., Geiger, K. (1992). "Optic atrophy reduces the pattern-electroretinogram for both fine and coarse stimulus patterns." Clin Vision Sci **7**: 327-333.
- Bach, M., M. Hawlina, et al. (2000). "Standard for pattern electroretinography. International Society for Clinical Electrophysiology of Vision." Doc Ophthalmol **101**(1): 11-18.
- Bach, M., P. Hiss, et al. (1988). "Check-size specific changes of pattern electroretinogram in patients with early open-angle glaucoma." Doc Ophthalmol **69**(3): 315-322.

- Bach, M., P. Hiss, et al. (1988). "[Pattern electroretinography with luminance stimuli in normal persons and patients with optic atrophy]." Fortschr Ophthalmol **85**(3): 308-311.
- Bach, M. and M. Mathieu (2004). "Different effect of dioptric defocus vs. light scatter on the pattern electroretinogram (PERG)." Doc Ophthalmol **108**(1): 99-106.
- Bach, M. and T. Meigen (1999). "Do's and don'ts in Fourier analysis of steady-state potentials." Doc Ophthalmol **99**(1): 69-82.
- Bach, M. and A. Speidel-Fiaux (1989). "Pattern electroretinogram in glaucoma and ocular hypertension." Doc Ophthalmol **73**(2): 173-181.
- Bach, M., F. Sulimma, et al. (1997). "Little correlation of the pattern electroretinogram (PERG) and visual field measures in early glaucoma." Doc Ophthalmol **94**(3): 253-263.
- Bach, M., A. S. Unsoeld, et al. (2006). "Pattern ERG as an early glaucoma indicator in ocular hypertension: a long-term, prospective study." Invest Ophthalmol Vis Sci **47**(11): 4881-4887.
- Baez, K. A., A. I. McNaught, et al. (1995). "Motion detection threshold and field progression in normal tension glaucoma." Br J Ophthalmol **79**(2): 125-128.
- Bankes, J. L., E. S. Perkins, et al. (1968). "Bedford glaucoma survey." Br Med J **1**(5595): 791-796.
- Bartz-Schmidt, K. U., G. Thumann, et al. (1999). "Quantitative morphologic and functional evaluation of the optic nerve head in chronic open-angle glaucoma." Surv Ophthalmol **44 Suppl 1**: S41-53.
- Bayer, A. U., K. P. Maag, et al. (2002). "Detection of optic neuropathy in glaucomatous eyes with normal standard visual fields using a test battery of

- short-wavelength automated perimetry and pattern electroretinography." Ophthalmology **109**(7): 1350-1361.
- Becker, B. and K. A. Hahn (1964). "Topical Corticosteroids and Heredity in Primary Open-Angle Glaucoma." Am J Ophthalmol **57**: 543-551.
- Becker, B., H. H. Unger, et al. (1963). "Plasma cells and gamma-globulin in trabecular meshwork of eyes with primary open-angle glaucoma." Arch Ophthalmol **70**: 38-41.
- Bengtsson, B. and A. Heijl (1998). "SITA Fast, a new rapid perimetric threshold test. Description of methods and evaluation in patients with manifest and suspect glaucoma." Acta Ophthalmol Scand **76**(4): 431-437.
- Bengtsson, B., J. Olsson, et al. (1997). "A new generation of algorithms for computerized threshold perimetry, SITA." Acta Ophthalmol Scand **75**(4): 368-375.
- Bennett, A. G., A. R. Rudnicka, et al. (1994). "Improvements on Littmann's method of determining the size of retinal features by fundus photography." Graefes Arch Clin Exp Ophthalmol **232**(6): 361-367.
- Berninger, T. and R. P. Schuurmans (1985). "Spatial tuning of the pattern ERG across temporal frequency." Doc Ophthalmol **61**(1): 17-25.
- Bland, J. M. and D. G. Altman (1986). "Statistical methods for assessing agreement between two methods of clinical measurement." Lancet **1**(8476): 307-310.
- Blaxter, P. L. (1950). "A note on the so-called enlargement of the blind spot in glaucoma." Br J Ophthalmol **34**(7): 442-444.
- Blondeau, P., J. Lamarche, et al. (1987). "Pattern electroretinogram and optic nerve section in pigeons." Curr Eye Res **6**(6): 747-756.

- Bodis-Wollner, I. and J. R. Brannan (1997). "Hidden visual loss in optic neuropathy is revealed using Gabor patch contrast perimetry." Clin Neurosci **4**(5): 284-291.
- Bonomi, L., G. Marchini, et al. (1998). "Prevalence of glaucoma and intraocular pressure distribution in a defined population. The Egna-Neumarkt Study." Ophthalmology **105**(2): 209-215.
- Bonomi, L., G. Marchini, et al. (2000). "Vascular risk factors for primary open angle glaucoma: the Egna-Neumarkt Study." Ophthalmology **107**(7): 1287-1293.
- Bossuyt, P. M., L. Irwig, et al. (2006). "Comparative accuracy: assessing new tests against existing diagnostic pathways." BMJ **332**(7549): 1089-1092.
- Bossuyt, P. M., J. B. Reitsma, et al. (2003). "Towards complete and accurate reporting of studies of diagnostic accuracy: the STARD initiative." BMJ **326**(7379): 41-44.
- Bowd, C., L. M. Zangwill, et al. (2006). "Structure-function relationships using confocal scanning laser ophthalmoscopy, optical coherence tomography, and scanning laser polarimetry." Invest Ophthalmol Vis Sci **47**(7): 2889-2895.
- Brais, P. and S. M. Drance (1972). "The temporal field in chronic simple glaucoma." Arch Ophthalmol **88**(5): 518-522.
- Budenz, D. L., M. J. Fredette, et al. (2008). "Reproducibility of peripapillary retinal nerve fiber thickness measurements with stratus OCT in glaucomatous eyes." Ophthalmology **115**(4): 661-666 e664.
- Bunce, C. and R. Wormald (2006). "Leading causes of certification for blindness and partial sight in England & Wales." BMC Public Health **6**: 58.
- Butt, Z., C. O'Brien, et al. (1997). "Color Doppler imaging in untreated high- and normal-pressure open-angle glaucoma." Invest Ophthalmol Vis Sci **38**(3): 690-696.

- Campbell, F. W. and D. G. Green (1965). "Optical and retinal factors affecting visual resolution." J Physiol **181**(3): 576-593.
- Chandler, P. A., W. M. Grant, et al. (1997). Chandler and Grant's glaucoma. Baltimore, Md. ; London, Williams & Wilkins.
- Chauhan, B. C. and P. H. House (1991). "Intratest variability in conventional and high-pass resolution perimetry." Ophthalmology **98**(1): 79-83.
- Chauhan, B. C., P. H. House, et al. (1999). "Comparison of conventional and high-pass resolution perimetry in a prospective study of patients with glaucoma and healthy controls." Arch Ophthalmol **117**(1): 24-33.
- Chauhan, B. C. and C. A. Johnson (1994). "Evaluating and optimizing test strategies in automated perimetry." J Glaucoma **3 Suppl 1**: S73-81.
- Chauhan, B. C., R. P. LeBlanc, et al. (1997). "Repeatable diffuse visual field loss in open-angle glaucoma." Ophthalmology **104**(3): 532-538.
- Chauhan, B. C., J. D. Tompkins, et al. (1993). "Characteristics of frequency-of-seeing curves in normal subjects, patients with suspected glaucoma, and patients with glaucoma." Invest Ophthalmol Vis Sci **34**(13): 3534-3540.
- Chia, W. L., I. Goldberg, et al. (1999). "Evaluation of oculokinetic perimetry." Aust N Z J Ophthalmol **27**(5): 306-311.
- Christoffersen, T., T. Fors, et al. (1995). "Glaucoma screening with oculokinetic perimetry in general practice: is its specificity acceptable?" Eye (Lond) **9 (Pt 6 Su)**: 36-39.
- Cockerham, K. P., C. Pal, et al. (1997). "The prevalence and implications of ocular hypertension and glaucoma in thyroid-associated orbitopathy." Ophthalmology **104**(6): 914-917.

- Colotto, A., B. Falsini, et al. (1996). "Transiently raised intraocular pressure reveals pattern electroretinogram losses in ocular hypertension." Invest Ophthalmol Vis Sci **37**(13): 2663-2670.
- Colotto, A., B. Falsini, et al. (2000). "Photopic negative response of the human ERG: losses associated with glaucomatous damage." Invest Ophthalmol Vis Sci **41**(8): 2205-2211.
- Curcio, C. A. and K. A. Allen (1990). "Topography of ganglion cells in human retina." J Comp Neurol **300**(1): 5-25.
- Cursiefen, C., M. Korth, et al. (2001). "The negative response of the flash electroretinogram in glaucoma." Doc Ophthalmol **103**(1): 1-12.
- Dacey, D. M. and M. R. Petersen (1992). "Dendritic field size and morphology of midget and parasol ganglion cells of the human retina." Proc Natl Acad Sci U S A **89**(20): 9666-9670.
- Dagnelie, G., M. J. de Vries, et al. (1986). "Pattern reversal stimuli: motion or contrast?" Doc Ophthalmol **61**(3-4): 343-349.
- Damato, B. E. (1985). "Oculokinetic perimetry: a simple visual field test for use in the community." Br J Ophthalmol **69**(12): 927-931.
- Dandekar, S., J. Ales, et al. (2007). "Methods for quantifying intra- and inter-subject variability of evoked potential data applied to the multifocal visual evoked potential." J Neurosci Methods **165**(2): 270-286.
- Dannheim, F. and S. M. Drance (1971). "Studies of spatial summation of central retinal areas in normal people of all ages." Can J Ophthalmol **6**(4): 311-319.
- Dannheim, F. and S. M. Drance (1974). "Psychovisual disturbances in glaucoma. A study of temporal and spatial summation." Arch Ophthalmol **91**(6): 463-468.

- Davila, K. D. and W. S. Geisler (1991). "The relative contributions of pre-neural and neural factors to areal summation in the fovea." Vision Res **31**(7-8): 1369-1380.
- Davis, D. and C. Davis (1997). Sound system engineering. Boston, Mass. ; Oxford, Focal.
- de Oliveira Rassi, M. and M. B. Shields (1982). "Crowding of the peripheral nasal isopters in glaucoma." Am J Ophthalmol **94**(1): 4-10.
- Delgado, M. F., N. T. Nguyen, et al. (2002). "Automated perimetry: a report by the American Academy of Ophthalmology." Ophthalmology **109**(12): 2362-2374.
- Dielemans, I., P. T. de Jong, et al. (1996). "Primary open-angle glaucoma, intraocular pressure, and diabetes mellitus in the general elderly population. The Rotterdam Study." Ophthalmology **103**(8): 1271-1275.
- Drance, S. M. (1969). "The early field defects in glaucoma." Invest Ophthalmol **8**(1): 84-91.
- Drance, S. M. (1991). "Diffuse visual field loss in open-angle glaucoma." Ophthalmology **98**(10): 1533-1538.
- Drance, S. M. and D. R. Anderson (1985). Automatic perimetry in glaucoma : a practical guide. Orlando, Grune & Stratton.
- Drance, S. M., M. Fairclough, et al. (1977). "The importance of disc hemorrhage in the prognosis of chronic open angle glaucoma." Arch Ophthalmol **95**(2): 226-228.
- Drasdo, N., Y. H. Aldebasi, et al. (2001). "The s-cone PHNR and pattern ERG in primary open angle glaucoma." Invest Ophthalmol Vis Sci **42**(6): 1266-1272.
- Drasdo, N., D. A. Thompson, et al. (1987). "Complementary components and local variations of the pattern electroretinogram." Invest Ophthalmol Vis Sci **28**(1): 158-162.

- Duke-Elder, W. S. S. (1954). Textbook of ophthalmology : vol. 6. London, Kimpton.
- Embleton, S. J., S. L. Hosking, et al. (2002). "Effect of senescence on ocular blood flow in the retina, neuroretinal rim and lamina cribrosa, using scanning laser Doppler flowmetry." Eye (Lond) **16**(2): 156-162.
- European Glaucoma, S. (2008). Terminology and guidelines for glaucoma, Savona, Italy Editrice Dogma 2008.
- Evans, D. W., S. L. Hosking, et al. (2003). "Contrast sensitivity improves after brimonidine therapy in primary open angle glaucoma: a case for neuroprotection." Br J Ophthalmol **87**(12): 1463-1465.
- Felius, J., W. H. Swanson, et al. (1996). Spatial summation for selected ganglion cell mosaics in patients with glaucoma. Perimetry Update 1996/1997. M. Wall, Heijl, A.: 213-221.
- Fellman, R. L., J. R. Lynn, et al. (1989). Clinical importance of spatial summation in glaucoma. Perimetry Update 1988/89. A. Heijl. Berkeley, Kugler & Ghedini, 1989, The Hague (Netherlands) 313-324.
- Ferreras, A., L. E. Pablo, et al. (2008). "Mapping standard automated perimetry to the peripapillary retinal nerve fiber layer in glaucoma." Invest Ophthalmol Vis Sci **49**(7): 3018-3025.
- Finkelstein, I., G. E. Trope, et al. (1990). "Quantitative analysis of collagen content and amino acids in trabecular meshwork." Br J Ophthalmol **74**(5): 280-282.
- Fiorentini, A., L. Maffei, et al. (1981). "The ERG in response to alternating gratings in patients with diseases of the peripheral visual pathway." Invest Ophthalmol Vis Sci **21**(3): 490-493.

- Flammer, J., E. Eppler, et al. (1982). "[Quantitative perimetry in the glaucoma patient without local visual field defects]." Graefes Arch Clin Exp Ophthalmol **219**(2): 92-94.
- Flammer, J., S. Orgul, et al. (2002). "The impact of ocular blood flow in glaucoma." Prog Retin Eye Res **21**(4): 359-393.
- Ford, B. A., P. H. Artes, et al. (2003). "Comparison of data analysis tools for detection of glaucoma with the Heidelberg Retina Tomograph." Ophthalmology **110**(6): 1145-1150.
- Forte, R., L. Ambrosio, et al. (2010). "Pattern electroretinogram optimized for glaucoma screening (PERGLA) and retinal nerve fiber thickness in suspected glaucoma and ocular hypertension." Doc Ophthalmol **120**(2): 187-192.
- Fortune, B., B. V. Bui, et al. (2004). "Inter-ocular and inter-session reliability of the electroretinogram photopic negative response (PhNR) in non-human primates." Exp Eye Res **78**(1): 83-93.
- Friedman, D. S., R. C. Wolfs, et al. (2004). "Prevalence of open-angle glaucoma among adults in the United States." Arch Ophthalmol **122**(4): 532-538.
- Frisen, L. (1987). "High-pass resolution targets in peripheral vision." Ophthalmology **94**(9): 1104-1108.
- Frishman, L. J., F. F. Shen, et al. (1996). "The scotopic electroretinogram of macaque after retinal ganglion cell loss from experimental glaucoma." Invest Ophthalmol Vis Sci **37**(1): 125-141.
- Gabor, D. (1946). "Theory of Communication." J of the Inst of Elec Eng **93**(26): 429-457.
- Galloway, P. H., S. J. Warner, et al. (2003). "Helicobacter pylori infection and the risk for open-angle glaucoma." Ophthalmology **110**(5): 922-925.

- Garway-Heath, D. F. (2008). "Early diagnosis in glaucoma." Prog Brain Res **173**: 47-57.
- Garway-Heath, D. F., J. Caprioli, et al. (2000). "Scaling the hill of vision: the physiological relationship between light sensitivity and ganglion cell numbers." Invest Ophthalmol Vis Sci **41**(7): 1774-1782.
- Garway-Heath, D. F. and D. S. Friedman (2006). "How should results from clinical tests be integrated into the diagnostic process?" Ophthalmology **113**(9): 1479-1480.
- Garway-Heath, D. F., G. E. Holder, et al. (2002). "Relationship between electrophysiological, psychophysical, and anatomical measurements in glaucoma." Invest Ophthalmol Vis Sci **43**(7): 2213-2220.
- Garway-Heath, D. F., D. Poinosawmy, et al. (2000). "Mapping the visual field to the optic disc in normal tension glaucoma eyes." Ophthalmology **107**(10): 1809-1815.
- Garway-Heath, D. F., S. T. Ruben, et al. (1998). "Vertical cup/disc ratio in relation to optic disc size: its value in the assessment of the glaucoma suspect." Br J Ophthalmol **82**(10): 1118-1124.
- Garway-Heath, D. F., A. Viswanathan, et al. (1999). Relationship between perimetric light sensitivity and optic disc neuroretinal rim area. Perimetry Update 1998/1999. M. Wall, Wild, J.M., Kugler Publications The Hague, The Netherlands. : 381-389.
- Gilbert, C. D. and T. N. Wiesel (1992). "Receptive field dynamics in adult primary visual cortex." Nature **356**(6365): 150-152.
- Gilpin, L. B., W. C. Stewart, et al. (1990). "Threshold variability using different Goldmann stimulus sizes." Acta Ophthalmol (Copenh) **68**(6): 674-676.

- Gilpin, L. B., W. C. Stewart, et al. (1990). "Hemianopic offsets in the visual field of patients with glaucoma." Graefes Arch Clin Exp Ophthalmol **228**(5): 450-453.
- Glass, E., M. Schaumberger, et al. (1995). "Simulations for FASTPAC and the standard 4-2 dB full-threshold strategy of the Humphrey Field Analyzer." Invest Ophthalmol Vis Sci **36**(9): 1847-1854.
- Glezer, V. D. (1965). "The receptive fields of the retina." Vision Res **5**(9): 497-525.
- Goldmann, H. (1999). "Fundamentals of exact perimetry. 1945." Optom Vis Sci **76**(8): 599-604.
- Gonzalez-Hernandez, M., L. E. Pablo, et al. (2009). "Structure-function relationship depends on glaucoma severity." Br J Ophthalmol **93**(9): 1195-1199.
- Gordon-Bennett, P. S., A. S. Ioannidis, et al. (2008). "A survey of investigations used for the management of glaucoma in hospital service in the United Kingdom." Eye (Lond) **22**(11): 1410-1418.
- Gordon, M. O., J. A. Beiser, et al. (2002). "The Ocular Hypertension Treatment Study: baseline factors that predict the onset of primary open-angle glaucoma." Arch Ophthalmol **120**(6): 714-720; discussion 829-730.
- Gotoh, Y., S. Machida, et al. (2004). "Selective loss of the photopic negative response in patients with optic nerve atrophy." Arch Ophthalmol **122**(3): 341-346.
- Graham, N. and D. C. Hood (1992). "Modeling the dynamics of light adaptation: the merging of two traditions." Vision Res **32**(7): 1373-1393.
- Graham, S. L., S. M. Drance, et al. (1996). "Comparison of psychophysical and electrophysiological testing in early glaucoma." Invest Ophthalmol Vis Sci **37**(13): 2651-2662.

- Graham, S. L. and Vaegan (1991). "High correlation between absolute psychophysical threshold and the scotopic threshold response to the same stimulus." Br J Ophthalmol **75**(10): 603-607.
- Graham, S. L., V. A. Wong, et al. (1994). "Pattern electroretinograms from hemifields in normal subjects and patients with glaucoma." Invest Ophthalmol Vis Sci **35**(9): 3347-3356.
- Gramer, E., R. Gerlach, et al. (1982). "[Topography of early glaucomatous visual field defects in computerized perimetry]." Klin Monbl Augenheilkd **180**(6): 515-523.
- Gramer, E., D. Kontic, et al. (1981). "[Computer perimetry of glaucomatous visual field defects at different stimulus sizes (author's transl)]." Ophthalmologica **183**(3): 162-167.
- Greenstein, V. C., D. C. Hood, et al. (1989). "S (blue) cone pathway vulnerability in retinitis pigmentosa, diabetes and glaucoma." Invest Ophthalmol Vis Sci **30**(8): 1732-1737.
- Greve, E. L. (1973). Single and multiple stimulus static perimetry in glaucoma : the two phases of perimetry. Hague, Junk.
- Gur, M., Y. Y. Zeevi, et al. (1987). "Changes in the oscillatory potentials of the electroretinogram in glaucoma." Curr Eye Res **6**(3): 457-466.
- Harrington, D. O. (1965). "The Bjerrum Scotoma." Am J Ophthalmol **59**: 646-656.
- Harrison, J. M., P. S. O'Connor, et al. (1987). "The pattern ERG in man following surgical resection of the optic nerve." Invest Ophthalmol Vis Sci **28**(3): 492-499.
- Hart, W. M., Jr. and B. Becker (1982). "The onset and evolution of glaucomatous visual field defects." Ophthalmology **89**(3): 268-279.

- Harwerth, R. S., L. Carter-Dawson, et al. (1999). "Ganglion cell losses underlying visual field defects from experimental glaucoma." Invest Ophthalmol Vis Sci **40**(10): 2242-2250.
- Harwerth, R. S., L. Carter-Dawson, et al. (2004). "Neural losses correlated with visual losses in clinical perimetry." Invest Ophthalmol Vis Sci **45**(9): 3152-3160.
- Harwerth, R. S., L. Carter-Dawson, et al. (2005). "Scaling the structure--function relationship for clinical perimetry." Acta Ophthalmol Scand **83**(4): 448-455.
- Harwerth, R. S., M. L. Crawford, et al. (2002). "Visual field defects and neural losses from experimental glaucoma." Prog Retin Eye Res **21**(1): 91-125.
- Harwerth, R. S. and H. A. Quigley (2006). "Visual field defects and retinal ganglion cell losses in patients with glaucoma." Arch Ophthalmol **124**(6): 853-859.
- Harwerth, R. S., A. S. Vilupuru, et al. (2007). "The relationship between nerve fiber layer and perimetry measurements." Invest Ophthalmol Vis Sci **48**(2): 763-773.
- Harwerth, R. S., J. L. Wheat, et al. (2010). "Linking structure and function in glaucoma." Prog Retin Eye Res **29**(4): 249-271.
- Healey, P. R., P. Mitchell, et al. (1998). "Optic disc hemorrhages in a population with and without signs of glaucoma." Ophthalmology **105**(2): 216-223.
- Heidelberg-Engineering (2001). Heidelberg Retinal Tomograph II (manual), Heidelberg Engineering GmbH, Dossenheim.
- Heijl, A., B. Bengtsson, et al. (2009). "Natural history of open-angle glaucoma." Ophthalmology **116**(12): 2271-2276.
- Heijl, A., M. C. Leske, et al. (2002). "Reduction of intraocular pressure and glaucoma progression: results from the Early Manifest Glaucoma Trial." Arch Ophthalmol **120**(10): 1268-1279.

- Heijl, A., A. Lindgren, et al. (1989). "Test-retest variability in glaucomatous visual fields." Am J Ophthalmol **108**(2): 130-135.
- Heijl, A., G. Lindgren, et al. (1987). "Normal variability of static perimetric threshold values across the central visual field." Arch Ophthalmol **105**(11): 1544-1549.
- Heijl, A. and L. Lundqvist (1984). "The frequency distribution of earliest glaucomatous visual field defects documented by automatic perimetry." Acta Ophthalmol (Copenh) **62**(4): 658-664.
- Heilmann, K. and K. T. Richardson (1978). Glaucoma : conceptions of a disease : pathogenesis, diagnosis, therapy. Philadelphia ; London, Saunders [etc.].
- Henson, D. B. (1989). "An optimized visual field screening method." Surv Ophthalmol **33 Suppl**: 443-444; discussion 449-450.
- Henson, D. B. (1989). "Visual field screening and the development of a new screening program." J Am Optom Assoc **60**(12): 893-898.
- Henson, D. B. (1993). Visual fields. Oxford, Oxford University Press.
- Henson, D. B., S. Chaudry, et al. (2000). "Response variability in the visual field: comparison of optic neuritis, glaucoma, ocular hypertension, and normal eyes." Invest Ophthalmol Vis Sci **41**(2): 417-421.
- Henson, D. B., B. C. Chauhan, et al. (1988). "Screening for glaucomatous visual field defects: the relationship between sensitivity, specificity and the number of test locations." Ophthalmic Physiol Opt **8**(2): 123-127.
- Henson, D. B., J. Evans, et al. (1996). "Influence of fixation accuracy on threshold variability in patients with open angle glaucoma." Invest Ophthalmol Vis Sci **37**(2): 444-450.
- Holder, G. E. (1987). "Significance of abnormal pattern electroretinography in anterior visual pathway dysfunction." Br J Ophthalmol **71**(3): 166-171.

- Holder, G. E. (1997). "The pattern electroretinogram in anterior visual pathway dysfunction and its relationship to the pattern visual evoked potential: a personal clinical review of 743 eyes." Eye (Lond) **11 (Pt 6)**: 924-934.
- Holder, G. E. (2001). "Pattern electroretinography (PERG) and an integrated approach to visual pathway diagnosis." Prog Retin Eye Res **20(4)**: 531-561.
- Holder, G. E., M. G. Brigell, et al. (2007). "ISCEV standard for clinical pattern electroretinography--2007 update." Doc Ophthalmol **114(3)**: 111-116.
- Hollows, F. C. and P. A. Graham (1966). "Intra-ocular pressure, glaucoma, and glaucoma suspects in a defined population." Br J Ophthalmol **50(10)**: 570-586.
- Holopigian, K., J. Snow, et al. (1988). "Variability of the pattern electroretinogram." Doc Ophthalmol **70(1)**: 103-115.
- Hood, D. C., V. C. Greenstein, et al. (2002). "Visual field defects and multifocal visual evoked potentials: evidence of a linear relationship." Arch Ophthalmol **120(12)**: 1672-1681.
- Hood, D. C. and R. H. Kardon (2007). "A framework for comparing structural and functional measures of glaucomatous damage." Prog Retin Eye Res **26(6)**: 688-710.
- Hood, D. C., L. Xu, et al. (2005). "The pattern electroretinogram in glaucoma patients with confirmed visual field deficits." Invest Ophthalmol Vis Sci **46(7)**: 2411-2418.
- Horn, F. K., C. Y. Mardin, et al. (2009). "Correlation between local glaucomatous visual field defects and loss of nerve fiber layer thickness measured with polarimetry and spectral domain OCT." Invest Ophthalmol Vis Sci **50(5)**: 1971-1977.

- Hot, A., M. W. Dul, et al. (2008). "Development and evaluation of a contrast sensitivity perimetry test for patients with glaucoma." Invest Ophthalmol Vis Sci **49**(7): 3049-3057.
- Hulsman, C. A., J. J. Houwing-Duistermaat, et al. (2002). "Family score as an indicator of genetic risk of primary open-angle glaucoma." Arch Ophthalmol **120**(12): 1726-1731.
- Inui, T., O. Mimura, et al. (1981). "Retinal sensitivity and spatial summation in the foveal and parafoveal regions." J Opt Soc Am **71**(2): 151-163.
- Jansonius, N. M., J. Nevalainen, et al. (2009). "A mathematical description of nerve fiber bundle trajectories and their variability in the human retina." Vision Res **49**(17): 2157-2163.
- Johnson, C. A. (1994). "Selective versus nonselective losses in glaucoma." J Glaucoma **3 Suppl 1**: S32-44.
- Johnson, C. A. (2001). "Psychophysical measurement of glaucomatous damage." Surv Ophthalmol **45 Suppl 3**: S313-318; discussion S322-314.
- Johnson, C. A., A. J. Adams, et al. (1993). "Blue-on-yellow perimetry can predict the development of glaucomatous visual field loss." Arch Ophthalmol **111**(5): 645-650.
- Johnson, C. A., A. J. Adams, et al. (1993). "Progression of early glaucomatous visual field loss as detected by blue-on-yellow and standard white-on-white automated perimetry." Arch Ophthalmol **111**(5): 651-656.
- Johnson, C. A., B. C. Chauhan, et al. (1992). "Properties of staircase procedures for estimating thresholds in automated perimetry." Invest Ophthalmol Vis Sci **33**(10): 2966-2974.
- Johnson, C. A., P. A. Sample, et al. (2002). "Structure and function evaluation (SAFE): I. criteria for glaucomatous visual field loss using standard

- automated perimetry (SAP) and short wavelength automated perimetry (SWAP)." Am J Ophthalmol **134**(2): 177-185.
- Johnson, M. A., B. A. Drum, et al. (1989). "Pattern-evoked potentials and optic nerve fiber loss in monocular laser-induced glaucoma." Invest Ophthalmol Vis Sci **30**(5): 897-907.
- Jonas, J. B. and A. E. Grundler (1997). "Correlation between mean visual field loss and morphometric optic disk variables in the open-angle glaucomas." Am J Ophthalmol **124**(4): 488-497.
- Jonas, J. B., X. N. Nguyen, et al. (1989). "Parapapillary chorioretinal atrophy in normal and glaucoma eyes. I. Morphometric data." Invest Ophthalmol Vis Sci **30**(5): 908-918.
- Kanski, J. J. (1989). Glaucoma : a colour manual and treatment, Butterworths.
- Kasai, N., G. Takahashi, et al. (1993). An analysis of spatial summation using a Humphrey Field Analyzer. . Amsterdam / New York, Kugler Publications.
- Kass, M. A., D. K. Heuer, et al. (2002). "The Ocular Hypertension Treatment Study: a randomized trial determines that topical ocular hypotensive medication delays or prevents the onset of primary open-angle glaucoma." Arch Ophthalmol **120**(6): 701-713; discussion 829-730.
- Katz, J. (1999). "Scoring systems for measuring progression of visual field loss in clinical trials of glaucoma treatment." Ophthalmology **106**(2): 391-395.
- Katz, L. J., G. L. Spaeth, et al. (1989). "Reversible optic disk cupping and visual field improvement in adults with glaucoma." Am J Ophthalmol **107**(5): 485-492.
- Kelly, D. H. (1981). "Nonlinear visual responses to flickering sinusoidal gratings." J Opt Soc Am **71**(9): 1051-1055.

- Keltgen, K. M. and W. H. Swanson (2009). Estimation of spatial scale using Gabor stimuli. American Academy of Optometry. Orlando, Florida, American Academy of Optometry.
- Kerrigan-Baumrind, L. A., H. A. Quigley, et al. (2000). "Number of ganglion cells in glaucoma eyes compared with threshold visual field tests in the same persons." Invest Ophthalmol Vis Sci **41**(3): 741-748.
- Kitazawa, Y., T. Horie, et al. (1977). "Untreated ocular hypertension. A long-term prospective study." Arch Ophthalmol **95**(7): 1180-1184.
- Klein, B. E., R. Klein, et al. (1994). "Open-angle glaucoma and older-onset diabetes. The Beaver Dam Eye Study." Ophthalmology **101**(7): 1173-1177.
- Kobelt-Nguyen, G., U. G. Gerdtham, et al. (1998). "Costs of treating primary open-angle glaucoma and ocular hypertension: a retrospective, observational two-year chart review of newly diagnosed patients in Sweden and the United States." J Glaucoma **7**(2): 95-104.
- Korth, M., F. Horn, et al. (1989). "The pattern-evoked electroretinogram (PERG): age-related alterations and changes in glaucoma." Graefes Arch Clin Exp Ophthalmol **227**(2): 123-130.
- Korth, M., N. X. Nguyen, et al. (1994). "Scotopic threshold response and scotopic PII in glaucoma." Invest Ophthalmol Vis Sci **35**(2): 619-625.
- Kountouras, J., N. Mylopoulos, et al. (2001). "Relationship between Helicobacter pylori infection and glaucoma." Ophthalmology **108**(3): 599-604.
- Kountouras, J., N. Mylopoulos, et al. (2003). "Increased levels of Helicobacter pylori IgG antibodies in aqueous humor of patients with primary open-angle and exfoliation glaucoma." Graefes Arch Clin Exp Ophthalmol **241**(11): 884-890.

- Kwon, Y. H., H. J. Park, et al. (1998). "Test-retest variability of blue-on-yellow perimetry is greater than white-on-white perimetry in normal subjects." Am J Ophthalmol **126**(1): 29-36.
- Lachenmayr, B. J., S. M. Drance, et al. (1992). "Diffuse field loss and diffuse retinal nerve-fiber loss in glaucoma." Ger J Ophthalmol **1**(1): 22-25.
- Latham, K., D. Whitaker, et al. (1994). "Spatial summation of the differential light threshold as a function of visual field location and age." Ophthalmic Physiol Opt **14**(1): 71-78.
- Latham, K., D. Whitaker, et al. (1993). "Magnification perimetry." Invest Ophthalmol Vis Sci **34**(5): 1691-1701.
- Lau, L. I., C. J. Liu, et al. (2003). "Patterns of visual field defects in chronic angle-closure glaucoma with different disease severity." Ophthalmology **110**(10): 1890-1894.
- Le, A., B. N. Mukesh, et al. (2003). "Risk factors associated with the incidence of open-angle glaucoma: the visual impairment project." Invest Ophthalmol Vis Sci **44**(9): 3783-3789.
- LeBlanc, E. P. and B. Becker (1971). "Peripheral nasal field defects." Am J Ophthalmol **72**(2): 415-419.
- Leipert, K. P. and I. Gottlob (1987). "Pattern electroretinogram: effects of miosis, accommodation, and defocus." Doc Ophthalmol **67**(4): 335-346.
- Leske, M. C., A. M. Connell, et al. (1994). "The Barbados Eye Study. Prevalence of open angle glaucoma." Arch Ophthalmol **112**(6): 821-829.
- Leske, M. C., A. M. Connell, et al. (1995). "Risk factors for open-angle glaucoma. The Barbados Eye Study." Arch Ophthalmol **113**(7): 918-924.

- Leske, M. C., A. M. Connell, et al. (2001). "Incidence of open-angle glaucoma: the Barbados Eye Studies. The Barbados Eye Studies Group." Arch Ophthalmol **119**(1): 89-95.
- Leske, M. C., S. Y. Wu, et al. (2002). "Incident open-angle glaucoma and blood pressure." Arch Ophthalmol **120**(7): 954-959.
- Leske, M. C., A. Heijl, et al. (2004). "Factors for progression and glaucoma treatment: the Early Manifest Glaucoma Trial." Curr Opin Ophthalmol **15**(2): 102-106.
- Levi, D. M. and S. A. Klein (1990). "Equivalent intrinsic blur in spatial vision." Vision Res **30**(12): 1971-1993.
- Leydhecker, G. (1950). "The electroretinogram in glaucomatous eyes." Br J Ophthalmol **34**(9): 550-554.
- Li, G., C. Luna, et al. (2007). "Sustained stress response after oxidative stress in trabecular meshwork cells." Mol Vis **13**: 2282-2288.
- Li, Y. and Y. Z. Yi (1985). "[Histochemical and electron microscopic studies of the trabecular meshwork in primary open-angle glaucoma]." Yan Ke Xue Bao **1**(1): 17-22.
- Lin, H. C., J. H. Kang, et al. (2010). "Hypothyroidism and the risk of developing open-angle glaucoma: a five-year population-based follow-up study." Ophthalmology **117**(10): 1960-1966.
- Luna, C., G. Li, et al. (2009). "Alterations in gene expression induced by cyclic mechanical stress in trabecular meshwork cells." Mol Vis **15**: 534-544.
- Lundberg, L., K. Wettrell, et al. (1987). "Ocular hypertension. A prospective twenty-year follow-up study." Acta Ophthalmol (Copenh) **65**(6): 705-708.

- Lundh, B. L. and E. Gottvall (1995). "Peripheral contrast sensitivity for dynamic sinusoidal gratings in early glaucoma." Acta Ophthalmol Scand **73**(3): 202-206.
- Lutjen-Drecoll, E., C. A. May, et al. (1998). "Localization of the stress proteins alpha B-crystallin and trabecular meshwork inducible glucocorticoid response protein in normal and glaucomatous trabecular meshwork." Invest Ophthalmol Vis Sci **39**(3): 517-525.
- Machida, S., Y. Gotoh, et al. (2008). "Correlation between photopic negative response and retinal nerve fiber layer thickness and optic disc topography in glaucomatous eyes." Invest Ophthalmol Vis Sci **49**(5): 2201-2207.
- Machida, S., D. Raz-Prag, et al. (2008). "Photopic ERG negative response from amacrine cell signaling in RCS rat retinal degeneration." Invest Ophthalmol Vis Sci **49**(1): 442-452.
- Maffei, L. and A. Fiorentini (1982). "Electroretinographic responses to alternating gratings in the cat." Exp Brain Res **48**(3): 327-334.
- Maffei, L., A. Fiorentini, et al. (1985). "Pattern ERG in the monkey after section of the optic nerve." Exp Brain Res **59**(2): 423-425.
- Mai, T. A. and H. G. Lemij (2008). "Longitudinal measurement variability of corneal birefringence and retinal nerve fiber layer thickness in scanning laser polarimetry with variable corneal compensation." Arch Ophthalmol **126**(10): 1359-1364.
- Mai, T. A., N. J. Reus, et al. (2007). "Structure-function relationship is stronger with enhanced corneal compensation than with variable corneal compensation in scanning laser polarimetry." Invest Ophthalmol Vis Sci **48**(4): 1651-1658.
- Maloney, L. T. (1990). "Confidence intervals for the parameters of psychometric functions." Percept Psychophys **47**(2): 127-134.

- Marc, R. E. and H. G. Sperling (1977). "Chromatic organization of primate cones." Science **196**(4288): 454-456.
- Marcelja, S. (1980). "Mathematical description of the responses of simple cortical cells." J Opt Soc Am **70**(11): 1297-1300.
- Martus, P., M. Korth, et al. (1998). "A multivariate sensory model in glaucoma diagnosis." Invest Ophthalmol Vis Sci **39**(9): 1567-1574.
- Maruyama, I., H. Ohguro, et al. (2000). "Retinal ganglion cells recognized by serum autoantibody against gamma-enolase found in glaucoma patients." Invest Ophthalmol Vis Sci **41**(7): 1657-1665.
- Mason, R. P., O. Kosoko, et al. (1989). "National survey of the prevalence and risk factors of glaucoma in St. Lucia, West Indies. Part I. Prevalence findings." Ophthalmology **96**(9): 1363-1368.
- Medeiros, F. A. (2007). "How should diagnostic tests be evaluated in glaucoma?" Br J Ophthalmol **91**(3): 273-274.
- Medeiros, F. A., D. Ng, et al. (2007). "The effects of study design and spectrum bias on the evaluation of diagnostic accuracy of confocal scanning laser ophthalmoscopy in glaucoma." Invest Ophthalmol Vis Sci **48**(1): 214-222.
- Medeiros, F. A., P. A. Sample, et al. (2004). "Frequency doubling technology perimetry abnormalities as predictors of glaucomatous visual field loss." Am J Ophthalmol **137**(5): 863-871.
- Medeiros, F. A., L. M. Zangwill, et al. (2004). "Comparison of the GDx VCC scanning laser polarimeter, HRT II confocal scanning laser ophthalmoscope, and stratus OCT optical coherence tomograph for the detection of glaucoma." Arch Ophthalmol **122**(6): 827-837.
- Metz, C. E. (1978). "Basic principles of ROC analysis." Semin Nucl Med **8**(4): 283-298.

- Miglior, S., N. Pfeiffer, et al. (2007). "Predictive factors for open-angle glaucoma among patients with ocular hypertension in the European Glaucoma Prevention Study." Ophthalmology **114**(1): 3-9.
- Mitchell, P., F. Hourihan, et al. (1999). "The relationship between glaucoma and myopia: the Blue Mountains Eye Study." Ophthalmology **106**(10): 2010-2015.
- Mitchell, P., E. Rochtchina, et al. (2002). "Bias in self-reported family history and relationship to glaucoma: the Blue Mountains Eye Study." Ophthalmic Epidemiol **9**(5): 333-345.
- Mitchell, P., W. Smith, et al. (1997). "Open-angle glaucoma and diabetes: the Blue Mountains eye study, Australia." Ophthalmology **104**(4): 712-718.
- Miyazaki, M., K. Segawa, et al. (1987). "Age-related changes in the trabecular meshwork of the normal human eye." Jpn J Ophthalmol **31**(4): 558-569.
- Morgan, J. E. (2002). "Retinal ganglion cell shrinkage in glaucoma." J Glaucoma **11**(4): 365-370.
- Mukesh, B. N., C. A. McCarty, et al. (2002). "Five-year incidence of open-angle glaucoma: the visual impairment project." Ophthalmology **109**(6): 1047-1051.
- Neoh, C., S. B. Kaye, et al. (1994). "Pattern electroretinogram and automated perimetry in patients with glaucoma and ocular hypertension." Br J Ophthalmol **78**(5): 359-362.
- Newman, E. A. and L. L. Odette (1984). "Model of electroretinogram b-wave generation: a test of the K⁺ hypothesis." J Neurophysiol **51**(1): 164-182.
- Nicolela, M. T., S. M. Drance, et al. (1996). "Color Doppler imaging in patients with asymmetric glaucoma and unilateral visual field loss." Am J Ophthalmol **121**(5): 502-510.

- North, R. V., A. L. Jones, et al. (2010). "Electrophysiological evidence of early functional damage in glaucoma and ocular hypertension." Invest Ophthalmol Vis Sci **51**(2): 1216-1222.
- O'Brien, C. and Z. Butt (1999). "Blood flow velocity in the peripheral circulation of glaucoma patients." Ophthalmologica **213**(3): 150-153.
- O'Donoghue, E., G. B. Arden, et al. (1992). "The pattern electroretinogram in glaucoma and ocular hypertension." Br J Ophthalmol **76**(7): 387-394.
- Ohba, N., K. Nakao, et al. (2007). "The 100 most frequently cited articles in ophthalmology journals." Arch Ophthalmol **125**(7): 952-960.
- Otto, T. and M. Bach (1997). "[Reproducibility of the pattern electroretinogram]." Ophthalmologe **94**(3): 217-221.
- Pan, F. and W. H. Swanson (2006). "A cortical pooling model of spatial summation for perimetric stimuli." J Vis **6**(11): 1159-1171.
- Papst, N., M. Bopp, et al. (1984). "Pattern electroretinogram and visually evoked cortical potentials in glaucoma." Graefes Arch Clin Exp Ophthalmol **222**(1): 29-33.
- Parisi, V. (2003). "Correlation between morphological and functional retinal impairment in patients affected by ocular hypertension, glaucoma, demyelinating optic neuritis and Alzheimer's disease." Semin Ophthalmol **18**(2): 50-57.
- Parisi, V., G. Manni, et al. (2001). "Correlation between optical coherence tomography, pattern electroretinogram, and visual evoked potentials in open-angle glaucoma patients." Ophthalmology **108**(5): 905-912.
- Parisi, V., G. Manni, et al. (1999). "Visual function correlates with nerve fiber layer thickness in eyes affected by ocular hypertension." Invest Ophthalmol Vis Sci **40**(8): 1828-1833.

- Pfeiffer, N. and M. Bach (1992). "The pattern-electroretinogram in glaucoma and ocular hypertension. A cross-sectional and longitudinal study." Ger J Ophthalmol **1**(1): 35-40.
- Pfeiffer, N., D. Birkner-Binder, et al. (1991). "[Pattern ERG in ocular hypertension and glaucoma. Effect of pattern size, contrast and retinal eccentricity]." Fortschr Ophthalmol **88**(6): 815-818.
- Pfeiffer, N., B. Tillmon, et al. (1993). "Predictive value of the pattern electroretinogram in high-risk ocular hypertension." Invest Ophthalmol Vis Sci **34**(5): 1710-1715.
- Piltz, J. R. and R. J. Starita (1990). "Test-retest variability in glaucomatous visual fields." Am J Ophthalmol **109**(1): 109-111.
- Pointer, J. S. and R. F. Hess (1989). "The contrast sensitivity gradient across the human visual field: with emphasis on the low spatial frequency range." Vision Res **29**(9): 1133-1151.
- Popovic, Z. and J. Sjostrand (2005). "The relation between resolution measurements and numbers of retinal ganglion cells in the same human subjects." Vision Res **45**(17): 2331-2338.
- Portney, G. L. and J. E. Hanible (1975). "A comparison of four projection perimeters. Instrument specifications." Surv Ophthalmol **20**(3): 220-223.
- Quigley, H. A. (1996). "Number of people with glaucoma worldwide." Br J Ophthalmol **80**(5): 389-393.
- Quigley, H. A. and A. T. Broman (2006). "The number of people with glaucoma worldwide in 2010 and 2020." Br J Ophthalmol **90**(3): 262-267.
- Quigley, H. A., G. R. Dunkelberger, et al. (1989). "Retinal ganglion cell atrophy correlated with automated perimetry in human eyes with glaucoma." Am J Ophthalmol **107**(5): 453-464.

- Quigley, H. A., R. M. Sanchez, et al. (1987). "Chronic glaucoma selectively damages large optic nerve fibers." Invest Ophthalmol Vis Sci **28**(6): 913-920.
- Racette, L., F. A. Medeiros, et al. (2007). "The impact of the perimetric measurement scale, sample composition, and statistical method on the structure-function relationship in glaucoma." J Glaucoma **16**(8): 676-684.
- Ramakrishnan, R., P. K. Nirmalan, et al. (2003). "Glaucoma in a rural population of southern India: the Aravind comprehensive eye survey." Ophthalmology **110**(8): 1484-1490.
- Read, R. M. and G. L. Spaeth (1974). "The practical clinical appraisal of the optic disc in glaucoma: the natural history of cup progression and some specific disc-field correlations." Trans Am Acad Ophthalmol Otolaryngol **78**(2): OP255-274.
- Redmond, T., D. F. Garway-Heath, et al. (2010). "Sensitivity loss in early glaucoma can be mapped to an enlargement of the area of complete spatial summation." Invest Ophthalmol Vis Sci.
- Redmond, T., M. Zlatkova, et al. (2010). "The effect of age on the area of complete spatial summation for chromatic and achromatic stimuli." Invest Ophthalmol Vis Sci.
- Reidy, A., D. C. Minassian, et al. (1998). "Prevalence of serious eye disease and visual impairment in a north London population: population based, cross sectional study." BMJ **316**(7145): 1643-1646.
- Reus, N. J. and H. G. Lemij (2004). "The relationship between standard automated perimetry and GDx VCC measurements." Invest Ophthalmol Vis Sci **45**(3): 840-845.

- Reus, N. J., Q. Zhou, et al. (2006). "Enhanced imaging algorithm for scanning laser polarimetry with variable corneal compensation." Invest Ophthalmol Vis Sci **47**(9): 3870-3877.
- Ringens, P. J., S. Vijfvinkel-Bruinenga, et al. (1986). "The pattern-elicited electroretinogram. I. A tool in the early detection of glaucoma?" Ophthalmologica **192**(3): 171-175.
- Robson, J. G. and N. Graham (1981). "Probability summation and regional variation in contrast sensitivity across the visual field." Vision Res **21**(3): 409-418.
- Rouland, J. F., G. Berdeaux, et al. (2005). "The economic burden of glaucoma and ocular hypertension: implications for patient management: a review." Drugs Aging **22**(4): 315-321.
- Ruben, S. T., G. B. Arden, et al. (1995). "Pattern electroretinogram and peripheral colour contrast thresholds in ocular hypertension and glaucoma: comparison and correlation of results." Br J Ophthalmol **79**(4): 326-331.
- Salgarello, T., A. Colotto, et al. (1999). "Correlation of pattern electroretinogram with optic disc cup shape in ocular hypertension." Invest Ophthalmol Vis Sci **40**(9): 1989-1997.
- Sample, P. A., C. F. Bosworth, et al. (2000). "Visual function-specific perimetry for indirect comparison of different ganglion cell populations in glaucoma." Invest Ophthalmol Vis Sci **41**(7): 1783-1790.
- Sample, P. A., F. A. Medeiros, et al. (2006). "Identifying glaucomatous vision loss with visual-function-specific perimetry in the diagnostic innovations in glaucoma study." Invest Ophthalmol Vis Sci **47**(8): 3381-3389.
- Sample, P. A. and R. N. Weinreb (1990). "Color perimetry for assessment of primary open-angle glaucoma." Invest Ophthalmol Vis Sci **31**(9): 1869-1875.

- Sample, P. A. and R. N. Weinreb (1992). "Progressive color visual field loss in glaucoma." Invest Ophthalmol Vis Sci **33**(6): 2068-2071.
- Sawusch, M., J. Pokorny, et al. (1987). "Clinical electroretinography for short wavelength sensitive cones." Invest Ophthalmol Vis Sci **28**(6): 966-974.
- Scheffrin, B. E., M. L. Bieber, et al. (1998). "The area of complete scotopic spatial summation enlarges with age." J Opt Soc Am A Opt Image Sci Vis **15**(2): 340-348.
- Schlottmann, P. G., S. De Cilla, et al. (2004). "Relationship between visual field sensitivity and retinal nerve fiber layer thickness as measured by scanning laser polarimetry." Invest Ophthalmol Vis Sci **45**(6): 1823-1829.
- Schuurmans, R. P. and T. Berninger (1984). "Pattern reversal responses in man and cat: a comparison." Ophthalmic Res **16**(1-2): 67-72.
- Schwartz, B., J. C. Rieser, et al. (1977). "Fluorescein angiographic defects of the optic disc in glaucoma." Arch Ophthalmol **95**(11): 1961-1974.
- Sieving, P. A., K. Murayama, et al. (1994). "Push-pull model of the primate photopic electroretinogram: a role for hyperpolarizing neurons in shaping the b-wave." Vis Neurosci **11**(3): 519-532.
- Sieving, P. A. and R. H. Steinberg (1987). "Proximal retinal contribution to the intraretinal 8-Hz pattern ERG of cat." J Neurophysiol **57**(1): 104-120.
- Sihota, R., P. Sony, et al. (2006). "Diagnostic capability of optical coherence tomography in evaluating the degree of glaucomatous retinal nerve fiber damage." Invest Ophthalmol Vis Sci **47**(5): 2006-2010.
- Silverstone, D. E. and J. Hirsch (1986). Automated visual field testing : techniques of examination and interpretation. East Norwalk, Conn., Appleton-Century-Crofts.

- Sloan, L. L. and D. J. Brown (1962). "Area and luminance of test object as variables in projection perimetry: Clinical studies of photometric dysharmony " Vision Res **2**(12): 527-541.
- Sommer, A., J. M. Tielsch, et al. (1991). "Relationship between intraocular pressure and primary open angle glaucoma among white and black Americans. The Baltimore Eye Survey." Arch Ophthalmol **109**(8): 1090-1095.
- Spahr, J. (1975). "Optimization of the presentation pattern in automated static perimetry." Vision Res **15**(11): 1275-1281.
- Spileers, W., F. Falcao-Reis, et al. (1993). "Evidence from human electroretinogram A and off responses that color processing occurs in the cones." Invest Ophthalmol Vis Sci **34**(6): 2079-2091.
- Spry, P. G., A. B. Bates, et al. (2000). "Simulation of longitudinal threshold visual field data." Invest Ophthalmol Vis Sci **41**(8): 2192-2200.
- Spry, P. G., C. A. Johnson, et al. (2001). "Variability components of standard automated perimetry and frequency-doubling technology perimetry." Invest Ophthalmol Vis Sci **42**(6): 1404-1410.
- Strouthidis, N. G., S. K. Gardiner, et al. (2010). "Predicting progression to glaucoma in ocular hypertensive patients." J Glaucoma **19**(5): 304-309.
- Stroux, A., M. Korth, et al. (2003). "A statistical model for the evaluation of sensory tests in glaucoma, depending on optic disc damage." Invest Ophthalmol Vis Sci **44**(7): 2879-2884.
- Sugimoto, K., A. Schotzau, et al. (1998). "Optimizing distribution and number of test locations in perimetry." Graefes Arch Clin Exp Ophthalmol **236**(2): 103-108.
- Sustar, M., B. Cvenkel, et al. (2009). "The effect of broadband and monochromatic stimuli on the photopic negative response of the electroretinogram in normal

- subjects and in open-angle glaucoma patients." Doc Ophthalmol **118**(3): 167-177.
- Swanson, W. H., J. Felius, et al. (2000). "Effect of stimulus size on static visual fields in patients with retinitis pigmentosa." Ophthalmology **107**(10): 1950-1954.
- Swanson, W. H., J. Felius, et al. (2004). "Perimetric defects and ganglion cell damage: interpreting linear relations using a two-stage neural model." Invest Ophthalmol Vis Sci **45**(2): 466-472.
- Swanson, W. H., B. B. Lee, et al. (2010) "Ganglion Cell Responsiveness to Perimetric Stimuli: Frequency-Doubling Stimuli Are Not Better Than Conventional Stimuli in Separating M-Cells From P-Cells." Invest Ophthalmol & Vis Sci. E-abstract.
- Swanson, W. H., F. Pan, et al. (2008). "Chromatic temporal integration and retinal eccentricity: psychophysics, neurometric analysis and cortical pooling." Vision Res **48**(26): 2657-2662.
- Tafreshi, A., L. Racette, et al. (2010). "Pattern electroretinogram and psychophysical tests of visual function for discriminating between healthy and glaucoma eyes." Am J Ophthalmol **149**(3): 488-495.
- Tafreshi, A., P. A. Sample, et al. (2009). "Visual function-specific perimetry to identify glaucomatous visual loss using three different definitions of visual field abnormality." Invest Ophthalmol Vis Sci **50**(3): 1234-1240.
- Teikari, J. M. (1987). "Genetic factors in open-angle (simple and capsular) glaucoma. A population-based twin study." Acta Ophthalmol (Copenh) **65**(6): 715-720.
- Tezel, G., D. P. Edward, et al. (1999). "Serum autoantibodies to optic nerve head glycosaminoglycans in patients with glaucoma." Arch Ophthalmol **117**(7): 917-924.

- Thibos, L. N. (1998). "Acuity perimetry and the sampling theory of visual resolution." Optom Vis Sci **75**(6): 399-406.
- Thomas, J. P. (1978). "Spatial summation in the fovea: asymmetrical effects of longer and shorter dimensions." Vision Res **18**(8): 1023-1029.
- Thylefors, B. and A. D. Negrel (1994). "The global impact of glaucoma." Bull World Health Organ **72**(3): 323-326.
- Tielsch, J. M., J. Katz, et al. (1994). "Family history and risk of primary open angle glaucoma. The Baltimore Eye Survey." Arch Ophthalmol **112**(1): 69-73.
- Tielsch, J. M., J. Katz, et al. (1995). "Hypertension, perfusion pressure, and primary open-angle glaucoma. A population-based assessment." Arch Ophthalmol **113**(2): 216-221.
- Tielsch, J. M., A. Sommer, et al. (1991). "Racial variations in the prevalence of primary open-angle glaucoma. The Baltimore Eye Survey." JAMA **266**(3): 369-374.
- Traquair, H. M. (1938). An introduction to clinical perimetry. [S.l.], Henry Kimpton.
- Trick, G. L. (1992). "Pattern electroretinogram: an electrophysiological technique applicable to primary open-angle glaucoma and ocular hypertension." J Glaucoma **1**(4): 271-279.
- Trick, G. L., M. Bickler-Bluth, et al. (1988). "Pattern reversal electroretinogram (PRERG) abnormalities in ocular hypertension: correlation with glaucoma risk factors." Curr Eye Res **7**(2): 201-206.
- Turpin, A., A. M. McKendrick, et al. (2003). "Properties of perimetric threshold estimates from full threshold, ZEST, and SITA-like strategies, as determined by computer simulation." Invest Ophthalmol Vis Sci **44**(11): 4787-4795.
- Tyler, C. W. (1981). "Specific deficits of flicker sensitivity in glaucoma and ocular hypertension." Invest Ophthalmol Vis Sci **20**(2): 204-212.

- Uchida, H., S. Ugurlu, et al. (1998). "Increasing peripapillary atrophy is associated with progressive glaucoma." Ophthalmology **105**(8): 1541-1545.
- Vaegan, S. L. Graham, et al. (1991). "Selective reduction of oscillatory potentials and pattern electroretinograms after retinal ganglion cell damage by disease in humans or by kainic acid toxicity in cats." Doc Ophthalmol **77**(3): 237-253.
- van den Berg, T. J., F. C. Riemslag, et al. (1986). "Pattern ERG and glaucomatous visual field defects." Doc Ophthalmol **61**(3-4): 335-341.
- van der Schoot, J., N. J. Reus, et al. (2010). "The ability of short-wavelength automated perimetry to predict conversion to glaucoma." Ophthalmology **117**(1): 30-34.
- Varma, R., H. A. Quigley, et al. (1992). "Changes in optic disk characteristics and number of nerve fibers in experimental glaucoma." Am J Ophthalmol **114**(5): 554-559.
- Viswanathan, S., L. J. Frishman, et al. (2000). "The uniform field and pattern ERG in macaques with experimental glaucoma: removal of spiking activity." Invest Ophthalmol Vis Sci **41**(9): 2797-2810.
- Viswanathan, S., L. J. Frishman, et al. (1999). "The photopic negative response of the macaque electroretinogram: reduction by experimental glaucoma." Invest Ophthalmol Vis Sci **40**(6): 1124-1136.
- Viswanathan, S., L. J. Frishman, et al. (2001). "The photopic negative response of the flash electroretinogram in primary open angle glaucoma." Invest Ophthalmol Vis Sci **42**(2): 514-522.
- Wakili, N., F. K. Horn, et al. (2008). "The photopic negative response of the blue-on-yellow flash-electroretinogram in glaucomas and normal subjects." Doc Ophthalmol **117**(2): 147-154.

- Wall, M. and K. M. Ketoff (1995). "Random dot motion perimetry in patients with glaucoma and in normal subjects." Am J Ophthalmol **120**(5): 587-596.
- Wall, M., K. R. Woodward, et al. (2009). "Repeatability of automated perimetry: a comparison between standard automated perimetry with stimulus size III and V, matrix, and motion perimetry." Invest Ophthalmol Vis Sci **50**(2): 974-979.
- Wanger, P. and H. E. Persson (1983). "Pattern-reversal electroretinograms in unilateral glaucoma." Invest Ophthalmol Vis Sci **24**(6): 749-753.
- Wassle, H., M. H. Chun, et al. (1987). "Amacrine cells in the ganglion cell layer of the cat retina." J Comp Neurol **265**(3): 391-408.
- Watson, A. B. and D. G. Pelli (1983). "QUEST: a Bayesian adaptive psychometric method." Percept Psychophys **33**(2): 113-120.
- Weber, J., F. Dannheim, et al. (1990). "The topographical relationship between optic disc and visual field in glaucoma." Acta Ophthalmol (Copenh) **68**(5): 568-574.
- Weih, L. M., M. Nanjan, et al. (2001). "Prevalence and predictors of open-angle glaucoma: results from the visual impairment project." Ophthalmology **108**(11): 1966-1972.
- Weinreb, R. N. and P. T. Khaw (2004). "Primary open-angle glaucoma." Lancet **363**(9422): 1711-1720.
- Weinreb, R. N. and J. P. Perlman (1986). "The effect of refractive correction on automated perimetric thresholds." Am J Ophthalmol **101**(6): 706-709.
- Weinstein, G. W., G. B. Arden, et al. (1988). "The pattern electroretinogram (PERG) in ocular hypertension and glaucoma." Arch Ophthalmol **106**(7): 923-928.
- Werner, E. B. and J. Beraskow (1979). "Peripheral nasal field defects in glaucoma." Ophthalmology **86**(10): 1875-1878.

- Westcott, M. C., F. W. Fitzke, et al. (1998). "Abnormal motion displacement thresholds are associated with fine scale luminance sensitivity loss in glaucoma." Vision Res **38**(20): 3171-3180.
- Westheimer, G. (1966). "Focusing responses of the human eye." Am J Optom Arch Am Acad Optom **43**(4): 221-232.
- Whalen, W. R. and G. L. Spaeth (1985). Computerized visual fields : what they are and how to use them. Thorofare, Slack.
- Wild, J. M., R. P. Cubbidge, et al. (1998). "Statistical aspects of the normal visual field in short-wavelength automated perimetry." Invest Ophthalmol Vis Sci **39**(1): 54-63.
- Wild, J. M., J. M. Wood, et al. (1987). "Spatial summation and the cortical magnification of perimetric profiles." Ophthalmologica **195**(2): 88-96.
- Wilensky, J. T. and A. E. Kolker (1976). "Peripapillary changes in glaucoma." Am J Ophthalmol **81**(3): 341-345.
- Wilensky, J. T., J. R. Mermelstein, et al. (1986). "The use of different-sized stimuli in automated perimetry." Am J Ophthalmol **101**(6): 710-713.
- Wilson, M. E. (1967). "Spatial and temporal summation in impaired regions of the visual field." J Physiol **189**(2): 189-208.
- Wilson, M. E. (1970). "Invariant features of spatial summation with changing locus in the visual field." J Physiol **207**(3): 611-622.
- Wirtschafter, J. D., W. L. Becker, et al. (1982). "Glaucoma visual field analysis by computed profile of nerve fiber function in optic disc sectors." Ophthalmology **89**(3): 255-267.
- Wolfs, R. C., C. C. Klaver, et al. (1998). "Genetic risk of primary open-angle glaucoma. Population-based familial aggregation study." Arch Ophthalmol **116**(12): 1640-1645.

- Wollstein, G., D. F. Garway-Heath, et al. (1998). "Identification of early glaucoma cases with the scanning laser ophthalmoscope." Ophthalmology **105**(8): 1557-1563.
- Wong, T. Y., B. E. Klein, et al. (2003). "Refractive errors, intraocular pressure, and glaucoma in a white population." Ophthalmology **110**(1): 211-217.
- Wood, J. M., J. M. Wild, et al. (1988). "Factors affecting the normal perimetric profile derived by automated static threshold LED perimetry. I. Pupil size." Ophthalmic Physiol Opt **8**(1): 26-31.
- Wyatt, H. J., M. W. Dul, et al. (2007). "Variability of visual field measurements is correlated with the gradient of visual sensitivity." Vision Res **47**(7): 925-936.
- Yamada, N., P. P. Chen, et al. (1999). "Screening for glaucoma with frequency-doubling technology and Damato campimetry." Arch Ophthalmol **117**(11): 1479-1484.
- Yang, A. and W. H. Swanson (2007). "A new pattern electroretinogram paradigm evaluated in terms of user friendliness and agreement with perimetry." Ophthalmology **114**(4): 671-679.
- Yin, Z. Q., Vaegan, et al. (1997). "Widespread choroidal insufficiency in primary open-angle glaucoma." J Glaucoma **6**(1): 23-32.
- Yucel, Y. H., N. Gupta, et al. (1998). "Relationship of optic disc topography to optic nerve fiber number in glaucoma." Arch Ophthalmol **116**(4): 493-497.
- Zalta, A. H. and J. C. Burchfield (1990). "Detecting early glaucomatous field defects with the size I stimulus and Statpac." Br J Ophthalmol **74**(5): 289-293.
- Zangwill, L. M., S. Jain, et al. (2007). "The effect of disc size and severity of disease on the diagnostic accuracy of the Heidelberg Retina Tomograph Glaucoma Probability Score." Invest Ophthalmol Vis Sci **48**(6): 2653-2660.

Zeyen, T. G., M. Zulauf, et al. (1993). "Priority of test locations for automated perimetry in glaucoma." Ophthalmology **100**(4): 518-522; discussion 523.